

**Department of Chemical Engineering
Clean Gas Technologies Australia**

CO₂ Separation by Cryogenic and Hydrate

Daria Surovtseva

**This thesis is presented for the Degree
Doctor of Philosophy
of
Curtin University of Technology**

September 2010

To the best of my knowledge and belief this thesis contains no material previously published by any other person except where due acknowledgement has been made. This thesis contains no material which has been accepted for the award of any other degree or diploma at any university.

Acknowledgements

Sincere gratitude is expressed to my supervisor, Professor Robert Amin, for his professional guidance and continuous encouragement throughout my research. His dedication and enthusiasm for scientific research is unsurpassed, and his vast knowledge and incisive insight have been inspiring.

I wish to express my thanks to Associate Professor Ahmed Barifcani, for his assistance during the experiments, helpful discussions and valuable advices. In addition, I would like to thank all staff at Clean Gas Technologies Australia, Associate Professor David Pack, Ms. Sabine Isbarn, Mr. Saif Gahdban and fellow PhD students for their enormous support and help.

I gratefully acknowledge the financial support to this work from CO2CRC with especial thanks to Barry Hopper Hopper for his leadership, and professional guidance for the past 5 years of research work.

Last but not least, I would like to acknowledge my family back home in Russia for their encouragement and support.

Abstract

According to the Intergovernmental Panel on Climate Change Fourth Assessment Report (IPCC AR4), fossil fuels are utilised to produce more than 80% of the world's energy and this is likely to remain unchanged in the nearest future, especially as industrialisation is pursued by such economic giants as China. Without substantial change in energy policies with primary focus on the development of sustainable technologies for power generation, mitigation of associated Green House Gas (GHG) emissions cannot be fully implemented, and will require continual improvement in order to achieve objectives set by the Kyoto protocol. Research and development in the field of Carbon Capture and Sequestration is therefore being thoroughly explored. In this work a new sustainable technology for CO₂ capture from IGCC power stations is developed and discussed in detail. This technology is based on cryogenic condensation integrated with gas hydrate formation.

With the massive global reduction in recoverable oil and the potential size in a few decades time, the accent started to shift towards the other available fossil fuels such as gas and coal. The amount of Natural Gas trapped in the form of solid hydrate sunk in the deep ocean and permafrost areas cannot be estimated precisely, however, the scientific community agrees that values in order of 10¹⁵ to 10¹⁷ cubic metres are realistic. This has caused overwhelming research into gas hydrates as storage media for different gases. Gas hydrates are highly organized crystalline structures with molecules of light gases encaged in a framework created by water molecules. They can form at any place where free water in intimate contact with hydrate forming gas is exposed to elevated pressures and low temperatures. The ability to store large quantity of gas per unit volume makes gas hydrates an attractive option for any application requiring gas preservation. One of such modern applications for gas hydrates has arisen from the global warming problem and addresses the potential capability to efficiently capture and safely store the CO₂.

Coal remains the main energy source in the world; for example, in Australia it is providing 40% of total energy and up to 80% of electricity (Cuevas-Cubria et al., 2010). The main advantages of coal over the other fossil energy resources are its abundance, its easy recoverability and lower cost. Massive pollution produced during burning of this fuel forced the creation of new technologies that allow for GHG

reduction. Integrated Gasification Combined Cycle (IGCC) is the most favoured advanced option for energy recovery from a variety of sources, particularly coal, the so-called 'clean coal technology'. IGCC generates a high pressure shifted syngas stream composed essentially of Hydrogen and Carbon Dioxide. Historically, the CO₂ was separated from rich sources (such as natural gas) via the Ryan-Holmes cryogenic condensation process. However, applied at the gas or oil refinery this method can consume up to 50% of the generated energy to bring the CO₂ levels down to pipeline requirements which does not seem attractive in terms of cost of CO₂ avoided. High temperatures utilised for coal gasification are also not favourable for the implementation of cryogenic condensation to an IGCC stream.

On the other hand, high pressure and high CO₂ content in the IGCC flue gas provide the ideal conditions for CO₂ capture in the form of solid hydrates. This option has been investigated under the guidance of the US Department of Energy by a team of researchers (Los Alamos National Laboratory, Nexant, Inc., and SIMTECHE) since 1999 and at the Chinese Academy of Science. A few proof-of-concept reports can be found stating that the utilisation of the hydrate formation phenomenon for purification of gas streams is less energy intensive than any of the other existing CO₂ capture methods. The ability to encapsulate significant amounts of gas in little space and relatively mild conditions of storage make the hydrates an extremely attractive option for easy handling of high rates of GHG emissions. However, this research is still on a laboratory scale.

In this thesis a new method is developed for cost and energy efficient CO₂ sequestration from IGCC sources based on a simple configuration. High feed pressure facilitates bulk removal of CO₂ by cryogenic methods, and high energy recovery is achieved through process integration with hydrate formation. Liquid CO₂ produced as a result of condensation carries most of the cold energy required for initial refrigeration, and the hydrate unit does not consume any substantial additional energy. Separated CO₂ is characterised by high purity sufficient for utilisation in enhanced oil and gas recovery processes. The hydrate can be easily handled and stored. Although the focus is made on IGCC flue gas application, the method can be extended to other sources with high CO₂ levels and supplied at high pressure.

Additional value is brought to this research by extensive investigation of the phase behaviour of gas mixtures containing CO₂. Particular attention is paid to the distinctive features of gas hydrates produced in different systems including mixtures

with hydrocarbons and non-hydrocarbons in various concentrations and in the presence of chemicals dissolved in water. This knowledge will contribute to the future development in the field of hydrates and will be useful for both academic research and industrial application.

Research Summary

This project focuses on capture of Carbon Dioxide from product gases of the Oxyfuel and IGCC combustion processes. These technologies are gaining favour as options for power generation from fossil fuels. Separation of Hydrogen from the product gas of these reforming processes promises significant productivity gains when compared with current processes. The work described in this thesis is an exploration of a combined cryogenic and gas-hydrate process which offers effective separation over a wide range of process conditions and gas compositions

Following a review of pertinent literature, both the cryogenic condensation stage and the hydrate precipitation stage are investigated by means of process simulation and experiment.

Deficiencies in the performance of the simulation programs over the range of gas compositions and process temperatures and pressures are identified. A modified equation of state is developed for Carbon Dioxide-Hydrogen mixtures to address this problem.

Conditions for formation of Carbon Dioxide hydrate are explored and the effects of various hydrate-promoting agents on the equilibrium phase envelope are examined for optimal dosage. A new promoter is identified and is applied to improve the efficiency of the precipitation process.

Development of the combined cryogenic and hydrate process to pilot-plant scale is discussed. Particular features of a continuously operating plant are identified and attention is directed to favourable process conditions and to qualities of the process stream relevant to handling and further utilisation.

This research has resulted in five journal papers, one of which is published in the Chemical Engineering Research and Design Journal (Surovtseva, Amin & Barifcani, 2010), two are submitted to the Fluid Phase Equilibria Journal, and two are prepared for submission. Also an Australian provisional patent application number 2010902902 entitled "Process and apparatus for removing carbon dioxide from a gas stream" was filed on 30 June 2010 in the name of CO2CRC Technologies Pty Ltd.

Nomenclature

Acronyms and Abbreviations

(p-)TSA	(Para-) Toluene Sulphonic Acid
CCGT	Combined Cycle Gas Turbine
CCGT	Combined Cycle Gas Turbine
CCS	Carbon Capture and Sequestration
CFZ	Controlled Freezing Zone technology by Exxon Mobil
CGTA	Clean Gas Technologies Australia
CMC	Critical micelle concentration
CO2CRC	Cooperative Research Centre for Greenhouse Gas Technologies, Australia
CoP	ConocoPhillips IGCC Plant
DOE	Department of Energy
EOS	Equation of state
GE	General Electric
GEE	GE Energy IGCC Plant
GPSA	Gas Processors Suppliers Association
H	Hydrate phase
HDT	Hydrate Dissociation Temperature
HFT	Hydrate Formation Temperature
IGCC	Integrated Gasification Combined Cycle
JT	Joule-Thompson effect
L	Liquid hydrocarbon or CO ₂ phase
LABSA	Linear Alkyl Benzene Sulphonic Acid
LNG	Liquefied Natural Gas
m	Meta stable fluid
MEG	Monoethylene Glycol
MSDS	Material Safety Data Sheet
NETL	National Energy Laboratory
NG	Natural Gas
NRTL	Non-random two-liquid equation
NRTL	Non-random two liquid model

NRU	Nitrogen Rejection Unit
PEG	Polyethylene Glycol
PR	Peng-Robinson equation of state
PT	Pressure-temperature characteristics
PVT	Pressure-Vapor-Temperature
S	Solid phase
SDS	Sodium Dodecyl Sulphate
SRK	Soave-Ridlich-Kwong equation of state
SVLE	Solid-Liquid-Vapor equilibrium
TBAB	Tetrabutyl Ammonium Bromide
TBAC	Tetrabutyl Ammonium Chloride
THF	Tetrahydrofuran
UNIFAC	Universal Functional Activity Coefficient
US	United States
V, G	Hydrocarbon or CO ₂ in vapour phase
VLE	Vapor-Liquid equilibrium
WAT	Cloud point (Wax Appearance Temperature)
WRF	Woodside Research Foundation

Parameters

a,b,A,B	Constants of a fluid in various equations
C,c	Heat capacity, concentration
F	Fugacity
g,G	Gibbs Energy
h	Enthalpy
k	Boltzman constant, kJ/K
K	Phase distribution parameter
K _H	A Constant in Hammerschmidt formula
M	Molecular weight
n	Amount of component, mol
P, p	Pressure in specified units
q	Fugacity coefficient
R	Universal gas constant, J/(mol·K), radius
r	Radius or distance

T	Temperature in specified units
t	Time, s
V, v	Volume
W	Water content, amount of inhibitor
x, y	Mole fraction of a component
Z, z	Compressibility factor, initial total composition, cavity coordination number
α	Kihara core diameter
$\alpha(T)$, $b(T)$	Functions of temperature
γ	Activity coefficient
δ	Binary interaction parameter
δ	Binary interaction parameter
ϵ	Kihara energy of a molecule
μ	Viscosity, chemical potential
ρ	Density in specified units
σ	Collision radius
ω	Acentric factor

Subscripts

C, c	Critical properties
eq	Equilibrium
exp	Experimental
H	Hydrate
W	Water, weight
m	Meta stable state of fluid
i, j	Components
0, o	Reference state
fr	Solidification or freezing

Table of Contents

Chapter 1. Introduction to the Research	1
1.1. Introduction	1
1.2. Objectives of this Research	3
1.3. Significance of this Research	4
1.4. Thesis Chapter Outline	6
Chapter 2. Literature Review	8
2.1. Introduction	8
2.2. Low Temperature Technologies for CO ₂ Abatement	9
2.2.1. Gas Hydrates	9
2.2.1.1. Natural Gas Hydrates. Inhibition.	14
2.2.1.2. Hydrate Promoters for Gas Separation and Storage ..	16
2.2.2. Cryogenic Separation of CO ₂	20
2.2.2.1. Ryan-Holmes Process	22
2.2.2.2. Controlled Freezing Zone by Exxon	23
2.2.2.3. CryoCell® Technology	25
2.2.2.4. Other Competitors and Testing Programs	26
2.3. Modern Options for CO ₂ Abatement	28
2.3.1. IGCC Power Plants for CO ₂ Capture	28
2.3.2. Oxyfuel Technology for CO ₂ Capture	33
2.4. Summary of the Existing Options for CO ₂ Capture	35
2.5. Phase Behaviour of CH ₄ -CO ₂ and H ₂ -CO ₂ Mixtures	36
2.5.1. Methane-Carbon Dioxide system	37
2.5.2. Hydrogen-Carbon Dioxide System	42
2.6. Theoretical Models for Phase Transitions Prediction	44
2.6.1. Cubic Equation of State and Shortcoming	45

2.6.2. Excess Free Energy and Activity Coefficient Based Models	.48
2.6.3. Comparison of Different Models49
2.7. Conclusion49
Chapter 3. Cryogenic Separation of CO ₂52
3.1 Introduction52
3.2 Theoretical Modelling of Phase Behaviour of H ₂ -CO ₂ mixtures53
3.3 Experimental Investigation of CO ₂ Condensation and Freezing54
3.3.1 Experimental Procedures56
3.3.2 Dew Point Determination Technique58
3.4 Results and Discussion60
3.4.1 Dew Point Results61
3.4.2 Total CO ₂ Capture Rates63
3.4.3 Stickiness of Solid CO ₂65
3.5 Thermodynamic Modelling of CO ₂ Condensation and Freezing69
3.6. Conclusion73
Chapter 4. CO ₂ Separation by Hydrate74
4.1. Introduction74
4.2. Water Content of Sour Gases75
4.3. Materials and Procedures78
4.4. Results and Discussion80
4.4.1. Hydrotropes Testing80
4.4.2. Optimisation of TBAC Content84
4.4.3. Quantifying TBAC Performance85
4.5. Thermodynamic Modelling of CO ₂ Hydrate86
4.5.1. Van der Waals-Platteeuw (VdW-P) Model87
4.5.2. Calculation of $\Delta\mu_W$87

4.5.3. Calculation of $\Delta\mu_H$	88
4.5.4. Improvements to the Model	89
4.6. Conclusion	90
Chapter 5. Hydrate Management and MEG Concentration	91
5.1. Introduction	91
5.2. Experimental	94
5.2.1. Sample Preparation	95
5.2.2. Experimental Procedures.	95
5.3. Hydrate Formation Temperature (HFT) and Hydrate Dissociation Temperature (HDT)	96
5.3.1. Experimental HFT vs HDT	97
5.3.2. Assessment of the Accuracy of Prediction	99
5.4. Effect of Methane/CO ₂ Ratio on Hydrate Formation and Dissociation	103
5.5. Conclusion	105
Chapter 6. Gas Hydrates in Presence of Condensate and Wax	108
6.1. Introduction	108
6.2. Experimental Investigation of the Condensate Influence on Hydrate Formation	110
6.3. Hydrate Dissociation Curves in the Presence of Condensate	111
6.4. Hydrate-Wax Interaction	112
6.5. MEG-Wax Interaction	114
6.6. Fluid Viscosity Change During Hydrate Formation	115
6.7. Conclusion	117
Chapter 7. Pilot Plant Design	118
7.1. Introduction	118
7.2. Flue Gas Description	119

7.3. Flow Scheme Description	121
7.4. Servicing streams	124
7.5. IGCC GE Case Study	125
7.5.1. Mass and Energy Balance	125
7.5.2. Equipment Design	126
7.5.3. Overall CO ₂ Capture and Purity	127
7.5.4. Heat Recovery	127
7.6. IGCC Shell Case Study	127
7.6.1. Mass and Energy Balance	128
7.6.2. Equipment Design	128
7.6.3. Overall CO ₂ Capture and Purity	129
7.6.4. Heat Recovery	130
7.7. Conclusion	130
Chapter 8. Laboratory Set-up for the Technology Testing	132
8.1. Introduction	132
8.2. Laboratory Set-up Description	134
8.3. Equipment and Specifications	136
8.4. Operating Procedures	137
8.5. Safety	140
8.6. Experimental Results and Discussion	140
8.6.1. Cryogenic Section	140
8.6.1. Hydrate Section.....	142
8.6.1.1. Experimental Description	142
8.6.1.2. Theoretical Modelling	142
8.7. Conclusion	143

Chapter 9. Case Study. Cool Energy Cryogenic CO ₂ Removal Project Developer	
Model	144
9.1. Introduction	145
9.2. Current Market Place Overview for CO ₂ Removal Technologies.....	147
9.2.1. Chemical Solvents	147
9.2.2. Physical Solvents	148
9.2.3. Membranes	149
9.2.4. Hybrid Membrane and Chemical Solvents	150
9.3. CryoCell® Position in the CO ₂ Removal Market	151
9.3.1. Comparison with Chemical Solvents	151
9.3.1.1. Capital Cost	151
9.3.1.2. Operating Cost	152
9.3.1.3. Conclusion for Chemical Solvents	152
9.3.2. Comparison with Physical Solvents and Membranes	152
9.3.3. CryoCell® Competitive Position for CO ₂ Removal	154
9.4. Competing Technologies in the CO ₂ Capture Market	154
9.4.1. Cryogenic Distillation (Ryan-Holmes)	155
9.5. CryoCell® position in the CO ₂ capture Market	155
9.5.1. Comparison with Solvents and Membranes	155
9.5.1.1. Capital Cost	156
9.5.1.2. Operating Cost	157
9.5.1.3. Emissions from fuel gas	157
9.5.2. Comparison with Ryan-Holmes	159
9.5.3. CryoCell® Competitive Position for CO ₂ Capture	159
9.6. Potential Competition in the CO ₂ Capture Market	159
9.6.1. CFZ™ – Controlled Freeze Zone	160

9.6.2. The Cimatech Process	161
9.6.3. Advanced Solvents	162
9.6.4. IFPexol IFPex 2	162
9.6.5. Sprex® CO ₂	163
9.7. Future Markets Overview	163
9.7.1. Competing Technologies in LNG Market	164
9.7.1.1. Large Scale LNG	164
9.7.1.2. Medium Scale LNG	165
9.7.1.3. Small scale LNG	166
9.7.2. Other Technologies in Syngas and Other Potential Markets..	168
9.8. Conclusion	171
Chapter 10. Conclusion and Recommendations	173
10.1. Research Summary	175
10.2. Significance	176
10.3. Recommendations	177
Reference List	180
Appendix A. High Pressure Full-Vision Sapphire Cell	203
Appendix B. Gas Sample Preparation and Transfer Procedure	207
Appendix C. CO ₂ condensation and freezing.....	209
Appendix D. Gas Compositions for Hydrate Testing.....	242
Appendix F. CO ₂ -Natural Gas Multiphase Flash Model	254
Appendix G. Observations During Gas Mixture Preparation.....	262

List of Figures

Figure 1.1 Block diagram of the Integrated Cryogenic and Hydrate Technology for Carbon Dioxide capture	2
Figure 2. 1 Types of hydrate network structures	10
Figure 2. 2 Phase Diagram for Gas Hydrate	12
Figure 2. 3 Moles of gas consumed in dissolution and hydrate formation in a typical experiment.....	13
Figure 2. 4 The effect of THF on hydrate formation from CO ₂ -N ₂ gas mixtures.....	18
Figure 2. 5 Principal scheme of the Ryan-Holmes process for Natural Gas sweetening	22
Figure 2. 6 Tower arrangement for CFZ process	24
Figure 2. 7 Block diagram of CoolEnergy's technology	26
Figure 2. 8 Schematic of IGCC process	29
Figure 2. 9 Comparison of Total Plant Cost for the IGCC cases with and without CO ₂ capture	32
Figure 2. 10 Comparison of Net Plant Efficiency for the IGCC cases with and without CO ₂ capture	32
Figure 2. 11 Oxyfuel combustion by Vattenfall	33
Figure 2. 12 Topology of the binary system CO ₂ -N ₂ in PT diagram	37
Figure 2. 13 Comparison of experimental phase diagrams obtained by Donnelly and Katz (1954) and Davis et al. (1962)	39
Figure 2. 14 Experimental data on phase envelope CO ₂ -CH ₄ mixture	40
Figure 2. 15 The possibility of separation of different compositions Methane-Carbon Dioxide	41
Figure 2. 16 Isotherms for Hydrogen-Carbon Dioxide mixtures	43
Figure 2. 17 Bubble point curves for H ₂ -CO ₂ mixtures from Bezanehtak (2002) and Spano et al. (1968)	43

Figure 2. 18 Density of liquid phase during condensation of Hydrogen-Carbon Dioxide mixtures	44
Figure 3. 1 Dew point simulation results	54
Figure 3. 2 Liquid CO ₂ collected in the cell at -55°C	57
Figure 3. 3 Typical gas volume changes during cooling-heating cycle	59
Figure 3. 4 Dew point observation on Pressure-Temperature curve	60
Figure 3. 5 Phase envelope of mixtures with different CO ₂ content in the range of pressures 30 to 60 bar	62
Figure 3. 6 Comparison of theoretical and experimental dew point results	62
Figure 3. 7 CO ₂ capture rates at 50 to 57 bar	64
Figure 3. 8 Freezing of Carbon Dioxide from mixtures with Natural Gas	68
Figure 4. 1 McKetta-Wehe chart for estimation of Natural Gas saturation (1958)....	76
Figure 4. 2 Calculation sheet developed as part of this work	77
Figure 4. 3 Slurry of CO ₂ hydrate formed from 14 mol% H ₂ -CO ₂ mixture in the presence of 1 wt% TBAC solution at 1.2°C	82
Figure 4. 4 Effect of TBAC concentration on CO ₂ hydrate formation	84
Figure 5. 1 Comparison of HFT and HDT for Sample 2 synthetic gas in contact with 0 to 65 wt% MEG-water solutions	99
Figure 5. 2 Type 1 Hydrate curve for Sample 2 with 0 to 25 wt% MEG	102
Figure 5. 3 Type 2 Hydrate curve for Sample 2 with 40 to 50 wt% MEG	102
Figure 5. 4 Type 3 Hydrate curve for Sample 2 with 55 to 70 wt% MEG	102
Figure 5. 5 Hydrate curve for Sample 1 with 40 wt% MEG	102
Figure 5. 6 Experimental Hydrate curves for Sample 3 with and without MEG in comparison with simulation results	103
Figure 5. 7 Effect of composition on HDT in the presence of MEG	105
Figure 6. 1 PT characteristics during cold start-up and extended shut-in	110
Figure 6. 2 Hydrate dissociation in waxy and de-waxed condensate on S3	112

Figure 6. 3 Hydrates formation in de-waxed Condensate @ 120 bar.....	113
Figure 6. 4 Hydrates formation in waxy condensate at 60 bar. The formation of egg shape structure due to the rotation of the mixer	114
Figure 6. 5 WAT as function of MEG concentration	115
Figure 6. 6 MEG freezing as function of concentration	115
Figure 6. 7 Viscosity as a function of temperature and concentration	116
Figure 7. 1 Block diagram for the IGCC process with CO ₂ capture by cryogenic and hydrate	121
Figure 7. 2 Flow diagram for integrated cryogenic and hydrate CO ₂ capture.....	122
Figure 7. 3 Feed gas drying, chilling and liquefaction of CO ₂	123
Figure 7. 4 Hydrate CO ₂ capture	123
Figure 7. 5 CO ₂ rich gas drying and compression	124
Figure 8. 1 Laboratory rig for integrated cryogenic and hydrate testing	133
Figure 8. 2 Measuring equipment	133
Figure 8. 3 Mixing section	134
Figure 8. 4 Cryogenic section	135
Figure 9. 1 CoolEnergy Demonstration Site	145
Figure 9. 2 Cost comparison between CryoCell and Amine for CO ₂ removal only	151
Figure 9. 3 Cost comparison of CryoCell® and amine including CO ₂ capture	156
Figure 9. 4 Comparison of emissions from fuel gas for CryoCell and Amine plants	157
Figure 9. 5 CFZ Clear Lake Pilot Plant	160
Figure 9. 6 Simplified Spretx Process Flow Diagram	163
Figure 10. 1 Contribution to CO ₂ emissions from various sources	174
Figure A. 1 Photograph of the Sapphire Cell	203

List of Tables

Table 2. 1 Parameters for models based on the activity coefficient approach	48
Table 3. 1 Natural Gas composition	55
Table 3. 2 Dew point data for gas mixtures containing 27 to 52 mol% CO ₂	63
Table 3. 3 Percentages of CO ₂ collected at -55°C at different pressures for different compositions	65
Table 3. 4 Results on CO ₂ freeze out from mixtures with Natural Gas	66
Table 4. 1 CO ₂ content in gas streams during processing with a new technology ..	74
Table 4. 2 List of chemicals potentially promoting hydrate formation	79
Table 4. 3 The effect of tested chemicals on CO ₂ hydrate formation.....	83
Table 4. 4 Choice of optimum concentration of TBAC	84
Table 4. 5 CO ₂ capture from H ₂ -CO ₂ mixtures by 1 wt% TBAC-water solution ..	86
Table 5. 1 K _H constant for Hammerschmidt equation for calculation of necessary amount of inhibitor	93
Table 5. 2 Guidelines for gas hydrate inhibition and gas dehydration	94
Table 5. 3 Compositions used.....	95
Table 5. 4 Experimental HFT and HDT for Sample 2 synthetic gas	97
Table 5. 5 Experimental HDT for S2 in comparison with design figures	101
Table 5. 6 Effect of composition on HDT in the presence of MEG	104
Table 6. 1 Fluid composition for experimental testing	111
Table 6. 2 WAT and MEG freezing at 85 bar.....	115
Table 6. 3 WAT and MEG freezing at 5 bar	115
Table 6. 4 Viscosity as Function of Temperature and concentration	116
Table 7. 1 Coal composition used in the IGCC	119
Table 7. 2 IGCC GE and Shell compositions and conditions	11200

Table 7. 3 Servicing streams	124
Table 7. 4 Mass and Energy balance	125
Table 7. 5 Vessels	126
Table 7. 6 Pumps	126
Table 7. 7 Heat exchangers	126
Table 7. 8 Compressors	127
Table 7. 9 Mass and Energy balance	128
Table 7. 10 Vessels	129
Table 7. 11 Pumps	129
Table 7. 12 Heat Exchangers	129
Table 7. 12 Compressors	129
Table 8. 1 Dimensions of the vessels used in laboratory set-up	137
Table 8. 2 First and second feed gas compositions	138
Table 8. 3 Summary of Cryogenic stage performance	141
Table 8. 4 Estimated Hydrate stage performance	143
Table 9. 1 Comparison of CryoCell and Amine plant fuel and power requirements	156
Table B. 1 Equipment used for sample preparation	208
Table C. 1 Gas composition for CO ₂ freezing testing	209
Table C. 2 Experimental conditions for CO ₂ stickiness experiments	210
Table D. 1 Gas composition for CO ₂ hydrate testing	242
Table D. 2 Compositions prepared for hydrate testing	242

Chapter 1. Introduction to the Research

1.1. Introduction

The concentration of CO₂ in our atmosphere is promoted by the combustion of fossil fuels for the generation of electricity. Capturing CO₂ from flue-gas streams is an essential parameter for the carbon management for sequestering of CO₂ from our environment. Cost-effective carbon capture is a critical step in any gas processing plant containing CO₂ or fossil fuel power plant. With 50% of Australian electricity and most of CO₂ emissions coming from coal, carbon capture technologies are essential to the future of energy and coal-related industries. The most recent need for CO₂ capture is related to the process streams from the modern power stations such as IGCC plants. In this research the emphasis is on the implementation of low temperature condensation and hydrate techniques for CO₂ separation from such sources, while several other methods exist and are commercialised.

Technologies currently available on the market do not offer sequestration options for captured CO₂, resulting in the CO₂ removed from the gas being vented into the atmosphere. With increasing awareness of climate change impacts and calls for reductions in emissions it has been recognized that in future an emphasis will be placed on technologies which not only remove CO₂ from the gas stream, but also enable its capture in a form suitable for storage or further use.

The baseline approach for the process of cryogenic condensation is to refrigerate the feed gas containing CO₂ at elevated pressure down to temperatures where Carbon Dioxide can be condensed and/or solidified and removed. In the cases of Natural Gas processing and Enhanced Oil Recovery (EOR), the CO₂ can be separated as a solid from partially liquefied hydrocarbons. Liquid CO₂ of high purity can be obtained from IGCC flue gas, while Hydrogen stays in the gas phase. Similar research involving cryogenic separation of CO₂ is being conducted at Brigham Young University by Dr. Larry Baxter for post-combustion CO₂ capture from power plants (Cryogenic Carbon Capture Technology, 2009).

A stand-alone cryogenic technique for CO₂ separation from flue gases from power plants does not appear to be a competitive method due to high energy demand for refrigeration. In this research, process integration involving utilisation of gas hydrate formation for CO₂ sequestration is proposed (Figure 1.1). In the first stage the most

of the CO_2 will be removed from the flue gas via cryogenic condensation, and in the second stage the remainder of CO_2 will be captured in form of solid hydrate. Majority of the energy required for cooling of the feed gas will be recovered from the process streams.

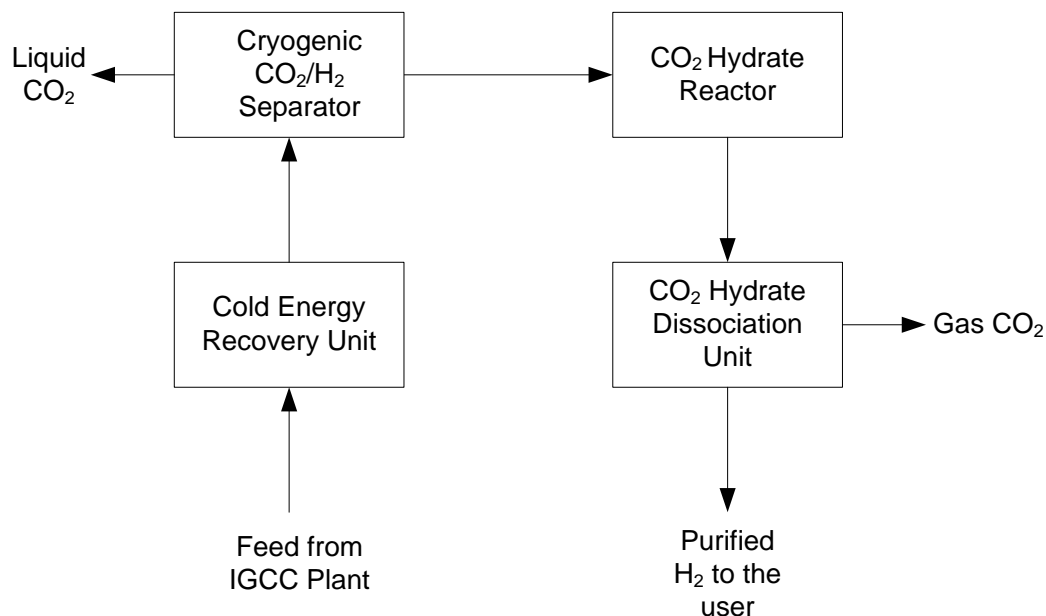


Figure 1.1 Block diagram of the Integrated Cryogenic and Hydrate Technology for Carbon Dioxide capture

The majority of low molecular weight gases including CO_2 , form solid crystalline structures in the presence of water at low temperature and high pressure conditions specific for each gas. The use of promoters can increase selectivity of this process, and therefore CO_2 can be relatively easily captured from a mixture of gases in the form of a solid hydrate. The research is based on work previously conducted at Clean Gas Technology Australia (CGTA), formerly the Woodside Research Foundation (WRF) at Curtin University of Technology. This concerns the field of cryogenic separation of CO_2 from Natural Gas (CryoCell Technology) and utilisation of hydrotropes as hydrate promoters for Methane clathrate formation (Gnanendran and Amin, 2003). A multi-stage hydrate formation method is proposed for CO_2 removal and being investigated by SIMTECHE in conjunction with the Nexant research group under the US Department of Energy, however, there are no data available on the current status of this project.

Building on this knowledge, this research involves an extensive theoretical and bench-scale study of the effectiveness of CO_2 removal by combined cryogenics and hydrates and is supported by experimentation on a semi-continuous laboratory-scale

pilot plant specially constructed as part of the contract with project sponsor CO2CRC Australia. The rig is capable of processing 500 cc/min of gas mixture. The technology produces liquid CO₂ in the first cryogenic condensation stage, and fine CO₂ hydrate slurry in the second stage. Hydrate is easily dissociated to produce ultra-pure gaseous CO₂ and water. Liquefied CO₂ can be pumped to storage through the enhanced oil and gas recovery processes. High pressure of both gaseous and liquefied CO₂ products significantly reduces energy consumption in the final stage of compression to required pressure of 110 bar. Identification of a suitable promoter capable of facilitating CO₂ hydrate formation from lean gas mixtures at temperatures higher than the freezing point of water is considered the most significant and difficult part of this research. The design and commissioning of the reactor for hydrate formation is described in Battah (2002). A semi-continuous operation to produce hydrate from synthetic Natural Gas was performed by Gnanendran (2004). The technology has been tested for CO₂ separation from IGCC and Oxyfuel gas mixtures, however its application can be extended to other high-CO₂ containing sources supplied at high pressure.

1.2. Objectives of this Research

To develop and test the cryogenic-hydrate technology capable of separating Hydrogen and Carbon Dioxide from synthesis gas streams at high temperature and pressure, with high purity and recovery at low energy penalty. This is achieved through the following steps:

- Evaluation of the effectiveness of cryogenic CO₂ capture (capture rate): The method proposed in this research includes separation of CO₂ in liquid phase from GE and Shell IGCC, and Oxyfuel process gases. In addition, CO₂ freezing out from mixtures with light hydrocarbons is investigated in order to study the potential of build-up of frozen matter in pipelines. An extensive study is conducted using state-of-the-art PVT equipment in order to: i) build reliable phase envelope curves for mixtures of interest because the results of a theoretical examination conducted show inconsistency; and ii) by analysis of gas and liquid phases at equilibrium, conduct quantitative assessment of the CO₂ which can be captured.

- Analysis of hydrate formation: Various chemicals of hydrotropic structure were tested in regards to their promotion of CO₂ hydrate formation from the lean gas stream obtained after cryogenic separation. Efficiency of separation is determined in terms of the reduction in CO₂ concentration in the gas phase and also referred to as *capture rate*. In order to better understand the governing laws of hydrate formation in the presence of other substances, inhibiting effects of monoethylene glycol MEG and condensate are studied using gas mixtures of CO₂ with Natural Gas with different compositions. The effect of wax precipitation is also assessed.

- Pilot plant development, operation and optimisation: The optimal integration of the capture process with the power plant is necessary to ensure a low energy requirement for CO₂ capture, but it is also needed in order to reduce the investment costs of the interfacing. The pilot is an essential step in the development of a cost-effective carbon capture technology. To establish the viability of the technology during continuous operation is one of the most important challenges facing any new technology development. Process schemes of a pilot plant which will allow for efficient energy recovery as well as optimised utilisation of water and promoter are developed for GE and Shell IGCC, and Oxyfuel. Operational conditions for the combined cryogenic and hydrate technology for CO₂ capture are optimised on the basis of the obtained study results. Experimental work is performed on the pilot plant in order to establish the required scale-up data for the development of a field plant.

The global aim of this research as defined by the contract with the sponsors is to design, build and operate a rig for CO₂ capture from a mixture of gases similar to the IGCC flue gases for both Shell and GE processes and Oxyfuel process gases. Experimentation on this rig will enable a commercially viable scaled-up process to be realised in the future.

1.3. Significance of this Research

IGCC processes are becoming the most promising technologies for gasification of coal. The syngas produced by these processes is rich in Hydrogen and also contains a high percentage of Carbon Dioxide. The CO₂ after its capture and separation from the syngas could be compressed and handled separately. The syngas rich in H₂ above 85 mol% could be used as clean fuel for power generation. There are basically two

established gasification processes namely GE & Shell processes. The pressures used are in the range of 30 bar for the Shell process to 60 bar for the GE process. Each process has its own advantages and merits and the CO₂ capture scheme from the syngas gasification process plays a major role for evaluation and comparison of these processes.

CO₂ capture by the hydrate method could be used in many cases especially when CO₂ concentration in the flue gases is high. The IGCC process represents an ideal case for CO₂ capture by the hydrate method as both processes provide the gas at high pressure, therefore eliminating the energy requirements for the compression stage. The other advantage is that once CO₂ is captured it could be easily released from the hydrate in the dissociation stage which only requires 5-10 degrees of temperature rise and/or 10-20 bar decrease in pressure. The CO₂ produced could therefore be compressed from these high process pressures to 110 bar, which is the required product pressure also decreasing the compression stage energy demand.

In this project, highly efficient energy and heat recovery is achieved through utilisation of the high feed gas pressure for condensation and capture of CO₂ in the cryogenic stage. Liquefied CO₂ can be used for cooling and partial condensation of the CO₂ in the feed gas. Utilisation of less equipment, simple configuration and low initial energy consumption also contribute to lower cost.

The overall efficiency of CO₂ capture can be estimated in terms of the following data.

- Overall capture is above 90 mol% of CO₂
- Captured CO₂ is more than 95 mol% purity

Furthermore, the CO₂ captured both by cryogenic and hydrate is ready for transportation and storage with no further treatment and energy required. Along with CO₂, high purity Hydrogen is produced at high pressure of over 50 bar.

A comprehensive, fundamental study of CO₂ and Methane hydrates formation in the presence of various chemicals and condensates also makes a useful contribution to future research in the field of hydrates. Extensive equilibrium data for a vast variety of gas compositions, thorough the description of interfacial and bulk properties can play an important role in hydrate prediction knowledge. A new experimental technique for hydrate formation prediction based on viscosity changes is developed within this research. A study of the effect of wax deposition on Natural Gas hydrate

formation can be an inestimable contribution to the industry as this phenomenon has not been thoroughly investigated before.

Experimental investigation of $\text{H}_2\text{-CO}_2$ mixtures has shown that existing theoretical models overestimate achievable CO_2 capture rates for mixtures with low CO_2 content. Results obtained from simulation software are found to be inconsistent in prediction of dew points, especially in the region of high pressures and low concentrations of CO_2 . A new method for experimental dew and bubble point determination based on PVT changes has been developed and proved to give very accurate results. A new modification to the SKR-Peneloux equation of state is made to improve its predicting capability for such mixtures.

1.4. Thesis Chapter Outline

This research consists of three divisions as outlined in the project objectives. Chapter 2 contains a literature review of existing low-temperature techniques for CO_2 removal from gas streams, and also presents results of previous experimental and theoretical studies for Hydrogen- CO_2 and Methane- CO_2 gas mixtures, which is useful for understanding the major milestones of this research. Chapters 3 through to 8 contain details of the theoretical and experimental work conducted in this research. The first objective, namely utilisation of cryogenic methodology for CO_2 separation, is addressed in Chapter 3 which contains theoretical simulation results and compares them with experimental quantitative analysis of CO_2 condensation from IGCC and Oxyfuel gas mixtures as well as CO_2 freeze-out from mixtures with hydrocarbons. A new modification to the equation of state is proposed for a more accurate description of phase envelopes of $\text{H}_2\text{-CO}_2$ mixtures. Chapters 4 through to 6 deal with the investigation of CO_2 and Methane hydrates. Chapter 4 is dedicated to finding a promoter which enables CO_2 hydrate slurry formation in water from overhead gas after condensation. Also in this Chapter the optimal concentration of the promoter is identified. The inhibition effect of MEG on hydrate formation is quantitatively estimated in Chapter 5 using CO_2 -hydrocarbon gas mixtures as an example. Development and utilisation of a new method for hydrate formation prediction based on changes in bulk properties of an aqueous phase is also described. In Chapter 6, the effect of condensate and wax deposition on hydrates is illustrated. Pilot plant design and operation is presented in Chapters 7 and 8 respectively. Basic design, simulation results and flow diagrams for the rig are included in Chapter 7. Chapter 8 contains a

description of the laboratory equipment and its arrangement, the operation manuals, encountered problems and their solutions during process optimisation, as well as the results of experimental testing of the developed technology for CO₂ capture from GE and Shell IGCC, and Oxyfuel flue gases. Conclusions are made according to a comparison of model and obtained data. The current marketplace and the potential for the enhanced cryogenic technique for CO₂ capture is discussed in Chapter 9. Research findings are outlined and summarised in Chapter 10, and recommendations for further research and scale-up are given. The relevant information not included in the main Chapters is given in the Appendices.

Chapter 2. Literature Review

2.1. Introduction

Several research groups are investigating effectiveness and efficiency of various options for CO₂ capture around Australia under control of CO₂CRC. Existing pilot plants being tested at Hazelwood Power Station and the Mulgrave Project include membrane separation, adsorption by solids, and absorption by solvents facilities. These alternatives comprise a clearly competitive environment to low-temperature separation, especially from low-CO₂ process streams. Chemical and physical solvent technologies account for approximately 90% of the worldwide installed base of CO₂ removal technologies; and membrane technologies account for nearly all the remaining 10%. Each of these techniques allows for significant reduction in CO₂ emissions; however, they still have some critical problems associated with high energy consumption, corrosion, foaming, low capacity, and significant cost of start-up and maintenance. Besides, current CO₂ removal procedures do not include means for permanent storage or sequestration in geological formations. Only three amine-based carbon capture projects (Statoil's Sleipner West Gas Field in the North Sea off Norway; their Snøhvit Field LNG and CO₂ storage projects in the Barents Sea, Norway; and the Sonatrach–BP–Statoil operated Gas Processing Plant in In Salah, Algeria) have been developed for carbon capture and underground storage to prevent its release into the atmosphere (Rubin et al., 2010).

Two general trends in carbon capture research have emerged. The first is to address the inefficiencies of conventional absorption processes currently in use. The second is to develop alternative capture technologies that have the potential to achieve substantial cost reductions.

According to the US Electric Power Research Institute (EPRI) (Prism/MERGE Analyses 2009 Update, 2009; Advanced Coal Power Systems with CO₂ Capture: EPRI's CoalFleet for Tomorrow Vision, 2008), efficiency improvements can be expected to provide reductions of 20% to 30% in the near-term and 40% to 50% in the medium-term. Improvements in the near-term can result from the use of new reagents, improved absorber design, and better stripping conditions. The discussion rapidly becomes technical, with other quoted improvements being: faster kinetics,

lower oxidation losses, and improved absorbers (geometry, packing, staging, and lower-cost construction materials).

The second trend is to find altogether new chemistries and processes that will reduce the cost of carbon capture by a factor of two to four (Electric Power Research Institute, 2009). The chance of success is lower for this research route and the research timescale extends further into the future. The hydrate formation phenomenon is one of the modern prospective approaches that have appeared recently promising to save energy. Advantages of application of hydrate formation for CO₂ capture and storage over conventional techniques are discussed in detail further.

Within the scope of this work, the accent is made on the investigation of process integration of a well-established low-temperature condensation technique with a new concept of use of gas hydrate formation for carbon capture from non-hydrocarbon gas mixtures (IGCC and Oxyfuel flue streams) and for improved performance. Utilisation of cryogenic separation of CO₂ is widely used in natural gas sweetening, therefore detailed comparison of the process implementation for the two cases (CO₂ capture from hydrocarbon and non-hydrocarbon mixtures respectively) is provided. Phase behaviour of the hydrogen-CO₂ gas mixture is thoroughly investigated using both theory and experiment to account for the possible changes of the flue gas composition from the source (power station). The main advantage of this method is that it does not offer venting of the captured CO₂ into the atmosphere but produces CO₂ in amenable for transportation, injection and permanent storage form.

2.2. Low Temperature Technologies for CO₂ Abatement

2.2.1. Gas Hydrates

Water molecules tend to arrange themselves around molecules of dissolved gases in polyhedral structures, which at certain pressure, temperature and saturation solidify in a form resembling ice. These non-stoichiometric ice-like clathrate compounds, where molecules of low molecular weight gases or volatile liquids are hosted within cavities created via Hydrogen-bonding, are known as gas hydrates. Although the structural characteristics are very similar to common ice, liquid to solid transition occurs at temperatures sometimes significantly higher than water freezing point. This phenomenon is caused by the stabilisation effect of guest molecules on long range

ordering in water. The first mention of hydrates dates back to 1810 and Sir Humphry Davy.

Depending on the type of guest molecules, particularly the size, the form of the polyhedron formed by surrounding water can vary. According to the accepted classification (Sloan and Koh 1998), there are three possible crystal structures in which hydrates can exist, namely cubic structure I (sI), cubic structure II (sII), and hexagonal structure (sH). The first two structures were classified in terms of the sizes of guest molecules by Stackelberg (1949). Common structure I formers include Methane, Ethane, Carbon Dioxide, Hydrogen Sulphide and other molecules in the range of 0.40 to 0.55 nm (Sloan, 2003). Structure II contains larger cages which can be occupied by 0.60 to 0.70 nm guests such as Propane or iso-butane molecules which in turn stabilise the lattice for housing smaller molecules such as Nitrogen. Structure H was first reported substantially later by Ripmeester and Ratcliffe (1990), and it was found to enclathrate Tetrahydrofuran, Neohexane and other hydrocarbons with carbon number not exceeding 7 and size about 0.80 to 0.90 nm. The latter structure, similar to sII, also contains smaller cavities available for lowest molecular weight inclusions of Nitrogen and noble gases. Crystal structures, number of cavities and potential hydrate formers for each described type are presented in Figure 2.1.

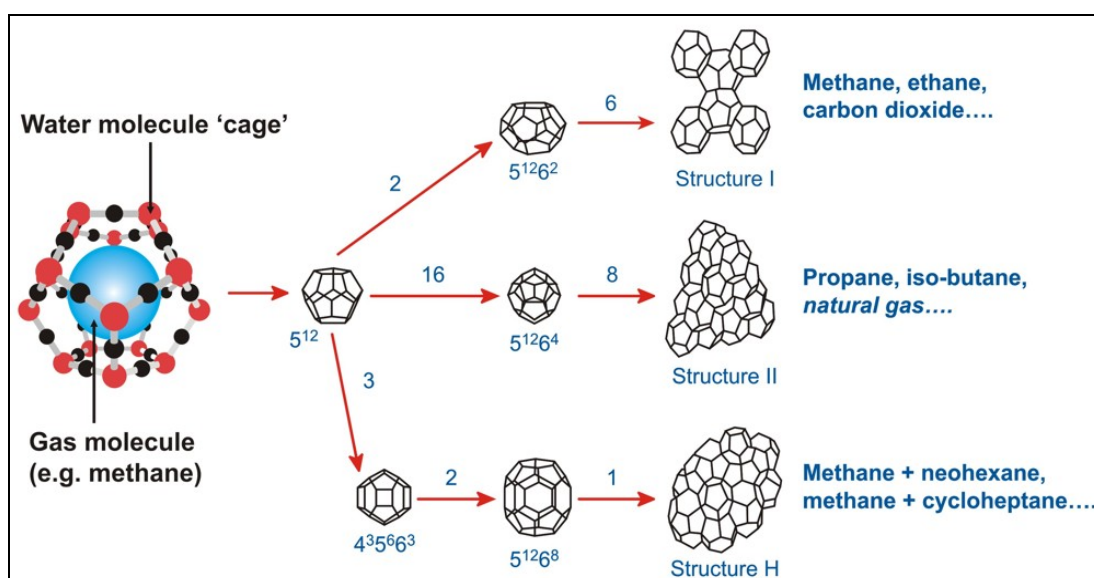


Figure 2. 1 Types of hydrate network structures (Sloan, 1998)

The water to gas molecular ratio in gas hydrate compounds is usually about 85% (Sun & Duan, 2005), which contributes to a high affinity to ice. However,

macroscopic properties such as heat of formation and equilibrium physical conditions are fully determined by crystalline structure.

Traditionally, gas hydrates have been of a great importance for the oil and gas production industry due to their annoying tendency to plug pipelines and damage the equipment (Hammerschmidt, 1934; Davies et al., 2008). In this regard, significant research is focusing on finding creative and effective ways to prevent or defer the hydrate formation from light hydrocarbons (Kelland et al., 1995; Lederhos et al., 1996). These include inhibition techniques and the study of hydrate equilibrium and dissociation (Behar et al., 1991; Long, 1994; Lachance et al., 2009). Since large deposits of Methane hydrate were found in permafrost areas and in the sea beds, the interest in hydrate research attained a new direction and expanded widely (Dillon et al., 1992). For example, a dynamic in-field study on gas hydrates as a potential source of clean energy is being conducted within the Mallik 2002 Gas Hydrate Research Well Program in the Canadian Arctic region (Takahashi et al., 2003; Holder et al., 1988; Lee and Holder, 2001; Burshears et al., 1986; Jadhawar et al., 2006). However, this process is outside the scope of the current research. Utilisation of gas hydrate phenomenon for Natural Gas transportation and storage existed since early 1940's (Benesh, 1942; Miller and Strong, 1946; Parent, 1948), and the newest concept in the field of hydrates started in the early 1990's pertaining to gas hydrates as a means for CO₂ capture and storage. This technique involves the use of additives which can facilitate hydrate formation and improve gas-to-hydrate conversion (Kang et al., 2001; Seo et al., 2001). To explore other technological applications, the research has also expanded to the determination of fundamental physical properties of gas clathrates including heat of formation/dissociation, thermal conductivity, heat capacity, crystal structure and gas molecule behaviour inside a water lattice. A large number of studies are dedicated to investigation of kinetics of the formation and dissociation processes in pure water and in the presence of various additives. The latest comprehensive review of the main trends in gas hydrates research can be found in (Sloan & Koh, 2008).

Any hydrate former, such as Natural Gas or CO₂, and water comprise a two-component system for which a pressure-temperature phase diagram is given in Figure 2.2.

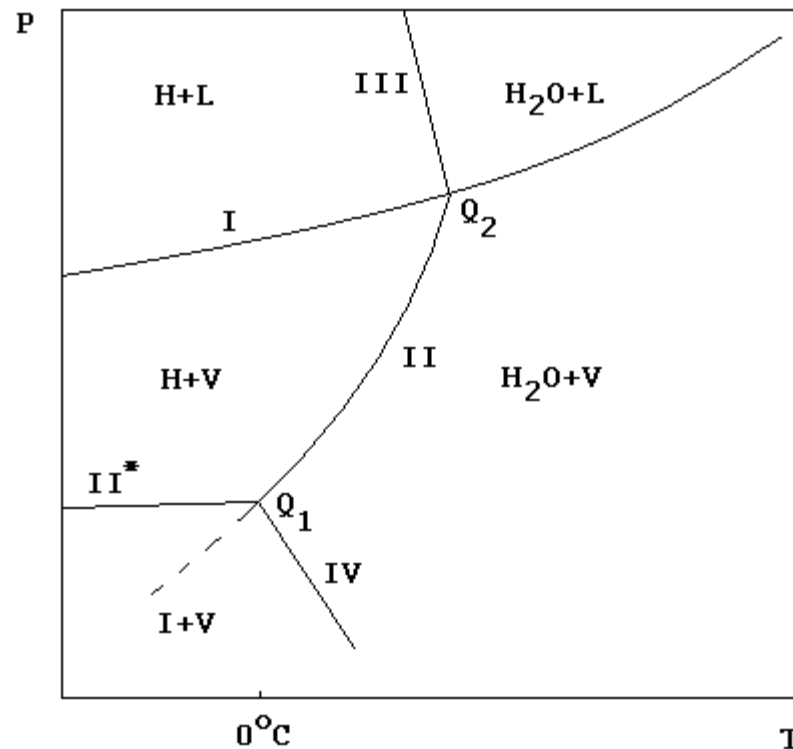


Figure 2. 2 Phase Diagram for Gas Hydrate (single component). I – Saturation pressure of the pure component, II – Saturation pressure of the hydrate ($T > 0^\circ\text{C}$), II* - saturation pressure of the hydrate ($T < 0^\circ\text{C}$), III – Dissociation curve of the hydrate, IV – Depression of freezing point of water as a result of dissolution of hydrate forming component.

According to Gibb's phase rule, two phases coexist in areas on this diagram, lines represent three phases, and quadruple states correspond to points. Quadruple point Q_1 is where Ice, Water, Hydrate and Vapour coexist. State Q_2 describes equilibrium between Water, hydrate former in Liquid phase, Vapour and Hydrate. The three phase lines of Ice-Hydrate-Vapour and Water-Hydrate-Vapour equilibrium are of particular interest for both industrial and academic applications where hydrate formation is encountered. Three-phase equilibria for a wide variety of hydrate forming systems have been studied (Rodger 1990; Holder et al., 1980). The most important for current research are the works concerning Natural Gas hydrate formation in the presence of heavier hydrocarbons and inhibitors and CO_2 hydrate formation with and without promoting substances.

Gas hydrates form in any location when a hydrate-forming gas is in contact with free water and exposed to appropriate pressure and temperature conditions. Laboratory investigations of hydrate formation are confined most often to gradual reduction of temperature of the pressurised water-gas system, or to gradual pressure increase in an isothermal regime. The most important factors defining the intensity of hydrate

accumulation are the state of the water and diffusivity of the hydrate-former, degree of agitation, and degree of metastability and supersaturation of the system (Makogon 1997, Kashchiev and Firoozabadi, 2002). Crystallization of the hydrate in the solution is analogous to the precipitation process and passes all stages from nucleation to critical size build-up. Figure 2.3 demonstrates typical gas consumption during the hydrate formation process. When a sufficient quantity of hydrate-former (n_{eq}) is dissolved in the solution to achieve saturation, the reactor has to undergo stirring for additional time t_{tb} (about 800 seconds in this case) before first crystals of hydrate appear and start assembling. Numerous works support the view that seeding of hydrate particles is stochastic (Radhakrishnan and Trout, 2002), usually substantial overcooling and supersaturation in conjunction with long periods of vigorous agitation is necessary for the first nuclei to appear. This causes ambiguity in observation of hydrate formation conditions; therefore, for the current research, hydrate equilibrium conditions are determined as hydrate dissociation conditions. The hydrate is first formed in an overcooled vigorously stirred system, and then slowly heated with no mixing. The point at which bubbles of trapped gas start coming out of the aqueous phase is taken as the hydrate equilibrium condition.

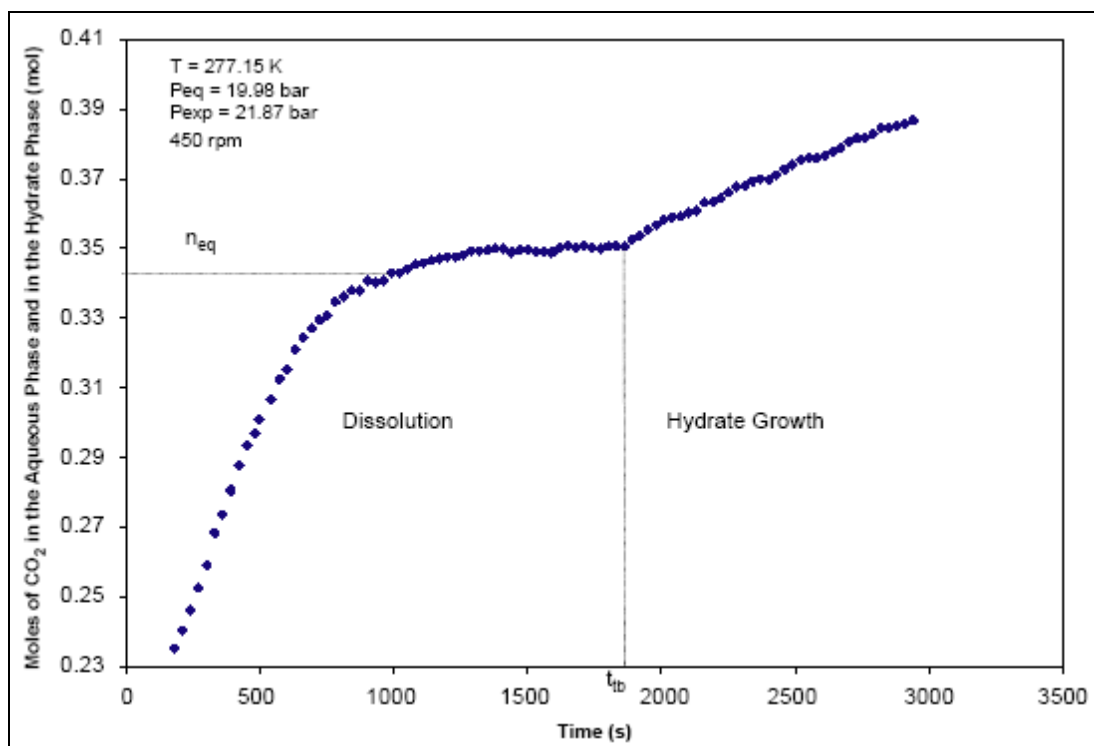


Figure 2. 3 Moles of gas consumed in dissolution and hydrate formation in a typical experiment (Clarke and Bishnoi, 2005)

Mass transfer effects have the biggest impact on the kinetics of hydrate nucleation and growth (Clarke and Bishnoi, 2005; Kim et al., 1987; Bishnoi and Natarajan, 1996; Natarajan et al., 1994; Skovborg and Rasmussen, 1994). A mechanistic model based on the rate of diffusion of a hydrate former into solution was developed in Bishnoi's works. Some practical schemes for calculation of hydrate nucleation based on the differences in free surface energies were proposed by Kashiev and Firoozabadi (2002a, 2002b, 2003). Hydrate formation is seen as an interfacial phenomenon, as in the majority of studies the hydrate was observed to first form a thin crispy film on the surface of an aqueous solution (Uchida et al, 1999). The nuclei tend to occur on the water/hydrate-former interface regardless of the state of the latter (Zhang, 2003; Holder et al., 2001) or even on the surface of solid impurities present in the solution.

2.2.1.1. Natural Gas Hydrates. Inhibition.

Many attempts have been made to explain the inhibition mechanism (Xhang et al., 2009; Zhang, 2009); however, this is still an open question. Thermodynamic and kinetic effects of hydrate preventing chemicals are necessary for understanding of possibilities for hydrate promotion studied in this work.

Development of the effective methods for combating hydrates during gas and oil exploration and processing is still the major research area in the field of gas hydrates. The most prominent chemicals used in industry include alcohols, glycols and ionic salts. As shown in the study performed by Ng and Robinson (1985), Methanol and glycols exhibit sufficient inhibiting action only when present at high concentrations in an aqueous phase. Surfactants were found to have similar effect when present in significantly lower quantities (ref Profio et al., 2005). Recently the use of a certain type of surfactants known as *hydrotropes* was shown to be contradictory in their ability to promote and inhibit hydrates formation (Gnanendran and Amin, 2003; Rovetto et al., 2006).

Chemicals used for hydrate inhibition belong to one of the two groups distinguished by Makogon (1994), namely thermodynamic and kinetic inhibitors. Thermodynamic inhibitors prevent hydrate formation at usual forming conditions by depressing the fugacity of water. Usually these are chemicals capable of creating Hydrogen bonds with water molecules and destructing its long range ordering followed by depression of fugacity. This action is similar to the water freezing point depression phenomenon

due to the considerable similarity between ice and hydrate structures. Monoethylene glycol and Methanol are typically used for industrial applications. Quantitatively, the inhibiting affect can be described in terms of the following figures: 10 wt% content of Methanol in water allows for 5°K reduction of Methane hydrate formation temperature at the same pressure, and 40°K difference can be observed in the case of the concentration of Methanol reaching 50 wt% (Munck et al., 1988). One of the earliest models for calculation of the hydrate formation temperature deviation in the presence of inhibitors is the Hammerschmidt model (described in Carroll, 2002. Initially proposed in Hammerschmidt, 1939). It is very simple in use; however, it is valid only for concentrations lower than 20 to 30 wt% of glycols and Methanol. Nielsen and Bucklin (1983) proposed another model which extended the range of concentrations of the inhibitor up to 80 wt% Methanol. This model was modified in Carroll (2002) to account for an activity coefficient, and therefore made the prediction more accurate and enabled its application to other chemicals. Described methods are not capable of prediction of hydrate formation conditions and are used only for estimation of temperature depression at constant pressure.

Ions exhibit a strong dipole-dipole effect on the arrangement of water molecules and reduce the ability to cluster in a manner similar to alcohols and glycols. The effects of electrolytes, including salts (Edmonds et al., 1996) producing different pH-media (Lamorena and Lee, 2009), and methods for calculations are most fully described in Anderson and Prausnitz (1986). Nevertheless, such chemicals are not popular in industry because of their corrosive nature. A comprehensive review of gas hydrate inhibition techniques and prediction models can be found in Sloan (2008).

Surfactants constitute another class of compounds found to affect hydrate formation. Commonly their effect is described as either inhibition of nucleation which occurred as a delay for many hours or days, or anti-agglomeration and prevention of hydrate particle growth and coalescence. Surfactants are known to change interfacial tension between an aqueous phase and the gas phase of a hydrate-former, therefore changing the mass transfer pattern which is vitally important in hydrate kinetics. Polyvinyl chains containing lactam rings were found to cause significant delay of Methane hydrate formation compared to pure water (Lederhos et al., 1995). The initiation period of hydrate seeding can be prolonged to 10 to 16 hours using 0.5 wt% additive according to the data presented in this paper. This type of chemical is also claimed to prevent plugging due to an anti-agglomeration effect. After the hydrate nuclei have

formed, molecules of inhibitor can adsorb on the surface preventing assemblage of larger structures (Zhang et al., 2009; Lo et al., 2009; Aman et al., 2009). The main advantage of kinetic inhibitors over glycols and alcohols currently used in industry is that the concentration of a chemical required for a significant inhibition effect is rarely higher than 0.5-2 wt% (Koh, 2002; Lachance et al., 2009). There are also reports (Arjmandi et al., 2003) on development of environmentally friendly substances effectively preventing hydrate formation in subsea conditions. New novel kinetic inhibitors are being developed using computer modelling (Storr et al., 2004). Investigation of the effect of corrosion inhibitors on hydrate formation is ongoing in the Chemical Engineering Department at Curtin University under supervision of Professor Moses Tade and Professor Rolf Gubner. Nevertheless, surfactants still did not receive wide application for industrial purposes of hydrate inhibition due to the lack in understanding the mechanism of their action (Sloan 2003). Urdahl et al. (1995) showed that the effect of additives in laboratory simulations can be erroneously interpreted, and more realistic situations reflecting industrial conditions should be studied. Following this, new and more accurate methods for the experimental examination of the effect of inhibitors on the kinetics of hydrate formation were developed (Lachance et al., 2009).

Recently (Gnanendran & Amin, 2003; Rovetto et al., 2006) hydrotropes were shown to significantly affect the thermodynamics of hydrate formation; however the authors draw opposite conclusions. These two papers are the only information available in this area, and current research contains further investigation of the impact of surfactants on the thermodynamics of hydrate equilibrium.

Hydrate inhibition is especially crucial during cold start-up experiments due to subcooling. Low temperatures also lead to partial condensation of gas and wax precipitation, however the effect of this phenomenon on hydrate formation has not been widely investigated. Research on integrated wax-hydrate modelling is being conducted at Heriot-Watt Institute of Petroleum Engineering (Tabatabaei 2000). Gao (2008) has shown that wax deposition can promote hydrate nucleation, however taking care of one issue can alleviate another problem.

2.2.1.2. Hydrate Promoters for Gas Separation and Storage

Utilisation of hydrate formation as a means of CO₂ capture is the latest concept in the field of reduction of greenhouse gases emissions. Hydrates were first proposed as a

storage medium for Natural Gas in 1942 (Benesh, 1942). Theoretical capacity for Natural Gas storage is estimated at 1 mole of gas per 5.75 moles of water which constitutes to theoretical value of 180:1 gas to hydrate volume ratio; however, in order to achieve this value, the gas-water system has to be exposed to hydrate formation conditions over substantial period of time which does not contribute to the viability of this technology for industrial exploitation. Certain techniques and chemicals can facilitate thermodynamics and/or kinetics of this process making hydrates a competitive option for CO₂ capture (Sun et al., 2003). In this research only the shift in thermodynamic conditions is addressed.

One method proposed for facilitating gas hydrate formation is described in a patent (Spencer and North, 1996; Spencer, 1997). A hydrate precursor is prepared by dissolving the hydrate former in water under pressure of 10 to 20 bar and temperature between -20° and -10°C. This method utilises the so-called memory effect of water which has already once formed a hydrate and is reused after dissociation. In this case, the water is saturated with hydrate forming gas, and therefore the time required for dissolution is eliminated.

A number of chemicals have been reported to shift hydrate equilibrium conditions to a more favourable region of lower pressures and higher temperatures. Where structural analysis was conducted, it was shown that in the presence of some promoters, CO₂ and Methane form sII or sH crystals instead of the sI framework indicated for these gases (Khokhar et al., 1998). This is because the majority of additives used are able to form sII or structure sH hydrates, where molecules of promoters being large in size, occupy large cavities and molecules of Carbon Dioxide and/or Methane are occluded in small cages. Large hydrate frameworks, especially type sH, are capable of storing greater quantities of gas per unit volume (Khokhar, 1998) and occur at milder PT-conditions (Sloan & Koh, 2008). Common thermodynamic promoters include THF, 1,4-Dioxane (Jager et al., 1999), Propane ((Kumar et al., 2006; Kumar et al., 2008), Hydrogen Sulphide, and many others. The major drawback of using the mentioned technique for promoting hydrate formation is the negative impact on the selectivity of separation and purity of trapped gas.

One of the most powerful reported thermodynamic promoters for CO₂ hydrate formation is Tetrahydrofuran (THF) (Figure 2.4). Equilibrium pressure at 275K in the presence of 1 mol% solution of THF in water is reduced by almost 95% compared to that of pure water. Although THF substantially reduces hydrate

formation pressure, about 1 order of magnitude, the resulting separation capability decreases. For example, a CO₂-enriched stream recovered after hydrate dissociation will contain about 60 mol% Carbon Dioxide if a 17 mol% CO₂ gas mixture formed the hydrate with pure water. If 1 mol% THF is added, released gas will hold only about 35 mol% CO₂. This hindered disagreement in promoter action can delay direct application of hydrate technology to gas separation (Kang & Lee, 2000). The major disadvantage of using THF in an industrial-scale hydrate facility is the toxicity.

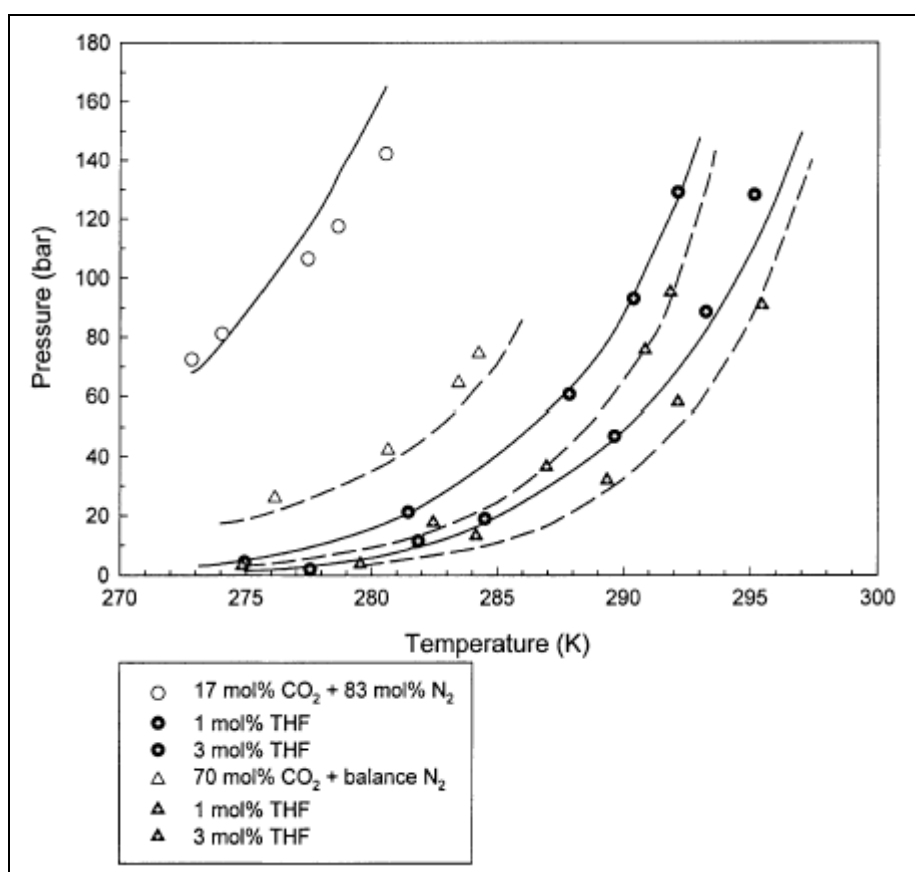


Figure 2. 4 The effect of THF on hydrate formation from CO₂-N₂ gas mixtures (Lee & Kang, 2001)

A CO₂ capture by hydrate from a shifted syngas stream project undertaken by SIMTECHE and Nexant was launched in the USA in 1999 (US DOE 2008&2009; Deppe et al., 2001&2004). In the first stage, an analytical and theoretical study of CO₂ hydrates formation was accomplished and the results were presented at the Third Annual Conference on Carbon Capture and Sequestration. Utilisation of CO₂ hydrate formation was shown to be capable of capturing 68% CO₂ from syngas at a single pass in the presence of Hydrogen Sulphide and pure water. The inventors claimed that the overall capture rate can be increased up to 90% by using

Ammonium salts additives as a promoter; however the current status of the project is unknown.

Since hydrate formation occurs on the water surface, very low concentrations of surfactants can be recommended for reduction of interfacial tension and therefore promotion of mass transfer from the vapour to aqueous phase (Watanabe et al, 2005; Imai et al, 2005). Other authors (Zhong and Rogers, 2000) suggest that the promotion action also occurs due to the self-aggregation mechanism, and the hydrate grows on the subsurface of the micelles. The first effect takes place in shortening the induction time needed for initial seeding of hydrate crystals, and the second mechanism explains improved rates of structure growth. Abundant data on successful utilisation of Sodium Dodecyl Sulphate (Link et al. 2003, Gayet et al. 2005), linear alkyl benzene Sulphonic acid (Kraaslan et al., 2001&2002), para-Toluene Sulphonic acid (p-TSA) (Gnanendran & Amin, 2003) and other anionic surfactants taken in concentrations lower than 1600 ppm (Zhang, 2004) are available. Notably, non-ionic surfactants exhibit significantly less promotion effect on hydrate formation, and cationic surfactants usually act as inhibitors in all range of concentrations except at very low concentrations (Kalogerakis et al, 1993; Pakulski, 2007). All surfactants taken in amounts exceeding critical micelle concentration (CMC) were reported to prolong hydrate nucleation and growth (Karaaslan et al., 2000). Usually the peak of positive influence falls in the range of concentrations about 10 times lower than CMC. Commonly used surfactants are solid and rarely encountered in vapour form due to low volatility; therefore, their use as hydrate promoters for gas transportation is more prudent as they do not contaminate the gas phase.

Although surfactants are found to promote hydrate formation kinetics and increase the hydrate/water ratio, they were not believed to demonstrate any significant influence on the hydrate equilibrium properties (Zhang et al., 2004) until recently. According to the study conducted at WRF in 2004, a very small amount of p-TSA is able to promote the CH₄ hydrate formation increasing the temperature of formation by 5°K (Gnanendran & Amin, 2004) in a sprayed tank. However, Sloan et al. (2006) have shown that p-TSA did not promote the hydrate formation of CH₄ containing gas mixtures in a stirred reactor. This disagreement might be explained by different turbulence patterns during the experiment.

Similar controversy in data published by different research groups can be found on Tetrabutyl Ammonium Bromide (TBAB) (Li et al., 2010). A process resembling the

high-pressure SIMTECHE method for CO₂ separation from an IGCC flue stream by means of catalytic hydrate formation has been studied in the Chinese Academy of Science. TBAB in the range of concentrations from 0.14 to 2.67 mol% is used to decrease equilibrium pressure at the same temperature. A maximum of 92% reduction in equilibrium pressure is achieved in the case of a 0.29 mol fraction of the chemical at 278.75K compared to pure water. The best result shows 54% capture of CO₂ from the feed gas mixture consisting of 60.8 mol% Hydrogen and 39.2 mol% Carbon Dioxide by single stage. In the second stage, hydrate is formed from an 18 mol% CO₂-H₂ gas mixture, and the pressure-temperature conditions can be brought up to 284K at 5MPa by means of using a 1 mol% TBAB solution. No data are reported regarding the final possible CO₂ separation. More concentrated aqueous solutions of TBAB (up to 50%) were also investigated as a gas storage media (Arjmandi et al., 2007) due to TBAB forming semi-clathrate structures in cold water enabling encapsulation of small gas molecules. At the same time, TBAB was reported to strongly inhibit hydrate formation (Kelland, 2006).

p-TSA and TBAB belong to the *hydrotropes*, amphiphilic compounds which have short bulky hydrophobic regions and thus differ from classical surfactants. Because hydrophobic and hydrophilic regions in such molecules are more balanced, micelles formed in the solution are characterised by a loose configuration. This assemblage provides greater access to the hydrophobic regions, consequently, enhancing the solubility of non-polar compounds (Balasubramanian et al., 1989). Although, the formation of micelles at hydrate formation conditions is questionable since the concentration of the additive is remarkably lower than distinctive CMC. Due to their distinctive structure, hydrotropes were suggested to create aggregated clusters and stabilise water lattice at substantially lower concentrations than necessary for critical micellisation (da Silva, 1999). This phenomenon supports the common observation that hydrophobic molecules can be dissolved in larger quantities and with higher selectivity in the presence of hydrotropes rather than surfactants. A positive effect of hydrotropes on PT-characteristics of CO₂ hydrate formation is proven in this thesis.

2.2.2. Cryogenic Separation of CO₂

Cryogenic CO₂ removal technology is not new to the oil and gas industry (Bocquet, 1959). Any hydrocarbons produced must be sweetened from such impurities as Carbon Dioxide, Hydrogen Sulphide, oxides of Nitrogen and others. The original

flue mixture produced from a reservoir, especially in the case of tertiary oil recovery, may contain over 40 mol% CO_2 (Goddin, 1984). The above mentioned acid gases lower the heating capacity of the gas mixture and must therefore be removed from the stream of mainly Methane and other hydrocarbon gases prior to commercial use as a fuel. On the other hand, trapped acid gases are marketable themselves and are required to be of high purity for such implementations as in the food industry, for example. Cryogenic distillation is considered as one of the most successful methods for separation of $\text{CH}_4\text{-CO}_2$ mixtures with content of Carbon Dioxide varying between 5 and 95 mol% (Ozero et al., 1986). However, operating temperatures below -60°C often lead to solid CO_2 formation and consequently plugging of the tower and the flow lines. Eggeman and Chaffin (2003) have claimed that this is a major obstacle in the light hydrocarbon/ CO_2 separation process due to the unreliable prediction of CO_2 freeze out temperatures made by several conventional simulation programs. Operating at pressures higher than 40 to 50 bar will result in higher process temperatures, but this may also result in the formation of inseparable supercritical $\text{CH}_4\text{-CO}_2$ fluid. Therefore the operating conditions are limited within a relatively narrow range between the critical state of the feed mixture and freezing conditions of Carbon Dioxide. Besides, if performed as a single distillation column, this will result in production of a Methane stream containing up to 10 to 15% CO_2 while a sales specification of about 2 to 4% is usually desired for pipeline gas. Helium and Natural Gas liquids recovery processes require less than 1% Carbon Dioxide content; ultra-pure product require less than 100 ppm CO_2 as specified for use in Natural Gas liquefaction plants and Nitrogen rejection process (Heichberger, 1987).

Cryogenic separation of carbon dioxide from natural gas is viable due to considerable difference in critical properties and triple point conditions of the components. Similarly, a flue stream at a power plant comprises gases which can be separated in the same manner. It is therefore beneficial for understanding of this work to look in more detail at the existing options for natural gas sweetening. In addition, this work includes extensive experimental and theoretical study of the effect of varying concentration of CO_2 on solid-liquid-vapor equilibrium of hydrogen-carbon dioxide mixtures.

2.2.2.1. Ryan-Holmes Process

In order to improve the efficiency and effectiveness of separation, Ryan and Holmes proposed the injection of heavier hydrocarbons into the distillation column. These additives are said to shift the CO_2 freezing point, therefore allowing for better separation at lower temperatures and prevention of plugging. The principal scheme for a legacy Ryan-Holmes distillation process is presented in Figure 2.5 (Holmes& Ryan, 1982a,b).

The process is applicable for Methane separation from mixtures containing acid gases such as Carbon Dioxide, for a wide range of compositions. The produced overhead stream is enriched in Methane and substantially free of acid gas components. The bottom products contain mainly CO_2 and other acid gases, higher alkanes and preferably not more than 1 mol% of Methane. Although the tower is operated at pressure-temperature conditions at which solid CO_2 can potentially form, the solids formation is avoided by introduction of 5 to 30 moles of non-polar additives such as $\text{C}_2\text{-C}_5$ hydrocarbons per 100 moles of feed into the column. The additives can be optionally introduced externally and/or as a recycled fraction of the bottom products.

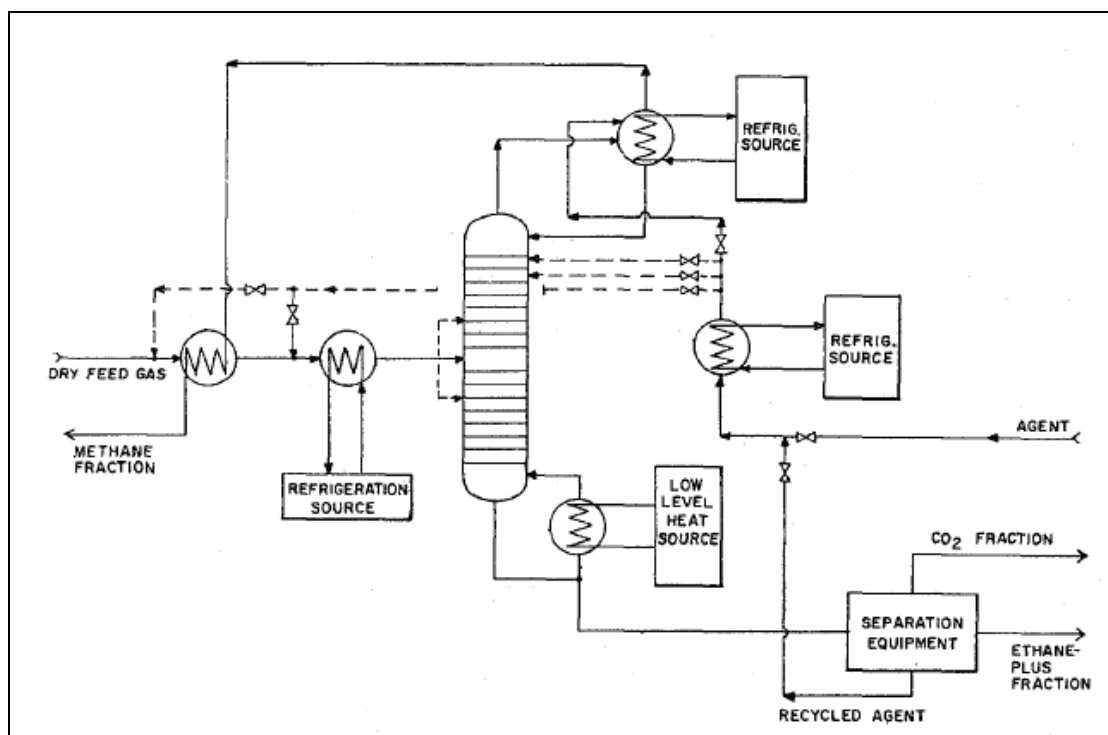


Figure 2. 5 Principal scheme of the Ryan-Holmes process for Natural Gas sweetening (Holmes&Ryan, 1982)

Additives are also said to raise the critical conditions of $\text{CH}_4\text{-CO}_2$ mixtures allowing therefore operation at higher pressures which in turn improves the effectiveness and economics of separation especially from high CO_2 containing sources. Natural Gas liquids, if present in the feed, can also be separated in the same distillation tower from Methane providing a marketable by-product. The high-pressure liquid CO_2 stream produced by this technique can be removed from the system and collected for injection into deep sea or for enhanced recovery from a depleted reservoir. By recycling this low temperature stream it can be employed in refrigeration systems eliminating the need for any external chilling units and therefore reducing energy requirements and capital cost.

There are a number of difficulties associated with the separation of the Ethane- CO_2 and Propane- CO_2 azeotropic mixtures. However, additives could be used to resolve this problem. Ancillary CO_2 purification requirements have motivated further research in this field. Numerous improvements (O'Brien et al., 1983 & 1987) have been made to this process recently including recycling of heavier hydrocarbon fractions (Goddin & McGalliard, 1984; Goddin, 1983), distribution of distillation and CO_2 concentration zones (Durr et al., 1994), multistage distillation (Sapper, 1987; Sapper & Kick, 1987), thermal coupling, and the introduction of other substances for shifting the CO_2 freezing point (Eakman & Marshall, 1979; Valencia & Denton, 1985, Gottier, 1988).

Modified Ryan-Holmes processes are successfully implemented in industrial processing of Natural Gas for Methane-Carbon Dioxide separation due to the significant difference in volatilities of components; however, it is not suitable for non-hydrocarbon sources such as IGCC and Oxyfuel process gases. The main reason is that all of the above mentioned processes involve the use of additives, mainly hydrocarbons, in order to improve separation, and therefore the recovered CO_2 must be separated from them in the subsequent stages.

2.2.2.2. Controlled Freezing Zone by Exxon

Another low temperature process for separation of CO_2 is the Controlled Freezing Zone (CFZ) technology by Exxon (Valencia & Denton, 1985). In this process the CO_2 freezing is not avoided, but permitted in a controlled manner. Therefore the method consists of two separate parts. In the first stage CO_2 is condensed in a manner similar to the one described above. Up to 15% of CO_2 may still remain in the

gas phase, mixed with hydrocarbons in the product gas stream from this stage. In the second stage, the overhead gas stream from the distillation tower is directed into the freezing zone, engineered in such a way as to prevent the introduction of solids in the distillation zone. There, the gaseous mixture is brought in contact with at least one cold liquid sprayed through nozzles placed in the upper part in order to solidify CO₂ in a form resembling snow. The liquid sprayed into the freezing zone is conventionally a C₁-rich stream containing 3-8 mol% of CO₂ (Haut et al., 1989) and is in counter current to the distillation zone product stream. A second spraying liquid could be liquefied Nitrogen as when the CFZ method is applied for the Nitrogen rejection unit as described by Potts and Thomas (1992), or any other highly volatile component. A second distillation zone may be added for further purification of the overhead stream from the freezing zone. A typical arrangement for this process is shown in Figure 2.6.

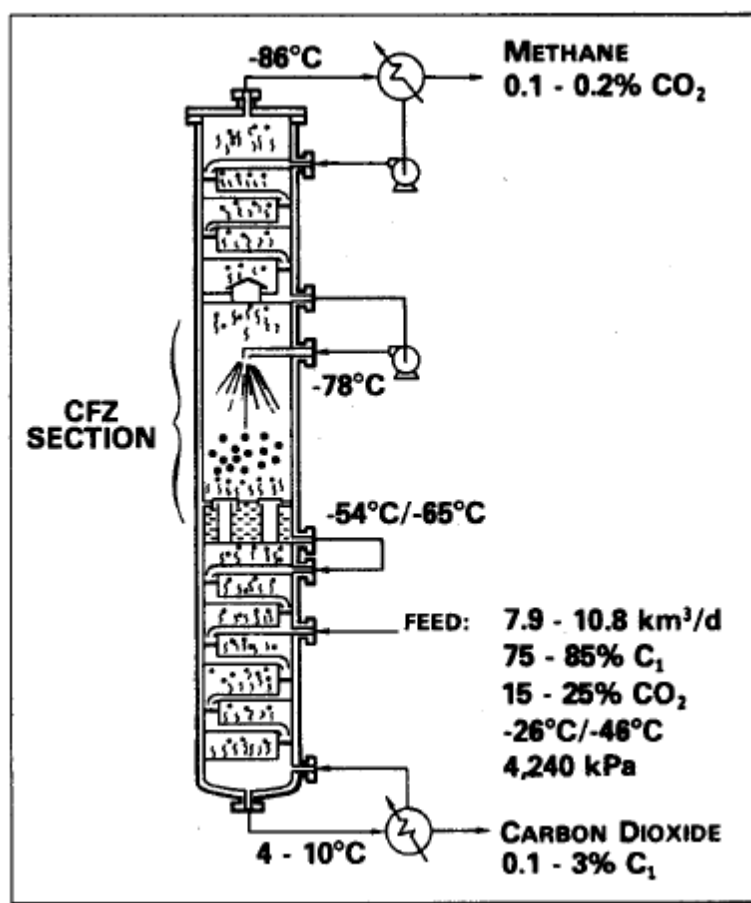


Figure 2. 6 Tower arrangement for CFZ process (Valencia & Denton, 1985)

During start-up it is essential to prevent freezing outside the freezing zone, and therefore substantially pure Methane stream must be used while the tower is chilled to the low operating temperatures. Another way avoid CO₂ solidification at this stage

is to inject small quantities of heavier hydrocarbons such as Propane or Butane or Methanol. This leads to the use of other techniques for CO₂ removal before the column reaches the required conditions. One of the methods is described in (Haut et al., 1991) and utilises pressure-temperature swing adsorption on Linde molecular sieves. The Methane-rich stream can then be condensed and used as a spraying liquid in the freezing zone of the tower. During continuous operation, the adsorption stripping section can be utilised for additional purification of the overhead product stream; however introduction of this supplementary unit will inevitably increase the capital cost.

The CFZ technique can produce an overhead product enriched in Methane and containing 700 ppm to 2 mol% CO₂ and bottoms composition ranging from 0.5 to 1 mol% Methane in CO₂ from a feed composition of 15 to 65 mol% CO₂ (Haut et al., 1989). This method of CH₄-CO₂ separation is usually associated with liquefied Natural Gas production (Cole et al., 1999) and utilises so-called Cold Energy of LNG (Takeuchi, 2000) produced at -160°C. Despite the possibility to obtain high purity products, this method is not suitable for non-hydrocarbon sources such as IGCC and Oxyfuel gases.

The ExxonMobil Controlled Freeze Zone (CFZ) technology was originally tested at the Clear Lake CFZ Demonstration Plant during the 1980's. ExxonMobil is now proceeding with a commercial demonstration plant in conjunction with a gas treatment plant near the LaBarge gas field in Wyoming. The CFZ technology has been successfully tested at a 14 mmscfd facility (Valencia et al., 2008; Northrop & Valencia, 2009).

2.2.2.3. CryoCell® Technology

One of the latest improvements to Natural Gas sweetening technologies was made by Amin et al. in 2005. The technology known as CryoCell® has been patented (Amin, 2006; Hart & Amin, 2007; Amin & Kennaïrd, 2008). Cold liquid hydrocarbons C₂-C₄ are utilised for CO₂ absorption in conjunction with the Joule-Thomson expansion effect in order to cool the feed gas down to temperatures where CO₂ freezes out and precipitates at the bottom of the vessel. CO₂ is then heated and can be pumped to appropriate pressure and sequestered. The process is highly scalable and applicable to a wide range of tasks, easily operatable and inexpensive. Due to the absence of chemicals involved in gas treatment, no corrosion issues are involved. This

technology has been tested for a number of years at the 2 mmscfd CoolEnergy demonstration site in Dongara, Western Australia launched in 2006, and the block diagram of the process is shown in Figure 2.7.

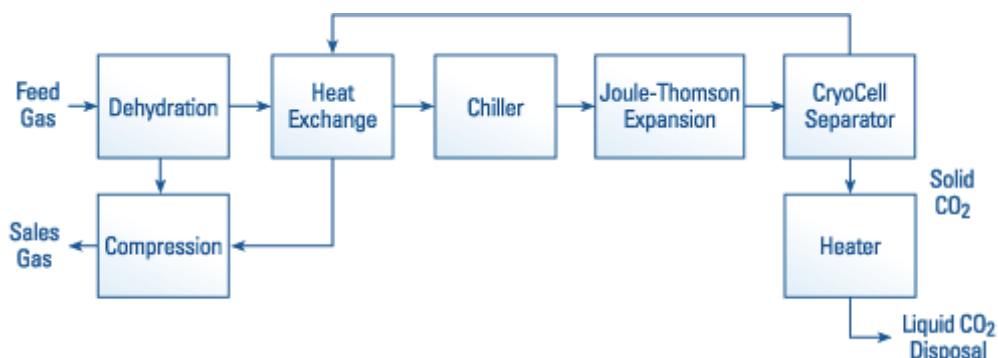


Figure 2.7 Block diagram of CoolEnergy's technology (Cool Energy corporate website)

The CryoCell step reduces CO₂ concentration down to less than 3 mol%, and the CryoZorbTM utilises absorption by cold Methanol to further reduce CO₂ to ppm level. Further information about this technology can be found in (Amin et al., 2005). The principal experience gained during the development of the CryoCell technology at Woodside Research Foundation was favourably utilised in this work.

A case study to assess the competitiveness of the cryogenic methodology for CO₂ separation is given in Chapter 9.

2.2.2.4. Other Competitors and Testing Programs

With the exception of the above mentioned processes, the commercial rollout of cryogenic technologies for CO₂ removal from hydrocarbons appears to be quite limited, with no more than a handful of licenses having been sold by each vendor. Four other technologies have been identified that have been commercialised or are being commercialised. These are:

- IFP/Total's Spretx CO₂ process.
- BCCK Engineering's (Cimarex) process.
- Acrion Technologies' CO₂ Wash process.
- A process developed by Prometheus Energy.

A joint venture comprising IFP, Total and Prosernat has developed a CO₂ removal technology called Spretx CO₂. Spretx CO₂ is an enhancement of a relatively new H₂S removal technology called Spretx, also developed by Total/IFP/Prosernat. Spretx is an acronym for "Special PRe-EXtraction". The Spretx process is designed to bulk pre-

extract H_2S from very sour gas and is used upstream of a conventional amine based sweetening process. The Spretex technology was tested at an industrial pilot unit operated at Total's Lacq field in south-west France from early 2005 to mid-2006 (Huydghé et al., 2008). Current status of the testing program for Spretex CO_2 is not disclosed. The Spretex process is a technology based on a patent filed by IFP in 1994, and subsequent patents filed by IFP and Total refer to (Minkkinen et al., 1996 & 1998).

BCEK Engineering Inc. is an “international Natural Gas engineering company” (BCEK Engineering Inc., corporate website). The company has numerous technology offerings in the area of gas removal and separation. Patented Nitex NRU (Nitrogen Rejection Unit) technology has found a new application for removing CO_2 from Natural Gas streams utilising cold Methanol to a level between 1 and 5 ppm, suitable for use in LNG. This technology will be implemented in a 200 mmscf/d grassroots gas processing facility under development as part of the Cimarex Helium-Methane Recovery project at Big Piney in Wyoming (Streater, 2010). The unit is expected to be online in late 2011 (Ballou, 2009).

Acrion owns a proprietary technology called CO_2 Wash which is used to clean landfill gas. According to the company, Acrion's CO_2 Wash process “converts landfill Methane to medium Btu gas, electricity, pipeline gas, LNG or Methanol, and enables recovery of CO_2 in liquid form.” (Acrion Technologies, Inc. corporate website). The technology is commercialised and implemented at a landfill gas processing facility built by Acrion's partner FirmGreen, Inc. in Ohio.

Prometheus Energy is a private company based in Seattle, Washington. The company specialises in small-scale LNG production using Methane recovered from waste sources such as landfill projects and coal bed Methane. The company owns a patented CO_2 removal technology based on cryogenic freezing (Barclay et al., 2000 Natural Gas). Four operational projects utilising the company's cryogenic CO_2 removal technology: the Bowerman landfill project in Irvine and a site in Fresno County, California; the Lisbon, Utah landfill project; and a facility at the Krupinski Coal Mine in Poland.

The extent to which these technologies are, or will be, competitive is a function of; 1) technical nuances of the process; 2) the marketing, financial and people resources of the vendor and 3) the strategy adopted by the vendor regarding third party use of its technology.

Membrane, solvent and hybrid membrane/solvent CO₂ removal technologies represent the most competitive environment for any newly developing technology, particularly in low CO₂ environments where they are more cost effective.

Application of low temperatures to the power plant's flue gases is a very new concept and is not yet widely known. Cryogenic condensation has been proposed at Brigham Young University by Dr. Larry Baxter (Cryogenic CC Technology, 2009) for post-combustion CO₂ capture from power plants. Relatively low CO₂ content in the feed (less than 15 mol%) and pressures slightly above atmospheric dictate the use of temperatures in the order of -120° to -135°C. At these temperatures, CO₂ forms a solid and, therefore, does not contain any substantial amount of impurities. Capture rates as high as 90 to 99 mol% CO₂ are claimed to be achievable using this technology. Very low pressure of the flue gas will require substantial energy supply for compression.

A more detailed overview of the current marketplace is given in Chapter 9 where a case study for the Cool Energy Cryogenic CO₂ Removal Project Developer Model is taken as an example.

2.3. Modern Options for CO₂ Abatement

New options for fuel treatment with lower emissions have been proposed in the last few decades. In this work, flue gases obtained from two technologies are addressed, namely, IGCC gases and Oxyfuel streams. Syngas containing mainly CO₂ and Hydrogen is produced by the first method. Hydrogen purified from CO₂ can be used in fuel cells and as high quality low emissions fuel. A second option produces a rich in CO₂ gas stream which can be pumped to storage pressure with minimal further treatment, however, the amount of impurities in the stream (up to 10%) excludes it from utilisation in EOR process.

2.3.1. IGCC Power Plants for CO₂ Capture

Integrated Gasification Combined Cycle (IGCC) is a modern technique for energy production, which is claimed to be the most environmentally friendly fossil fuel fired power generation technology. The most important features of an IGCC based power plant is a low or zero level of green house gases emissions and pure Hydrogen stream production. Schematic of such a plant is shown on Figure 2.8.

Integrated Gasification / Combined Cycle Power Plant

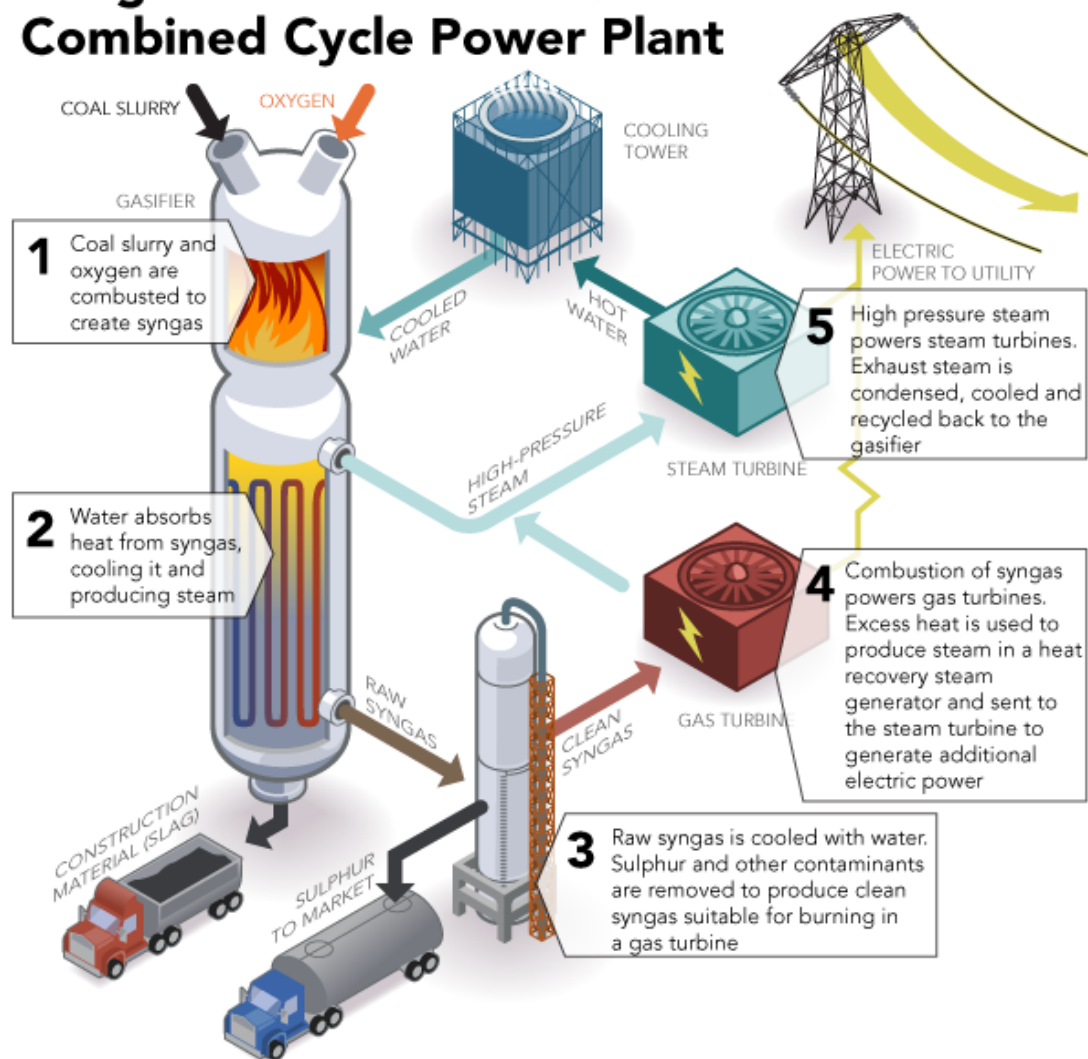


Figure 2. 8 Schematic of IGCC process (source <http://www.bantrel.com>)

IGCC is the process of converting low value fuels such as coal, petroleum coke, orimulsion, biomass, and municipal wastes into a high value, low Btu, environmentally friendly Natural Gas-type fuel, also called “synthesis gas” or simply “syngas”, through partial oxidation.

Coal gasification has been used in the US since it was first mentioned by the Baltimore Gas Company in 1842 to produce gas for domestic consumption and streetlights; however the concept of combining the gasifier with a gas turbine appeared to be viable only recently (US DOE, retrieved 5 March 2010). Practical feasibility of IGCC was demonstrated in 1984 when Cool Water, the first pilot IGCC facility, was launched in California (GE Energy, retrieved 18 May 2010).

After the coal is fed into a high-temperature pressurized container and burnt in a steam, it is then passed through a shift-converter producing synthesis gas or syngas which mainly consists of Carbon Dioxide and Hydrogen. In order to remove undesirable components, such as Carbon Dioxide and Sulphur, syngas is cooled. The processed gas can be used as a fuel or further processed and concentrated into a chemical or liquid fuel.

The IGCC system comprises a coal gasification unit connected to a power generation unit which in turn combines gas and steam fired turbines, and known as a combined cycle. In the first stage followed by shift-conversion, the solid coal is gasified as mentioned above in a stream containing a controlled amount of Oxygen. In the second stage, the cleaned gas stream is fed to the conventional gas turbine and burnt there to produce electrical energy. Hot exhaust gas from this stage is utilized for boiling water, creating the feed for a steam turbine for additional power generation. Typically, about 65% of the energy is produced by the gas turbine and 35% by the steam turbine.

Detailed comparison of applicability of different types of gasifiers to IGCC process can be found in (Cormos et al., 2007; Starr et al., 2006). The stream produced by an *entrained flow gasifier* contains mainly Hydrogen and carbon Monoxide and Dioxide with not more than 5 mol% (Guo et al, 2007) of Sulphur and Nitrogen containing compounds. After purification and shift-conversion, the flue gas is essentially represented by about 60 mol% Hydrogen and 40 mol% CO₂. This stream is utilized in Combined Cycle Gas Turbine (CCGT) described in (Brdar & Jones, retrieved 13 January 2010; Jones & Shilling, retrieved 21 October 2009). The most important feature of the produced gas stream is that it occurs at high pressure and contains a high level of CO₂ in mainly Hydrogen providing an excellent opportunity for Carbon Dioxide capture. CO₂ reduction in this case is more favorable than from a conventional steam plant, reaching 90 to 95 mol% capture rates.

There are basically two established gasification processes and these are the GE (former Texaco) & Shell processes. The pressures used are in the range of 30 bar for the Shell process to 60 bar for the GE process. Slurry feed gasifier and subsequent water quench is used in GE IGCC plants. Shell technology is represented by dry feed gasifier combined with a heat recovery boiler. An increase in pressure for the Shell gasifier has no significant influence on total energy output of the plant; however it reduces the electrical efficiency and provides a higher level of CO₂ emissions

(Davison et al., 2004). The same situation can be observed if GE technology is implemented at pressures about 40 bar.

In the Shell cases, dried ground coal is fed to the gasifier (Zheng & Furinsky, 2005). High heat recovery is achieved due to generation of high pressure steam in a heat recovery boiler used for cooling the gasified stream. A hydrolysis technique is used for purification from COS, and acid gases including CO₂ and H₂S are usually removed with a physical or chemical absorbent. In order to improve decarbonisation, raw quenched gas can be first introduced into the shift-converter. A large amount of steam is required in this stage. Because the steam has to be taken from the cycle, CO₂ capture (CCS) in the Shell case implies a high energy penalty.

In the case of the GE IGCC plant, slurry of milled coal in water is fed into the gasifier and burnt in a flow of Oxygen. Excess water and minor impurities are removed from the saturated produced gas when it is cooled with 15°C water. COS and acid gases are separated from flue gas in a similar manner as in the Shell case. Due to high initial water content, additional heat is required for its evaporation in the gasification stage resulting in lower coal to fuel conversion efficiency. Extra oxidation also requires higher amounts of Oxygen increasing auxiliary power consumption. Use of water for chilling of the raw processed gas displays relatively low heat recovery rates. However, high levels of steam in the fuel gas improve the overall performance of the shift-converter and therefore significantly decrease the energy penalty for CO₂ capture. In both cases, flue gas is subsequently expanded and fed into the gas turbine.

Comparison of total cost for Shell and GE configurations with and without CCS is shown in Figure 2.9 (Klara & Wimer, 2007). Results indicate that Shell station requires higher investment than GE regardless of combination with a supplementary CO₂ capture unit. Installation of equipment for Carbon Dioxide capture causes a 32 to 35% rise in total cost.

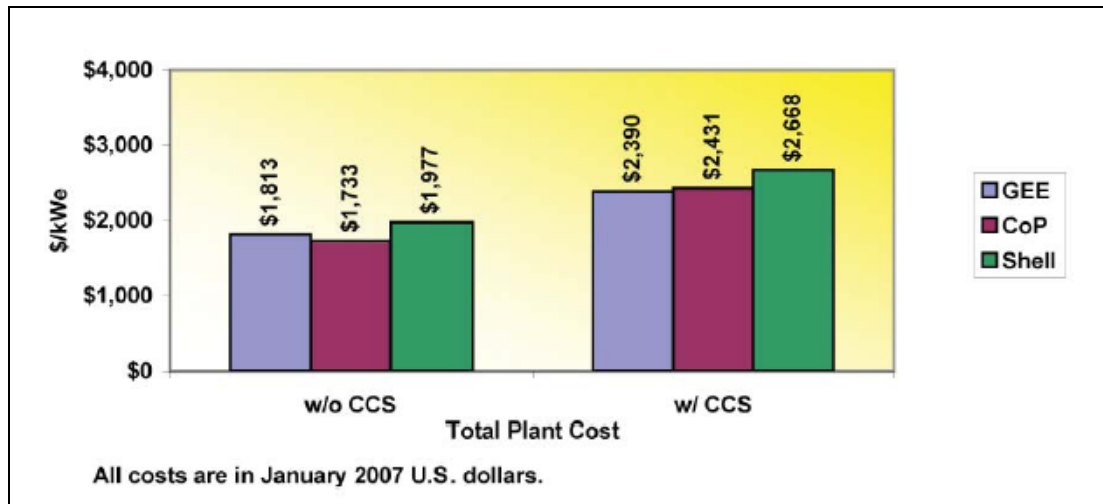


Figure 2. 9 Comparison of Total Plant Cost for the IGCC cases with and without CO₂ capture (Klara & Wimer, 2007)

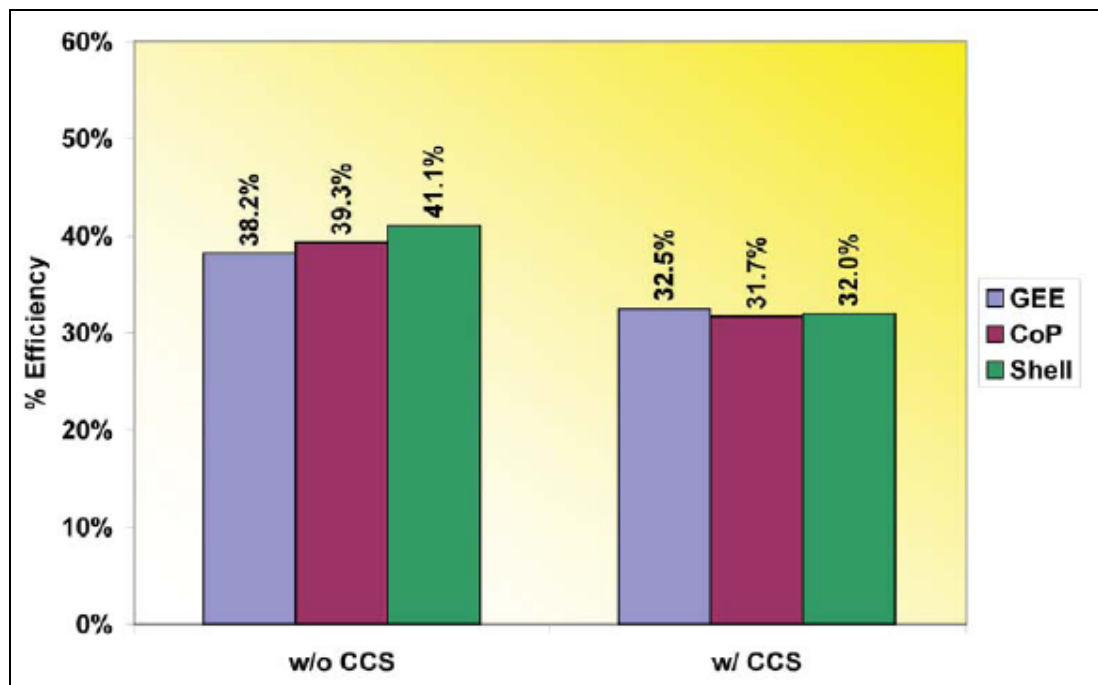


Figure 2. 10 Comparison of Net Plant Efficiency for the IGCC cases with and without CO₂ capture (Klara & Wimer, 2007)

The CCS cases require a significant amount of auxiliary power and extraction steam for the process, which reduces the energy output as shown in Figure 2.10 (Klara & Wimer, 2007). The GE configuration in terms of Net Plant Efficiency is more viable than Shell providing the least loss in efficiency compared to the arrangement without carbon capture.

Each process has its own advantages and merits and the CO₂ capture scheme from the syngas gasification process plays a major role in the evaluation and comparison of these processes (Linga et al., 2007).

The main aspect in this work will be made on the assessment of the feasibility of CO₂ capture by the cryogenic and hydrate method. This technique is proposed to be efficient for many cases especially when CO₂ concentration in the flue gases is high. The IGCC process represents an ideal case for CO₂ capture by the cryogenic and hydrate method as both processes provide the gas at high pressures.

2.3.2. Oxyfuel Technology for CO₂ Capture

Another promising way for clean gasification of coal is the so-called CO₂-O₂ recycle, or Oxyfuel technology (Gross, 2002a & 2002b) presented in Figure 2.11.

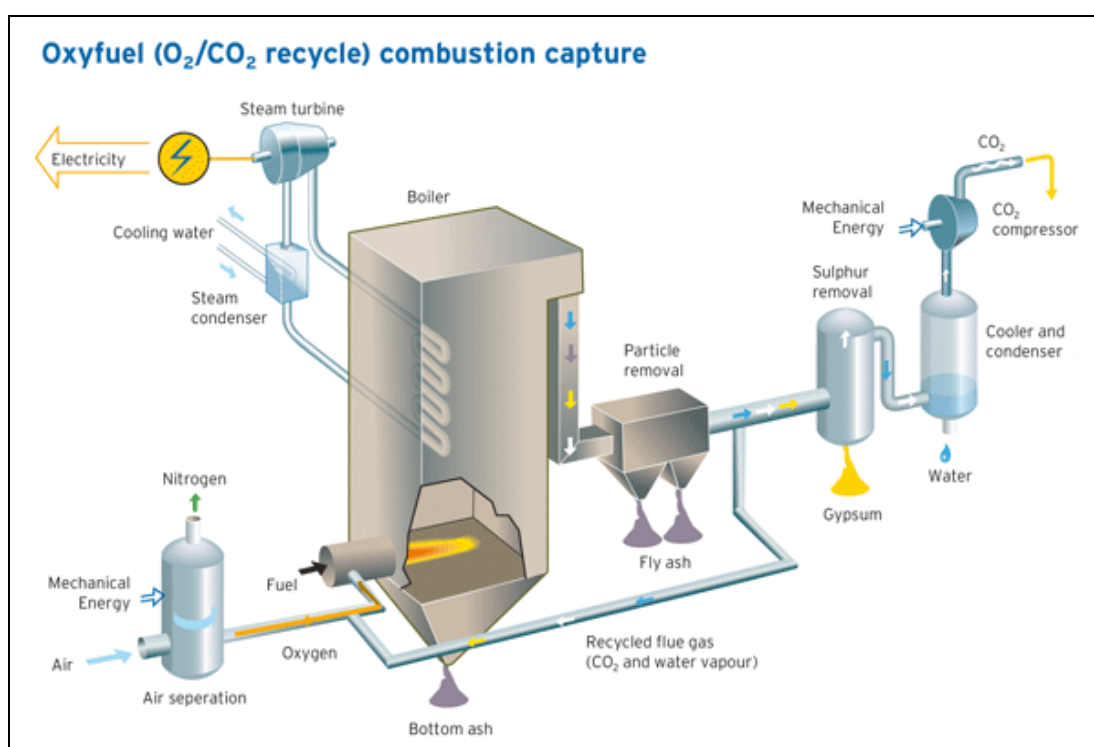


Figure 2. 11 Oxyfuel combustion by Vattenfall (Vattenfall corporate website)

This technology implies fossil fuel gasification in a stream of more than 95 mol% pure Oxygen supplied by an external air separation unit rather than air, resulting in production of flue gas rich in Carbon Dioxide and potentially eliminating Nitrogen oxides emissions. High temperatures in the boiler are utilised to create high pressure steam powering a steam turbine, similar to the IGCC case. A large part (about 70 to 80%) of the flue gas containing mainly CO₂ and steam is recycled into the boiler in order to maintain the combustion temperature and also volumetrically compensate for the absence of Nitrogen.

One substantial distinction from IGCC power plants lies within the choice of the fuel which is limited to bituminous coal, lignite and to a small extent heavy oil. Some sources (Thompson, 2005) suggest, however, that the fuel flexibility can be brought to the same levels as for IGCC cases via variation of the recycle rate.

In Canada in 1994 (Croiset & Thambimuthu, 1998), CANMET Energy Technology Centre launched a pilot testing facility capable of burning coal and/or Natural Gas in a flow of Oxygen or air (Tan et al., 2005). The main research at this facility is aimed at the development of oxy-firing technology for CO₂ abatement from power plants.

In a study conducted by Jupiter Oxygen Corporation in conjunction with US DOE and CoalTech (Ochs et al., 2004, Chui et al., 2003), about 28 vol% concentration of Oxygen in the combustion gas was shown to be optimal for increased thermal efficiency and total power output compared to air-fired boilers. Both characteristics gradually increase with higher Oxygen feed rates till its content in Oxygen supported recycled stream reaches 28 vol%. Beyond this point, efficiency and capacity drop rapidly and constitute about 2/3 of the values in the case of air-combustion when Oxygen concentration hits 35 vol%. Optimal heat transfer and steam generation rates are also achieved at recycle rates providing 28 vol% Oxygen flue gas. Exhaust from the boiler undergoes 5 stages of cryogenic condensation for pollutant gas removal. In the first two stages essentially all water is removed, and in the subsequent stages CO₂ content is gradually reduced. The final stream contains as little as 8.5 vol% CO₂, 57.6 vol% Oxygen and 33.9 vol% Nitrogen. Concentrations of CO₂ in the separated stream constitute 92 to 98 vol% depending upon the type of coal. This rich in CO₂ stream in many cases can be sequestered without any further treatment, although this purity is not enough for use in enhanced oil recovery.

One considerable disadvantage mentioned for Oxyfuel technology is that recycling and high Oxygen content promote SO₂ to SO₃ conversion, which can seriously damage the equipment due to strong corrosive properties. Other challenges with deployment of CO₂-O₂ recycling for CO₂ emissions reduction purposes include flame instability and uneven heat transfer (Buhre et al., 2005). Construction challenges include thorough sealing to prevent any leakage of air into the flue gas and, therefore, an unacceptable rise in Oxygen and Nitrogen concentrations. Flanges and joints along the flue gas ducts are especially vulnerable to leakage occurrence with plant ageing.

Results of studies conducted (van Hassel et al., 2005) have shown the potential for retrofitting Oxyfuel technology to conventional pulverised coal-fired power generating stations with reduced risk and cost involved compared to IGCC technologies. CO₂ capture cost in Oxyfuel plants is comparable with other existing CO₂ abatement technologies. Conceptually, emissions of SO_x and NO_x can be also eliminated with deployment of this technology (Kim et al., 2007; Liu & Okazaki, 2003; Croiset & Thambimuthu, 2001), and consequently the costs linked to scrubbing equipment can be reduced.

Existing operating pilot-plant Oxyfuel power generating units include a testing facility inaugurated by CANMET in Canada in 1994 (Croiset & Thambimuthu, 1998). Development of Oxy-firing technology for retrofitting at existing pulverised-fuel boilers is underway by Hitachi, Japan, for a 820 MW facility (Wu et al., nd). Results of the numerical study conducted to date were confirmed on four state-of-the-art coal-fired pilot units located in Germany, UK, and Japan. A 30 MW Oxyfuel pilot plant was launched at Schwarze Pumpe in Germany (Vattenfall corporate website) in 2008. This unit is constructed near the existing 1600 MW lignite-fired station. A 30 MW facility is under construction at the Callide Project in Australia with inauguration planned in mid-2011 (Callide Oxyfuel Project Schedule). Jupiter Oxygen Corporation is currently testing their 15 MW facility in Indiana (Ochs et al., 2009) fired with pure Oxygen instead of an Oxygen-enriched recycled gas stream.

Overall, Oxygen-firing fossil fuels combustion is a potentially feasible technology for multi-pollutant emissions reduction, and it is applicable for retrofit at existing pulverised-coal fired stations (Buhre et al., 2005). However, this technology reduces overall power plant performance in terms of fuel-to-electricity conversion by 9% (Cottrell et al., 2003).

Oxyfuel technology is still not widely accepted and not yet commercialised.

2.4. Summary of the Existing Options for CO₂ Capture from non-hydrocarbon sources

There is no vital commercialised process for separation of CO₂ from non-hydrocarbon gases based on cryogenic condensation. This problem however, attracts interest if condensation is considered as a method for trapping CO₂ from the process gases from power plants such as IGCC and Oxyfuel. The gas stream in this process consists mainly of CO₂ and Hydrogen with small quantities of Argon and Nitrogen in

case of IGCC gases. In the Oxyfuel case, the process stream contains 90% CO₂ with minor amounts of Oxygen, Nitrogen and Argon. Due to the considerable difference in critical properties and triple point conditions of the gases composing the mixture, cryogenic separation appears an effective way for CO₂ pre-combustion capture from IGCC/Oxyfuel flue streams. Elevated pressures of the process gas stream provide some initial advantage to the cryogenic separation of CO₂; however, elevated temperatures are not beneficial for the process economics and energy consumption. In case of IGCC this technique can yield pure liquefied CO₂ which can be reused as a refrigerant or in the beverage industry and purified Hydrogen, which is claimed as an alternative energy source.

2.5. Phase Behaviour of CH₄-CO₂ and H₂-CO₂ Mixtures

Despite a considerable number of investigations of the phase equilibrium conditions of pure components, in the case of the gas mixtures this knowledge appears to be insufficient for the phase envelope prediction. Since cryogenic distillation appears to be one of the most known methods for CO₂ separation from light hydrocarbon gases, a substantial number of studies devoted to the description and prediction of phase envelopes for such mixtures have been conducted throughout the last three decades. The main reason for the continuous experimental work in this direction is that the conventional models used for theoretical prediction of dew/bubble/freezing points and compositions of equilibrium phases of the gas mixtures produce inconsistent results, especially in the vicinity of the critical point. Because the first part of the current research is dealing with CO₂ separation from Natural Gas, IGCC and Oxyfuel gas mixtures using cryogenic technique, a brief review of the available experimental results on phase envelope investigation is presented below.

Two types of gas mixtures addressed in this work (methane-CO₂ and hydrogen-CO₂, representing natural gas and syngas mixtures accordingly) show significantly different topologies of the phase envelope. According to the study conducted by van Konynenburg and Scott in 1980, binary systems exhibit different behaviours in relation to the strength of intermolecular interaction and relative location of the critical points. In the case of strong attractive interactions, for example CO₂-Methanol, mixing of the two components is characterized as exothermal at low temperatures allowing for complete mixing, and therefore the critical locus of the mixture simply connects the critical conditions of the end-members. On the other

hand, when attractive forces are not very strong, mixing appears as an endothermic process. If the differences in critical properties of the end-members is not very large, for example a Methane (-82.4°C and 46 bar)-Carbon Dioxide (31°C and 73.8 bar) system, the critical locus is the same as in the previous case. However, within the boundaries of vapour-liquid coexistence, liquid-liquid immiscibility can occur. This phenomenon has been observed by several investigators (Berdnikov, 1987, Van den Kerkhof et al., 1994). Critical properties of Hydrogen (-240°C and 55 bar) and Carbon Dioxide (31°C and 73.8 bar) are greatly different leading to the absence of a continuous liquid-gas critical curve (Figure 2.12) for $\text{H}_2\text{-CO}_2$ mixture. Intricate behaviour of Hydrogen- CO_2 mixtures during cooling was confirmed by a few researches as described below, and should be monitored during the experimental work performed here.

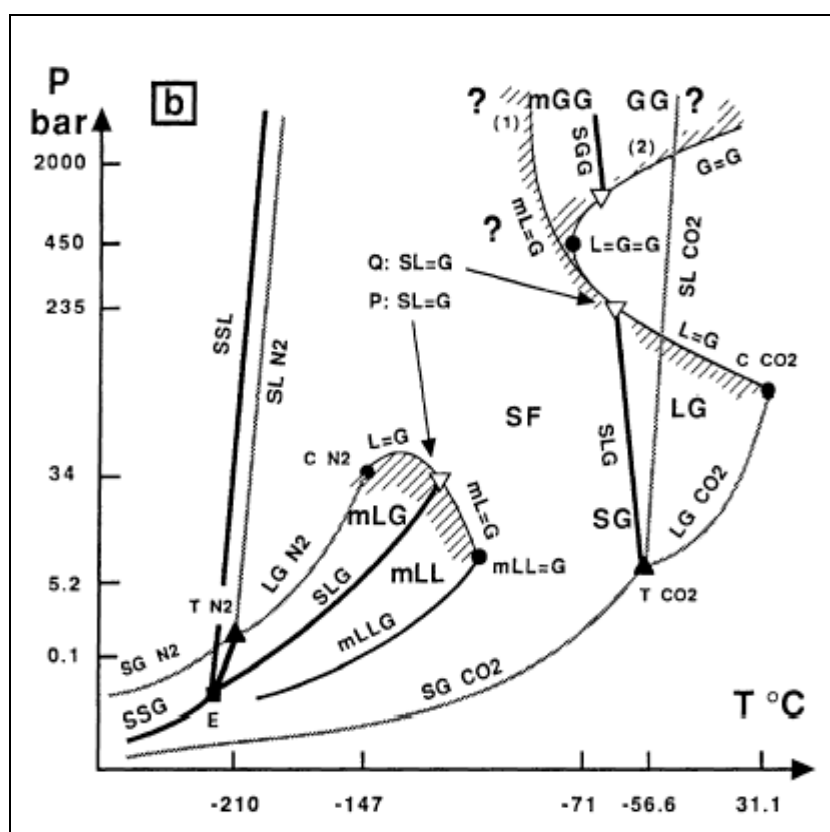


Figure 2. 12 Topology of the binary system $\text{CO}_2\text{-N}_2$ in PT diagram (Thiery et al., 1994)

2.5.1. Methane-Carbon Dioxide system

Phase diagrams of a 29.5 mol% Methane-Carbon Dioxide mixture in the range of temperatures between -100°C and 30°C at 46.4 and 34.5 bar were experimentally built by Donnelly and Katz in 1954. The three phase locus composed of these results

is included in the PT diagram in Figure 2.13 in comparison with the data from (Davis et al., 1962). Two critical loci for liquid-vapour and liquid-solid coexistence are presented in this diagram as was theoretically estimated by Konynenburg and Scott (1980). At fixed temperatures below the pure CO₂ triple point, the data by Davis et al. (1962) are about 3 bar above those presented in the Donnelly and Katz (1958) data set.

Fairly good agreement between the two data sets is observed except near the highest pressure for Solid-Vapour-Liquid equilibrium. The reason lies within the measurement techniques used by the two research groups as explained below.

Results of Donnelly and Katz (1958) were used by Ryan-Holmes, Valencia and other inventors to design the process units used for CO₂-hydrocarbon separation (see Chapters 2.2.2.1, 2.2.2.2 and 2.3.2). Based on these diagrams, higher pressure is more advantageous for distillation of such mixtures due to the wider Vapour-Liquid equilibrium temperature range and relatively narrow Vapour-Solid coexistence range. The operating conditions for distillation of a mixture containing mainly Methane and CO₂ can be confined in the region between -62° and -9°C at 46.4 bar. The best separation can be expected between -62° and -51°C. The Controlled Freezing Zone technique used for separation of Methane and Carbon Dioxide and described in the previous section can be also adjusted to about 44.8 bar and -62° to -51°C in the distillation zone and normally operates at temperatures below -81°C inside the freezing zone, allowing for CO₂ freeze out. Thus, separation of Methane-Carbon Dioxide mixture occurs at temperatures above the pure Methane critical temperature and below the CO₂ triple point, and therefore inside the region where gaseous and/or liquid Methane and liquid or solid CO₂ are present. Even a small content of Methane in CO₂ flue gas leads to significant changes in the freezing point defined for pure CO₂ at -56.6°C for a wide range of pressures above 5.2 bar. At temperatures below -70.5°C no solid forms from mixtures containing less than 7 mol% CO₂. Because the gas composition changes significantly during separation and the process conditions can vary depending upon the feed composition, interest in further study of Methane-Carbon Dioxide mixtures has arisen.

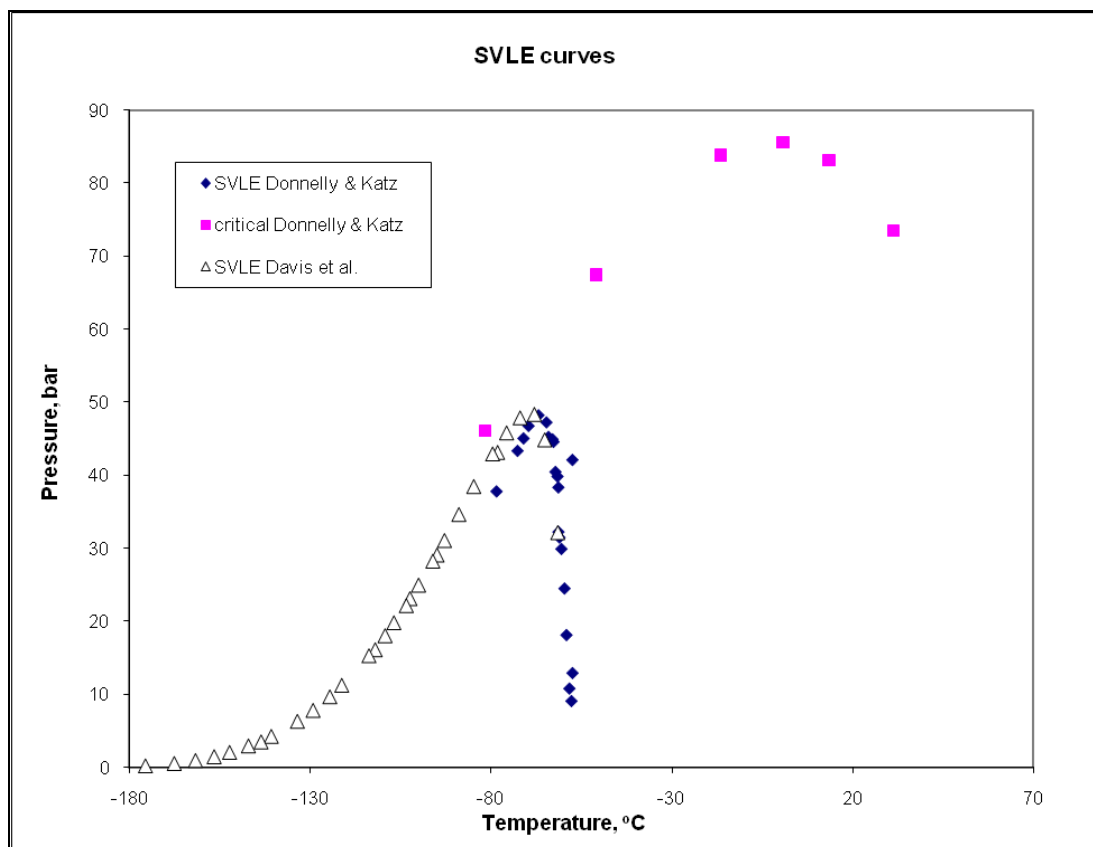


Figure 2. 13 Comparison of experimental phase diagrams obtained by Donnelly and Katz (1954) and Davis et al. (1962)

One of the most extensive experimental studies on phase transitions in $\text{CH}_4\text{-CO}_2$ systems with up to 24 mol% CO_2 in the range of temperatures between -120° and -53°C at pressures below 70 bar was conducted by Hwang et al. in 1976. The results of this research in comparison with other results are presented in Figure 2.14. It can be seen that the curves from previous works, including the data obtained by Donnelly and Katz (1958), are in good agreement with the referred investigation. Nevertheless, at temperatures below -50°C noticeable qualitative and quantitative discrepancies between isotherms obtained by Donnelly and Katz (1958) and others can be observed. This can be explained in terms of the technique used for the dew and frost point determination. Donnelly and Katz (1958) measured these points by extrapolation of the three phase locus while in the referred study Hwang et al. directly observed actual condensation conditions (see also below). The confining conditions of about 41.4 bar at -60°C for CO_2 solidification and critical pressure of the mixtures ranging between 55.16 and 65.5 bar depending upon the composition remain the same. The dew point isotherms for a Methane-Carbon Dioxide system at

temperatures below the critical temperature of Methane are linear, as shown by Hwang et al. (1976).

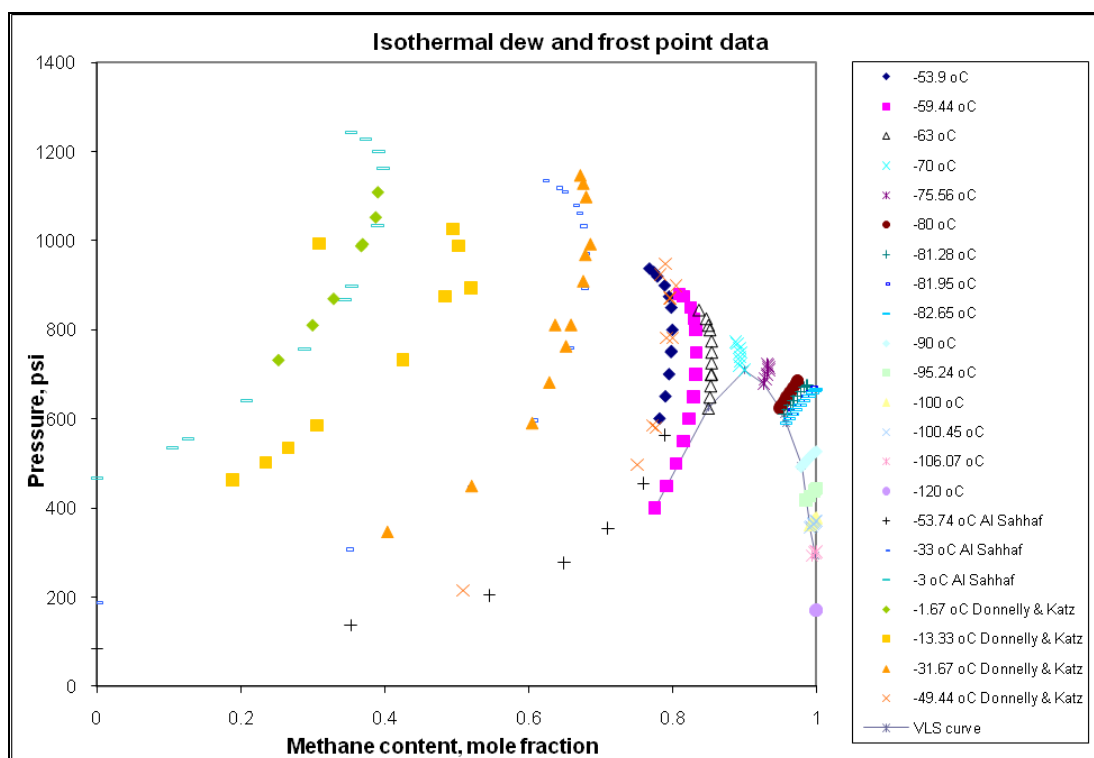


Figure 2. 14 Experimental data on phase envelope CO₂-CH₄ mixture published in (Hwang, 1976; Donnelly & Katz, 1954; Al Sahaf et al., 1983).

At lower temperatures a wider range of compositions can be separated at lower pressures, whereas at higher temperatures even high pressures may be insufficient for separation of mixtures containing a substantial amount of CH₄. Vapour-Liquid equilibrium points obtained by different researchers are compared in the P-x diagram presented as Figure 2.15. Good qualitative and quantitative agreement between the majority of the data sets can be observed. However, the dew point data from Hwang et al. qualitatively disagree with the other two curves. The experimental results by Arai et al. (1971) are also shown on this graph, however in this case the method used for the dew and bubble point measurement was indirect. Consequently, Arai's results deviate from the data obtained by other researchers.

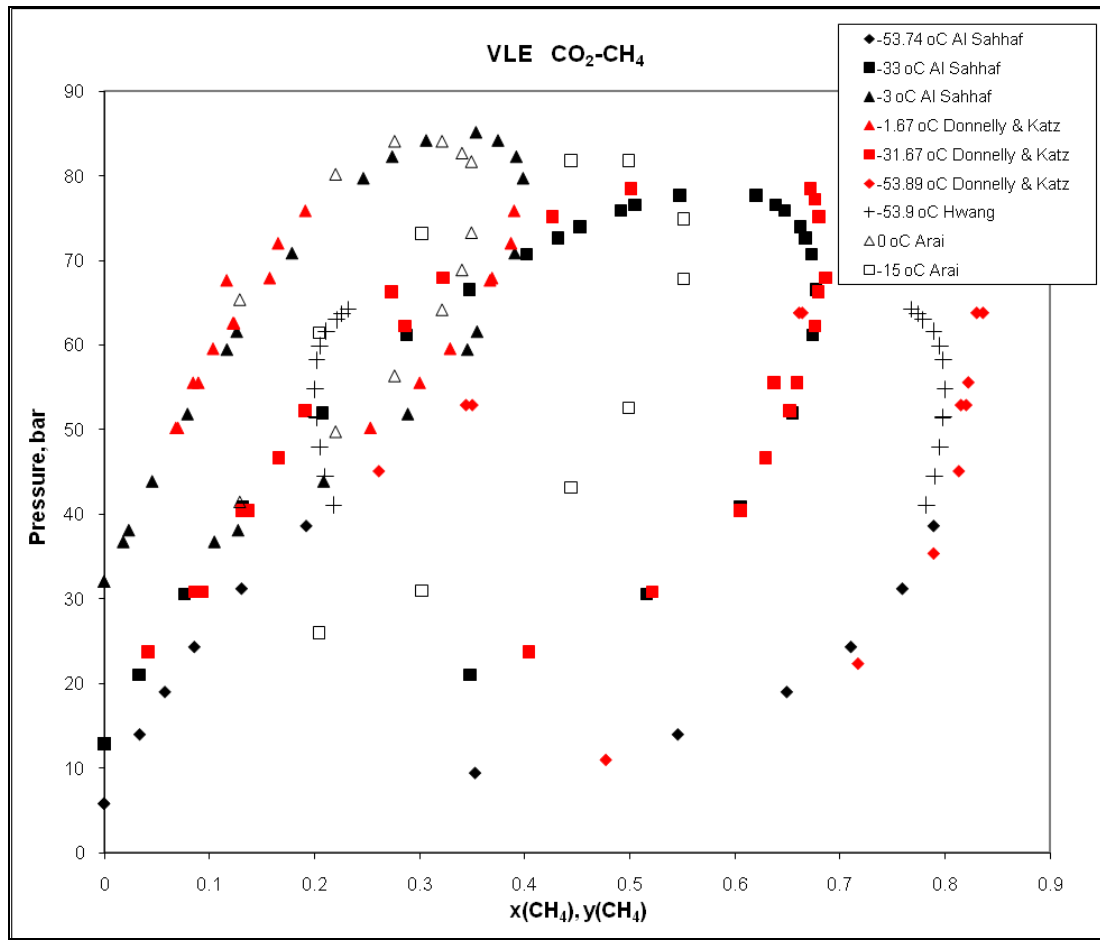


Figure 2. 15 The possibility of separation of different compositions Methane-Carbon Dioxide (Donnelly & Katz, 1958; Arai et al., 1971; Hwang et al., 1976; Al Sahhaf et al., 1983)

As described in Van den Kerkhof and Thiery (2001), about 5°C undercooling is necessary for the bubble nucleation in the metastable liquid phase during isochoric cooling. This is also the case for Gas to Solid and Liquid to Solid transformation in a steady state vessel. Therefore, more accurate results can be collected during heating when observation of the bubble disappearance or melting is performed. In the case of high density fluids, the melting point is not apparent for observation due to similar refractive indices of solid and liquid phases. Low density fluids tend to exhibit Gas-Solid transformation which is usually accompanied by a sudden invertible change in pressure and/or temperature. In the case of measuring the dew point, the chilling process is preferred due to the difficulties in observation of the disappearance of a thin film of liquid on the walls of the equilibrium cell during heating. The study also indicates that the frost point of CO₂ is suppressed in the presence of Methane to a higher degree than in the presence of Nitrogen. For the current research this implies increased risk of CO₂ freezing in pipelines during cryogenic separation.

2.5.2. Hydrogen-Carbon Dioxide System

A binary mixture containing CO₂ and Hydrogen was subjected to investigation in the study conducted by Bezanehtak et al. in 2002. The results include vapour-liquid equilibrium data for mixtures containing up to 20 mol% H₂ at 278.15 K, 290.15 K, and 298.15 K for pressures between 20 bar and 200 bar and are presented in Figure 2.16. The bubble point curve almost does not change with the temperature change, while the dew point curve shifts towards lower contents of Hydrogen in the vapour phase with temperature increase.

Another study was conducted for Hydrogen-Carbon Dioxide mixture in the temperature range between 220 and 290 K by Spano et al. in 1968. The two data sets are in good qualitative and quantitative agreement at pressures below 100 bar; however, the results of Spano et al. (1968) are consistently 10 bar higher than those of Bezanehtak et al. (2002) as shown in Figure 2.17. Deviations, mainly for liquid phase composition, can be noticed at higher pressures and temperature of 290 K (Figure 2.16). This disagreement was addressed to deal with experimental difficulties in this system (Bezanehtak et al., 2002) and most probably is related to the difficulty described by Konynenburg & Scott (1980). The data set obtained by Spano et al. (1968) shows the same effect of temperature on the liquid phase composition as that observed by Bezanehtak et al. (2002).

Hydrogen content in the liquid phase increases with pressure according to the data presented in Figure 2.17. Generally, Hydrogen solubility in liquid CO₂ increases with temperature at pressures above 100 bar. Temperature impact is such that higher concentrations of Hydrogen in the vapour phase are obtained at low and moderate pressures than at high pressures.

Density of liquid phase was also measured for the whole experimental range. As shown in Figure 2.18, the density is lower at higher temperatures indicating higher H₂ solubility in the liquid phase. Overall, the density tends to decrease with pressure providing yet another indication of higher Hydrogen content. In current research, this fact restricts application of high pressure during CO₂ condensation in order to meet the proposed purity requirements (e.g. to produce liquid CO₂ suitable for EOR application).

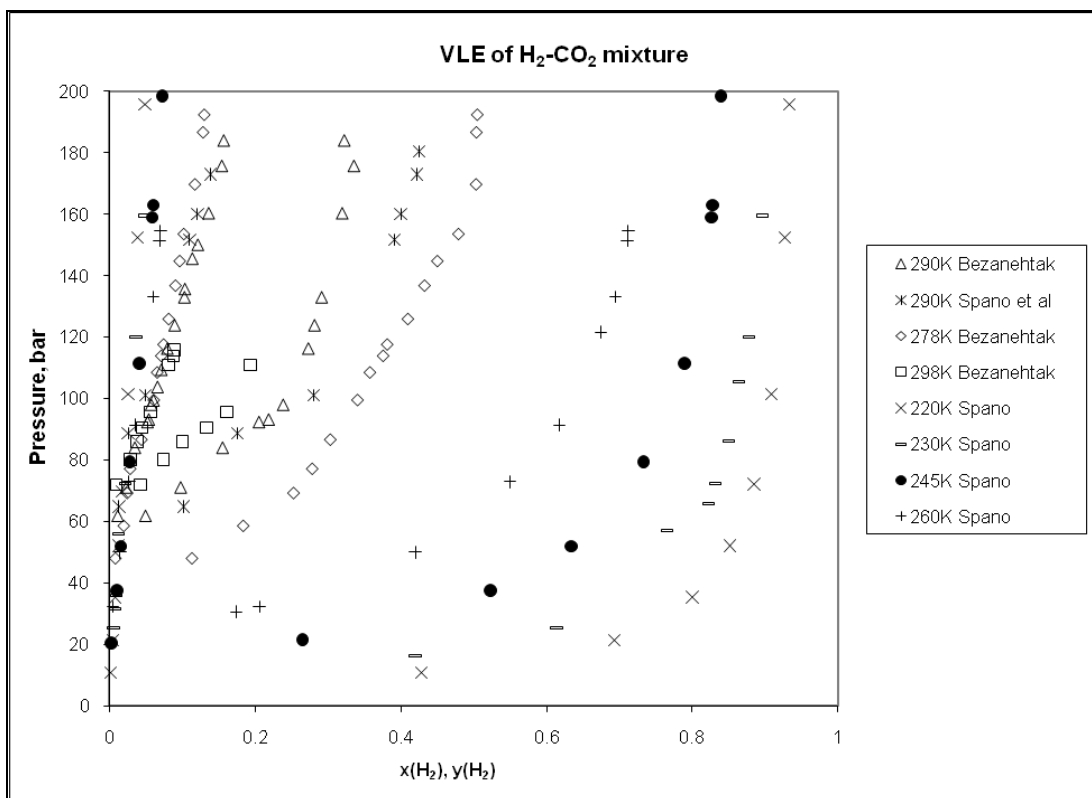


Figure 2. 16 Isotherms for Hydrogen-Carbon Dioxide mixtures

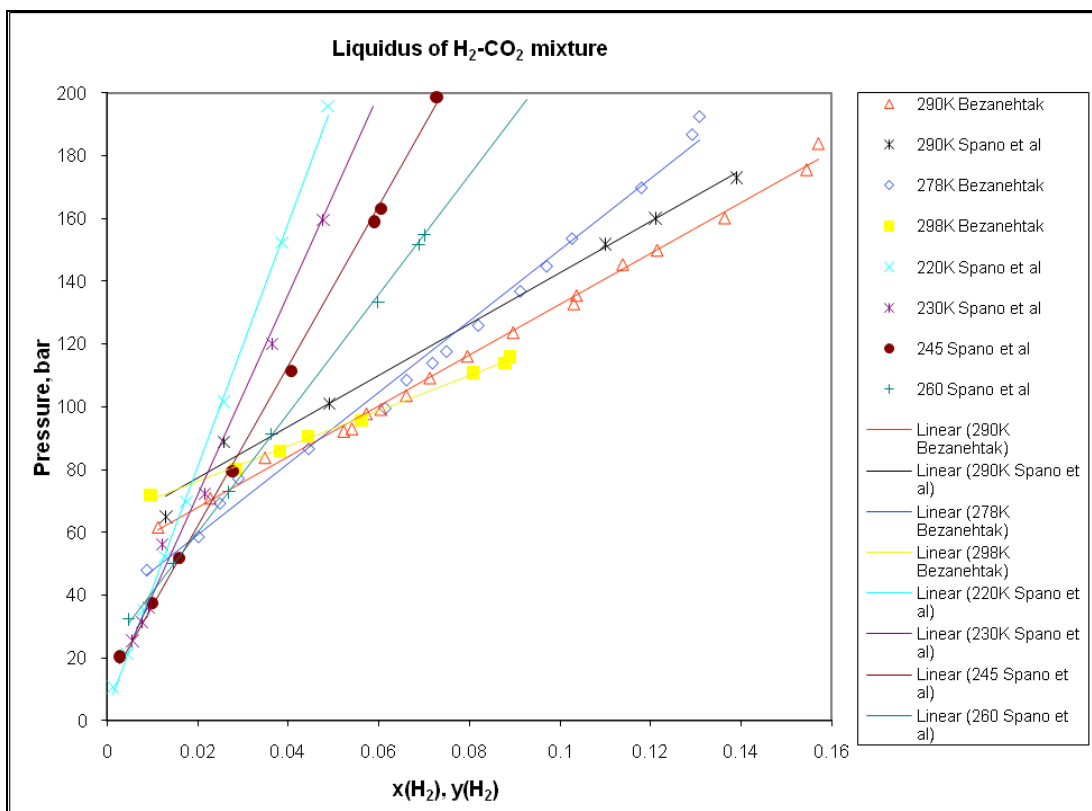


Figure 2. 17 Bubble point curves for H₂-CO₂ mixtures from Bezanahtak (2002) and Spano et al. (1968)

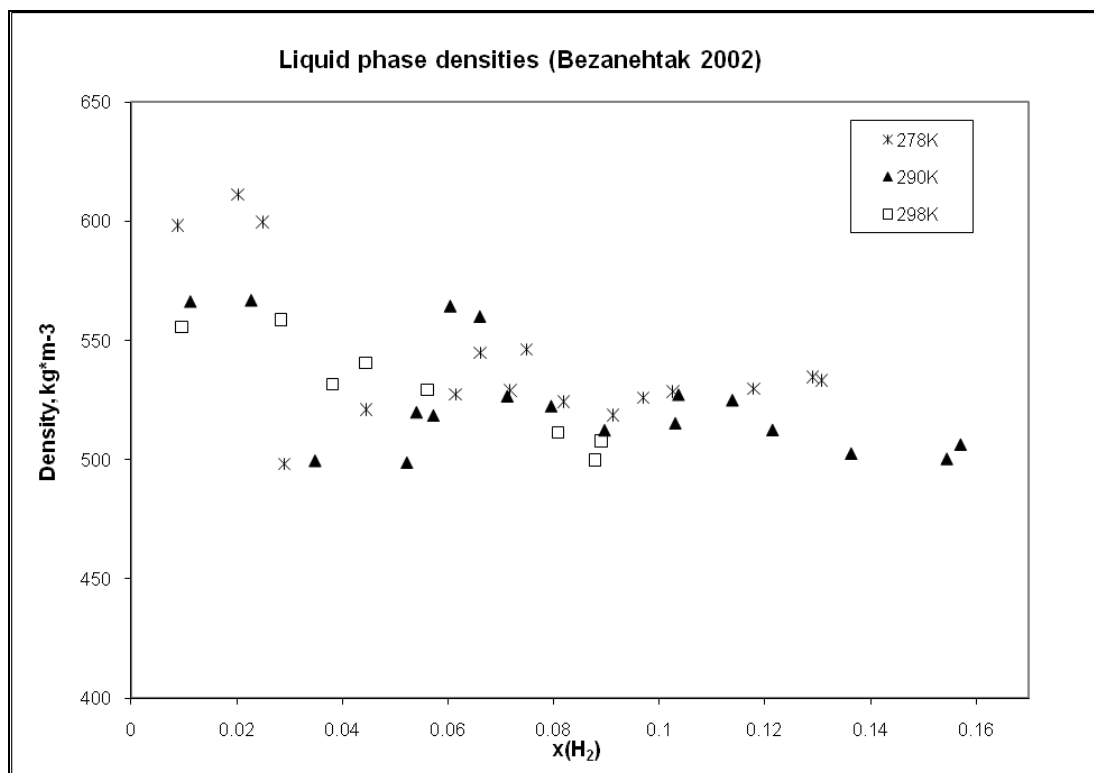


Figure 2. 18 Density of liquid phase during condensation of Hydrogen-Carbon Dioxide mixtures

Extensive study has been conducted in terms of the investigation of the feasibility of purification of Methane from Carbon Dioxide by cryogenic distillation. Numerous technologies have been developed and are now used in industry for Natural Gas sweetening. Unfortunately, phase behaviour of mixtures containing mainly Hydrogen and CO₂ did not undergo thorough analysis. In this work the main accent is made on separation of CO₂ from flue gases from IGCC pilot plants. In this regard, comprehensive experimental and theoretical investigation has been conducted for Hydrogen-Carbon Dioxide gas mixtures in a range of compositions.

2.6. Theoretical Models for Phase Transitions Prediction

The lack of accurate experimental work over the whole pressure-temperature-composition region has resulted in many theoretical models have been developed for a limited number of applications. Applied thermodynamics tools are still not advanced enough to allow the simultaneous prediction of VLSE by either activity coefficient models or equations of state unless sufficient experimental data are available. Below is the review of the most commonly applied theoretical models which were used in this research for the phase transitions predictions.

2.6.1. Cubic Equation of State and Shortcoming

Currently used statistical thermodynamics methods are mainly based on a cubic equation proposed by van der Waals and Platteeuw (1959) given in general form by equation 2.1.

$$\left(P + \frac{a}{v^2}\right)(v - b) = RT \text{ or } P = \frac{RT}{v - b} - \frac{a}{v^2}, \text{ where}$$

(2.1)

P – Pressure, Pa,

T – Temperature, K

V – Volume, m³/mol

R – Universal gas constant

The improvements made throughout decades included corrections of binary interaction parameters to account for temperature dependency, critical or non-critical state, polarity, acentric factor, and so on. Peng-Robinson Equation 2.2 is now widely used in chemical engineering design for phase envelope prediction and was used in this work for modelling.

$$P = \frac{RT}{mV - b} - \frac{a(T)}{mV(mV + b) + b(mV - b)}, \text{ where}$$

(2.2)

P – Pressure, Pa,

T – Temperature, K

V – Volume, m³/mol

R – Universal gas constant

$a(T)$ – a gas constant dependent on temperature given by

$$a(T) = \frac{0.45724R^2T_c^2\alpha(T)}{P_c}, \text{ where}$$

P_c – Critical Pressure, Pa

T_c – Critical Temperature, K

V_c – Critical Volume, cm³/mol

$\alpha(T)$ – function of temperature described by

$$\sqrt{\alpha} = 1 + m\left(1 - \sqrt{T/T_c}\right), \text{ where}$$

m – is a function of acentric factor, which is equal 0.2249 for CO₂, and described by

$$m = 0.37464 + 1.54226\omega - 0.26992\omega^2$$

b – a constant for a certain fluid given by

$$b = \frac{0.07780RT_c}{P_c}$$

The EOS can be expressed in terms of the compressibility factor, z :

$$z^3 - (1 - B)z^2 + (A - 3B^2 - 2B)z - (AB - B^2 - B^3) = 0, \text{ where}$$

$$z = PV/RT$$

$$A = aP/(RT)^2$$

$$B = bP/RT$$

Here constants A & B are dependent on the values of the constant a & b . A cubic Equation for z is solved to get one real root that gives molar volume from which the density is obtained.

The Chung et al. (1988) method is one of the widely used methods to find the viscosity of dense gases. This method includes density along with temperature and pressure, as the input for calculating the viscosity. Chung et al. suggested the following expression for describing the fact that the fluid gas has a high viscosity for high pressure.

$$\mu = \frac{\mu_1 \cdot 36.344 \cdot \sqrt{MT_c}}{V_c^{2/3}}, \text{ where}$$

μ – viscosity, μP

M – molecular weight, g/mol

And μ_1 is given by equation

$$\mu_1 = \frac{(T^*)^{0.5}}{\Omega_v} \left\{ F_c \left[(G_2)^{-1} + E_6 y \right] \right\} + \mu^{**}, \text{ where}$$

$$T^* = 1.2593T_r$$

$$F_c = 1 - 0.2756\omega$$

$$\Omega_v = A_1 (T^*)^{-B_1} + C_1 \exp(-D_1 T^*) + E \exp(-F_1 T^*)$$

$$A_1 = 1.16145$$

$$B_1 = 0.14874$$

$$C_1 = 0.52487$$

$$D_1 = 0.77320$$

$$E = 2.16178$$

$$F_1 = 2.43787$$

$y = \rho V_C / 6$, where

ρ – molar density, mol/cc

$$G_2 = \frac{E_1 \{ [1 - \exp(-E_4 y)] / y \} + E_2 G_1 \exp(E_5 y) + E_3 G_1}{E_1 E_4 + E_2 + E_3}, \text{ where}$$

$$G_1 = \frac{1 - 0.5y}{(1 - y)^3}$$

$$\mu^{**} = E_7 y^2 G_2 \exp[E_8 + E_9 (T^*)^{-1} + E_{10} (T^*)^{-2}]$$

And the parameters E_1 to E_{10} are shown in the table

Table Chung et al. (1988) coefficients to calculate $E_i = a_i + b_i \omega$

i	a_i	b_i
1	3.324	50.412
2	1.210E-3	-1.154E-3
3	5.283	254.209
4	6.623	38.096
5	19.745	7.630
6	-1.9	-12.537
7	24.275	3.450
8	0.7972	1.117
9	-0.2382	0.06770
10	0.06863	0.3479

In cases of solid deposition from a liquid phase, particularly hydrate formation, the Soave-Redlich-Kwong equation of state with the Peneloux modification (Peneloux & Rauzy, 1982; Abdoul et al., 1991) was developed to better fit the experimental results than the PR EOS described above. This modification is brought about by utilisation of the Rackett compressibility factor instead of the compressibility factor to correct the repulsive term in the equation of state. Resulting values therefore better describe properties of liquid phases except for associated compounds, and make better predictions in the high pressure region.

A number of investigators suggested further amendments to the cubic EOS to enable more reliable hydrate prediction. These include for example, the development by Kashchiev and Firoozabadi (2002a) for estimation of induction time.

EOS approach involves numerous binary interaction parameters specific for each case which results in large error margin.

2.6.2. Excess Free Energy and Activity Coefficient Based Models

Another approach to the description of the equilibrium relationship is in terms of the excess free Gibbs energy and activity coefficient. The generalised form of this equation is given by expression 2.3 (Renon & Praustitz, 1968), and essentially three models are derived based on this approach: the Wilson model, the Heil model and the non-random two liquid (NRTL) model. Values of constants and limitations of each model are given in Table 2.1. All equations are equally good for the description of fluids with little deviation from non-ideality.

$$\frac{g^E}{RT} = -q \left[x_1 \ln(x_1 + x_2 G_{21}) + x_2 \ln(x_2 + x_1 G_{12}) \right] + p x_1 x_2 \left[\frac{\tau_{21} G_{21}}{x_1 + x_2 G_{21}} + \frac{\tau_{12} G_{12}}{x_2 + x_1 G_{12}} \right] \quad (2.3)$$

In Equation 2.3

g^E – excess Gibbs energy due to phase transition

R – Universal gas constant

T – Temperature, K

q, p – parameters different for each model and given in Table 2.1

x_1, x_2 – overall mole fraction of molecules 1 or 2 type

$G_{12} = \rho_{12} \exp(-\alpha_{12} \tau_{12})$ and $G_{21} = \rho_{21} \exp(-\alpha_{21} \tau_{21})$, where

ρ_{ij}, α_{ij} – are given in Table 2.1 and α accounts for non-ideality and non-randomness of the fluid

$\tau_{12} = (g_{12} - g_{22}) / RT$ and $\tau_{21} = (g_{21} - g_{11}) / RT$, where

g_{12}, g_{21} – energies of interaction between molecules 1 and 2, $g_{12} = g_{21}$

g_{11}, g_{22} – residual Gibbs energy in pure 1 or 2

Table 2. 1 Parameters for models based on the activity coefficient approach

Equation	p	q	ρ_{ij}	α_{ij}^0	limitations
Wilson	0	1	v_i/v_j	1	Does not account for partial miscibility, or when splitting occurs at low degree of non-ideality. Good for alcohol-hydrocarbon systems
Heil	1	1	v_i/v_j	1	Not recommended for strongly self-associated systems where phase splitting occurs at very high values of activity coefficients and high degree of non-randomness
NRTL	1	0	1	α_{ij}	Properly selected parameter α can adjust the equation for essentially any application. $\alpha = 0.2$ for low non-ideality and low non-randomness case, and $\alpha = 0.55$ for strongly non-ideal cases

2.6.3. Comparison of Different Models

Eggeman and Chafin (2003) evaluated the predicting ability of different models for CO₂ freezing by comparing the generated results with the second generation graph adopted from Pikaar's PhD thesis (1959). The original data have never been published outside this thesis, and it could not be accessed to be used in this thesis. The activity coefficient model given by Equation 2.3 in NRTL approximation produced a very good fit to Pikaar's experimental data; however, two major limitations were found to cause the error: 1) a large number of non essential interaction parameters have to be generated due to the limited accuracy of the produced key parameters, and 2) Henry's law is not suitable for use in the supercritical region. The Peng-Robinson EOS is able to generate a very close fit to the experimental data; however, "the CO₂-Methane binary interaction parameter has to be changed by approximately 13% from the value used in VLE calculations". Eggeman and Chafin (2003) also suggest that the most accurate way to solve the cubic EOS is through the false position method. Results of the current research show that SRK model better describes hydrate formation than PR model.

The accuracy of the prediction of phase transitions by any of the presented models is often limited, and this question was addressed in few recent papers (Eggeman & Chafin, 2003&2005; Hlavinka et al, 2005). The current thesis also contains a comparison of simulated results using different models against experimental data.

2.7. Conclusion

An overview of available information on low temperature gas separation techniques such as gas hydrates and cryogenic distillation is given in this Chapter. The main focus is on current developments in both fields concerning Methane and CO₂. Natural gas where Methane is the main component is gaining recognition as being the major energy source in the foreseeable future due to the depletion of recoverable oil. Particularly, vast deposits of Natural Gas hydrates in the sea bed attract the interest of researchers. Thermodynamics and kinetics of hydrate formation and decomposition is being thoroughly studied. In the mean time gas hydrates remain a crucial problem encountered in flow assurance engineering, and a large part of investigations is conducted in order to improve existing inhibiting techniques. Traditionally, injection of alcohols and glycols, specifically Methanol and monoethylene glycol, is deployed in industry to prevent formation of plugs in

transmitting pipelines during oil and gas production. Despite apparent economic profit which includes lower concentrations of chemicals needed to suppress hydrate formation and less impact on purity of trapped gas, surfactants are still not widely used for this purpose because of corrosive nature. The research is however being undertaken with the intent to developing non-corrosive, non-toxic and more effective inhibitors. Gas hydrates formation phenomenon also bears a prospective opportunity for CO₂ capture and sequestration. Pragmatic interest in chemicals able to promote nucleation and crystal growth has therefore appeared. Similar to inhibitors, there are substances alleviating thermodynamic conditions but causing a negative impact on the purity and selectivity of separation, and surfactants which improve kinetics, however the mechanism of their action is extremely poorly understood.

Separation of carbon dioxide is a vital step in any process involving CO₂. Traditional cryogenic processes for capture of Carbon Dioxide from gas streams involve removal of acid gases from raw Natural Gas, and therefore can be described as CH₄-CO₂ separation. There are three major competing technologies for it, the Ryan-Holmes process (O'Brien et al., 1987), Controlled Freezing Zone (Haut et al., 1989), and CryoCell (Amin and Jackson, 2004). Establishment and improvement of each of these existing methods prompted detailed investigation of phase transitions of systems of interest. The same technologies can be applied for CO₂ separation from other gas mixtures where the components have significantly different critical and triple point conditions, for example flue gases at power plants. Modern power stations such as IGCC, however, require the development of completely new approaches for purification of flue streams due to different compositions. Very little research has been done in the field of low temperature H₂-CO₂ separation, and there is no viable commercialised process based on cryogenics. The evaluation of the competitiveness of cryogenic procedure is discussed in Chapter 9.

The central goal of this research is to develop a new creative technology for pre-combustion separation of Carbon Dioxide from IGCC flue gases. The idea is to combine well known cryogenic distillation, which does not appear economically attractive on a stand-alone basis, with a novel concept of utilisation of hydrate formation for CO₂ capture. A fundamental study of both phase envelopes and hydrate formation curves of H₂-CO₂ mixtures is conducted to justify the choice of optimum operating conditions, including the suitable promoter and its concentration.

Considerable similarity of Methane and Carbon Dioxide hydrate structure suggest that the behaviour of the two is the like. Therefore it is considered worthwhile to utilise the abundant information available on Methane hydrates in order to better understand the trends of CO₂ hydrate formation/dissociation. In this regard, the hydrate research performed in this work includes investigation of the influence of different factors on Methane hydrate formation. Such factors as high concentration of a chemical dissolved in water and the presence of another condensed phase (condensate or wax) are addressed.

Chapter 3.

Cryogenic Separation of CO₂

3.1 Introduction

In the first stage of the proposed combined cryogenic and hydrate technology for CO₂ removal from IGCC flue gases, the stream will undergo substantial refrigeration in order to condense most of the CO₂. Performance of this stage is quantified by the amount of liquefied Carbon Dioxide which can be collected. A theoretical study using two well-known models was conducted as a first step of assessment of the effectiveness of separation. The Peng-Robinson equation of state (EOS) (Peng & Robinson, 1976) was chosen for use in the HYSYS computer simulation software because this is an appropriate method conventionally used in chemical engineering for process modulation. The Soave-Redlich-Kwong equation, modified by Peneloux (Abdoul et al., 1991) better describes the properties of a liquid phase whenever it is present in the system and this EOS is available in the PVTsim simulation environment.

Inconsistency in the simulation results and the scarcity of available experimental data required a laboratory investigation of phase behaviour and a quantitative evaluation of separation. Mixtures of Hydrogen and Carbon Dioxide were chilled to low temperatures just above CO₂ freezing point at various pressures, and the amount and the degree of separation was determined. The volume of the liquid and its composition are relatively easy to measure under laboratory conditions with less error than for other properties, therefore they were chosen as measured parameters for evaluation of the effectiveness of CO₂ capture. Effectiveness of CO₂ separation is referred to as *capture rate*. The dew point curves were obtained and described for each investigated gas mixture for better understanding of the effect of possible deviations in process conditions. Data on kinetics of condensation were recorded in most cases to provide supplementary material for calculations. The method employed here ensured stable and repeatable experimental conditions such as gas composition, pressure maintenance, cooling rate, time required for the system to reach equilibrium, and temperature control. Because near-freezing temperatures are involved in operational conditions, and thus pipeline blockage can be encountered, experiments were conducted in order to assess whether or not frozen CO₂ could stick to the walls or could be flashed and carried out with the gas flow.

The composition of the IGCC process gas is essentially given at 40 mol% CO₂ and 60 mol% Hydrogen (Klara & Sravastava, 2002) at pressures between 30 and 60 bar. In addition to these basic cases, gas mixtures containing different amounts of Carbon Dioxide at various pressures were also investigated in order to better understand phase behavior and the influence of flow instability. Laboratory testing of cryogenic condensation of CO₂ from H₂-CO₂ gas mixtures of various compositions was crucial for prudent choice of operating conditions of the laboratory rig constructed for testing of the combined cryogenic and hydrate technology. A new model for prediction of the dew point curves for H₂-CO₂ systems was developed on the basis of the Peneloux-SRK EOS and experimental data obtained in this research.

Particular attention was paid to the means of avoiding blockages in case CO₂ freezing occurred in pipelines as this can be a limiting factor for the demonstration facility design and operation. Different coatings were tested with regards to sticking of frozen matter, and therefore expediting the build-up of a solid plug.

The effectiveness of cryogenic condensation for additional CO₂ purification from an Oxyfuel gas mixture at -55°C and pressures between 10 and 12 bar was also estimated.

3.2 Theoretical Modelling of Phase Behaviour of H₂-CO₂ mixtures

Figure 3.1 shows phase envelopes generated by the two models for the gas mixtures containing 29 to 52 mol% CO₂ mixed with Hydrogen. Simulation results display a high degree of inconsistency, especially for low concentrations of CO₂ in the region of elevated pressures. In general, according to the SRK-P EOS, condensation occurs at lower temperatures and higher pressures than forecast by the PR model. At pressures of interest, about 60 bar, the difference in dew point temperatures varies between 2°C for high CO₂ content to 4°C for low concentration of Carbon Dioxide. This difference leads to erroneous results for prediction of capture rates and, therefore, poor quality of overall design simulation.

Performance of PR model was compared in two software packages (HYSYS and PVTsim) and the obtained results were within 0.5% discrepancy, therefore the use of different simulation environments was not considered to be an issue. Comparison of the results produced by SRK-P model was not conducted because this EOS is not available in HYSYS.

Because a lower dew point temperature is obtained by the SRK method, the amount of CO_2 which can be condensed is lower than in case of the PR model; therefore there is a discrepancy in estimated capture rates of the order of 2 mol% for mixtures containing 52 mol% CO_2 in the feed to 5 mol% for low CO_2 content.

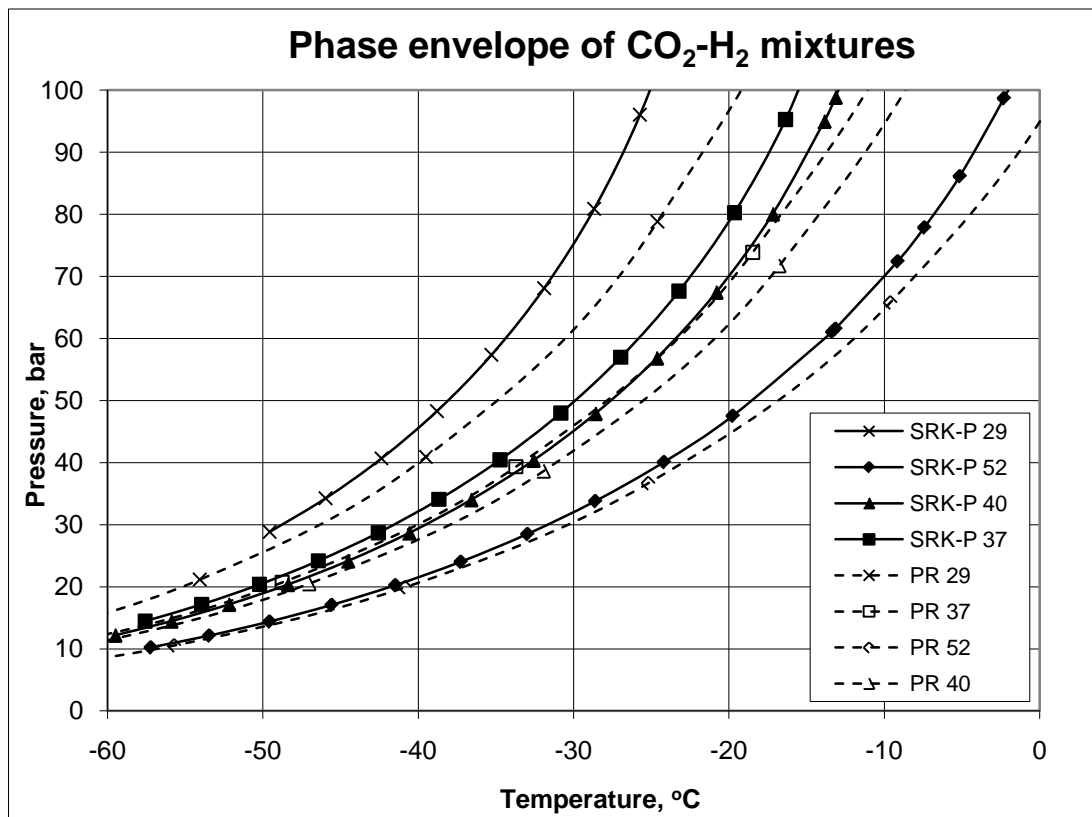


Figure 3. 1 Dew point simulation results. SRK-P relates to SRK-P EOS used in PVTsim, and PR relates to PR EOS used in HYSYS. Also in the legend mol% of CO_2 in the mixture is given.

Therefore an extensive experimental study of phase envelopes for a range of H_2 - CO_2 mixtures was conducted in order to assess the achievable figures for CO_2 capture by cryogenic condensation from the mixtures of interest.

3.3 Experimental Investigation of CO_2 Condensation and Freezing

The gas compositions used in the experiments are tabulated in Appendix C, preparation of the gas mixtures is described in Appendix B and the apparatus description is given in Appendix A.

Condensation of carbon dioxide from CO_2 mixtures with hydrogen, nitrogen and argon was studied to determine the efficiency of cryogenic step for CO_2 removal from flue gases of IGCC power plants, capture rates and phase behavior. IGCC Shell gas contains 36-37 mol% CO_2 and IGCC GE contains 40 mol% CO_2 . Also

condensation from Oxyfuel-like gas mixture containing about 80 mol% CO₂ was studied.

Experimental investigation of CO₂ condensation from mixtures containing 23 to 52 mol% CO₂ with Nitrogen, Argon, but mainly Hydrogen was performed using a state-of-the-art high pressure sapphire cell described in Appendix A. Phase envelopes for mixtures were analysed at pressures between 30 and 60 bar. All mixtures were prepared *in situ* on a mass basis (described in Appendix B) prior to each experiment using industrial grade pure gases supplied by BOC Australia, and the composition was monitored by sampling using a Gas Alarm Systems' CO₂ analyser. The same gas mixture was used to conduct a series of tests to obtain dew points at various pressures and determine the efficiency of separation at near-freezing temperature. For comparison purposes, the final temperature for condensation and time allowed for equilibrium was the same in all experiments. Experiment for each gas mixture was repeated at least three times for repeatability.

CO₂ freezing and stickiness to different materials was studied to determine the potential for pipeline plugging during condensation process. In pipelines the flow of gas can carry the frozen particles away if they do not adhere to the walls; however in the cell the gas phase does not move fast enough. Therefore, CO₂ freeze out from mixtures with natural gas was studied. At operational temperatures of about -60°C some of natural gas is liquefied, and CO₂ forms solid crystals inside the liquid phase. When the mixer is turned, liquid phase can carry solid particles if they do not adhere to the stirrer. The stirrer was made of stainless steel with the base made of titanium. Stainless steel was mechanically coated with Teflon and ceramics to study the stickiness of frozen CO₂ to different materials.

Observations of the properties of frozen CO₂ in terms of adhesion to the mixer coated with different materials were made during low-temperature experimentations with 20, 45 and 70 mol% CO₂ in Natural Gas mixtures purchased from Alinta Gas (Table 3.1). At experimental conditions Methane is partially condensed from the gas phase and forms a liquid which can carry frozen CO₂ particles during stirring. Behaviour of the solid matter when the mixer is stopped was monitored and conclusions were made.

Table 3. 1 Natural Gas composition (dry basis)

Component	CO ₂	N ₂	C1	C2	C3	C4	C5	C6
Mol%	2.49	2.33	86.28	6.58	1.88	0.36	0.06	0.02

3.3.1 Experimental Procedures

Two sets of condensation tests were conducted with gas mixtures containing 23 to 52 mol% CO₂ with content analysed before and after each experiment. All experiments were conducted in the high-pressure full-vision cell described in Appendix A with the mixtures prepared on a weight basis according to the technique described in Appendix B.

On the basis of the data produced in the first set of experiments, phase envelope diagrams for mixtures of different compositions were developed. Once prepared, the same mixture was used to conduct a series of experiments for determination of dew points at different pressures. Tests were carried out by lowering the cell temperature at a rate of 2 degrees per hour at constant pressure until the first liquid droplets appeared. The mixer was running at the same speed in all experiments to ensure even temperature distribution inside the cell. The pressure and temperature of the cell and displacement of the pump were monitored and recorded during the experiment. The system was then heated to temperatures 5 to 10°C higher than the observed dew point temperatures and left for at least 30 minutes to ensure the absence of any liquefied CO₂. The pressure was then lowered by 5 bar and the experiment repeated. Dew points for the pressure ranges of 30 to 60 bar were obtained for each mixture.

In the second stage, liquefied CO₂ was collected in the cell (Figure 3.2), and its volume and composition measured at -55°C and the capture rates calculated for the above mixtures. The mixer was replaced with a cylinder with horizontal marks 1.5 mm apart which allowed calculating the volume of condensed liquid phase. The sapphire cell was pressurised with a sample and insulated from the external pump. The system was then chilled at a rate of 10 to 15°C/hr to -55°C and the dynamic dew point (temperature at which condensation occurred at this fast cooling) was also observed. The level of liquid and the pressure were recorded during cooling, and after the cell was cooled and held at -55°C for about 1 hour to achieve equilibrium. The level of liquid was then used to calculate the volume of condensed CO₂. A portion of equilibrium gas was then quickly removed and analysed. During this operation, liquid CO₂ froze due to the temperature drop resulting from depressurisation. The cell was then heated to room temperature and all CO₂ was gasified and analysed. Taking into account the gas remaining after depressurisation, the composition of the collected liquid CO₂ was calculated.

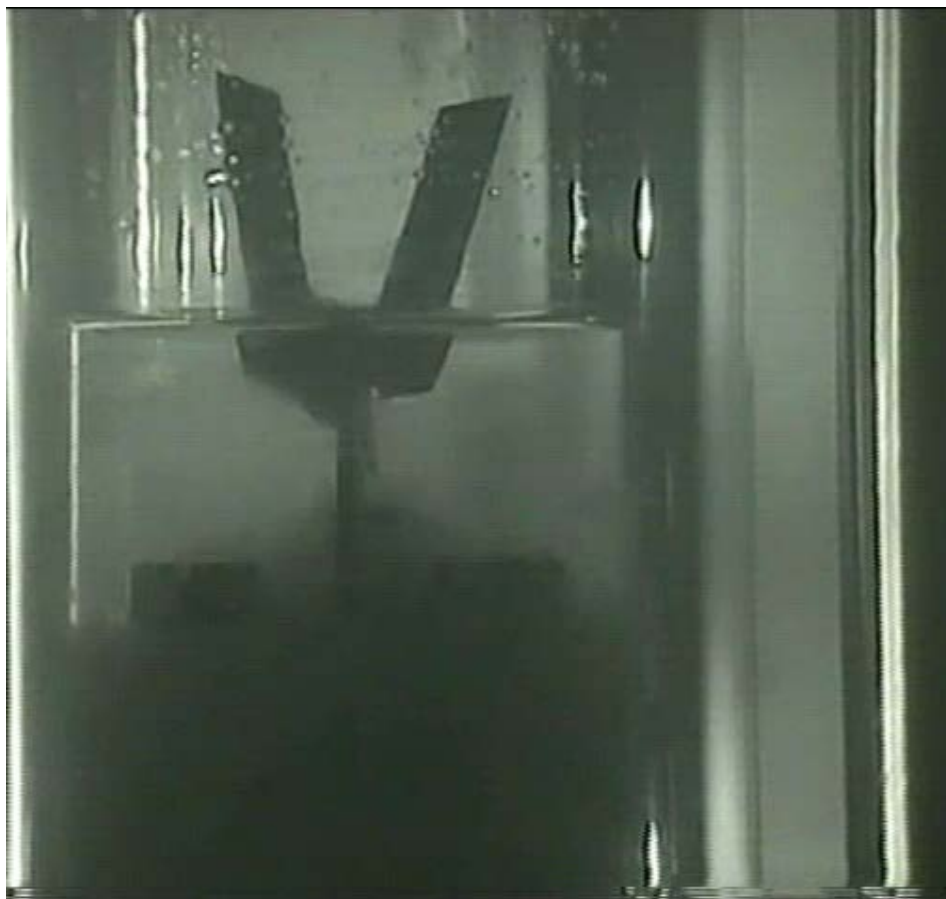


Figure 3. 2 Liquid CO₂ collected in the cell at -55°C

In all experiments the dew point was detected by visual observations and read as the breaking point on the pressure (volume) vs. temperature graph (see Figures 3.3 and 3.4). The optical element signal was recorded in some cases, and the dew point was also observed as a drop in this signal. The marked scale for liquid phase level measurements was calibrated every time after experimentation with water or pentane at atmospheric conditions. In some cases, condensed liquid was slowly evaporated by heating from -55°C at a rate of 5°C per hour and changes in displacement were also recorded.

Three mixtures containing 20, 45 and 70 mol% Carbon Dioxide with Natural Gas (NG) supplied by Alinta Gas were subjected to an investigation of the stickiness of solid CO₂ to different materials. During preparation CO₂-NG compositions were treated as two component mixtures because Natural Gas of known composition was supplied. The gas mixture was fed into the cell and chilled until a substantial amount of solid CO₂ froze out from the liquefied fraction composed of mainly CO₂ and Methane, usually to -65°C. Pressure was kept constant throughout the experiments at 12, 18 or 30 bar. The mixture underwent vigorous agitation during each experiment

allowing fine particles of solid CO₂ to form and suspend in the liquid hydrocarbon phase. When the stirrer was manually stopped, the tendency of solids to precipitate on the mixer was monitored. The entire stirrer was made of stainless steel and coated with Teflon or ceramic for the examination of different surfaces. Eggeman & Chafin (2003) have shown that there is large inconsistency in prediction of CO₂ freezing by conventional computer software. Therefore, frost point temperatures were recorded for each case in this study, and conditions were plotted and compared with those available from Hwang et al. (1974).

3.3.2 Dew Point Determination Technique

During all experiments dedicated to the study of the phase envelope of CO₂-N₂-Ar-H₂ mixtures total displacement of the pump was measured as an indication of the amount of feed gas needed to sustain the pressure drop due to cooling. In other words, these values reflect gas volume change in the cell during the experiment. Figure 3.3 is a typical plot of the difference in gas volume changes during condensation and evaporation for an experiment with 40 mol% of CO₂ in the feed at 65.3 bar.

Gas volume change during cooling above the dew point (which was visually observed at -20.1°C and 65.3 bar) occurs due to the temperature drop alone, while the volume change at lower temperatures is due to both condensation and temperature changes. Thus, the slope becomes steeper below the dew point. Above the dew point the inclination tangent is equal to $-0.76^{\text{CC}}/^{\circ}\text{C}$ and after the liquid started accumulating, the tangent became equal to $-1.93^{\text{CC}}/^{\circ}\text{C}$.

Evaporation does not follow the same path compared with condensation due to the difference between the dew and bubble points, which is usual for multicomponent gas mixtures. However, the same trend of the slope change can be observed on heating curve. The gas expands slowly at low temperatures and the slope becomes steeper at higher temperatures when evaporation takes place.

The straight lines above and below the dew point were found using the least-squares method and the approximate coefficients are shown on the graph. The intersection of the two lines was found to represent the dew point. The dew point temperature found from this graph is equal to -19.9°C, which is slightly higher than temperature observed visually. This can be caused by some delay in observation of the first

droplets is possible because the eye is not able to catch the appearance of fine moisture in the cell.

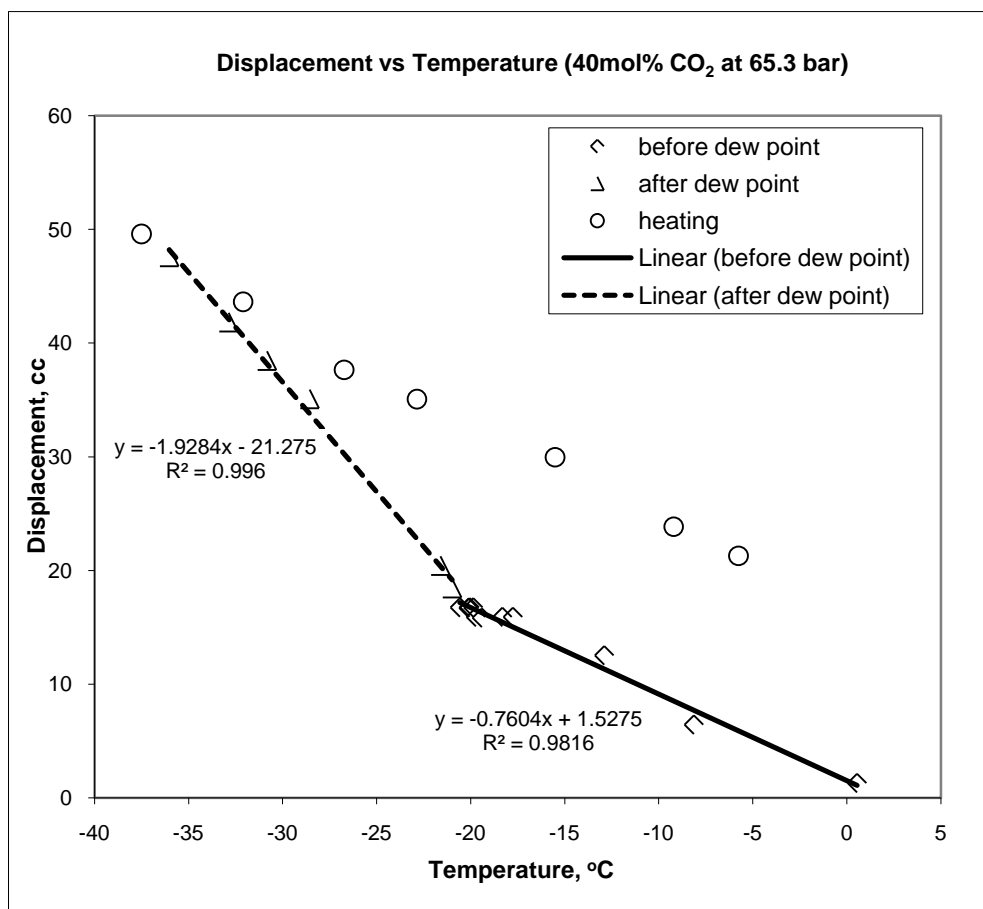


Figure 3. 3 Typical gas volume changes during cooling-heating cycle

In some cases the system was insulated from external environment (the pump) straight after loading the sample. In this case the pressure change during cooling was recorded and can be plotted against temperature. The pressure-temperature curve obtained during the experiment using the 37mol% CO₂ gas mixture is presented in Figure 3.4. The change in slope indicates that the dew point can also be observed on this graph. The calculated value of -41.5°C is again in very good agreement with the observed dew point temperature of -41.3°C. As expected, this plot is increasing with temperature in contrast with the volume-temperature graph due to the inverse relationship between pressure and volume.

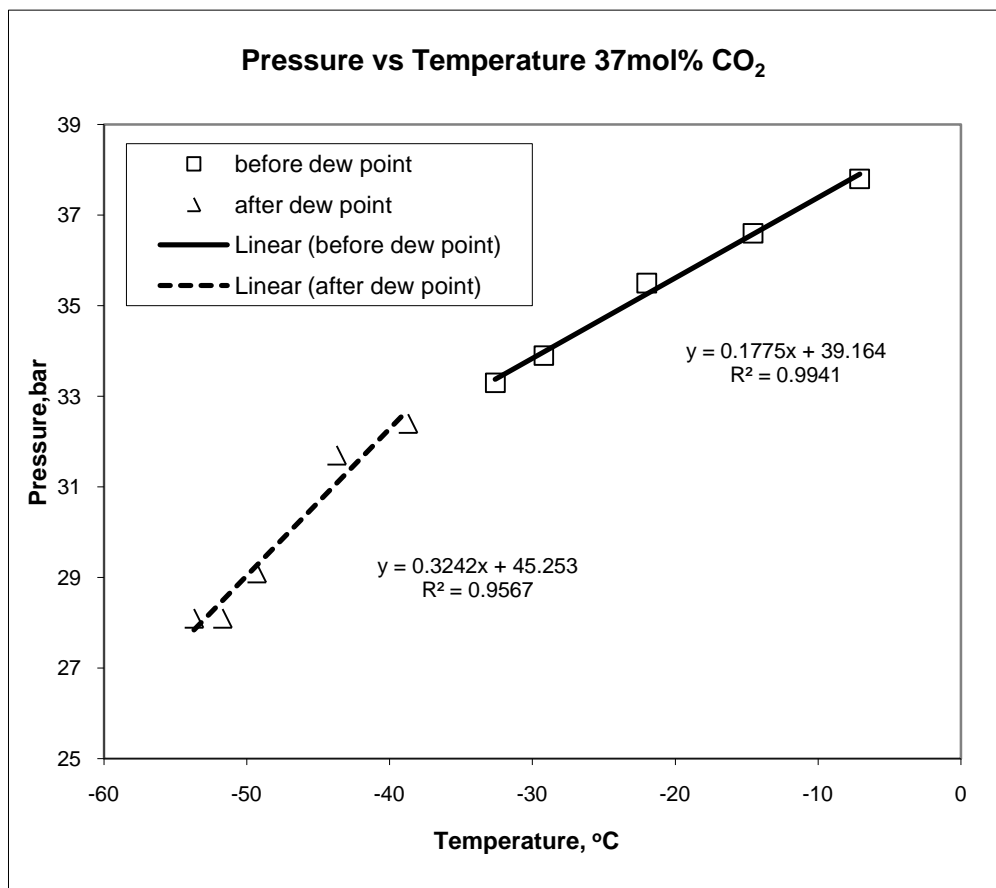


Figure 3. 4 Dew point observation on Pressure-Temperature curve

Similar dependencies were found for all conducted experiments.

3.4 Results and Discussion

The phase behaviour results and CO₂ capture rates for the separation of H₂-CO₂ mixtures were compared with results obtained from computer simulation software described in Section 3.2. Experimental results from the first set of experiments agree closely with those generated by the conventional SRK-Peneloux model, however minor modification is necessary to improve the predictive capability. Overall, achievable capture rates are better described by the PR model using HYSYS simulation software.

Study of the stickiness of frozen CO₂ crystals to different materials has produced the following results. Solid CO₂ has shown the least adherence to ceramics and strong adherence to stainless steel. Teflon protects stainless steel from accumulation of CO₂ on it at low concentration of CO₂ in the feed; however at high concentration it demonstrates the same adherence properties as stainless steel.

3.4.1 Dew Point Results

A series of experiments was conducted for compositions containing 27 to 52 mol% CO₂ with Hydrogen at pressures between 30 and 60 bar. The phase envelope curves obtained are as shown in Figure 3.5 and tabulated in Table 3.2. The results are in fairly good agreement with those obtained by Spano et al. (1968) for the same concentrations of CO₂ (as in Figure 2.16). Slight deviation between the two sets of data can be explained by the presence of small amount of highly volatile components (nitrogen and argon) in the gas mixtures studied in this work.

Condensation occurred at lower temperatures for lower pressures and lower CO₂ concentrations. At 60 bar the dew point for 27 mol% CO₂ gas mixture was found to be -40.1°C whereas a mixture containing 52 mol% CO₂ started liquefying at -15.5°C. At 40 bar the dew appeared first at -45.1°C and -26.84°C respectively for these two compositions. These values represent the border conditions for the conducted experimental work. The dew point temperatures for the same mixture at different pressures tend to be lower with decreasing pressure. At the same pressure, mixtures with higher CO₂ content condense at higher temperatures.

In all cases the dew point temperatures change by approximately 2°C for a pressure difference of 5 bar at pressures higher than 50 bar. At pressures below 50 bar, the dew point temperature decreases by approximately 3°C for a 5 bar pressure drop. In other words, the temperature increase with pressure is higher for higher values of pressure than for lower values.

In all cases, the dew points calculated with the SRK-P model are in better agreement with experimental results than predicted by PR model as shown in Figure 3.6 and Table 3.2. The agreement is very good at high concentration of CO₂ in the mixture, however, at lower concentrations disagreement increases. This is due to the fact that thermodynamic properties of Carbon Dioxide are usually poorly represented by cubic equations of state (Berro et al., 1996).

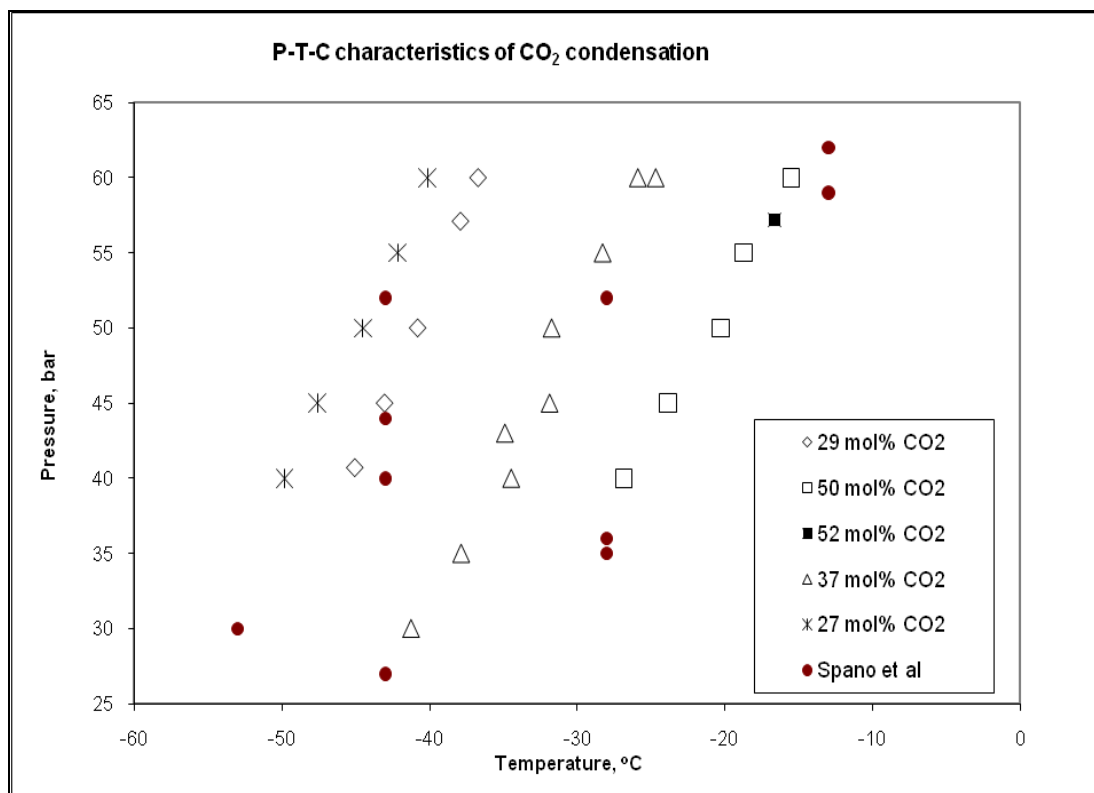


Figure 3. 5 Phase envelope of mixtures with different CO₂ content for the range of pressures 30 to 60 bar

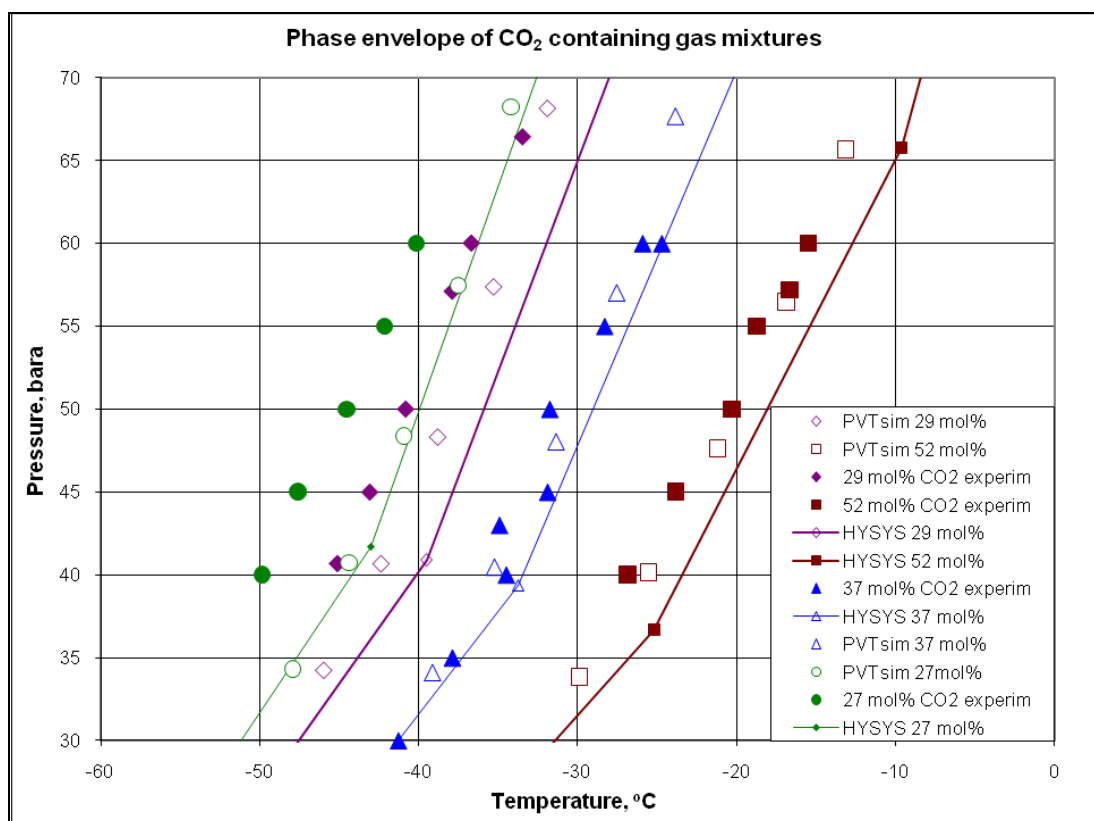


Figure 3. 6 Comparison of theoretical and experimental dew point results

Table 3. 2 Dew point data for gas mixtures containing 27 to 52 mol% CO₂

CO ₂ , mol%	27				29				
Pressure, bar	60	55	50	45	40	66.4	60	57.1	50
T(SRK- P), °C	-40.2	-41.8	-43.6	-45.6	-48	-31.8	-33.8	-34.8	-37.5
T(PR), °C	-35.4	-37.2	-39.3	-41.6	-44.1	-28.9	-31.2	-32.2	-35.2
T(exp), °C	-40.1	-42.2	-44.5	-47.6	-49.8	-33.5	-36.7	-37.9	-40.8
CO ₂ , mol%	29		37						
Pressure, bar	45	40.7	60	57.3	55	50	45	43	40
T(SRK- P), °C	-39.7	-41.8	-25.8	-26.8	-27.35	-29.9	-31.85	-33.3	-34.5
T(PR), °C	-37.6	-39.8	-23.8	-24.9	-25.6	-28.1	-30.4	-31.8	-33.3
T(exp), °C	-43	-45.1	-25.3	-27.1	-28.3	-31.8	-31.9	-34.9	-34.5
CO ₂ , mol%	37		50	52					
Pressure, bar	35	30	57.2	60	55	50	45	40	
T(SRK- P), °C	-37.6	-41.6	-16	-13.9	-16.1	-18.6	-21.3	-24.3	
T(PR), °C	-36.8	-40.3	-13.5	-12.2	-14.5	-17	-19.8	-23	
T(exp), °C	-37.9	-41.3	-16.65	-15.5	-18.7	-20.3	-23.8	-26.8	

3.4.2 Total CO₂ Capture Rates

The amount of liquid CO₂ which can be collected at -55°C is also dependent on the CO₂ concentration in the feed stock and the pressure as tabulated in Table 3.3.

According to the results obtained, high rates of CO₂ capture between 70 and 80% of the total CO₂ feed amount are achievable at pressures of 35 to 60 bar from mixtures containing 35 to 80 mol% CO₂ in the feed as a result of a single flash condensation. A total of about 55 to 65% CO₂ capture is achievable from mixtures initially containing less than 30 mol% CO₂. For the Shell case 50 to 60% capture was achieved at a process pressure of 28 to 33 bar and at 53 bar the capture rate increased to 78 to 79% of CO₂. More than 90% of CO₂ was captured from the Oxyfuel gas mixture at a process pressure of 10 to 12 bar. The remainder of CO₂ from the overhead gas is to be captured on the next stage by hydrate.

It can be noticed from Table 3.3 that higher rates of CO₂ capture are obtainable if higher pressure is exerted upon the system with higher initial CO₂ content as could be predicted from conventional gas-vapour equilibrium calculations.

It can be also noticed that in most cases the SRK-P model is in closer agreement with the experimental results compared with PR model. A significant difference between the theoretical and the experimental results occurs for the Shell case and low- CO_2 cases (containing less than 30 mol% CO_2).

Total CO_2 capture rates at pressures of 50 to 57 bar from mixtures containing different initial amount of CO_2 are also shown on Figure 3.7. The percentage of CO_2 which can be captured rises sharply from 55 to 85 mol% as the CO_2 concentration in the feed increases from 20 to 40 mol%. The subsequent addition of CO_2 to the feed mixture does not exhibit any significant impact on the total capture rate. The dashed line shows the results based on a simulation using PR EOS. The change follows the same trend as the experimental data, however, capture rates are overestimated throughout the whole region with significant differences at low concentrations of CO_2 , while the deviation diminishes at concentrations above 40 mol%. The dotted line shows the trend built on the basis of SRK-P data. Although the trendline has a slightly different shape, constantly increasing, separate points fall very close to those determined experimentally. Also the rate of increase falls when concentration reaches 40 mol%.

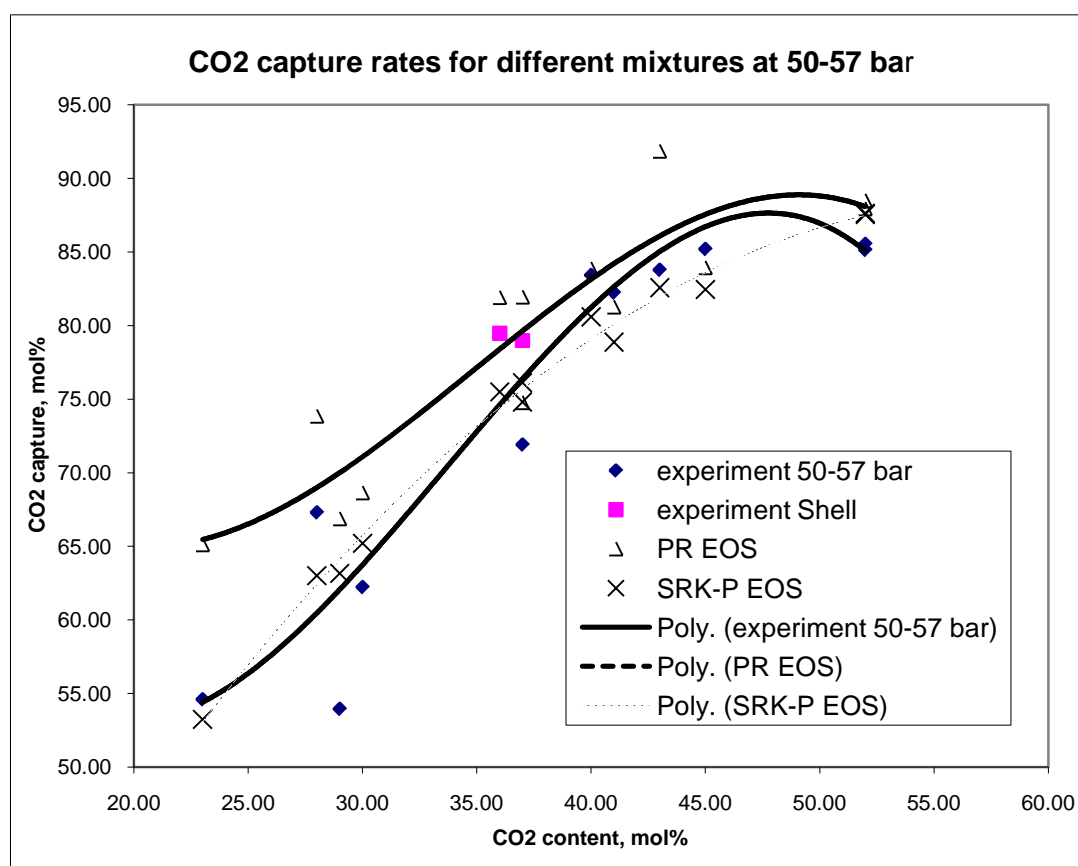


Figure 3. 7 CO_2 capture rates at 50 to 57 bar

Table 3. 3 Percentages of CO₂ collected at -55°C at different pressures for different compositions

CO ₂ content, mol%	Pressure, bar	CO ₂ liquid collected, mol%		
		SRK-P	PR	experim
Mixtures with Hydrogen				
23	50.9	53.24	65.11	54.61
27	28.9	32.37	54.20	55.41
28	55.0	63.01	73.84	67.30
29	51.5	63.16	66.87	53.96
30	55.7	65.21	68.63	62.23
36	60.6	77.28	78.94	81.07
37	47.3	72.78	72.25	74.43
36	52.4	74.81	74.76	71.91
37	53.0	75.50	81.90	79.47
37	54.2	76.12	81.94	78.98
37	27.2	55.03	59.59	52.18
38	26.3	55.92	60.06	59.29
38	33.3	64.00	58.20	77.33
38	28.0	57.94	48.84	63.78
40	50.2	80.59	83.86	83.43
41	56.8	78.87	81.26	82.23
43	53.1	82.58	91.85	83.78
45	53.3	82.45	83.93	85.20
52	54.4	87.64	87.93	85.54
52	56.0	87.55	88.49	85.14
52	57.2	87.40	86.72	81.56
80	35.5	94.73	58.66	68.64
Mixtures with Oxygen				
84	7.2	65.75	78.07	82.37
88	10.0	92.78	99.43	95.41
93	12.0	96.01	88.61	91.47

3.4.3 Stickiness of Solid CO₂

The purpose of this study is to measure the solid CO₂ properties in terms of sticking to different surfaces, carried out at various pressures, temperatures, and compositions, and observing the stickiness behaviour as a function of time, when in contact with Teflon, stainless steel and ceramic. The results are summarised in Table 3.4. Pictures are included in Appendix C. Temperatures of CO₂ freeze out were also recorded in some cases.

Carbon Dioxide crystal deposition started on the sapphire cell walls because the cell wall was colder due to the heat transfer from the air bath, especially where the cooling rate was fast, causing uneven heat distribution. The solid CO₂ disconnecting itself from the sapphire walls and falling into the liquid phase can be related to the release of the heat of fusion as a consequence of the CO₂ solidification process shortly after formation. After reaching equilibrium, the solid sank to the bottom of the cell and the

stirring, set at high speed, accelerated that process. CO₂ agglomerates if left at static conditions for more than 60 minutes. This causes the formation of agglomerates or lumps of solid Carbon Dioxide flakes which restricted the movement of the magnetic stirrer on some occasions. The static nature of the test procedures may contribute to the non-uniform CO₂ particle distribution in the cell in the sense that there is no simultaneous liquid and solid formation which can drive solid particles down the vessel wall. In the static case, liquid hydrocarbons can occur before the CO₂ solidification depending on pressure and temperature. Hence problems with CO₂ solubility in liquid hydrocarbons can play a significant role in the solidification. In other words, the liquid hydrocarbon must be saturated before freezing can occur. Further, solid CO₂ crystal agglomeration occurs through a coalescence process, driven by surface energy and the electrostatic properties of CO₂ crystals.

Table 3. 4 Results on CO₂ freeze out from mixtures with Natural Gas

Coating material	CO ₂ mol%	Temp, °C	Pressure, bar	Freezing temp, °C	Stickiness
SS	70	-65	30	-61.4	Yes
SS	70	-65	18	-56.4	Yes
SS	70	-65	12	-57.1	Yes
SS	45	-65	30	-63.8	Yes
SS	45	-65	18	-61.2	Yes
SS	45	-65	12	-60.3	Yes
SS	20	-90	30	-72.5	Yes
SS	20	-90	18	-69.7	Yes
SS	20	-98.8	12	-97.6	Yes
Teflon	70	-65	30	-61.4	Yes
Teflon	70	-65	18		Yes
Teflon	70	-65	12		Yes
Teflon	45	-65	30		Yes
Teflon	45	-65	18	-62.7	Yes
Teflon	45	-65	12	-59.7	Yes
Teflon	20	-93	30	-73.4	No
Teflon	20	-90	18	-71.8	No
Teflon	20	-100	12	-80	No
Ceramic	70	-65	30	-60.5	No
Ceramic	70	-65	18	-59.7	No
Ceramic	70	-65	12		No
Ceramic	70	-65	12	-58	No
Ceramic	20	-90	30	-71.7	No
Ceramic	20	-90	18	-70.4	No
Ceramic	20	-100	12	-77.2	No
Ceramic	45	-65	30	-64.9	No
Ceramic	45	-65	18	-62.4	No
Ceramic	45	-65	12	-61.2	No

In some cases frozen matter stuck to the base of the mixer therefore blocking its movement. This happened only when the blades of the mixer were coated with a different material, and the bottom part remained stainless steel. A ceramic coating performed best in regards to non-stickiness of solidified Carbon Dioxide in all ranges of envisaged concentrations and pressures in a stirred cell. Teflon can safely be used in the flow of low-CO₂ containing mixtures, and high turbulence is required to prevent solid build-up if CO₂ concentration is above 20 mol%. Stainless steel was found to be the worst material to be used where freezing of CO₂ might occur because it adheres strongly to the surface, quickly causing blockages even when exposed to vigorous agitation.

CO₂ freezing curves obtained as a result of the current study fall inside the Solid-Liquid-Vapour equilibrium region published in (Donnelly & Katz ,1954) and (Davis et al., 1962) as shown in Figure 3.8. Good qualitative agreement with the data presented by Hwang (Figure 2.14) and Eggeman and Chafin (2003) can also be noted. Overall, higher Methane content delays precipitation.

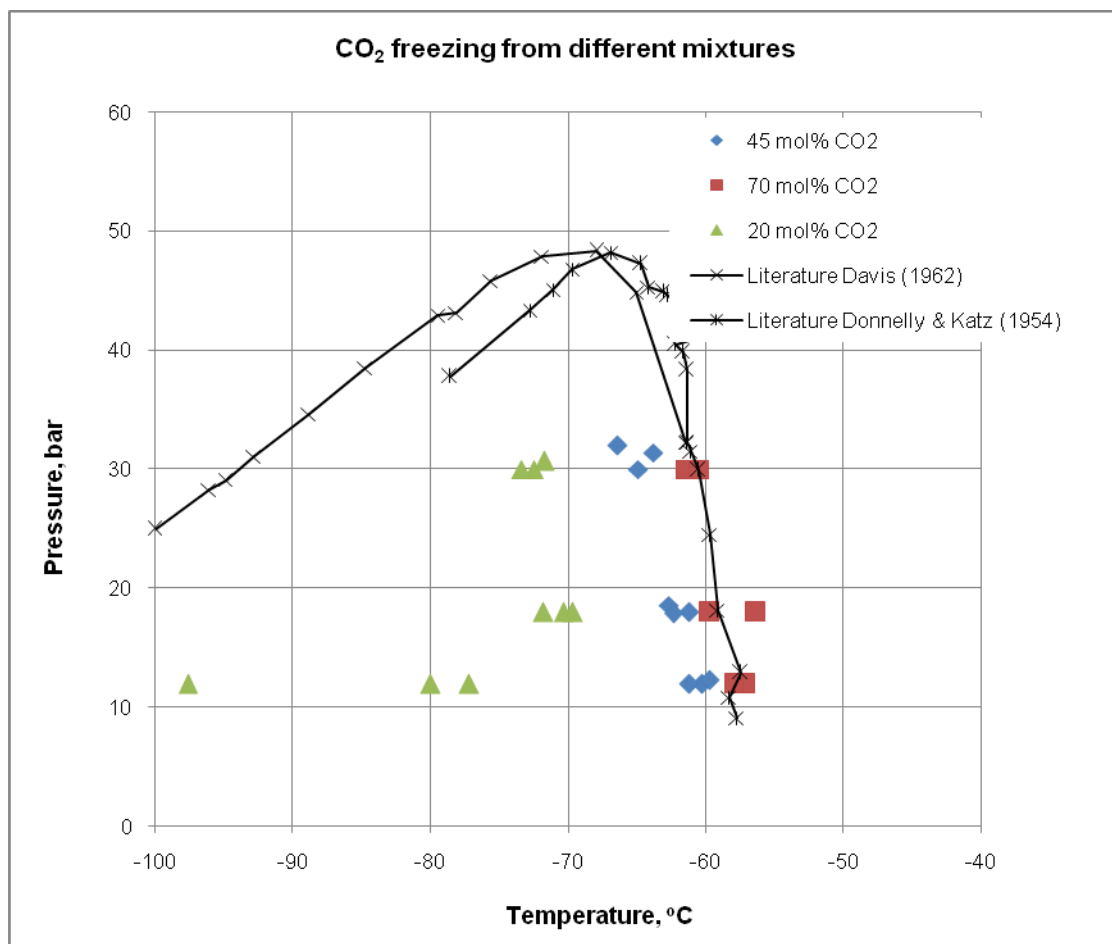


Figure 3. 8 Freezing of Carbon Dioxide from mixtures with Natural Gas

3.5 Thermodynamic Modelling of CO₂ Condensation and Freezing

The cool temperatures and high pressures encountered in much of the cryogenic condensation process lead to far from ideal thermo-chemical behaviour of the gas mixtures, in particular as CO₂ undergoes phase changes. In the ideal approximation, CO₂, mole fraction times total pressure, which is equal to partial pressure, provides the same behaviour as CO₂ vapour pressure. That is, in ideal systems CO₂ forms two phases through condensation or freezing whenever its partial pressure exceeds the vapour pressure of CO₂. The dew point and other lines produced by this approximation are not quantitatively or even qualitatively accurate over the entire range of temperatures and pressures. That is, CO₂ in light gases does not form an ideal system under these conditions. In the liquid region, the liquid that forms is a mixture of CO₂ and light gases. This fact makes prediction of phase changes a challenging process.

With the modern simulation options, the data and predictions agree reasonably well over most of the region and represent a substantial improvement compared with the ideal predictions. As temperature decreases, the size of the two-phase region increases. However, decreasing the temperature further forms solid rather than liquid CO₂. For example, at a nominal 20% CO₂ in Natural Gas, no solid forms at any pressure and temperature down to -70°C, in stark contrast to known ideal behaviour. However, the formation of a solid represents a substantial thermodynamic and energy advantage since the solid that forms contains essentially no other gases or impurities and does not have to go through a subsequent distillation process. Liquid distillation in air separation units represents the largest energy demand, mostly associated with cooling for the condenser. The operational challenges are commonly associated with solids handling.

As was mentioned above (Eggeman & Chafin, 2003), PR EOS does not predict CO₂ freezing very well; therefore a model based on the Soave-Redlich-Kwong EOS combined with the Michelsen stability algorithm was developed (Appendix F) as part of this research in order to better describe multiple phase behaviour of the gas mixtures with CO₂. The model was developed for CO₂-NG mixture rather than for CO₂-H₂ mixtures because in this research CO₂ freeze out from gas mixtures with natural gas was studied. The model can be easily modified for use with other gas mixtures by changing the input parameters such as composition, critical properties and binary interaction parameters.

Freezing temperature of the mixture at given pressure is calculated using data obtained with SRK EOS as follows

$$T_{fr} = \frac{V_m}{R_c} \frac{(P - V_p)}{\ln \left[\frac{(z_0)F_{cg}(z)_0 P}{V_p F_{cg} CO_2(V_p)} \right]}$$

Where

V_p – vapour pressure of solid CO_2 which can be found from Antoine Equation

$$\log_{10}(V_p) = A - \frac{B}{T + C}$$

With $A = 6.81128$, $B = 1301.679$ and $C = -3.494$ (NIST Chemistry webbook)

z_0 – compressibility factor calculated from SRK EOS

$$z^3 - z^2 + (A - B - B^2)z - AB = 0$$

With

$$A = \frac{\alpha a P}{R^2 T^2} \text{ and } B = \frac{b P}{R T}$$

Where

$$\alpha = \left[1 + (0.48508 + 1.55171\omega - 0.1561\omega^2)(1 - \sqrt{T_r}) \right]^2$$

With ω – acentric factor

T_r – ration of temperature over critical temperature

$$a = 0.42748 \frac{R^2 T_c^2}{P_c} \text{ and } b = 0.08664 \frac{R T_c}{P_c}$$

$F_{cg}CO_2(V_p)$ – fugacity of pure CO_2 at V_p calculated using SRK EOS as

$$\ln \phi = z - 1 - \ln(z - B) - \frac{A}{B} \ln \left(1 + \frac{B}{z} \right)$$

$F_{cg/cl}(z)_0$ – fugacity of CO_2 in the mixture (gas/liquid phase)

$$\ln \phi = (BB)_i(z - 1) - \ln(z - B) - \frac{A}{B} ((AA)_i - (BB)_i \ln \left[1 + \frac{B}{z} \right])$$

Where

$$(AA)_i = \frac{2}{(\alpha a)_m} \left[\sum_j^{n_c} (\alpha a)_{ij} \right] \text{ and } (BB)_i = \frac{b_i}{b_m}$$

With

$$(\alpha a)_m = \sum_i \sum_j y_i y_j (\alpha a)_{ij}$$

$$(\alpha a)_{ij} = \sqrt{(\alpha a)_i (\alpha a)_j (1 - k_{ij})}$$

$$b_m = \sum y_i b_i$$

V_m – molar volume of solid CO_2

$$V_m = \frac{M_w}{\rho}$$

With M_w – molecular weight

ρ - density

R_c – Universal gas constant

P – pressure of the system

Solubility of the solid can be also calculated using the values specified above as follows:

$$x(T) = \frac{V_p F_{cg} \text{CO}_2(V_p)}{P F_{cl}(z)_0} \exp \left[\frac{V_m}{R_c T} (P - V_p) \right]$$

Michelsen algorithm (Michelsen, 1982a,b) allows to assess the number of equilibrium phases by creating a second phase inside the given mixture and looking at its stability (negative free Gibbs energy) expressed in terms of the fugacity coefficients.

$$g(y) = \sum y_i (\ln y_i + \ln \varphi_i - h_i) \geq 0$$

Where

y_i – mole fraction in equilibrium phase

φ_i – fugacity calculated with SRK EOS as described above

$$h_i = \ln z_i + \ln \varphi_i(z)$$

With z – total mole fraction

Solution of this equation represents a global minimum on the free Gibbs energy surface, however it is important to have a good initial guess for y values. First guess can be obtained via flash-solution of the following equation

$$\sum \frac{z_i (k_i - 1)}{(1 + (k_i - 1)\beta)} = 0$$

Where k_i – equilibrium factor

β – amount of the corresponding phase

It is important to check the convergence on this step

$$\sum (R_i - 1)^2 < 10^{-10}$$

If it is not achieved, k_i should be corrected using the correction factor R_i as follows:

$$k_i^{(n+1)} = k_i^{(n)} R_i \text{ with } R_i = \frac{F_{cl}(x(k))_i}{F_{cg}(y(k))_i} \frac{1}{z_y}$$

Mole composition of the phases can then be found as

$$x_i = \frac{z_i}{1 + (k_i - 1)\beta} \text{ and } y_i = \frac{k_i z_i}{1 + (k_i - 1)\beta}$$

The freezing points of liquid and vapour are then found using corrected values for composition.

3.6. Conclusion

A comprehensive theoretical and experimental study of phase envelopes for mixtures containing 23 to 52 mol% CO₂ with Hydrogen was performed using a high pressure sapphire cell. Dew points were determined using two techniques: visual observations and by using a PT diagram. A fiber optic system fitted in the testing facility was also used in some cases to detect the phase change. Significant inconsistency in prediction of the dew points for the chosen mixtures especially at low concentrations of Carbon Dioxide under high pressures occurs if conventional simulation models are used. The experimental results were found to agree qualitatively with those known from the literature. This data describe thoroughly a narrow region of P-T-C conditions for such mixtures and can be used for development of an improved simulation model.

As part of the research on the new technology for CO₂ capture from IGCC flue gases, the amount of liquefied Carbon Dioxide which can be collected from the selected mixtures at different pressures was verified experimentally. More than 80% of the total CO₂ feed amount can be captured at pressures between 55 and 60 bar from mixtures containing about 40 mol% CO₂ in the feed (GE case). For the Shell case (37 to 38 mol% CO₂ in the feed) 50 to 60% capture was achieved at process pressures of 28 to 33 bar and at 53 bar the capture rate increased to 78 to 79% of the CO₂. More than 90% of CO₂ was separated from the Oxyfuel gas mixture at a process pressure of 10 to 12 bar.

Overall, it was shown that cryogenic condensation can be regarded as a prospective method for removal of CO₂ from process streams for power plants if energy consumption can be reduced by process integration with other techniques.

It was shown there was a high risk of plugging in stainless steel pipelines due to the CO₂ freezing. However, ceramic or Teflon coating can be suggested as a means for preventing blockage because solid CO₂ does not stick to such surfaces, and therefore can be carried through with the stream flow.

Following the discrepancy in prediction of the freezing points generated in conventional computer simulation software, a new modification to the Soave-Redlich-Kwong EOS was proposed based on the utilization of the Michelsen stability algorithm.

Chapter 4.

CO₂ Separation by Hydrate

4.1. Introduction

Cryogenic condensation, although shown to be effective for CO₂ capture from IGCC flue gases as a high purity liquid under pressure (Surovtseva et al., 2009a), needs substantial process integration to reduce energy requirements. A new prospective concept of utilisation of hydrate formation for economically feasible CO₂ abatement is proposed in this research for combination with a distillation technique.

Process gas obtained after cryogenic separation of CO₂ from IGCC gases at -55°C and 57 bar for the IGCC GE case, 28 and 53 bar in the IGCC Shell case have the compositions listed in Table (4.1).

Table 4. 1 CO₂ content in gas streams during processing with a new technology

Name of process	Pressure, bar	Initial CO ₂ content, mol%	CO ₂ content after cryogenic, mol%	Target CO ₂ after hydrate, mol%
IGCC GE	57	40	12	8
IGCC Shell	28	37	22	15
IGCC Shell	53	37	12	9

Further reduction of CO₂ by 30 to 40 mol% is targeted in this research through the utilisation of hydrate formation (see Chapter 7). Significantly lowered concentration of CO₂ in the feed compared to that addressed in the SIMTECHE/Nextant (US DOE NETL, 2008) and Chinese Academy of Science's (Li et al., 2010) projects constitutes the major obstacle for effective utilisation of the hydrate formation phenomenon. An appropriate chemical additive which would promote hydrate precipitation at reported conditions needs to be found. The most effective of the reported CO₂ hydrate promoters, Tetrahydrofuran (THF) was rejected due to its toxicity, and Hydrogen Sulphide had to be eliminated from the gas mixture due to laboratory safety restrictions. Based on previous experience in Methane hydrate promotion available at CGTA, in this study a new thermodynamic promoter for CO₂ removal by means of hydrate formation from mixtures listed in Table 4.1 was found. This finding can be a breakthrough for the developing field of CCS as there is an urgent need for capturing of Carbon Dioxide from streams containing low levels of CO₂.

4.2. Water Content of Sour Gases

Saturation properties of the gas phase, particularly water content, are crucial in the hydrate formation process. Engineers who design Natural Gas dehydration facilities or hydrate suppression systems in field gathering lines, roughly estimate the water content of gases with the McKetta-Wehe chart (Figure 4.1, GPSA, 2004). When natural gases contain substantial quantities of acid gases, H_2S and/or CO_2 , their water content can be considerably higher than the chart for sweet gas would indicate, especially at high temperatures and pressures above 1000 psi.

In this work the correlation by Kobayashi et al. (1987) is adopted for calculation of water content in a gas phase for all studied cases as shown in Figure 4.2 and by Equation 4.1. Hydrogen does not carry any significant amount of water due to low solubility, and low temperatures prevent significant saturation due to CO_2 present in gas phase. Therefore, the model is assumed to give a good approximation to the initial estimation of the feasibility of hydrate formation.

$$W = A.B^T, \text{ where} \quad (4.1)$$

W – water content in lb H_2O / mmscf wet gas

T – temperature, °F

A and B are constants defined as:

$$A = \sum_{i=1}^4 a_i \left(\frac{P-350}{600} \right)^{i-1}$$

$$B = \sum_{i=1}^4 b_i \left(\frac{P-350}{600} \right)^{i-1}$$

Although the model was initially developed to assess the water content in Natural Gas, it can be easily adjusted for use with any gas composition by varying coefficients a_i and b_i . The common result produced by this model and presented in Table 4.1 shows the saturation at the experimental conditions is insufficient for hydrate formation. As result, the hydrate promoters were the focus of this research.

In some of the recent models the vapour pressure of pure water is required as an input. Poor estimates of the vapour pressure will lead to poor estimates of the water content.

<div>Input data for calculating the water content:</div> <div><div>Pressure = 57.0 bar</div><div>Temperature = 1.0 °C</div></div> <div><div>Water content if T < 37 °C : 142.7 mg/m³_{std}</div><div>Water content if 37 °C < T < 82 °C : 211.4 mg/m³_{std}</div></div> <div><div>Water content = 142.7 mg/m³_{std}</div><div>187.3 ppmV</div></div>	calculated constants A, B			Constants used in equations:				
	A	T<37	37<T<82	Constants	Temperature ranges			
		3.09850	5.59001		T < 37 °C	37 °C < T < 82 °C		
	B	1.03174	1.02574		a1	4.34322	10.38175	
	°F -> °C:				a2	1.35912	-3.41588	
	°F = 9/5 (°C) +32				a3	-6.82391	-7.93877	
	Bar -> psi:				a4	3.95407	5.84950	
	1 bar = 14.504 psi				b1	1.03776	1.02674	
	lbs -> mg				b2	-0.02865	-0.01235	
	1 lb = 453592 mg				b3	0.04198	0.02313	
An assumption is made that due to low temperature and Hydrogen being the main component of the mixture, the water content estimation does not significantly differ from the real value, providing a good approximation	cf --> m3				The constants are used in an analytical expression describing the graphs referred to above.	$W = A.B^T$ $A = \sum_{i=1}^4 a_i \left(\frac{P - 350}{600} \right)^{i-1}$ $B = \sum_{i=1}^4 b_i \left(\frac{P - 350}{600} \right)^{i-1}$		
	1 cf = 0.0283 m3							
	lb/scf --> kg/m3std							
	1 lb/scf = 16.02 kg/m3std							
16.019 kg/m3std								

Water content is calculated according to the following:
W = water content in lbH₂O/MMscf
T = temperature (°F)
A and B are constants defined as:

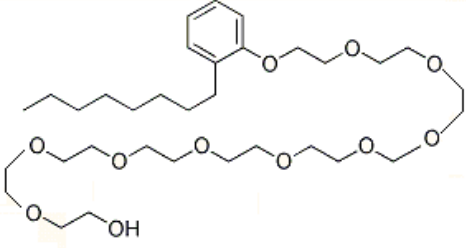
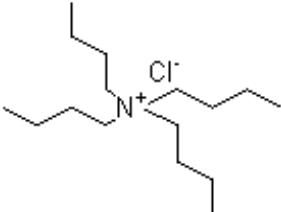
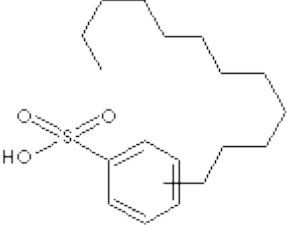
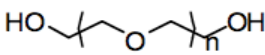
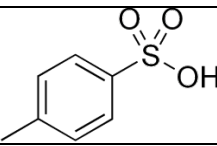
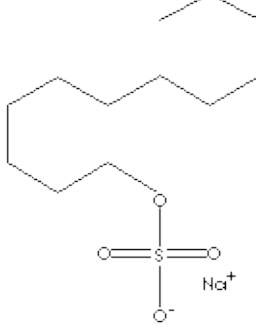
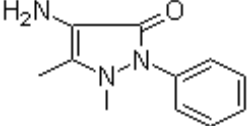
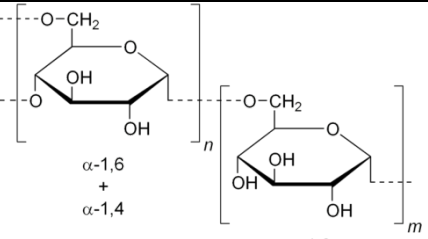
Figure 4. 2 Calculation sheet developed as part of this work

4.3. Materials and Procedures

Two sets of experiments were conducted to find a suitable promoter for additional separation of CO₂ from IGCC flue gases. In the first series, a thermodynamic promoter for CO₂ hydrate formation from pure CO₂, 47 mol% H₂-CO₂ and low-CO₂ gas mixtures containing 12 to 15 mol% CO₂ with H₂ was found using the full vision PVT sapphire cell described in Appendix A. Argon and Nitrogen do not form hydrate at the chosen conditions, therefore Argon and Nitrogen were eliminated and replaced with Hydrogen for simplicity. The chosen range of pressures and temperatures also does not allow for H₂-hydrate to form; therefore an error associated with such replacement of components is negligible. Compositions listed in Appendix D were prepared on a weight basis as described in Appendix B. The main focus was on hydrotropes as they were shown in (Gnanendran & Amin, 2004) to increase the hydrate formation temperature in case of Methane. Eight chemicals listed in Table 2 were tested and their effect on conditions of hydrate crystals nucleation and growth was evaluated. It was suggested according to the existing experience on promotion of hydrate formation that the optimum concentration of a promoter lies below 5 wt%, more often below 1 wt% as discussed in Chapter 2.2.1.2). A water-chemical solution was pressurised with a gas mixture to the desired pressure, and the cell was left overnight to reach equilibrium. The aqueous solution was constantly stirred to facilitate gas dissolution. The temperature of the cell was then lowered at between 2°C/hr and 4°C/hr till a solid was formed, and the temperature was recorded. The cell was then heated at 0.8°C/hr with no stirring and the behaviour of the solid was monitored, and hydrate dissociation conditions were recorded. Hydrate formation conditions are the same as dissociation conditions as discussed in Chapter 5.

When the solid hydrate dissociated, a sharp instant temperature drop was observed, and the pressure started rising rapidly. This temperature and pressure were taken as the hydrate formation conditions. If the solid phase started melting without any gas evolving, then it was frozen again, and the cell was depressurised. If there was no gas evolving, then the conclusion was made that no hydrate was formed. If some gas evolved from the frozen matter during depressurisation, the experiment was repeated. Each case when there was hydrate formation was repeated for confirmation.

Table 4. 2 List of chemicals potentially promoting hydrate formation

Name	Structure	Application
(Iso-)Octyl phenoxy polyethoxy Ethanol (Triton X-100)		Detergent. This is a mixture of alkylpolyglucosides, but the main component (about 80%) is Octylphenoxypolyethoxy Ethanol
Tetrabutyl Ammonium Chloride (TBAC)		Phase transfer catalyst; surface-active agents; antistatic agent; detergent; emulsifying agents
Sodium Dodecyl Benzene Sulphonate (SDBS)		Linear Alkyl Benzene Sulphonate is known from literature to promote pure CO ₂ and Methane hydrate formation
Polyethylene Glycol (PEG)		Used as inhibitor in high concentrations.
Para-Toluene Sulphonic acid (pTSA)		Was found to promote Methane hydrate formation (Gnanendran&Amin, 2004)
Sodium Lauryl Sulphate (SLS)		Based on the experience available at CGTA in Methane hydrate formation, low concentration of SLS can be used as a promoter
4-Amino phenazone (4-APh)		Analgesic and anti-inflammatory properties. Stimulates liver and is used to measure extracellular water.
Dextran		Blood volume expander, reduces viscosity of blood by increasing electronegativity.

In the second series, the optimum concentration of a chosen chemical was established using titanium cylinders having a 500 cc capacity and pressure rating of 100 bar. Three cylinders loaded with gas mixture and 170 cc water-promoter solution with different concentrations were used each time. Pressure in each bottle was monitored via pressure transducers connected to the metering equipment. The bottles were placed vertically on to the shaker contained in the cold room with temperature range from ambient to -25°C . To better agitate the aqueous phase, stainless steel rods were placed inside the testing cylinders. Temperature in the room is controlled electronically from outside, with accuracy of 1°C . Temperature was brought down to -5°C and the bottles were left on the shaker for 6 hours to ensure full conversion to hydrate and freezing of the excess water when the temperature inside the bottle reaches the ambient temperature. Freezing of any free water which was left unused for hydrate formation was necessary to ensure all gas stays trapped while equilibrium gas was fully vented and analysed. The fact of better preserving CO_2 hydrate at sub-zero temperatures was addressed in (Giavarini et al., 2007). After venting equilibrium gas through analyser, the bottles were insulated and left at room temperature between 20° and 30°C till all hydrate dissociated. The amount of the evolved gas was estimated on the basis of the pressure rise, and the composition was measured again. The effect of the promoter was quantified on the basis of achievable reduction in CO_2 concentration and is referred to as *capture rate*. The hydrate formation factor is not applicable in this case because of the excess water used, however the amount of CO_2 captured in the hydrate was calculated.

4.4. Results and Discussion

Hydrate cannot be formed from a low- CO_2 gas mixture at given pressures with liquid water without a promoter. Three hydrotropes out of eight tested surfactants displayed the ability to lift the hydrate formation temperature above the freezing point of water. Only one of these chemicals possesses properties suitable for its utilisation for large-scale hydrate production, and its optimum concentration is determined below.

4.4.1. Hydrotropes Testing

Results of the first series of experiments are summarised in Table 4.3. Sodium Lauryl Sulphate (SLS), Tetraethyl Ammonium Chloride (TEAC) and to a lesser extent 4-Aminophenazone (4-APh) were found to promote hydrate formation from gas

mixtures with low CO₂ concentration. At the proposed conditions, only CO₂ hydrate can be formed.

In the presence of 5 wt% 4-APh solids were formed from 14 mol% CO₂ mixture on the glass and above the surface during mixing at 58.9 bar and 2.9°C, and stayed there until ice was formed. This gas mixture would not form hydrate at this pressure with pure water. However, 5 wt% 4-APh did not cause any significant change in hydrate formation temperature from pure CO₂. Under pressure of 26.6 bar pure CO₂ would form hydrate at 6.35°C, and in the presence of 5 wt% 4-APh it has formed at 6.7°C. The effect of 4-Aminophenazone is not obvious, and further investigation is needed in order to conclude whether it can promote CO₂ hydrate formation within integrated cryogenic and hydrate technology.

Addition of 0.05 wt% SLS substantially increases the hydrate formation temperature from a gas mixture containing 14 mol% CO₂ (2.7°C at 60.6 bar), and can be used as a hydrate promoter. However, the solution foams abundantly during dissociation and stirring. Basically, all the aqueous phase is transferred into foam during depressurization. With this characteristic, the solution cannot be reused for hydrate formation as specified in the pilot plant design in Chapter 7.

Tetrabutyl Ammonium Chloride is an easily accessible chemical and is not dangerous. In the presence of 0.5 to 5 wt% TBAC in water, hydrate slurry is formed at temperatures about 1°C and pressure between 53 and 55 bar. When implemented in a larger scale hydrate forming facility, this slurry can be pumped into a separate vessel where the hydrate can be dissociated, and the released CO₂ can be further directed to storage and water recycled as described in Chapter 7. CO₂ release from the hydrate is accompanied by a slight foaming in the case of higher concentrations of the promoter, however, the foam settles down very quickly.

Other tested chemicals did not display any significant influence on phase transitions. In almost all cases the liquid phase became noticeably more viscous and jelly during cooling, especially at temperatures below 0°C. In some cases, experiments were repeated in the presence of pure Hydrogen, and the same phenomenon was observed. Therefore, this phenomenon was attributed to the effect of an additive on water during cooling.



Figure 4. 3 Slurry of CO₂ hydrate formed from 14 mol% H₂-CO₂ mixture in the presence of 1 wt% TBAC solution at 1.2 °C.

Table 4. 3 The effect of tested chemicals on CO₂ hydrate formation

CO2 in the feed mol%	Chemical	Chemical concentration, wt%	Phase change conditions		Aqueous phase description	Gas evolution after depressurisation
			P, bar	T, °C		
100			35.8	8.3	Hydrate	Yes
47			57.4	4.8	Hydrate	Yes
20			57.1	0.2	Ice	No
100	Triton X-100	~0.5 wt%	35.2	8.8	Hydrate	Yes
47	Triton X-100	~0.5 wt%	56.6	7.3	Hydrate	Yes
12	Triton X-100	~0.5 wt%	56.6	0.8	Gel	Little
12	TBAC	0.5 wt%	53.3	1.1	Viscous liquid	Yes
13	TBAC	5 wt%	53.2	0.9	Precipitating solid	Yes
13	TBAC	1 wt%	55.8	1.4	Slurry ¹	Yes
47	TBAC	1 wt%	54.2	7.3	Hydrate	Yes
12	SDBS	0.01 wt%	No changes until -5°C			
14	SDBS	0.05 wt%	56.7	0.1	Ice	Little
14	SDBS	0.1 wt%	No changes until -3.5°C			
13	PEG	0.1 wt%	59.5	0.9	Gel	Little
0	PEG	0.1 wt%	60.2	1.3	Gel to ice	No
16	PEG	0.5 wt%	59.4	-0.1	Viscous liquid	Little
15	PEG	1 wt%	No changes until -3°C			
15	pTSA	0.5 wt%	60	-0.3	Ice	Yes
47	Neutralised pTSA	0.5 wt%	59	5.3	Hydrate	Yes
13	Neutralised pTSA	0.5 wt%	98	-1.2	Ice	Yes
100	4-APh ²	5 wt%	26.6	6.7	Hydrate	Yes
14	4-APh ²	5 wt%	58.9	2.9	Belt of solid ³	
14	4-APh ²	0.5 wt%	55.2	0.6	Ice	No
14	4-APh ²	0.05 wt%	58.8	0.5	Ice	No
14	SLS ²	0.05 wt%	60.6	2.7	Thick Hydrate	Yes, Foam
14	SLS ²	0.5 wt%	58.4	0.2		Yes, Foam
15	Dextran	0.01 wt%	No changes until -4°C			
14	Dextran	0.05 wt%	57.5	0.7	Gel	Yes
14	Dextran	0.1 wt%	No changes until -2.6°C			
14	Dextran	1 wt%	59.3	1.1	Ice	Little

¹ See Figure 4.1² The results are not obvious, and experiments should be repeated for confirmation³ Some solid particles were sticking to the glass above the liquid surface and forming a 'belt'

4.4.2. Optimisation of TBAC Content

Aqueous solutions of Tetrabutyl Ammonium Chloride in the range of concentrations between 0.1 wt% and 2.5 wt% were tested to find the optimum amount of the promoter. It was expected on the basis of previous work (Gnanendran & Amin, 2004) to obtain a curve with maximum CO₂ capture at certain concentrations of the chemical, which is designated as optimum. For the specific case addressed in this research, such maximum was found at 1 wt% TBAC aqueous solution as represented in Table (4.4).

Table 4. 4 Choice of optimum concentration of TBAC

TBAC wt%	CO ₂ mol%		Pressure rise after hydrate dissociation, bar
	initial	equilibrium	
2.5	14	11	1.1
2.0	14	10	1.2
1.5	13	10	1.3
1.0	13	8	2.3
0.5	13	11	1.7
0.1	13	11	1.7

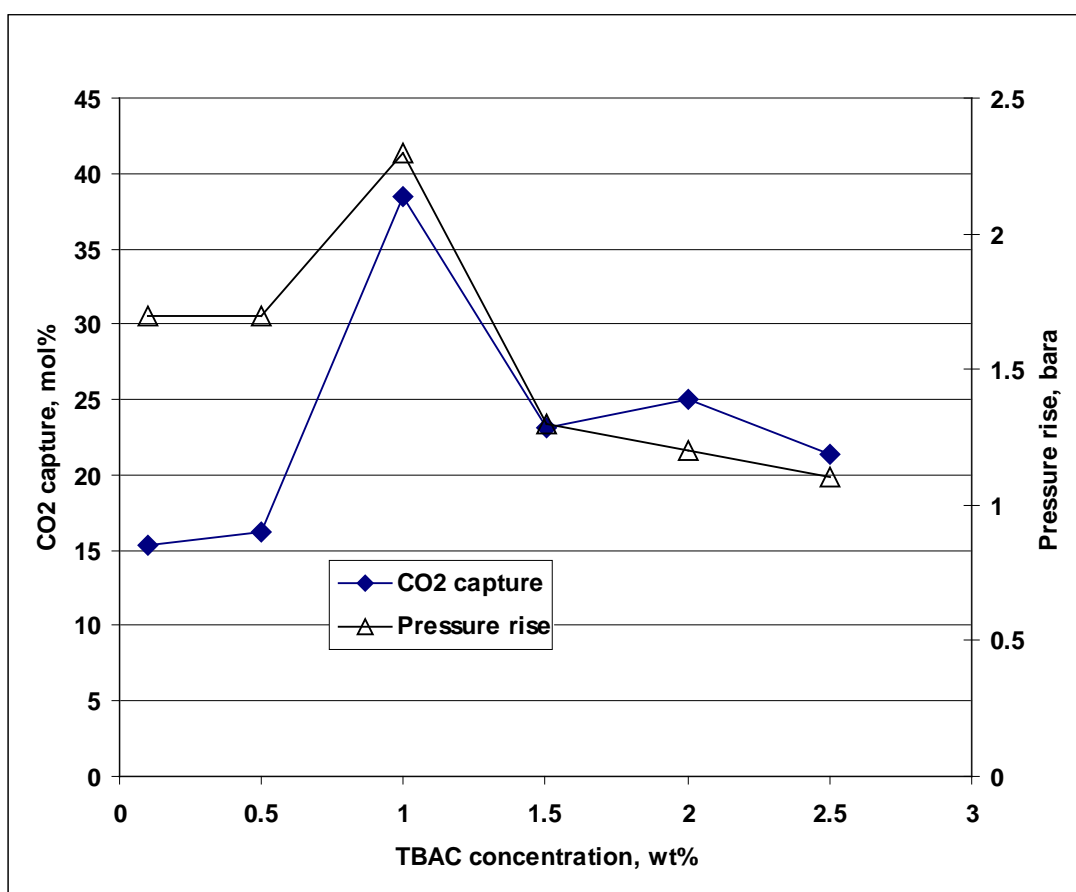


Figure 4. 4 Effect of TBAC concentration on the rate of CO₂ capture by hydrate

The ultimate reduction of Carbon Dioxide which can be achieved is 40 mol% of initial CO₂ content in the gas mixture. However, this figure may be lower at real process conditions because freezing of water will be avoided and therefore, higher temperatures will be involved. On the basis of the first set of experiments, operational temperatures should not be lower than -2°C to prevent freezing of the hydrate slurry.

The pressure rise after all hydrate has dissociated is indicative of the amount of CO₂ trapped inside the hydrate crystals. Best separation is achieved when most of the gas is converted into a solid, as is illustrated in Figure 4.4.

4.4.3. Quantifying TBAC Performance

The hydrate was formed in titanium bottles from 12 to 20 mol% H₂-CO₂ mixtures in the presence of 1 wt% TBAC-water solution. Three bottles were used at a time. The results from 3 sets of experiments are presented in Table 4.5. In the first set, bottles were filled with different compositions ranging between 11 and 20 mol% H₂-CO₂ mixtures. A reduction by 26.4 mol% on average was achieved at a pressure of about 60 bar and temperature of -1.5°C. Equilibrium gas was vented from each bottle to a pressure of 1 bar. After all hydrate dissociated, pressure was increased by 3 bar in the case of 17 mol% and 20 mol% initial CO₂ concentration, and by 2 bar in the case of the 11 mol% initial concentration. In all cases, a substantial increase in CO₂ concentration (up to 70mol% on average) in the gas phase was observed due to liberation of CO₂ from the hydrate.

The value for CO₂ capture obtained for the first mixture contained 20 mol% CO₂ appears to be erroneous (too low). This was caused by some of the solution transformed into hydrate staying in the valve through which the sample was taken. Therefore, the measured CO₂ concentration in the equilibrium gas exceeds the real value due to the presence of additional CO₂ from the hydrate in the valve. Liquid was also observed during venting in this case.

In the second set of experiments, the water-promoter solution from the first set was reused. In this case CO₂-nucleated water should lead to a higher capture rate. Three bottles were filled with 14 mol% H₂-CO₂ mixture to an average pressure of 64.4 bar. Reduction by 29 mol% CO₂ was achieved in all cases at -2°C and 58.5 bar.

In the third set, a fresh water with promoter solution was loaded in three bottles. The bottles were pressurised to 62.7 bar on average with 13.5 mol% H₂-CO₂ composition.

The bottles were placed vertically on the shaker to prevent any liquid in the sampling valve. Overall reduction by 30 mol% CO₂ was achieved in all cases at -2°C and pressure about 54 bar.

For calculations, an assumption is made that all gas trapped in the hydrate form is pure CO₂ because the temperatures and pressures involved exclude the possibility of Hydrogen-hydrate formation. This assumption was confirmed via calculating the amount of hydrogen remaining in gas phase after hydrate formation.

Table 4. 5 CO₂ capture from H₂-CO₂ mixtures by 1 wt% TBAC-water solution

Set No.	CO ₂ concentration, mol%		Amount of CO ₂ trapped in hydrate		Pressure rise after hydrate dissociation, bar	Temperature of formation, °C
	Initial	Equilibrium	Mol	Mol% of initial		
1	20	15	0.040	24	3	-1.5
	17	13	0.037	26	2.8	-1.5
	11	7	0.026	27	2	-1.5
2	14	11	0.034	29	2.6	-2
3	13.5	10	0.034	30	2.6	-2

4.5. Thermodynamic Modelling of CO₂ Hydrate

Initial estimation of the thermodynamic limits of hydrate formation is essential for any process involving hydrate deposition, particularly for hydrate utilisation as a means for gas capture and storage. Initial assumptions about the feasibility of CO₂ separation from Hydrogen by hydrate were made using the following sequence: chemical potentials of water in liquid and hydrate phase were calculated and equalised, fugacity of water was found, solubility of hydrate-forming gas was determined, and the activity coefficient of water in the presence of the promoter was estimated (Bouchemoua, 2009).

Any equilibrium implies the equality of chemical potentials of each component in all phases involved as defined by van der Waals-Platteeuw (1959). The Gibbs-Duhem theory is commonly used to describe equilibrium properties of liquid phases, for which the fugacity coefficients of components result from the solution of an equation of state (SRK, PR or others). Henry's law is usually applied for solubility calculations. In case any active additives such as hydrate promoters or inhibitors are involved, strongly non-ideal solutions will be best described by NRTL or UNIFAC (Universal Functional Activity Coefficient) models. Behaviour of gas molecules

encaged in a clathrate framework is regarded as being similar to an adsorption process based on Langmuir isotherms, however, with some distinctive differences.

4.5.1. Van der Waals-Platteeuw (VdW-P) Model

Early assumptions made by van der Waals-Platteeuw for application of classical statistical thermodynamics to hydrate equilibrium are as follows:

- Structure contains one guest gas molecule per cavity in the hydrate network.
- In a perfectly spherical cavity, gas-water interaction is described by binary potentials.
- Rotation of a gas molecule inside the cavity is not restricted.
- The only interactions taken into account are those between the gas molecules with the nearest neighbor water molecules.
- The shape of gas molecules does not influence the water packing pattern (the energy contribution from water is constant).

Chemical potentials of pure water and water in hydrate are equal at equilibrium,

$\mu_H = \mu_W$, where

μ_H – chemical potential of water in hydrate phase

μ_W – chemical potential of water in water or ice phase

This can be rewritten as

$\Delta\mu_H = \Delta\mu_W$, where

$\Delta\mu_W = \mu_p - \mu_W$, with

$\Delta\mu_H = \mu_p - \mu_H$

μ_p – is the reference chemical potential of an unoccupied hydrate lattice

4.5.2. Calculation of $\Delta\mu_W$

The Gibbs-Duhem expression describing an ideal solution relationship for the water and dissolved gas phase is written as follows:

$$\frac{\Delta\mu_W}{RT} = \frac{\Delta\mu_W^0}{RT_0} - \int_{T_0}^{T_F} \frac{\Delta h_W}{RT^2} dT + \int_0^P \frac{\Delta v_W}{RT} dP - \ln \gamma_W x_W, \text{ where}$$

$\Delta\mu_W^0$ – experimentally determined reference chemical potential determined by the structure of the hydrate lattice

x_W – is the mole fraction of water in the water-rich phase

γ_W – is the activity coefficient which should be calculated using NRTL or UNIFAC model in case inhibitors or promoters are used

$$\Delta h_W = \Delta h_W^0 + \int_{T_0}^T \Delta C_{P_W} dT, \text{ where}$$

$$\Delta C_{P_W} = \Delta C_{P_W}^0 + b(T - T_0)$$

$\Delta C_{P_W}^0$ – is an experimentally determined reference heat capacity difference between the empty hydrate lattice and pure water phase in the reference temperature region

Δh_W^0 – is an experimentally determined reference enthalpy difference

b – adjustable parameter determined for a number of substances by Holder and Manganiello (1982).

The chemical potential of water in different types of hydrates differs substantially due to characteristic distortions imposed by various guest molecules. This will be particularly important in the case of a multiple component gas mixture forming a hydrate. Lee and Holder (2000&2002) suggested the following improvement to the calculation of $\Delta\mu_W^0$ accounting for excess free energy:

$$\Delta\mu_{mix}^0 = \Delta\mu_{mix}^{0,ideal} + \Delta\mu_{mix}^{0,excess}, \text{ where}$$

$$\Delta\mu_{mix}^{0,excess} = Z_1 Z_2 [A + B(Z_1 - Z_2)], \text{ where}$$

A, B – experimentally determined constants

Z_1, Z_2 – molar fractions of components 1 and 2 in hydrate

Solubility of hydrate-forming gases in water is calculated using Henry's law.

4.5.3. Calculation of $\Delta\mu_H$

Expression for chemical potential of water in the hydrate phase is given by a combined van der Waals-Plateeuw and Langmuir equation (Chen, 1996):

$$\Delta\mu_H = RT \sum v_i \ln(1 - \sum C_j^i f_j(T, P))$$

Langmuir constants for spherical molecules of j -component in i -cavity are determined by integrating the interaction potential over the cavity volume.

$$C_{ij} = \frac{1}{kT} \int_0^{2\pi} \int_0^\pi \int_0^R \exp\left(-\frac{W}{kT}\right) r^2 \sin \theta dr d\theta d\Phi, \text{ where}$$

k – Boltsman constant, J/K

In a perfectly spherical cell with even distribution of water molecules on the surface, the gas-water molecular interaction can be described in terms of the Kihara potential (Kihara, 1953; McKoy & Sinanoglu, 1963):

$$W(r) = 2Z\varepsilon \left[\frac{\sigma^{12}}{R^{11}r} \left(\delta^{10} + \frac{a}{R} \delta^{11} \right) - \frac{\sigma^6}{R^5 r} \left(\delta^4 + \frac{a}{R} \delta^5 \right) \right], \text{ where}$$

σ – is the collision radius between molecule of guest gas and water, pm

r – is the distance between the centres of gas and water molecules , pm

ε – Kihara energy per molecule parameter, J/molecule

a – Kihara core diameter, pm

Z – cavity coordination number

R – gas molecule radius, pm

$$\delta^n = \frac{1}{n} \left[\left(1 - \frac{r}{R} - \frac{a}{R} \right)^{-n} - \left(1 + \frac{r}{R} - \frac{a}{R} \right)^{-n} \right]$$

The Langmuir model is limited to symmetrical interaction with the closest water molecules which are in immediate contact with encapsulated gas molecules. John et al. (1985) has expanded this model to account for asymmetry through an acentric factor and additionally, included relations with remote water shells which can be calculated from virial coefficient data.

$$C_{ij} = \frac{4\pi}{kT} \int \exp \left(- \frac{W_1(r) + W_2(r) + W_3(r)}{kT} r^2 dr \right), \text{ where}$$

W_1, W_2, W_3 – contributions to the Kihara potential function from the first, second and third aqueous shell

4.5.4. Improvements to the Model

The effect of lattice stretching due to gas molecule size on the reference chemical potential difference between the empty lattice and water is calculated by Holder et al. (1993). A new concept, which included local stability, linked cavity, basic hydrate, and basic hydrate component, was proposed in the late 90's (Chen & Guo, 1996).

In 2001, Trout developed a method to extract potentials from the temperature dependence of Langmuir constants for clathrate hydrates by using an analytical “inversion” method based on the standard statistical model of van der Waals - Plateeuw (Martin et al., 2001).

Sloan proposed a method in 2002, which optimized the model by direct incorporation of spectroscopic data (Ballard & Sloan, 2002).

The model can be further improved by incorporating the effect of promoting substances into it. However, the mechanism of promoting action is not clear as discussed in Chapter 2.2.1.2; therefore obtaining reliable experimental results is vital.

4.6. Conclusion

The concept of the promotion of CO₂ hydrate formation from low concentration H₂-CO₂ gas mixtures was investigated using eight different surfactants. It was found that strongly diluted aqueous solutions of 4-Aminophenazone, Sodium Lauryl Sulphate or Tetrabutyl Ammonium Chloride have the potential to promote conversion of CO₂ into clathrate form.

The effect of 4-Aminophenazone was not studied thoroughly.

Equilibrium temperature for CO₂ hydrate formation in the presence of Sodium Lauryl Sulphate is remarkably higher at the same pressure than in the case of pure water. However, if the solution is to be recycled as proposed in the Integrated Cryogenic and Hydrate CO₂ Capture Project, SLS would not be a favourable additive due to the formation of tremendous amounts of foam forming during depressurisation of the system followed by hydrate dissociation.

On the basis of the current study, Tetrabutyl Ammonium Chloride has the prospective of being used for CO₂ capture in solid form from 12 mol% H₂-CO₂ gas mixtures which are obtained after CO₂ removal by cryogenic condensation. Three sets consisting of three single experiments have been conducted in order to confirm the CO₂ capture rates. It was shown that 21 to 28 mol% CO₂ can be removed from 12 to 15 mol% CO₂-containing gas mixture brought in contact with 1 wt% TBAC-water solution at -2°C and pressure about 55 bar.

Chapter 5.

Hydrate Management and MEG Concentration

5.1. Introduction

This work presents extensive experimental data and hydrate curves in various concentrations of MEG based on the hydrate dissociation point rather than formation curves. Temperature reduction at constant pressure is the most commonly employed technique for hydrate formation and detection in the laboratory. However, due to substantial induction time, the experiment is very time-consuming and some error in readings is unavoidable. According to the phase diagram, hydrate formation and decomposition happen at the same conditions. Hydrate dissociation is more apparent to observe both visually and when using basic equipment such as thermocouples and pressure indicators. Trapped gas begins to evolve from a water lattice leading to distinguishable bubble formation and free water release. This occurs at a threshold temperature, and accompanied by a continuous increase in pressure until all crystals have decomposed. A comparison of experimental hydrate formation and dissociation curves is presented in this Chapter.

The MEG effect on hydrate formation from three gas mixtures with different Methane/CO₂ ratios was quantified in terms of equilibrium temperature reduction, and the produced hydrate curves were plotted against the most commonly used commercial computer software. The results showed that the hydrate dissociation curves can vary widely compared to hydrate formation curves obtained using commercial PVT software. The error is critical for systems containing high concentrations of the phase-shifting chemicals (promoters and inhibitors) added to the hydrate forming system. This is particularly important for the development of the new prediction models.

As the aqueous phase was constantly mixed during cooling and prior to and during hydrate formation, the electric loading on the stirring system was measured. This allowed for the development of equations and graphs for determination of hydrate formation relying on viscosity changes. This technique bears great potential in the field of *in situ* monitoring of the hydrate formation and is being developed further at the School of Engineering and IT at Charles Darwin University for CO₂ hydrates application.

Common inhibitors used in industry for hydrate management are Methanol (MeOH) and glycols, particularly widely used are monoethylene glycol (MEG), diethylene glycol (DEG) and triethylene glycol (TEG).

Methanol is more effective in pipeline services due to its high vapour pressure and high miscibility with water presented in a vapour phase. The formed equilibrium system enables to the lowering of the fugacity of water to the levels where the inhibition effect is sufficient to prevent plugging of the pipeline. Methanol is also less expensive than glycol. However, when using Methanol as an inhibitor, safety constraints must be considered, due to its low flash point (58°F). Methanol is usually unrecoverable and therefore lost during the process.

Recoverability is one of the most fundamental factors considered at any process facility, and the advantages of glycols utilisation are obvious for such systems. Glycols stay in the liquid phase at the process conditions which allows for easy regeneration and reuse. To be truly effective in a pipeline, it has to travel far enough from the injection point to establish a thin film which uniformly coats the entire inner surface of the flow conduit. Any bare, uncoated surface will collect gas hydrate crystals when they form from the vapour phase and initiate the growth of a hydrate plug. A high flash point (about 200°F) eliminates safety issues during glycols utilisation. Glycols are also more suitable in low temperature environments.

When using glycol as an inhibitor in processes which comprise glycol regeneration, air contact with the aqueous solution must be avoided. If such contact occurs, the oxidized glycol solution generates acids which are corrosive and can damage the process equipment. Blanketing of the glycol tank by an inert gas, sweet and dry gas, or an air-free steam must be provided.

Injection system

The inhibitor can be injected by pumps (portables for small pipes or fixed) driven by gas expansion turbines, compressed air or motors. When glycol is used, spray nozzles are installed to atomize the glycol and spray it uniformly on any peripheral surfaces. For the hydrate inhibition of large flow lines, the inhibitor can be sent into the pipe under slug form locked by pigs and pushed by the flowing gas to completely coat the inner pipe wall.

Calculation of required inhibitor volumes

Rapid calculation of inhibitor rates or volumes to be injected is based on the Hammerschmidt formula:

$$W = \frac{100 * M * \Delta T}{K_H + M \Delta T}, \text{ where} \quad (5.1)$$

M – molar mass of the inhibitor in g/mol

ΔT – temperature depression required. Usually estimated as the difference between the gas hydrate-forming temperature without inhibition and the lowest temperature in the transportation pipe line or in the process unit.

K_H – a constant with value 1297 for temperature expressed in °C or 2355 for °F

W – final concentration of inhibitor in the aqueous solution. The aqueous solution comprises the water that condenses from the gas, the initial pipe line water content (if any) plus the inhibitor. The method used for estimation of water content in the gas phase is described in Chapter 4.

The above formula is fully adequate for glycol inhibition. When dealing with Methanol, one has to take in consideration the quantity of Methanol which is vaporized in the gaseous phase. Some authors suggest replacing the constant K_H in the Hammerschmidt formula by other values, specified for each inhibitor listed in Table 5.1.

Table 5. 1 K_H constant for Hammerschmidt equation for calculation of necessary amount of inhibitor

Inhibitor	Methanol	MEG	DEG	TEG
Constant (for °F)	2335	2200	4367	4400

Choice of hydrate prevention methods

Table 5.2 displays general guidelines for the choice of hydrate prevention methods according to the cases to be considered:

- Gas transportation in pipelines
- Gas processing
- Gas regeneration process

Table 5. 2 Guidelines for gas hydrate inhibition and gas dehydration

Gas from wells (Natural Gas / associated gas) is routed to:	Focus on	Hydrate inhibition			Gas dehydration	
		Pipeline heater	Methanol injection	Glycol injection	Glycol absorption	Dry desiccant absorption
Separation & Transportation	Hydrate formation	✓ ⁴	✓	✓	✓	
	Stress corrosion		✓ (+ corrosion inhibitor)	✓ (+ corrosion inhibitor)	✓	
	Water dew point				✓	
Gas refrigeration processes (LNG, NGL JT valve and condensate recovery)	External mechanical refrigeration			✓	✓	
	Internal valve refrigeration			✓	✓	
	Turbo expander			✓ ⁵	✓	✓
	LNG Plant					✓
Other processing facilities	Compression		✓		✓	

5.2. Experimental

Hydrate was formed in the presence of 0 to 65 wt% MEG aqueous solution in the high pressure stirred sapphire cell described in Appendix A from three mixtures containing CO₂, Nitrogen and hydrocarbons C1-C9 and in the range of pressures 10 to 300 bar. Pure industrial grade gases for samples were supplied by BOC Australia, and liquid hydrocarbons of at least 99.9% purity were obtained from Sigma Aldrich. Compositions listed in Table 5.3 were prepared on a weight basis as described in Appendix B in accordance with masses presented in Appendix D and confirmed by GC-analysis at CoreLab. Experimentally observed hydrate formation and dissociation conditions were recorded and plotted against data predicted using conventional EOS and process models in commercial computer software: HYSYS, Hydrate, PVTsim, PIPESim and Multiflash. Mixing was kept at the same speed

⁴ For small pipelines

⁵ Although some manufacturers of turbo expanders (like Mafi-Trenh) consider glycol injection upstream of the machine as not advisable, some operators use this method for hydrate-formation prevention

throughout the cooling cycle while the electrical current changed due to changes in viscosity of the solution, especially when the first nuclei of hydrate formed.

5.2.1. Sample Preparation

Synthetic gas was used in all the experimental work. The gas was mixed with water and inhibitor in a pressurized full visual sapphire-cell PVT system (Appendix A). The sample was left for 24 hours to reach equilibrium before carrying out the experiments. The temperature of the hydrate sample was maintained for 24 hours after loading it into the cell and pressurizing it to the desired pressure.

Liquid hydrocarbons were weighed separately in 10cc syringes and loaded into the evacuated cell. Aqueous solution with or without MEG was added next. Gaseous components were weighed in evacuated bottles and fully transferred into the cell. The system was left for 24 hours exposed to stirring at a pressure of about 300 bar and temperature of about +30°C to ensure all liquid components were in a gas phase.

Table 5. 3 Compositions used

Composition, mol%			
	Sample 1 (S1)	Sample 2 (S2)	Sample 3 (S3)
Nitrogen	3.98	8.159	1.25
Carbon Dioxide	5.54	1.987	10.69
Methane	81.54	83.257	76.31
Ethane	4.69	3.904	7.48
Propane	2.21	1.4	3.19
Butanes	1.21	0.676	0.94
Pentanes	0.48	0.29	0.08
C6 fraction	0.24	0.158	0.06
C7 fraction	0.07	0.172	
C8 fraction	0.02		
C9 fraction	0.01		

5.2.2. Experimental Procedures.

The hydrate formation tests were carried out by lowering the cell temperature at about 4 degrees per hour at constant pressure until hydrate crystals was observed. Further, the cell was left at constant conditions and agitated with a magnetic mixer to allow for transformation of all free water into solid hydrate. The temperature and pressure were monitored and recorded during hydrate formation.

After the hydrate formation, the process was reversed in order to study dissociation, that is, temperature was slowly increased at a rate of one degree per hour, with this rate reduced to 0.8°C degrees per hour for tests with high MEG concentrations of

over 50 wt% MEG. All experimental parameters (pressure, temperature, gas volume) were monitored, recorded and stored automatically. The hydrate melting point observation was determined by monitoring a few parameters. Ideally, when the pressure starts to rise at a threshold temperature indicating the start of the decomposition, the amount of gas consumed during formation was compared to the gas evolved to check on the mass balance closure. An important indication of hydrate dissociation was that the temperature sensor at the bottom of the cell started to read a lower temperature than the sensor placed on the top of the cell in the gas phase. Another indication was through the pressure control positive displacement pump which starts moving backwards to compensate for the evolved gas.

From further experiments it was deduced that the rate of crystallization of hydrate is also closely related to the rate of stirring. In this case, the experiments were set at three different stirring rates of 100, 150, and 200 rpm. It was also observed that the higher rate of stirring also increases the ultimate consumption of gas, before the appearance of a hydrate crystal.

The electrical load on the stirring system was recorded during experiments, and equations for determination of viscosity were developed as described in Appendix F. These can be used for early detection of hydrate formation and are applied in Chapter 6.

All hydrate formation and dissociation observed visually in each experiment was recorded on video. Pictures of hydrates formed in the experiments are presented in Appendix E along with some common observations.

5.3. Hydrate Formation Temperature (HFT) and Hydrate Dissociation Temperature (HDT)

Investigation of HFT and HDT was conducted for synthetic gases listed in Table 5.3, and experimental results were plotted against most often utilized commercial computer software:

- Hydrate
- HYSYS with Peng-Robinson (PR) Equation of State (EOS)
- PIPEsim with PR EOS
- PVTsim with Soave-Redlich-Kwong-Peneloux EOS
- Multiflash with CPA-Infochem model

Hydrate was formed and dissociated at five different pressures; the tests were repeated twice to confirm the results and repeatability. The aqueous solution contained between 0 and 65 wt% inhibitor MEG. Results produced during experimentation on Sample 1 synthetic gas in the presence of 40 wt% and 45 wt% MEG and the same pressures were also compared with theoretically predicted conditions of hydrate formation.

5.3.1. Experimental HFT vs HDT

First, comparison between experimentally found conditions for hydrate formation and decomposition was made (Table 5.4 and Figure 5.1). Generally, recorded HDT was 2 to 10°C higher than HFT in all cases with the difference increasing at lower pressures for each composition of the aqueous phase as shown in Table 5.4 and Figure 5.1. This is due to overcooling required for the first hydrate nuclei to reach critical size and start depositing. Common observations made were that

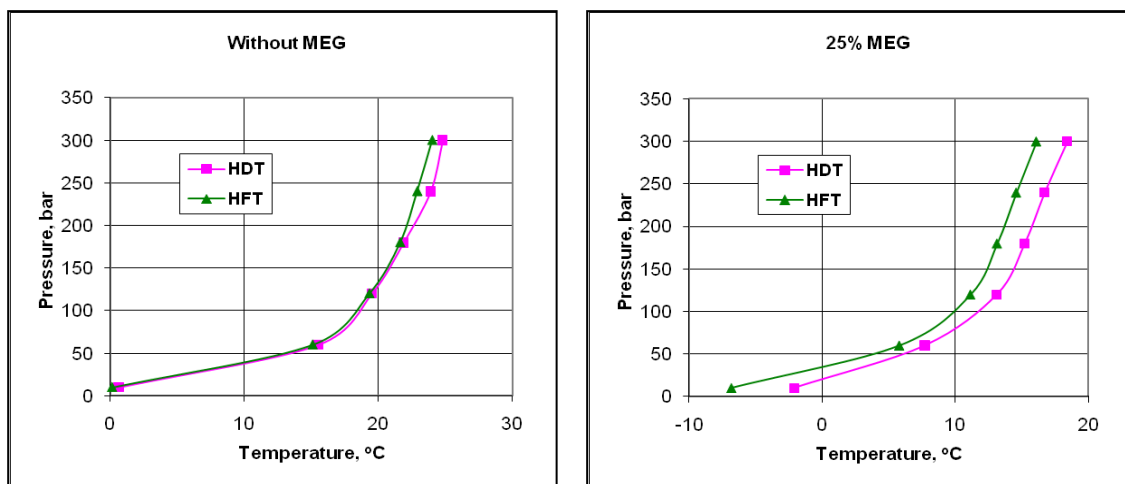
- The HDT is lower with higher concentration of MEG
- The HDT increases substantially when the HFT is below zero
- The HDT is slightly higher at higher pressure
- **Table 5. 4 Experimental HFT and HDT for Sample 2 synthetic gas**

Pressure, bar	without MEG		25% MEG		42% MEG		46% MEG	
	HFT	HDT	HFT	HDT	HFT	HDT	HFT	HDT
300	24.02	24.8	16.1	18.4	6.4	8	4	5.5
240	22.9	23.9	14.59	16.7	5.19	6.52	2.4	3.6
180	21.63	21.88	13.15	15.2	3.69	5.05	1.03	2.18
120	19.33	19.5	11.15	13.1	2.1	3.5	-0.31	1.06
60	15.1	15.5	5.81	7.7	-1.3	0.71	-4.5	-2.52
10	0.15	0.6	-6.8	-2.1				
Pressure, bar	50% MEG		57% MEG		61% MEG		65% MEG	
	HFT	HDT	HFT	HDT	HFT	HDT	HFT	HDT
300	0.56	2	-2.5	-0.54	-4.65	-3.92	-5.3	-4.2
240	-0.25	1.56	-3.2	-1.56	-7.26	-6.46	-8.31	-7
180	-1.49	0.13	-5	-3.27	-10.45	-9	-11.7	-10.24
120	-3.4	-2	-6.39	-5	-13.55	-11.75	-15.74	-13.47
60	-7.4	-4.73	-9.4	-7.67	-15.77	-14.08	-25.17	-20
10	-19.8	-13.54	-22.7	-13.54				

The increase in HDT when the HFT is below zero could be related to ice formation. If this assumption is valid, this signifies that the ice formation is not a welcome event during dissociation because it slows down the dissociation rate.

The MEG (hydrate inhibition) mainly dissolves in the free water phase thereby reducing the fugacity of water which reduces the tendency of hydrate formation. So the MEG modifies the properties of the water phases, not the hydrate phase. For example, the MEG depresses the ice point, reduces the vapour pressure of water, that is, it has a dehydrating effect on the vapour and hydrocarbon liquid phases (Mehta et al., 2006).

Some interesting observations were made during the experiments such as the increase of gas solubility before hydrate appearance at higher rates of agitation. The most interesting phenomenon was the liquid hydrocarbons in the water phase going from clear droplets to something like emulsion chain materials that disperse after the hydrate formation (this was captured on the video). This can be evidence of the fact that the MEG itself vaporises and also dissolves in the hydrocarbon liquid forming an emulsion just before the hydrate formation temperature. Another observation regarding the physical shape of the hydrates is that at first the hydrates are forming large but relatively dry lumps. With an increasing inhibitor concentration from 25 to 65 wt% the hydrates become more adhesive, depositing on the wall and agglomerating into larger chunks in the bulk fluid. At higher concentrations up to the full inhibition point, smaller hydrate particles form a suspension and gel-like structure in the bulk fluid.



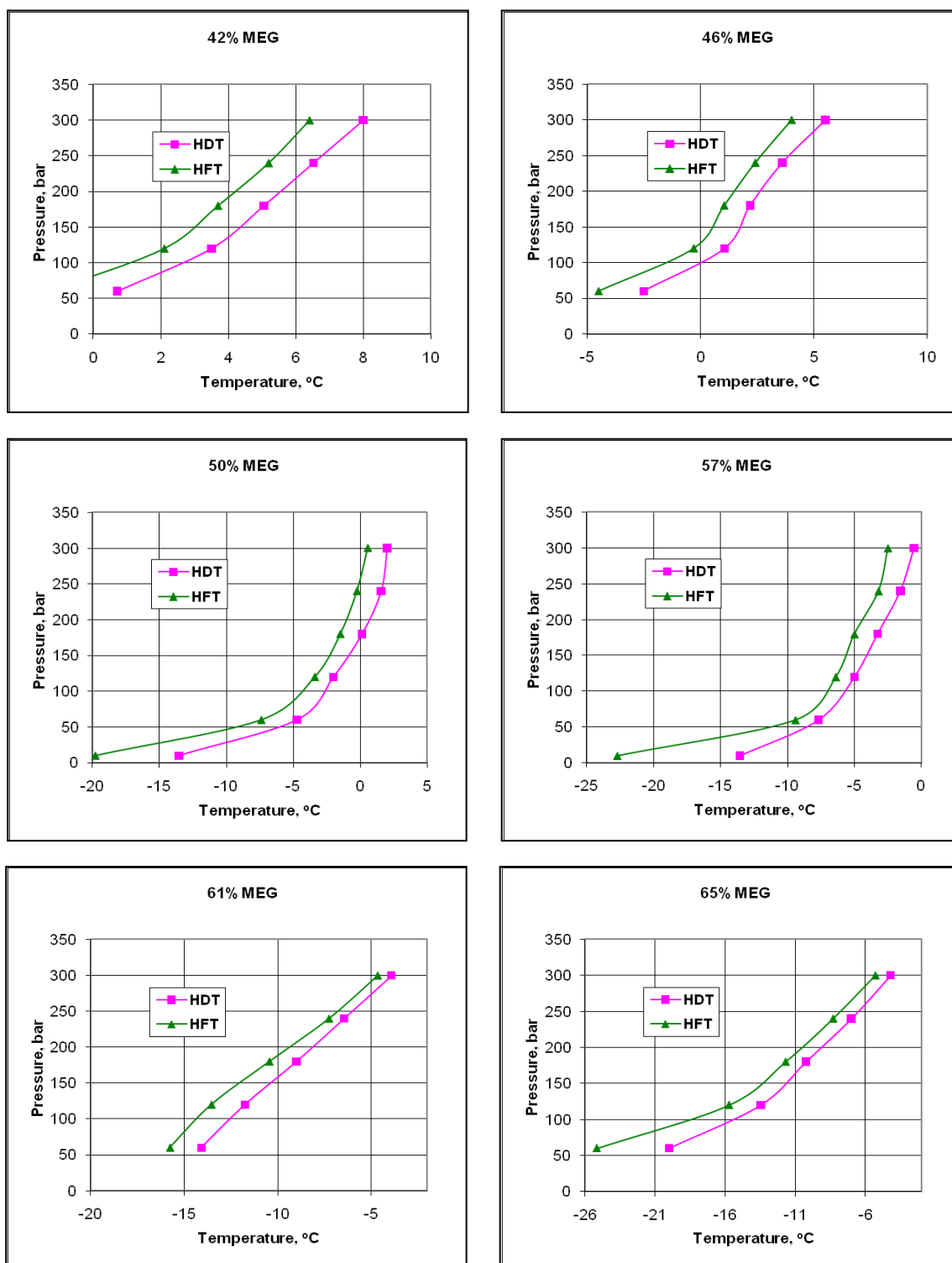


Figure 5. 1 Comparison of HFT and HDT for Sample 2 synthetic gas in contact with 0 to 65 wt% MEG-water solutions

5.3.2. Assessment of the Accuracy of Prediction

Numerical results for S2 hydrate equilibrium temperature obtained from PVTsim and PIPEsim computer simulation software and experimentally are given in Table 5.5. According to the phase diagram, formation and dissociation should occur at the same

conditions. Therefore experimental HDT has been compared with HFT generated by the different software packages. All results can be described by one of the three plots presented in Figures 5.2 to 5.4. In the first case, experimentally observed HDT is higher than theoretically predicted HFT. Systems with a concentration of MEG of 0 to 25wt% show this kind of behaviour. The difference in temperatures is about 1°C for all cases except when hydrate formed at sub-zero conditions at 10 bar in the presence of 25 wt% MEG. The same issue was addressed in the previous sub-Chapter and can be related to changes in the physical state of water. The second group represents hydrate formation from 40 to 50 wt% MEG in water solution and can be predicted quite well using the commercial computer program. Experiments conducted for Sample 1 synthetic gas in the presence of 40 MEG and 45 wt% MEG produced the same result in one simulation package predicting hydrate formation very good in the whole range of pressures tested (Figure 5.5). Systems with high MEG content belong to Type 3, where experimental results have a strongly deviating pattern of behaviour with the difference reaching 10°C.

Experimental points for Sample 3 synthetic gas are shown in comparison with the simulation results in Figure 5.6. Up to a concentration of 40 wt%, the discrepancies between experimental data and data generated in Multiflash for PIPEsim are less than 0.5°C, and for a concentration of 45 wt% of MEG, the maximum discrepancy is less than 1°C. For concentrations above 50 wt% MEG, the quality of the prediction decreases but is still acceptable as the maximum discrepancy is 1.5°C. There is also a good match between the experimental data and the prediction by HYSYS except for the zero MEG case; however, other software packages produce a higher discrepancy with the maximum error produced by PVTsim. In all cases with concentrations of the inhibitor above 45 wt%, the discrepancies increase, especially at high pressure.

Table 5. 5 Experimental HDT for Sample 2 in comparison with design figures

Pressure, bar	300	240	180	120	60	10
0 wt% MEG						
PVTsim	24.08	22.75	21.19	19.09	14.85	0.46
PIPEsim	23.1	21.8	20.23	18.3	14.1	0.16
experiment	24.7	23.8	21.78	19.4	15.4	0.5
25 wt% MEG						
PVTsim	17.34	16.06	14.59	12.67	8.71	-5.55
PIPEsim	15.8	14.5	13.1	11.1	7.2	-6.7
experiment	18.3	16.6	15.1	13	7.6	-2.2
42 wt% MEG						
PVTsim	10.45	9.22	7.83	6.09	2.42	-11.68
PIPEsim	7.3	6.1	4.9	3.1	-0.2	-14.2
experiment	7.9	6.42	4.95	3.4	0.61	
46 wt% MEG						
PVTsim	8.36	7.13	5.77	4.08	0.51	13.54
PIPEsim	4.8	3.5	2.1	0.6	-2.9	-16.8
experiment	4.26	2.66	1.1	-0.2	-3.88	
50 wt% MEG						
PVTsim	6.01	4.8	3.46	1.83	1.63	15.62
PIPEsim	1.7	0.6	-0.8	-2.2	-5.5	-19.3
experiment	0.9	0.04	-1.1	-2.83	-6.44	-18.1
57 wt% MEG						
PVTsim	1.12	-0.08	-1.37	-2.87	-6.09	-19.92
PIPEsim	-4.8	-5.8	-7	-8.5	-11.3	-25
experiment	-0.64	-1.66	-3.37	-5.1	-7.77	-13.64
61 wt% MEG						
PVTsim	-2.29	-3.47	-4.74	-6.15	-9.19	-22.9
PIPEsim	-9.1	-10.2	-11.5	-12.8	-15.5	-29
experiment	-4.02	-6.56	-9.1	-11.85	-14.18	
65 wt% MEG						
PVTsim	-6.27	-7.44	-8.67	-10	-12.81	-26.35
PIPEsim	-14.6	-15.6	-16.9	-17.9	-20.4	-33.7
experiment	-4.3	-7.1	-10.34	-13.57	-20.1	

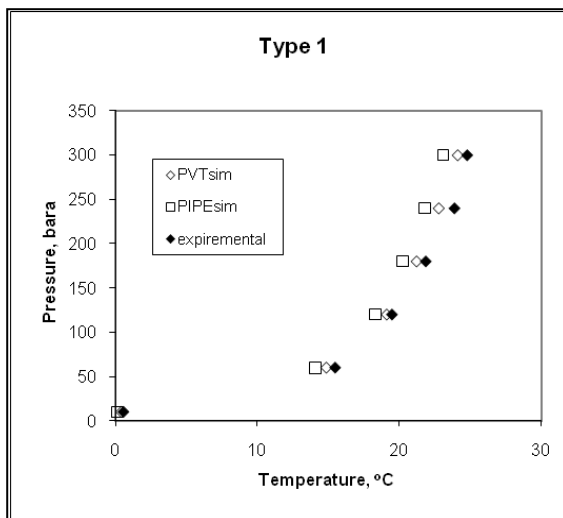


Figure 5. 2 Type 1 Hydrate curve for Sample 2 with 0 to 25 wt% MEG

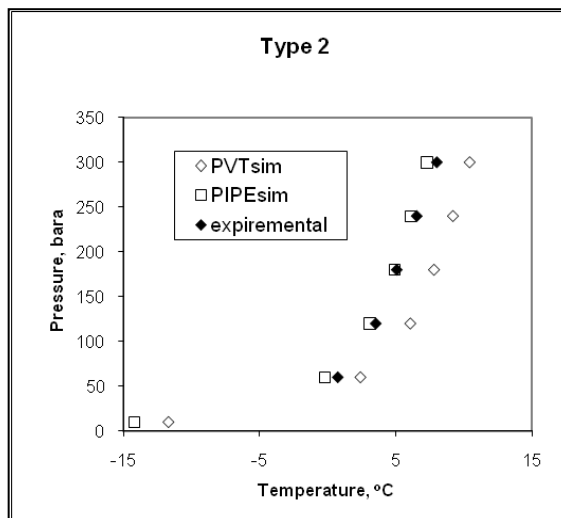


Figure 5. 3 Type 2 Hydrate curve for Sample 2 with 40 to 50 wt% MEG

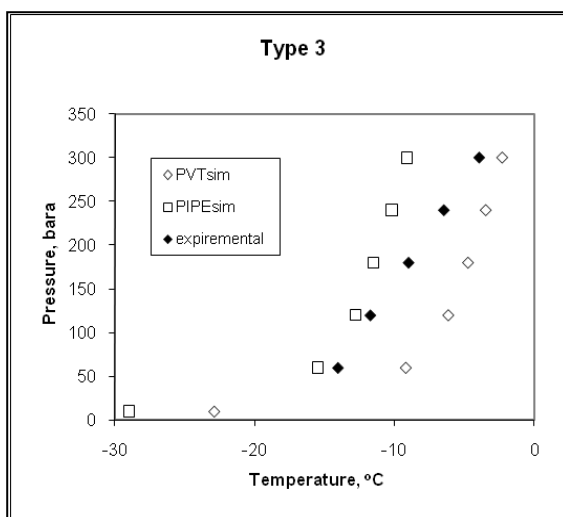


Figure 5. 4 Type 3 Hydrate curve for Sample 2 with 55 to 70 wt% MEG

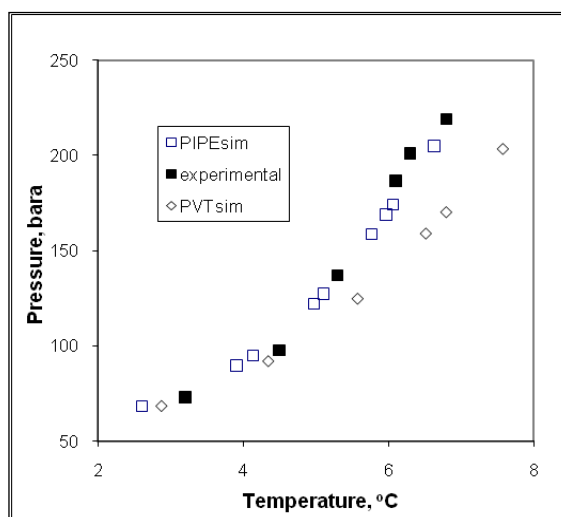


Figure 5. 5 Hydrate curve for Sample 1 with 40 wt% MEG

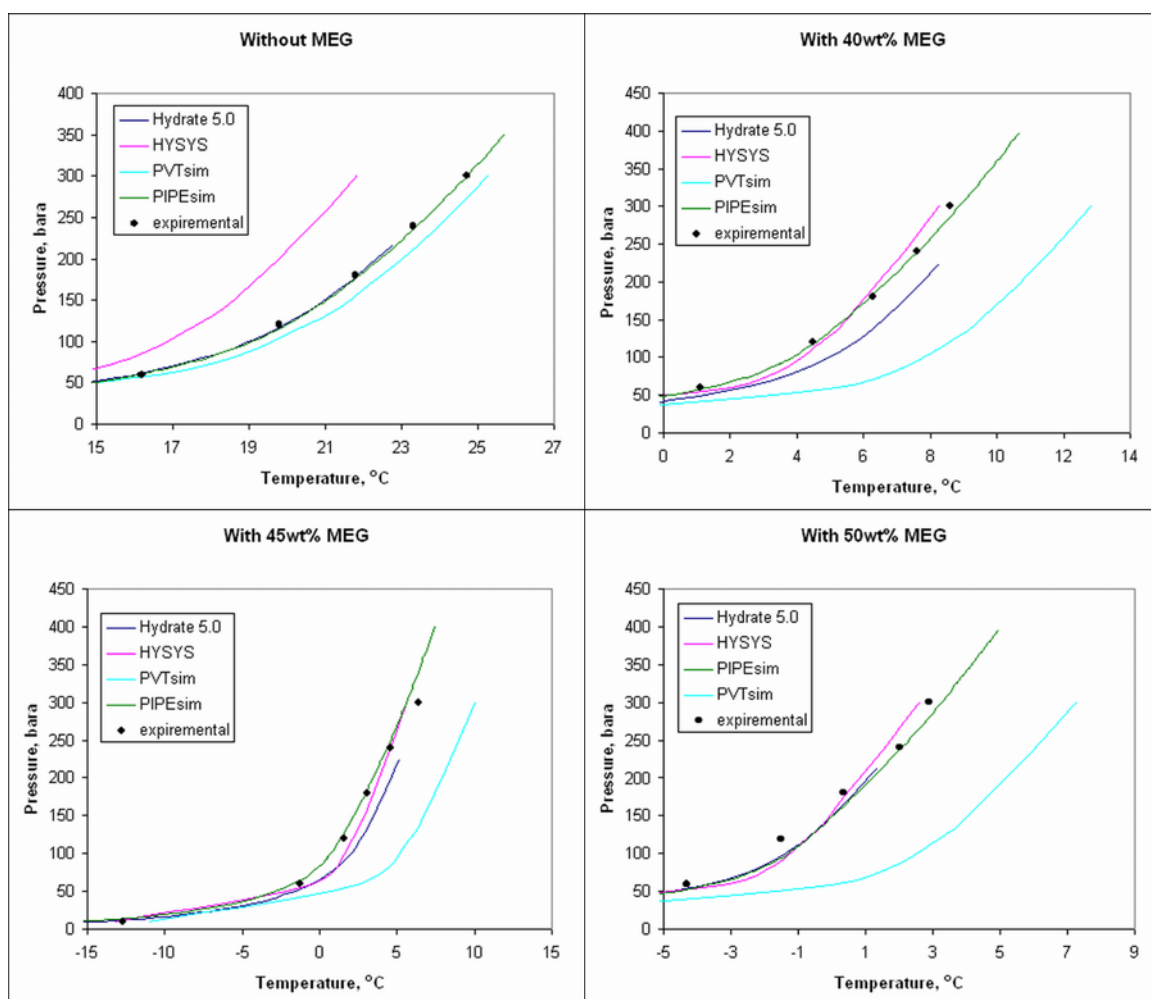


Figure 5. 6 Experimental Hydrate curves for Sample 3 with and without MEG in comparison with simulation results

5.4. Effect of Methane/CO₂ Ratio on Hydrate Formation and Dissociation

CO₂ content increases from under 2 mol% in Sample S2, to 5.5 mol% in S1 and to 9.6 mol% in S3 gas mixture. Accordingly, the amount of Methane and Nitrogen gradually decreases. A distinctive feature of the S1 gas mixture is that it contains heavy hydrocarbons which easily condense and form a film on top of the MEG-water solution in all cases.

Experiments were conducted at pressures in the range from 60 to 300 bar and in the presence of 40 and 45 wt% MEG in water solution. The amount of the solution was kept at 10 cc for each experiment. The hydrate equilibrium temperature was detected as the beginning of dissociation at a threshold temperature where the pressure starts rising. Results from three sets are compared in Table 5.6 and Figure 5.7.

Table 5. 6 Effect of composition on HDT in the presence of MEG

Sample 1 (S1)			Sample 2 (S2)			Sample 3 (S3)		
MEG	pressure	HDT@1.5	MEG	Pressure	HDT@2.5	MEG		HDT@2
40	219	6.8	42	300	7.90	40	300	7.3
	201.1	6.3		240	6.42		240	5.6
	186.8	6.1		180	4.95		180	5.0
	137.1	5.3		120	3.40		120	3.3
	97.9	4.5		60	0.61		60	0.7
	73	3.2						
45	186.8	4.5	46	300	4.26	45	300	4.0
	231.2	5.3		240	2.66		240	3.4
	198.4	4.6		180	1.10			
	168.9	4.0		120	-0.20			
	148.7	3.6		60	-3.88			
	130.3	3.0						
	93.2	1.4						
	75.6	0.9						

Experimental curves for S2 and S3 hydrate dissociation fall very close to each other with a large difference in dissociation temperature only at 300 bar. S1 hydrate, however, shows a wider stability region at both 40 and 45 wt% MEG, and dissociates at noticeably higher temperatures. In the presence of 40 to 42 wt% MEG S1 dissociates at consistently 1-2°C higher temperatures than S2 and S3, and in the presence of 45 to 46 wt% MEG the variation increases to almost 3°C.

It was noticed during the experiments that a condensed heavy hydrocarbon fraction was suppressing hydrate dissociation. This happened in all cases at pressures lower than 100 bar. During experiments with S1 mixture, some condensate was floating on top of the liquid phase at all times. Analysis of the results concluded that the presence of condensate is extending the hydrate stability region and will negatively influence hydrate dissociation.

Therefore the effect of condensate on hydrate dissociation was also investigated and is described in the following Chapter 6.

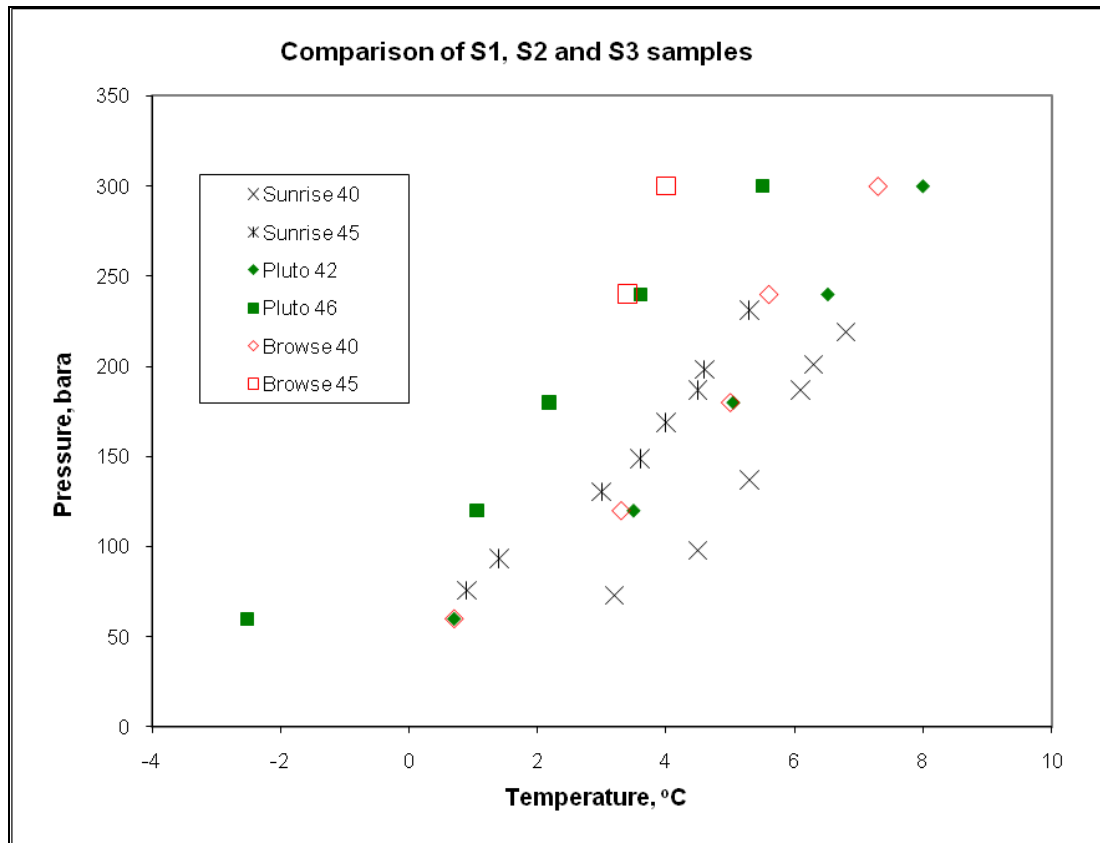


Figure 5. 7 Effect of composition on HDT in the presence of MEG

5.5. Conclusion

Experimental investigation of hydrate formation in the presence of high concentrations of inhibitor is shown to be necessary for the correct choice of operating procedures since design criteria obtained with commercial PVT computer software are not representative. The majority of the commercial software produced good result for low concentration MEG injection but started diverting from the presented experimental results as the MEG concentration went above 45 wt%. For example with the PIPEsim package which performed relatively better than the other packages, the discrepancy between experimental and modelled data up to a concentration of 40 wt%, are less than 0.5°C. For a concentration of 45 wt% of MEG, the maximum discrepancy is less than 1°C and thus a good match between the predicted and the experimental data. For concentrations above 50 wt% MEG, the quality of the prediction decreases as the maximum discrepancy is 1.5°C and the discrepancy is close to 5°C for a MEG concentration of 57 wt% and closer to 10°C for a MEG concentration of 65 wt%.

In this research the experimental hydrate dissociation temperatures at a given concentration of inhibitor MEG are compared with the hydrate dissociation curves from the following software packages:

- Hydrate
- HYSYS with PR EOS
- PVTsim with SRK-Peneloux EOS
- Multiflash for PIPEsim with CPA-Infochem model

The best match for the hydrate dissociation curve is the Multiflash for PIPEsim software with the CPA-Infochem EOS. PVTsim software shows the most conservative results. In general, HYSYS gives good matching results. Assuming an additional 5°C margin, the MEG concentration evolves between 45 wt% and 50 wt% inhibitor concentration, depending on the computer software selected.

When using the various software packages to generate a hydrate dissociation curve for systems at a pressure lower than 300 bar, the maximum temperature for the uncorrected margin is 5°C. For a dosage of MEG less than 30 wt%, the margin decreases to 4°C. These margins can be reduced by at least 2°C or 3°C by generating an experimental hydrate dissociation curve accurately measured in reputable laboratories.

The presence of condensate was found to suppress hydrate dissociation by 2 to 4°C in the presence of MEG. The effect was stronger in the case of higher MEG content in the aqueous phase. This effect was further tested as described in the next Chapter.

This part of the research has provided important information which was utilised during the study of CO₂ hydrates (Chapter 4). First, the hydrate dissociation conditions are indicative of the formation conditions. However, the presence of a third phase such as ice, hydrate of a heavier gas or oil can substantially suppress dissociation, in which case the hydrate is better preserved (as further discussed in Chapter 6). Second, there is discrepancy in predicting hydrate formation using conventional EOS, especially in the presence of high concentration of the phase-shifting agent. This fact has to be thoroughly investigated if a model for prediction of hydrate promotion is to be developed. Also, observations described in section 5.3.1 signify that the chemical-water interaction is particularly important to take into account during hydrate formation due to surfactant nature of the substances used.

Observation of the changing electrical load on the stirring system during hydrate formation produced scattered results and is not included in this thesis. However, it was obvious that as the system approaches the hydrate formation point, the stirring draws more current. This is attributed to the changes in kinematic viscosity and requires further investigation.

Chapter 6.

Gas Hydrates in Presence of Condensate and Wax

6.1. Introduction

The scope of this Chapter is related to the distinctive features of hydrate testing experiments for the S3 gas mixture discussed in the previous Chapter. The aim of this work is to see if there is any significant difference between the hydrates formed in an uninhibited system compared to an inhibited system and in the presence of the third phase (gas condensate).

First, a gas hydrate equilibrium curve using the S3 gas composition in the PVT cell combined with condensed water was established in Chapter 5. Measurements were carried out at six pressure intervals: 10 bar, 60 bar, 120 bar, 180 bar, 240 bar, and 300 bar. For each pressure the hydrate dissociation temperature was identified in the presence of 65 wt% MEG, 61 wt% MEG, 57 wt% MEG, 50 wt% MEG, 46 wt% MEG, 42 wt% MEG and finally 25 wt% MEG. The experimentally generated curve was then compared with the curve generated via the hydrate prediction computer software.

It is known that condensate (mainly C5) can promote hydrate formation under certain circumstances therefore in this study the experiments will be repeated with 5 wt% condensate. The above tests will be conducted for all pressure/temperature intervals and using condensed water inhibited with MEG at the dose rates indicated above. MEG mixed with condensed water saturated with gas is circulated up to a pressures of (10 to 300 bar). Pressure will be maintained constant for each test. The temperature of the mixture (water, MEG, condensate and gas) will be reduced at a cooling temperature ramp of 15°C per hour.

Observations of the density and porosity of the hydrate will be collected for each of the conditions above to assess the disassociation rate. Low porous, high density plugs take a longer time to dissociate than high porosity and low density plugs. Therefore, hydrate dissociation time for each sample will be measured as well, represented by the time frame from when gas evolution first emerged and finally stopped.

Finally, to replicate a cold start-up scenario, the cell will be cooled down to -28°C at 85 bar. For the initial test the cell will only condensate down to the minimum temperatures expected (-28 and -60°C) in the presence of MEG. Ideally during

cooling the cell pressure will remain constant at 5 bar or 85 bar. Furthermore during cooling, the cell will be observed for any changes to the liquid phase. In addition, the viscosity of the fluid in the cell will be measured. The cooling rate will be equivalent to the depressurisation cooling rate in a pipeline. Measurements will include:

1. Hydrate equilibrium curves for each pressure and temperature
 - a. temperature is gradually decreased at constant pressure
 - b. repeat above at sub-cooled end condition
 - c. pressure is gradually increased at constant temperature
 - d. repeat above conditions at choke pressure increase
2. Hydrate nucleation and formation peculiarities
3. Hydrate density of the fluid in the cell

Hydrate formation can accelerate at pressures higher than the equilibrium pressure and temperature lower than the equilibrium temperature, both conditions are likely to exist during cold pipeline start-up or extended wellhead shut-in where high pressure and low temperature is present (Figure 6.1). Cold start-up of a well with a large pressure differential across the sub-sea chokes can result in very low temperatures downstream of the sub-sea choke due to a Joule-Thomson (JT) cooling effect and pressure drop in order of 80 to 150 bar (Dayalath et al., 2004). Temperatures can drop down to -20°C or lower, depending on the gas composition and the initial differential pressure. At these conditions, phase separation will occur allowing for condensate separation and wax precipitation.

Based on data produced and described in Chapter 5, the condensate has noticeable impact of hydrate dissociation conditions, increasing the temperature by 2 to 4°C. The hydrate/wax interaction experiments (Gao, 2008) suggested that hydrate particle formation could assist wax to precipitate out of the solution and result in deposition. However, taking care of one issue can alleviate another problem. Therefore, if hydrate and wax risks coexist in the field, both hydrate and wax treatment programs must be concurrently effective at all times.

Because most of the heavier hydrocarbons contained in the condensate do not form any hydrate and their concentration in the gas phase is negligible compared to the concentration of hydrate-formers, current computer simulation software fails to account for the condensate presence in the flow. In this Chapter experimental S3 (see

Table 5.1) hydrate formation/dissociation conditions in the absence of condensate and in the presence of waxy or de-waxed condensate are compared.

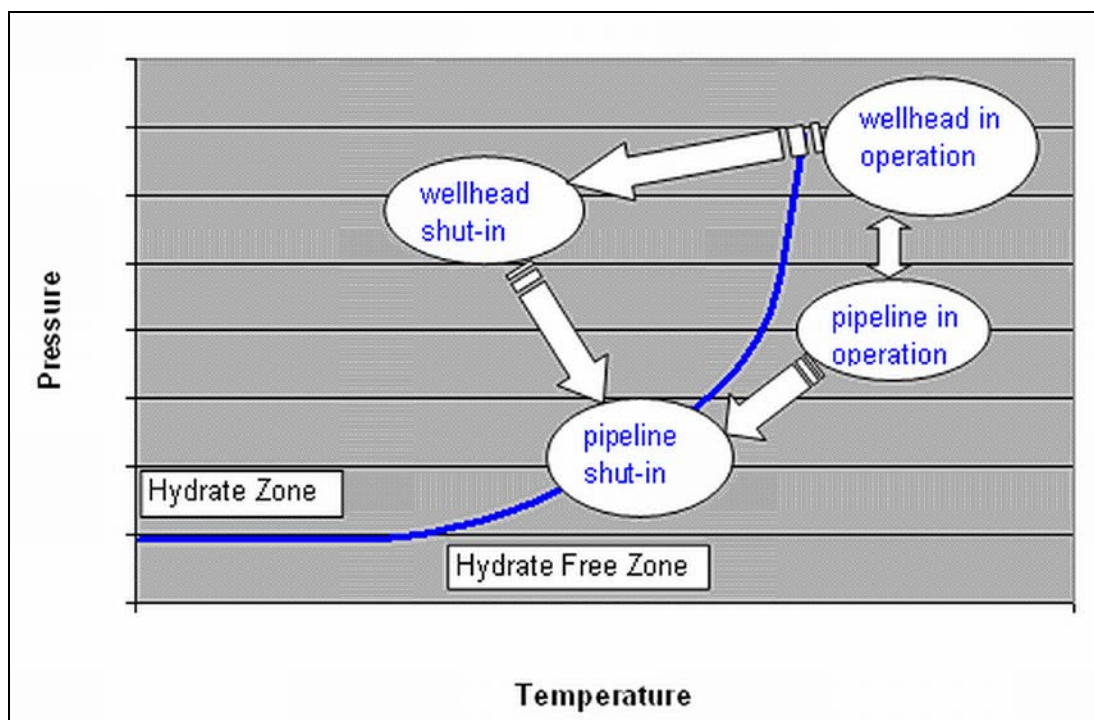


Figure 6. 1 PT characteristics during cold start-up and extended shut-in

6.2. Experimental Investigation of the Condensate Influence on Hydrate Formation

Synthetic gas S3 was used in all the experimental work, the gas was recombined with condensate (Table 6.1) obtained from the field and mixed with water and inhibitor (if any) in a pressurized full visual sapphire-cell PVT system described in Appendix A. The temperature of the hydrate sample was maintained for 24 hours after loading it into the cell and pressurizing it to the desire pressure equilibrium before carrying out the experiments. Then the temperature was decreased and the pressure maintained until full conversion of water into hydrate. The next step was to increase the temperature slowly and note when the hydrate began to melt down. Ideally, when the hydrate begins to melt, the temperature and pressure are maintained constant until the hydrate is totally melted, which was taken as the hydrate dissociation point.

The wax was removed from the condensate in one set of experiments by cooling the condensate to -6°C at a constant rate of 1 degree per hour with subsequent filtering to remove the wax.

Table 6. 1 Fluid composition for experimental testing

Synthetic Gas Composition		Condensate Composition	
Component	(mol%)	Component	(mol%)
CO ₂	10.69	CO ₂	0.7
N ₂	1.25	N ₂	
Methane	76.31	Methane	1.26
Ethane	7.48	Ethane	2.49
Propane	3.19	Propane	4.41
Butanes	0.94	Butanes	6.92
Pentanes	0.08	Pentanes	8.26
Hexanes	0.06	Hexanes	7.87
		C7	15.56
		C8	16.56
		C9	9.33
		C10	5.57
		C11	3.68
		C12	2.91
		C13	2.62

6.3. Hydrate Dissociation Curves in the Presence of Condensate

Figure 6.2 shows the impact of the condensates on the hydrate dissociation temperature for the following cases: Synthetic Gas only; Synthetic Gas and de-waxed condensate; and Synthetic Gas and waxy condensate. No MEG has been added for these tests.

The hydrate in all cases was floating on top of the condensate or was suspended in it unlike in the case of S1 described in the previous Chapter. The first sign of hydrate dissociation for the de-waxed condensate case was constantly 0.3°C lower than for the synthetic gas case. The released water transformed into hydrate again shortly after this first melting and at the same temperature. This phenomenon can be attributed to the formation of unstable hydrate from pentanes contained in the condensate during cooling, and this hydrate undergoes destruction faster than usual hydrates formed by light hydrocarbons. The released water is cold enough to encapsulate the excess lower hydrocarbons in its lattice forming new hydrate. However, the temperature margin is too small to draw many conclusions.

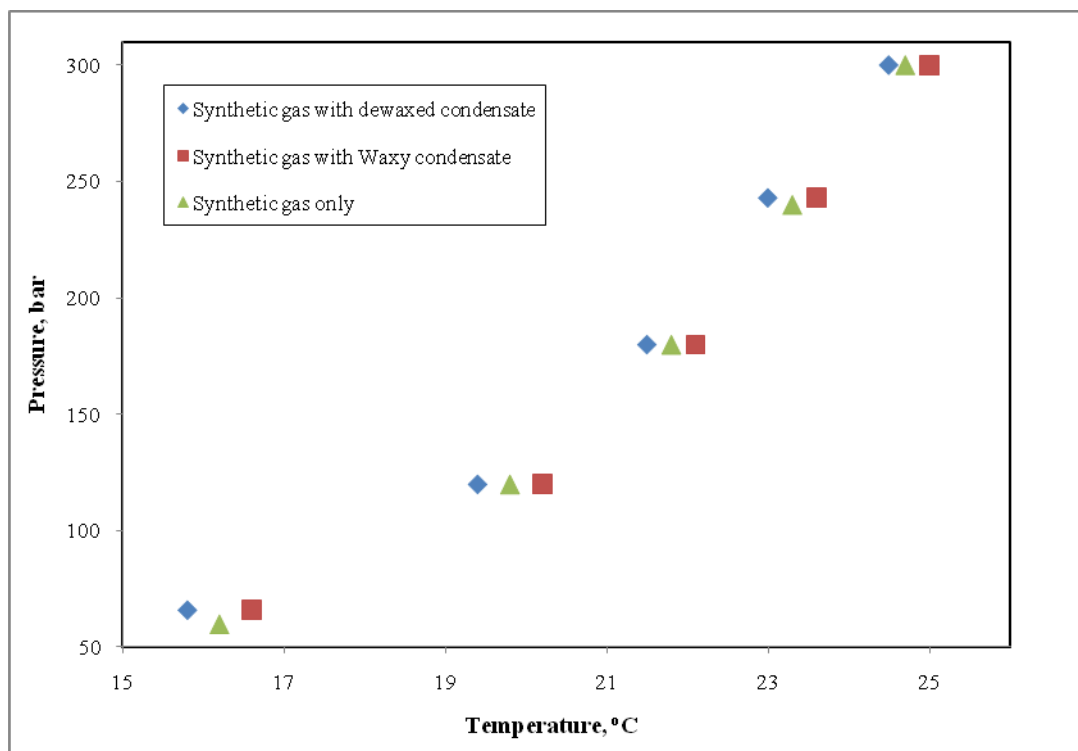


Figure 6. 2 Hydrate dissociation in waxy and de-waxed condensate on S3

The presence of a waxy condensate caused a slight increase in the dissociation temperature compared to the synthetic gas case. The variation is smaller than half a degree. The effect of wax is more related to the hydrate's intrinsic properties and possibly remediation as the crystal and overall form of the hydrate aggregate depend on the wax presence. Some literature (Gao, 2008) mentions that wax has the potential to stabilise the hydrate, thus shifting the hydrate dissociation curve towards higher temperatures. The examples are shown in the section below.

6.4. Hydrate-Wax Interaction

During cold start-up experiment, interaction between wax deposition and hydrate formation and its potential to put the flow assurance program at risk was also evaluated. To replicate a cold start-up scenario the cell was quickly cooled down from -28°C to -60°C at 85 bar, loaded with condensate recombined with the gas sample and the water-MEG solution.

The wax free condensate along with the gas from the same field and distilled water were recombined to generate a hydrate dissociation curve. This curve was then compared against the hydrate dissociation curve generated using the same method but this time with the same condensate containing wax. Comparison of the two

hydrate dissociation curves allows the determination of whether the deposition of wax and hydrates together has affected the hydrate dissociation temperature.

Figure 5.3 shows a picture of the test cell at 120 bar. Two kinds of hydrates co-exist at the same time and give to the mixture an appearance of baked beans.



Figure 6. 3 Hydrates formation in de-waxed Condensate @ 120 bar

Figure 6.4 shows two hydrate structures appearing at 60 bar. The first hydrate appears as shown on the picture on the left side. Then the eggs-shaped hydrates appear. It is likely that the presence of wax with the stirring causing tumbling keep adding layer after layer of hydrate and lighter wax molecules as the temperature is lowered.

Gas hydrate particles can facilitate wax crystals to come out of solution. A plausible explanation was that hydrate particles provided large solid surface areas and consequently created nucleation sites for wax crystals to deposit. Wax deposition in return can potentially cause hydrate particles to seed and agglomerate. The resulting hydrate/wax composite will decrease the fluid mobility and could ultimately result in a blockage. It is therefore recommended that both hydrate and wax risks are adequately addressed in order to ensure uninterrupted production.



**Figure 6. 4 Hydrates formation in waxy condensate at 60 bar.
The formation of egg shape structure due to the rotation of the mixer**

6.5. MEG-Wax Interaction

An initial test was carried out with the condensate cooled down to -28°C . During cooling the cell pressure was maintained constant at 85 bar. Furthermore, during cooling the cell was monitored for any changes to the liquid phase characteristics until it reached -60°C even though not much was happening beyond the freezing of the MEG at -28°C followed by wax precipitation on the vessel walls at -40°C . Wax appearance temperature (WAT) or cloud point of the recombined condensate was detected in the condensate with and without MEG. WAT is defined here as wax crystals can be seen through a 5x optical lines under polarized light.

Pressure was found to have little impact on WAT and MEG freezing points in systems containing 0 to 20 wt% of water (Tables 6.2 and 6.3). In the 90 to 10 wt% MEG/water system the MEG did not have any influence on either the MEG freezing temperature or the WAT. A decrease in MEG concentration to 80 wt% with water caused a 1°C drop in WAT and a 14°C reduction in MEG freezing temperature. Therefore, wax formed before the MEG solution froze. This may be related to the condensate impacting on the freezing point as the concentration of MEG in the MEG/water solution is lowered. Further reduction of MEG concentration to 70 wt% caused different behaviour of the system at high and low pressure. At low pressure WAT increased by 1°C , and MEG freezing occurred at 2°C lower compared to

higher MEG. At high pressure both WAT and MEG freezing increased by 2°C and 4°C respectively. In all cases WAT and MEG freezing is slightly lower at lower pressure.

Table 6. 2 WAT and MEG freezing at 85 bar

90-10 wt% MEG/water/Cond		80-20 wt% MEG/water/Cond		70-30 wt% MEG/water/Cond	
WAT	MEG Freezing	WAT	MEG Freezing	WAT	MEG Freezing
-39.7	-28.8	-41.12	-43	-39.38	-39.1

Table 6. 3 WAT and MEG freezing at 5 bar

90-10 wt% MEG/water/Cond		80-20 wt% MEG/water/Cond		70-30 wt% MEG/water/Cond	
WAT	MEG Freezing	WAT	MEG Freezing	WAT	MEG Freezing
-40.04	-30	-41.26	43.9	-40.2	-45

Cloud point temperature and MEG freezing temperature behave in a similar manner depending upon MEG concentration as shown in Figures 6.5 and 6.6. This may suggest some relation between the two.

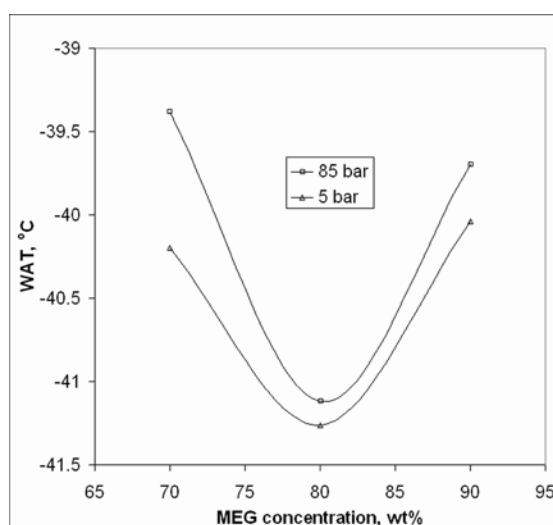


Figure 6. 5 WAT as function of MEG concentration

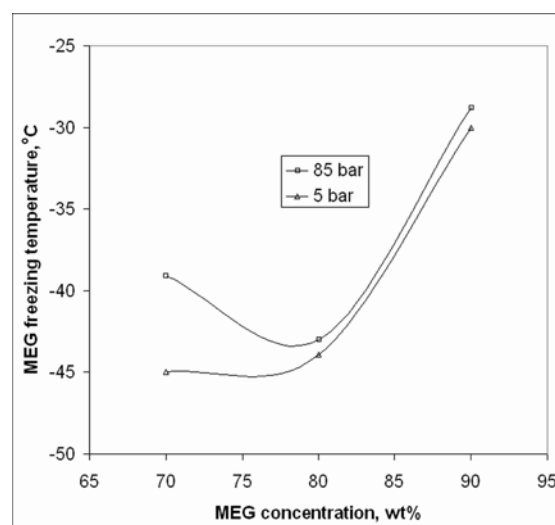


Figure 6. 6 MEG freezing as function of concentration

6.6. Fluid Viscosity Change During Hydrate Formation

Changes in viscosity of the liquid phase with temperature were analysed during the experiments. This was done by measuring and logging the change in the electrical loading on the stirring system. A polynomial extrapolation was used to convert the current to the viscosity of the fluid inside the cell. This method was tested for

calibration purposes on pentane (Appendix F). This should be further investigated in the future as viscosity measurement method.

Table 6. 4 Viscosity as Function of Temperature and concentration

90-10 wt% MEG/water		80-20 wt% MEG/water		70-30 wt% MEG/water	
Temperature °C	Viscosity cP	Temperature °C	Viscosity cP	Temperature °C	Viscosity cP
-1	40	-1	20	-1	9
-12	75	-12	50	-12	20
-18	105	-18	70	-23	60
-23	150	-23	100	-28	100
-28.8	260	-28	160	-34	192
		-34	282	-39.1	300
		-43	453		

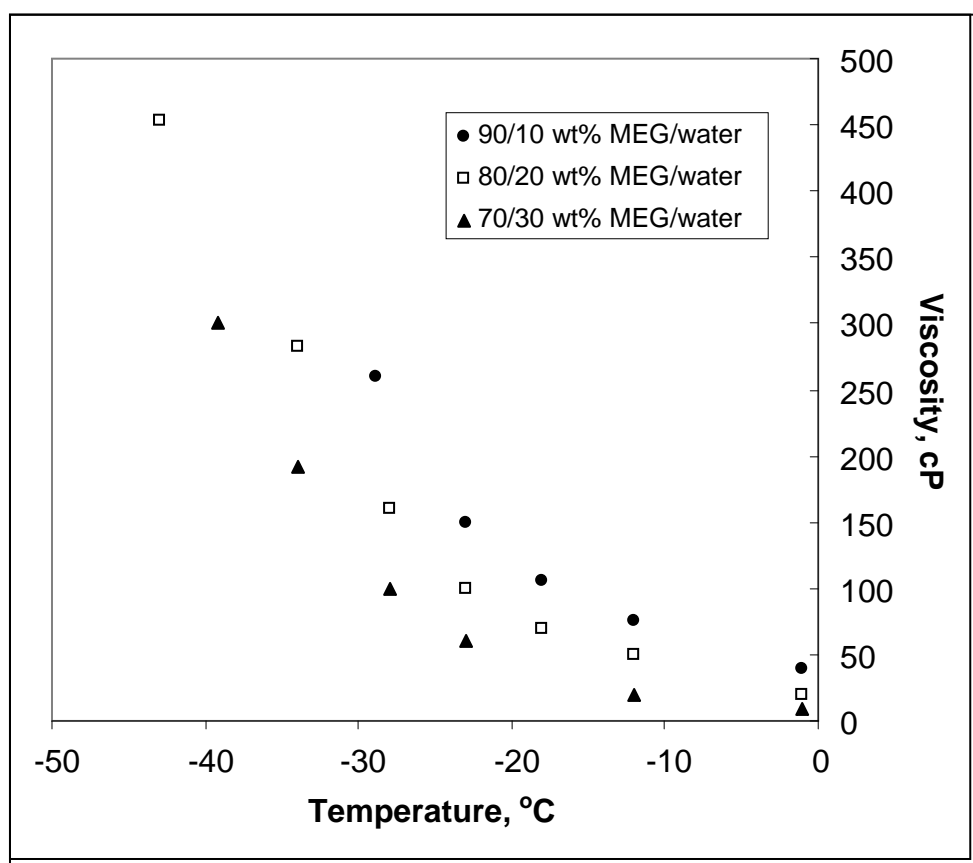


Figure 6. 7 Viscosity as a function of temperature and concentration

Figure 6.7 and Table 6.3 illustrate the changes in viscosity of the MEG/Condensate system, however, we believe the viscosity measured represents the MEG only at the bottom of the cell because the condensate floated on the top of the MEG due to its density gradient. The viscosity increased with decreased temperature until the

solidification temperature. At constant temperature, viscosity of less diluted MEG solution is higher.

6.7. Conclusion

Where gas condensation and wax deposition are expected to coincide with hydrate formation, the two flow assurance risks have to be addressed simultaneously. This study shows that the mutual effect of wax deposition and hydrate formation can be confined to mutual promotion of these phenomena and can aggravate the solid formation remediation (Gao, 2008). The presence of a liquid hydrocarbon phase played a role in affecting the hydrate dissociation temperature; however further tests will verify the final conclusion. Based on the results produced and described in this Chapter and Chapter 5, the effect of condensate on hydrate dissociation is most likely dependent on the condensate composition. Heavy hydrocarbons have almost zero impact, changing the hydrate dissociation temperature by only 0.3°C whereas C5 to C7 hydrocarbons delay the decomposition process by 2 to 4°C. Therefore, particular attention should be paid to the systems where multiphase flow is likely to occur.

This research has confirmed that the presence of the third liquid phase can delay hydrate dissociation via direct interaction with the hydrate particles. Therefore, impurities in form of liquid immiscible with water should be prevented during CO₂ reduction by hydrate if it is to be dissociated (Carbon Dioxide is then collected as gas, and the water can be reused for hydrate formation). Alternatively, small amount of liquid hydrocarbons can be added to the system to ensure that the hydrate is well preserved during removal from the system and transportation.

The effect of solid particles is dual. Hydrate forms and grows more quickly on the ‘nucleation centres’ presented as fine solid particles in the system, but this is unlikely to affect the dissociation. The effect of precipitation of solid on already formed hydrate crystals is not clear and requires further investigation.

Chapter 7.

Pilot Plant Design

7.1. Introduction

Separation techniques based on the differences in boiling points of components are the most important in the chemical process industry. More than 90% of separations are based on distillation, and this situation is not likely to change in the near future. Although there are a number of new developments for alternative CO₂ separation techniques, they tend to have technical limitations in terms of CO₂ content, pressure, or temperature that in many cases make them unattractive for practical purposes. In this project a hybrid system of cryogenic condensation and hydrate reactor that offers an interesting alternative for IGCC (GE and Shell) or Oxyfuel gases has been designed and tested. Cryogenic condensation alone is highly energy intensive, for example, separation energy for cryogenic distillation in the production of Natural Gas can be greater than fifty percent of the plant's total energy requirements. This proposed hybrid system consisting of different unit operations that are interlinked and optimized to achieve a desired outcome in terms of CO₂ content in the feed gas and waste stream. In this Chapter the focus is on the energy/cost savings in cryogenic distillation columns, by utilizing the heat available in the system and recovering the excess cooling. The commercial computer software Aspen HYSYS simulation is used to develop a rigorous dynamic simulation of the process plant equipment. Equipment specifications and operating conditions correspond to a typical gas processing plant. As a first step, the simulator is utilized to validate the design model for constant flow.

CO₂ capture by the cryogenic and hydrate method can be used in many situations, especially when CO₂ concentration in the flue gases is high. The IGCC process represents an ideal case for CO₂ capture by cryogenic and hydrate method as both processes provide the gas at high pressures. The other advantage is that once CO₂ is captured as a hydrate it can be released in the dissociation stage, which only requires a few degrees of temperature rise. The CO₂ produced can subsequently be compressed from these high process pressures to 110 bar, which is the required product pressure and also decreasing the energy demand in the compression stage.

Integrated Gasification Combined Cycle (IGCC) utilises low value fuel ranging from coal to municipal waste for high quality power generation. The major benefit of this cycle is the potential for zero greenhouse gas emissions including CO₂. There are basically two well established variations for IGCC plant arrangement, using the Shell or the GE (Texaco) gasification methods. In the first arrangement, dry ground coal is gasified under pressures of about 3 MPa, and high heat recovery is achieved due to the generation of high pressure steam in a heat recovery boiler used for cooling of the raw stream. A slurry fed gasifier, operating at pressures between 5 and 6 MPa combined with a subsequent water quench is used in the GE IGCC plants. Although additional heat and Oxygen supply is required for water evaporation in the latter case, the total energy penalty for CO₂ capture is lower due to a sufficient amount of steam for shift conversion (Zheng & Furinsky, 2005; Klara & Wimer, 2007).

Presented in this Chapter are the simulations study results on the integration of the cryogenic CO₂ separation process with synthetic hydrate formation for the reduction of the energy penalty. The work includes the pilot plant design details described in the current Chapter with its functionality discussed in Chapter 8.

7.2. Flue Gas Description

The composition of the process gas depends on the type of coal used by the process and the operating conditions. Based on Australian bituminous coal, the process gas has been identified with respect to its composition for both the GE and Shell processes. The Australian coal has the following composition (Table 7.1):

Table 7. 1 Coal composition used in the IGCC

Component	Composition wt %
Inherent moisture	9.5
Ash	12.2
Carbon	64.5
Hydrogen	4.38
Nitrogen	1.41
Oxygen	7.04
Sulphur	0.86
Chlorine	0.02
LHV, MJ/kg	25.87

Chilled flue gas after the gasifier is purified from COS by hydrolysis and from H₂S by chemical absorption. Raw gas containing mainly CO, Hydrogen and steam with small inclusions of CO₂ and inerts is passed through the shift-converter. Process gas

compositions and process conditions after shift-conversion based upon the IGCC GE and Shell processes selected for this study are shown in Table 7.2. The values were calculated for a 500 MW power generating plant utilizing the IGCC combustion technique with 38% overall efficiency (progress report 'CO₂ Separation by using single stage Hydrate Reactor and Cryogenic Condensation Process in Integrated Gasification Combined Cycle' by A.Barifcani & R.Amin dated 11 April 2007).

Table 7. 2 IGCC GE and Shell compositions and conditions

Component mol%	Compositions			
	GE process		Shell process	
	Initial	Dry basis	Initial	Dry basis
H ₂	55.04	55.145	56.51	56.686
CO	2.84	2.845	2.51	2.52
CO ₂	40.22	40.3	36.91	37.025
N ₂	0.68	0.681	3.10	3.11
O ₂	0.00	0.00	0.00	0.00
CH ₄	0.02	0.02	0.00	0.00
H ₂ S & COS	0.22	0. 22	0.18	0.181(no COS)
Ar	0.79	0.7915	0.48	0.481
H ₂ O	0.19	0.00	0.31	0.00
Process pressure bar	57.2		28.3	
Process temperature °C	38		38	
Syngas flow rate kgmol/hr	37276	37205	36998	36880
Molecular weight	20.2		19.25	
Process specifics				
Coal consumption, t/hr	323.1		273.1	
Gross power output, MW	972.8		896.2	
Net power output, MW	730.3		676.2	
Net efficiency, %	31.5		34.5	

Hydrogen sulphide presented in the gas mixture will be partially removed on the condensation stage together with the majority of the CO₂. The remainder will flow to the hydrate reactor. Detailed study of the SIMTECHE process (Deppe et al., 2004) reveals that this amount of H₂S is sufficient to promote CO₂ hydrate formation at the process conditions (53 to 57 bar and 1°C), with H₂S going into hydrate phase together with carbon dioxide.

Due to the safety reasons, the CO and H₂S cannot be used in the lab to reproduce the stream. Therefore in experimental set up, the CO stream is combined with an N₂ stream due to their close boiling points, critical temperature and pressures and having the same molecular weight; and H₂S is replaced with Hydrogen.

The stream produced in the Shell case is characterized by slightly lower CO_2 content given at significantly lower pressure. Utilization of high feed gas pressure is crucial in current research, therefore it is proposed to compress the Shell process stream to 53 bar prior to feeding into the CO_2 capturing unit.

7.3. Flow Scheme Description

Figure 7.1 shows a block diagram for the IGCC process with CO_2 capture unit.

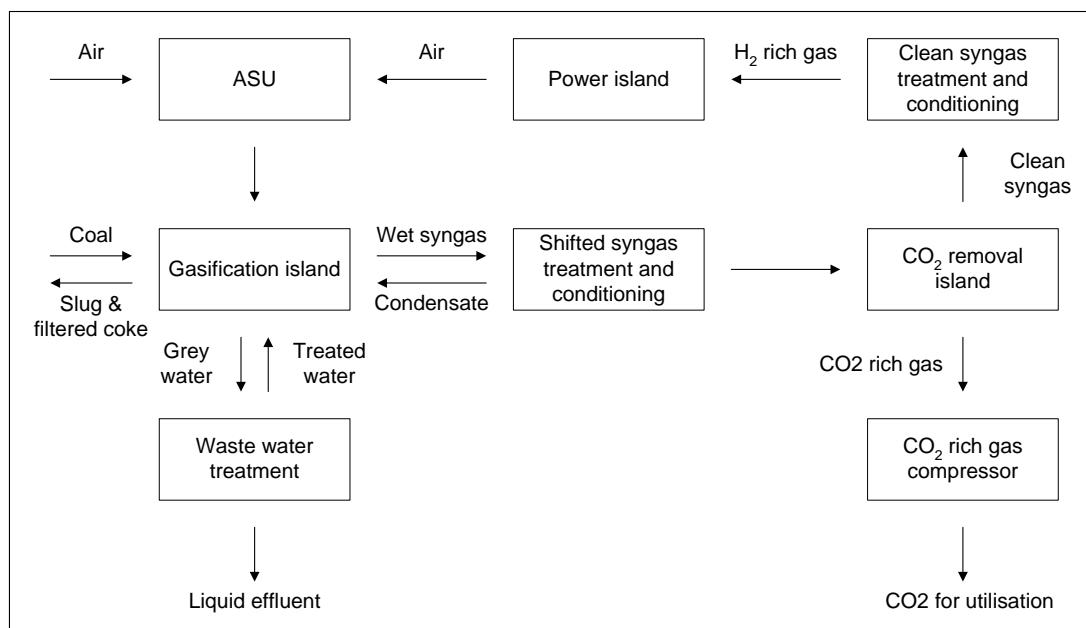


Figure 7. 1 Block diagram for the IGCC process with CO_2 capture

The purpose of this research is to develop an effective CO_2 removal technique which can be easily implemented at both new and existing power stations. An overall flow diagram for an integrated cryogenic and hydrate CO_2 separation module is shown in Figure 7.2 and in more detail in Figures 7.3-7.5. The proposed scheme possesses the following features:

- The feed gas pressure is utilized to condense and capture CO_2 in the hydrate form. Operating pressure for this process is between 55 and 60 bar.
- A substantial amount of energy is recovered due to utilization of liquefied CO_2 to cool and condense part of the CO_2 in the feed gas
- Reduction of compression energy requirements due to CO_2 hydrate gasification at high pressure

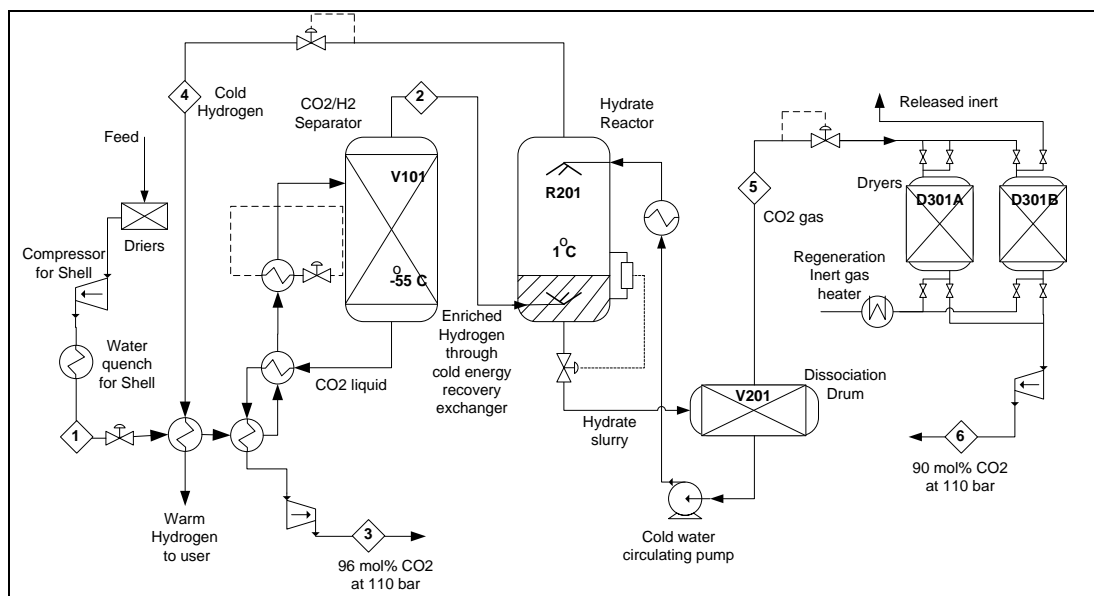


Figure 7. 2 Flow diagram for integrated cryogenic and hydrate CO₂ capture

CO₂ is mainly captured by cryogenic condensation and additional separation is achieved through utilization of the hydrate formation phenomenon. In the first stage (Figure 7.3) the feed with composition according to Table 7.2 enters the cryogenic energy recovery units and condensation exchangers after passing through the driers D101 A & B. Because the pressure of the Shell process is lower, initial compression in C102 is required; this results in the need for an additional cooler E106 when the Shell flue gas is treated. In heat exchanger E101 (first and second stages) cold purified hydrogen is utilised for initial cooling of the feed, and exchangers E102 & 103 utilise the cold energy of condensed CO₂ from cryogenic separator. The feed gas is further chilled to a temperature of -55°C by cooler E104 which results in substantial condensation of CO₂ at process pressure. The liquid CO₂ at -55°C separates from Hydrogen gas in V101 separator, flows through the heat recovery exchangers E102 & 103 and then CO₂ gas passes through the compressor to increase its pressure to 110 bar. Cold hydrogen rich gas from V101 is utilised to pre-cool the feed in the second stage of E101.

In the second stage, the Hydrogen rich gas flows to the hydrate reactor R201 at 1°C and process pressure where it makes contact with water sprayed from the top (Figure 7.4) forming hydrate as it flows down to the bottom of the reactor. The slurry then flows into the dissociation jacketed drum V201 at 20 bar where by an increase in its temperature to 10°C the hydrate is dissociated with CO₂ released from the cold

water. The CO₂ gas then passes through the dryers D301 and the compressor C301 to increase its pressure to 110 bar (see Figure 7.5).

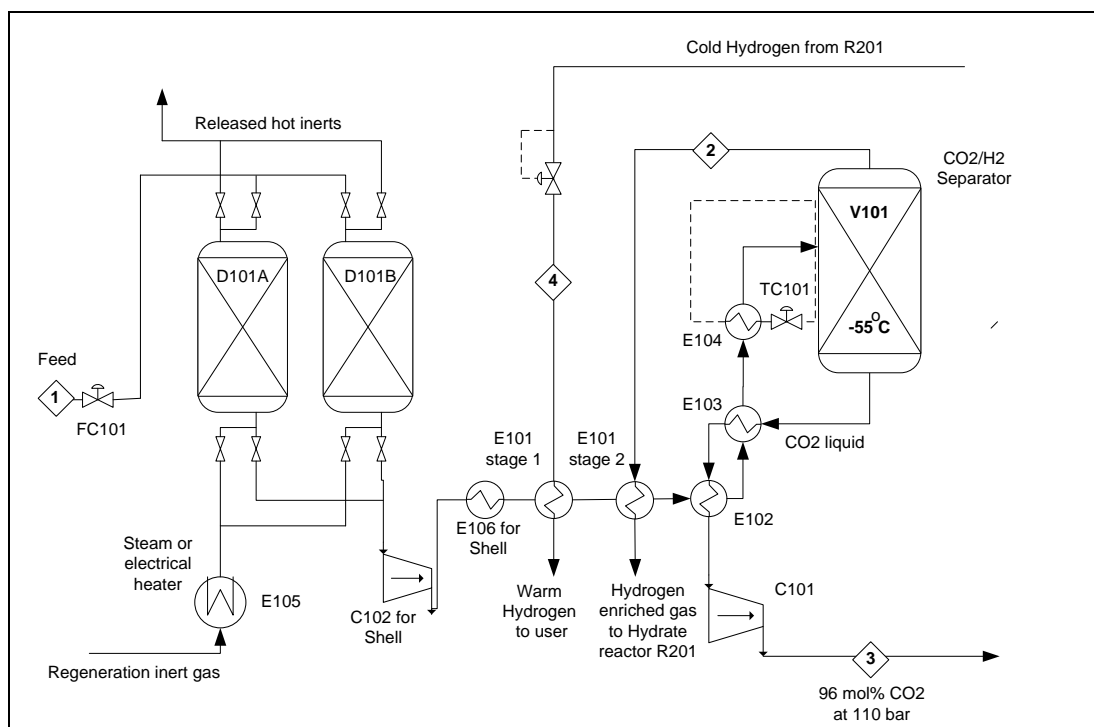


Figure 7. 3 Feed gas drying, chilling and liquefaction of CO₂

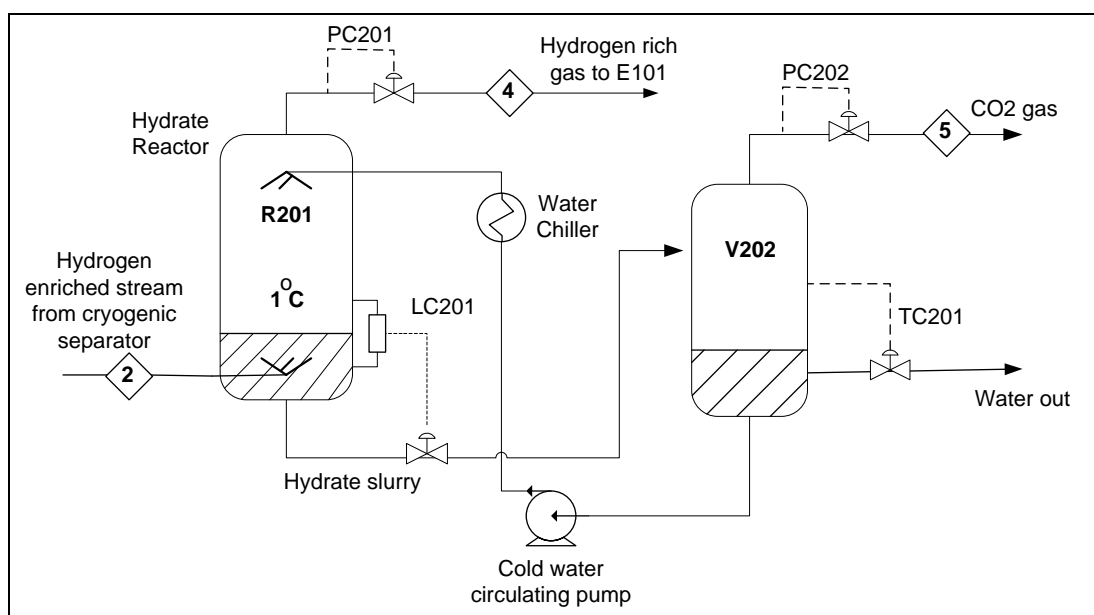


Figure 7. 4 Hydrate CO₂ capture

The Hydrogen gas passes from the top of reactor R201 through the first stage of exchanger E101 to cool down the feed gas as shown on Figure 7.2. The cold water from the dissociation drum is pumped by pump P201 and through a water chiller to be sprayed inside the hydrate reactor again.

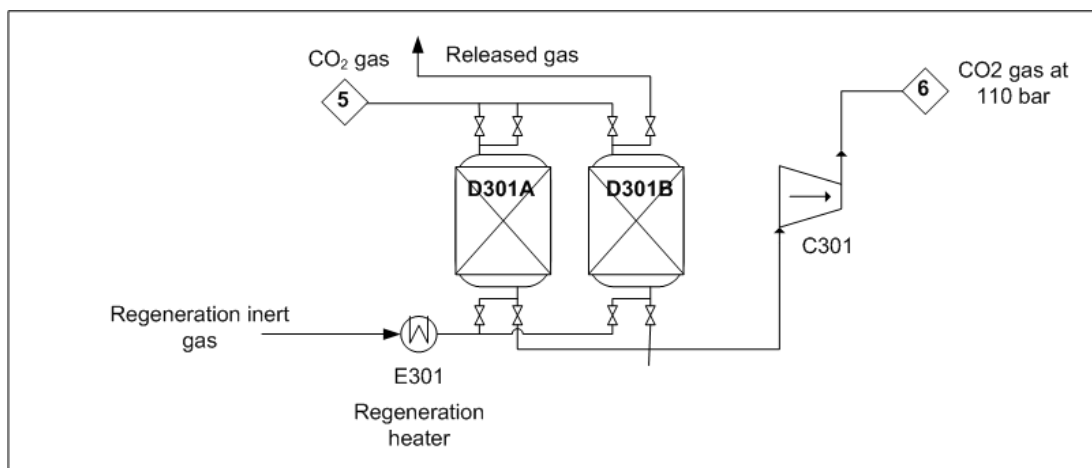


Figure 7. 5 CO₂ rich gas drying and compression

7.4. Servicing streams

Conditions for servicing streams required for normal operation of the CO₂ removal island are given in Table 7.3. Chemicals used include hydrate promoters as required by the process and 15 wt% aqueous solution of NaOH for pH control of effluent water.

Table 7. 3 Servicing streams

Supply stream	Conditions				
	Pressure, bar		Temperature, °C		Other
Seawater	Operating	2	Inlet	Depends on location	Filtered prior to use
	Design	4	Design	60	Once through basis
	Drop across exchangers	0.5	Increase across exchangers	10	Fouling factor 0.0002 hr•°C•cm ² /kcal
Cooling water	Supply	4.5	Inlet	17 to 29	Fouling factor 0.0002 hr•°C•cm ² /kcal
	Return	2.5	Increase across exchangers	12	
	Design	6.5	Design	60	
	Drop across exchangers	0.3			
Process water	Operating	3.5	Operating	Ambient	Supplied from storage tank
	Design	5.5	Design	60	
Demineralised water					pH 6.5 to 7.0
					Conductance 0.15 µs @ 25°C
					Salinity 0.1 mg/kg max

Steam	High	160	High	max 500	Available at power plant
	Medium	42	Medium	max 400	
	Low	4	Low	140	
Plant air	Operating	7	Operating	40	Filtered compressed air
	Design	9	Design	60	
Instrument air	Operating	7	Operating	40	Dew pt -25°C @ 7 bar
	Design	9	Design	60	Oil free
Nitrogen	Operating	7	Operating	40	Purity 99.9 mol%
	Design	9	Design	60	Dew pt -40°C @ 7 bar

7.5. IGCC GE Case Study

The IGCC GE flue gas composition to be purified from CO₂ is shown in Table 7.2 (dry basis). Properties of the process streams #1, 2 and 3 were simulated in the HYSYS computer simulation package using PR EOS (based on the results from Chapter 3). SRK-P EOS in PVTsim modelling software was used for equipment design and simulation of the hydrate stage (streams 4 and 5) based on the results discussed in Chapter 4. No promoting chemical was included in simulation due to the limitations of the existing models.

7.5.1. Mass and Energy Balance

The composition, flow rate, pressure and energy value of each stream is summarized in Table 7.3. Water circulation rate is 73092.57 kgmol/hr.

Table 7. 4 Mass and Energy balance

Feed component	Stream No.					
mol%	1	2	3	4	5	6
H ₂	55.145	80.8181	1.3218	86.65	0	0
CO + N ₂	3.525	5.0096	0.4125	4.961	4.8806	4.8806
Ar	0.79	1.0711	0.2006	0.849	3.6643	3.6643
CO ₂	40.3	13.0127	97.5073	7.512	90.5705	90.5705
H ₂ S	0.22	0.0616	0.552	0.0074	0.7905	0.7905
CH ₄	0.02	0.0268	0.0057	0.0211	0.0941	0.0941
MW						
Pressure bar	57.2	55.7	110	55.2	20	110
Flow rate kgmol/hr	37205	25190	12020	23490	1700	1700

7.5.2. Equipment Design

Design pressures are based on operating pressures and calculated by adding 2 bar. Design temperatures are calculated at 15°C plus the operating temperature but not less than 60°C for the highest design temperature. The lowest operating temperatures are used as the lowest design temperatures.

Driers designed to achieve -40°C dew point.

A special design has to be provided for E102 and E103 feed recovery coolers to recover the 48.28 MW available in liquid CO₂ as a chilling medium.

Table 7. 5 Vessels

Vessel No	Description	ID M	HT M	Thickness mm	Design P bar	Design T °C	material
D101A & B	Driers	2.5	7.5	80	59.2	295	CS
V101	H ₂ / CO ₂ liquid separator	2.5	10	65	58	-55	3½% Ni
R201	Hydrate reactor	2.4	15	75	57.5	60	CS (Teflon lined)
V201	Hydrate dissociation drum	2.4	18	74	57	60	CS (SS clad)
D301A & B	Driers	1.6	5	52	59	295	CS

Table 7. 6 Pumps

Equipment No	Description	Flow rate kgmol/hr	Power required MW
P201	Water pump	73092.6	1.45

Table 7. 7 Heat exchangers

Equipment No	Type	Description	Heat load MW
E101 stage 1	Shell & tube	Feed recovery cooler	4.975
E101 stage 2	Shell & tube	Feed recovery cooler	10.82
E102	Shell & tube	Feed recovery cooler	49.2
E103	Shell & tube	Feed recovery cooler	
E104	Package	Chiller	13.7
E201	Jacket	Dissociation drum heater	13
E105	Shell & tube	Heater	-
E301	Shell & tube	Heater	-

Table 7. 8 Compressors

Equipment No	Description	Flow rate kgmol/hr	Power required MW
C101	CO ₂ from liquefaction compressor	12020	4.61
C301	CO ₂ from hydrate compressor	1700	2.59

7.5.3. Overall CO₂ Capture and Purity

In the first cryogenic stage the feed stream is separated into Hydrogen enriched overhead containing 13 mol% CO₂ and the bottom product 97.5 mol% liquid CO₂. This implies that 11720.377 kgmol/h of CO₂ is removed from the initial stream containing 14993.615 kgmol/h of CO₂ by condensation. This is equivalent to 78.17 mol% capture efficiency.

In the second stage, a total of 1539.7 kgmol/h of CO₂ is regasified from hydrate which constitutes 47 mol% removal from an initial 3277.9 kgmol/h CO₂. The Hydrogen enriched stream contains 86.6 mol% Hydrogen and can be utilized for pure power generation.

Overall CO₂ capture is calculated as

$$\frac{1539.7(\text{kgmol} / \text{h}) + 11720.377(\text{kgmol} / \text{h})}{14993.615(\text{kgmol} / \text{h})} * 100 = 88.8\%$$

7.5.4. Heat Recovery

Recoverable heat from CO₂ liquid stream = 49.2 MW from -55°C to 15°C

Recoverable heat from first stage purified stream = 10.82 MW from -55°C to -5°C

Recoverable heat from second stage purified stream = 4.975 MW from 1°C to 25°C

7.6. IGCC Shell Case Study

This feed gas is based on IGCC Shell flue gas composition given in Table 7.2. The scheme is similar to the GE process except that the compression of the feed gas to 53 bar is added. Properties of the process streams #1, 2 and 3 were simulated in the HYSYS computer simulation package using PR EOS (based on the results from Chapter 3). SRK-P EOS in PVTsim modelling software was used for equipment design and simulation of the hydrate stage (streams 4 and 5) based on the results discussed in Chapter 4. No promoting chemical was included in simulation due to the limitations of the existing models.

7.6.1. Mass and Energy Balance

The composition, flow rate, pressure and energy value of each stream is summarized in Table 7.8. Water circulation rate in stream 2 is 81147.55 kgmol/hr.

Table 7. 9 Mass and Energy balance

Feed component	Stream No.					
mol%	1	2	3	4	5	6
H ₂	56.686	77.93	1.2	85.49	0	
CO	2.51	3.36	0.29	2.17	5.47	5.47
N ₂	3.11	4.18	0.32	5.3	1.83	1.83
Ar	0.481	0.62	0.11	0.437	2.215	2.215
CO ₂	37.025	13.85	97.57	6.46	89.835	89.835
H ₂ S	0.18	0.06	0.5	0.005	0.584	0.584
Heat flow, 10 ⁸ kJ/hr	54.92	16.29	39.6	6.98	8.428	8.63
Pressure bar	28.3	52	110	52	20	110
Flow rate kgmol/hr	36880	26670	10210	24310	2320	2320

7.6.2. Equipment Design

Design pressures are based on operating pressures and calculated by adding 2 bar. Design temperatures are calculated at 15°C plus the operating temperature but not less than 60°C for the highest design temperature. The lowest operating temperatures are used as the lowest design temperatures.

Driers designed to achieve a -40°C dew point.

A special design has to be provided for the E102 and E103 feed recovery coolers to recover the 41.9 MW available in liquid CO₂ as a chilling medium.

Table 7. 10 Vessels

Vessel No	Description	ID M	HT M	Thickness mm	Design P bar	Design T °C	material
D101A&B	Driers	2.4	7.5	39	30	295	CS
V101	H ₂ / CO ₂ liquid separator	2.5	10	60	54	-55	3½% Ni
R201	Hydrate reactor	2.4	15	70	54	60	CS (Teflon lined)
V201	Hydrate dissociation drum	2.4	18	28	22	60	CS (SS clad)
D301A&B	Driers	1.6	5	19	22	295	CS

Table 7. 11 Pumps

Equipment No	Description	Flow rate kgmol/hr	Power required MW
P201	Water pump	81148	1.43

Table 7. 12 Heat Exchangers

Equipment No	Type	Description	Heat load MW
E106	Shell & Tube	Feed gas water cooler	25.7
E101 stage 1	Shell & Tube	Feed gas cooler	4.82
E101 stage 2	Shell & Tube	Feed gas cooler	11.54
E102	Shell & Tube	Feed gas cooler	41.9
E103	Shell & Tube	Feed gas cooler	
E104	Package	Chiller	13.37
E201	Jacket	Dissociation drum heater	15.7
E105	Shell & Tube	Inert regeneration heater	
E301	Shell & Tube	Inert regeneration heater	

Table 7. 12 Compressors

Equipment No	Description	Flow rate kgmol/hr	Power required MW
C102	Feed gas compressor	36880	24.7
C101	CO ₂ from liquefaction compressor	10250	4.5
C301	CO ₂ from hydrate compressor	2320	3.54

7.6.3. Overall CO₂ Capture and Purity

In the first cryogenic stage the feed stream is separated into Hydrogen enriched overhead containing 13.7 mol% CO₂ and the bottom product 97.57 mol% liquid CO₂. This implies that 10001.3145 kgmol/h of CO₂ is removed from the initial stream

containing 13654.82 kgmol/h of CO₂ by condensation. This is equivalent to 73.24 mol% capture efficiency.

In the second stage, a total of 2084.172 kgmol/h of CO₂ is regasified from hydrate which constitutes 57 mol% removal from the initial 3653.5055 kgmol/h CO₂. The Hydrogen rich stream contains 85.5 mol% Hydrogen and can be utilized for clean power generation.

Overall CO₂ capture is calculated as

$$\frac{2084.172(\text{kgmol} / \text{h}) + 10001.3145(\text{kgmol} / \text{h})}{13654.82(\text{kgmol} / \text{h})} * 100 = 88.5\%$$

7.6.4. Heat Recovery

Recoverable heat from CO₂ liquid stream = 41.9 MW from -55°C to 15°C

Recoverable heat from first stage purified stream = 11.54 MW from -55°C to -5°C

Recoverable heat from second stage purified stream = 4.82 MW from 1°C to 25°C

7.7. Conclusion

Integrated Gasification Combined Cycle (IGCC) is an advanced technology for high efficiency power generation from a variety of fuels including domestic waste and other low Btu sources. Continued growth of the IGCC refinery segment however, is strongly dependent on how the current market requirements are addressed. Today's world is particularly demanding for clean energy production at low emissions level and overall environmental performance.

The above designs and simulations propose a novel method for CO₂ capture by cryogenic condensation and a single stage hydrate reactor system based on a simplistic approach and a minimum of equipment. Calculated capture rates show up to 88 mol% CO₂ abatement which results in production of a more than 85 mol% purity Hydrogen enriched stream. This stream can be used in fuel cells or for clean energy production with near-zero emissions of greenhouse gases. Slightly better separation and higher quality Hydrogen is generated in the IGCC GE case because of higher feed pressure than with IGCC Shell process. The difference is small and therefore in terms of environmental performance the proposed separation technique can be adapted to both power generating options.

Substantial amount of heat can be recovered via utilisation of the cold process streams for pre-cooling of the feed gas. In the Shell case 58.26 MW (51.5%) of the total energy consumed by heat exchangers can be recovered.

Chapter 8.

Laboratory Set-up for the Technology Testing

8.1. Introduction

The use of clathrate hydrate crystallization combined with cryogenic separation for the recovery of CO₂ from IGCC/Oxyfuel flue gas mixtures was demonstrated at the laboratory scale. It was shown that hydrate formation/decomposition coupled with cryogenic separation can result in an economical and efficient separation of CO₂ from a flue gas mixture. The laboratory process reported in this Chapter was specifically build for CO₂ recovery from IGCC (GE and Shell) Oxyfuel gas mixture. Also a chemical additive was found that lowers the operating pressure while maintaining the higher CO₂ recovery during hydrate production. This laboratory demonstration has shown that cryogenic and hydrate formation/decomposition cycles combined with the knowledge of the gas composition, pressure and temperature can be controlled to produce an optimum purification process for flue gases. In this Chapter, a multi-scale approach is used to address the formation of CO₂ hydrate in aqueous solutions.

A laboratory rig (Figure 8.1) has been constructed at Clean Gas Technologies Australia in order to trial-test combined cryogenic and hydrate CO₂ capture technology, the design for which is presented in previous Chapters. The skid-mounted unit was commissioned in mid-2008 and the operation commenced in September 2008. In order to improve the performance and simplify the operation, some changes to the initial design were made and they are described in this Chapter. Detailed description of the instrumentation and operating procedures is also provided.

Only a limited number of experiments was conducted. The two stages of the proposed technology for CO₂ capture from IGCC flue gases were tested separately due to the absence of a continuous feed supply. First, the cryogenic stage was tested, and the overhead gas composition was determined. Next, the measured composition was recombined and the hydrate precipitation experiment was performed. The results obtained from both stages were compared with the expected values indicated in Chapter 7, and used for overall estimation of anticipated efficiency of the combined continuous process.



Figure 8. 1 Laboratory rig for integrated cryogenic and hydrate testing

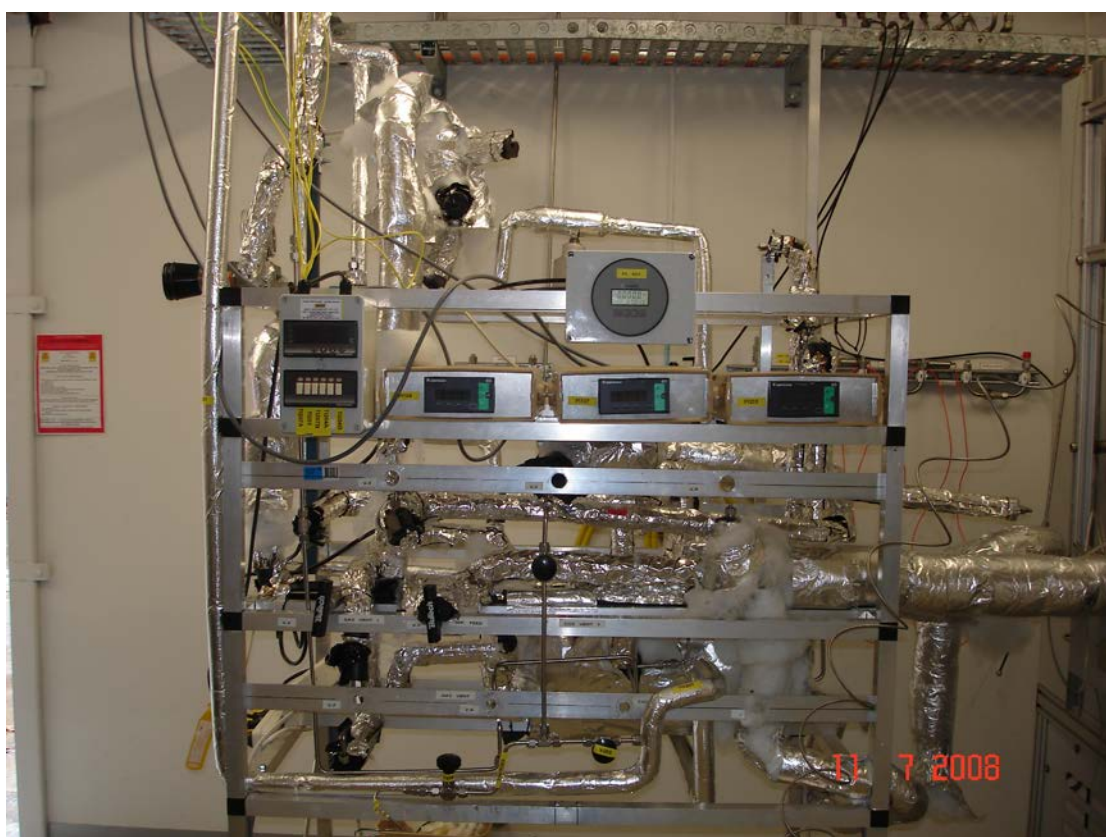


Figure 8. 2 Measuring equipment

Experiments were conducted for gas mixtures essentially resembling those of dry IGCC GE and Shell compositions as presented in Table 8.2. Hydrogen Sulphide and carbon Monoxide were eliminated from the composition due to laboratory safety regulations and the resulting compositions are shown in Table 8.2. Hydrogen was added to account for the volume of the removed Hydrogen Sulphide, and carbon Monoxide was replaced with Nitrogen due to their close boiling points, critical temperature and pressures and having the same energy value. Cryogenic separation was also trial-tested using a mixture similar to Oxyfuel feed gas, however, a hydrate could not be formed at the low pressures at which the flue gas is supplied in this process.

8.2. Laboratory Set-up Description

The laboratory set-up flow diagrams are shown in Figures 8.3 to 8.5. The CO₂ capturing unit consists of three essential parts: a mixing section, a cryogenic section, and the hydrate reactor. The mixtures to be purified from CO₂ are recombined in mixing drum D101 using industrial grade pure gases from 40 liter cylinders through high pressure regulators V103 and V106, and the composition is checked by sampling through top SP101 (V113 open, V114 closed) and bottom SP102 (V114 open, V113 closed) sample points on the vessel. The vessel is equipped with a cooling package PA101, which can be optionally cooled down to -10°C.

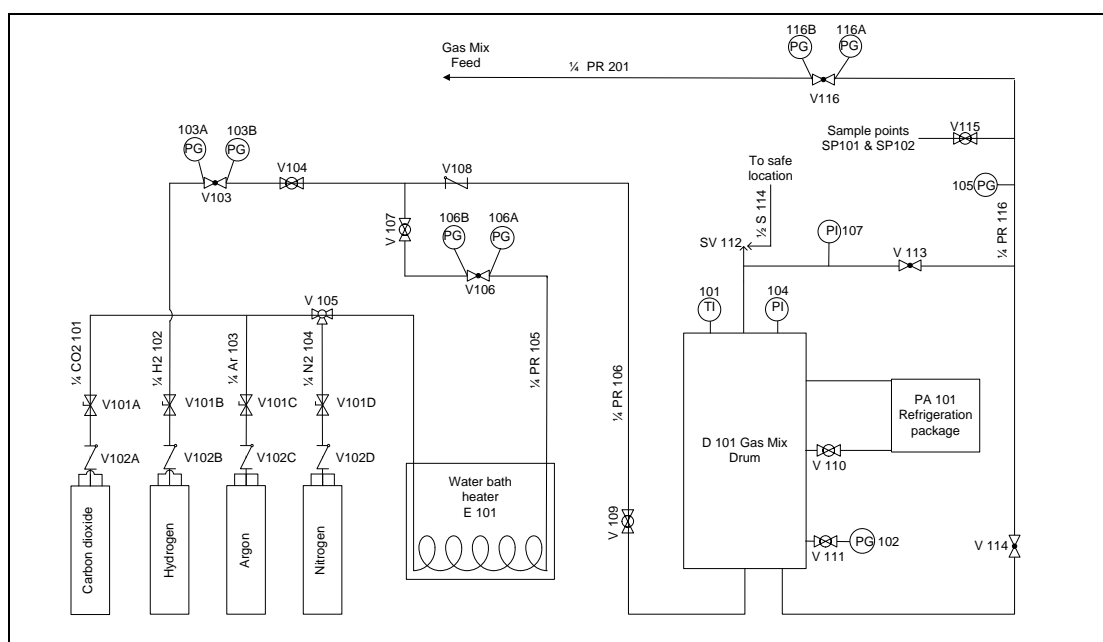


Figure 8. 3 Mixing section

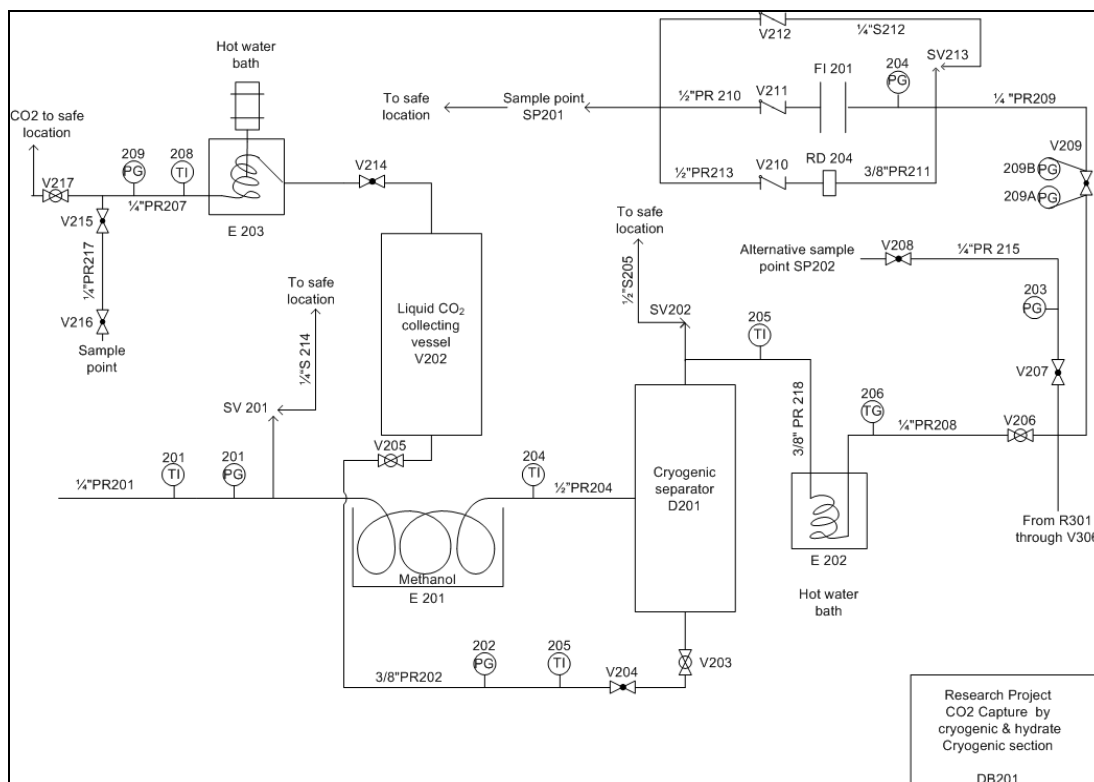


Figure 8. 4 Cryogenic section

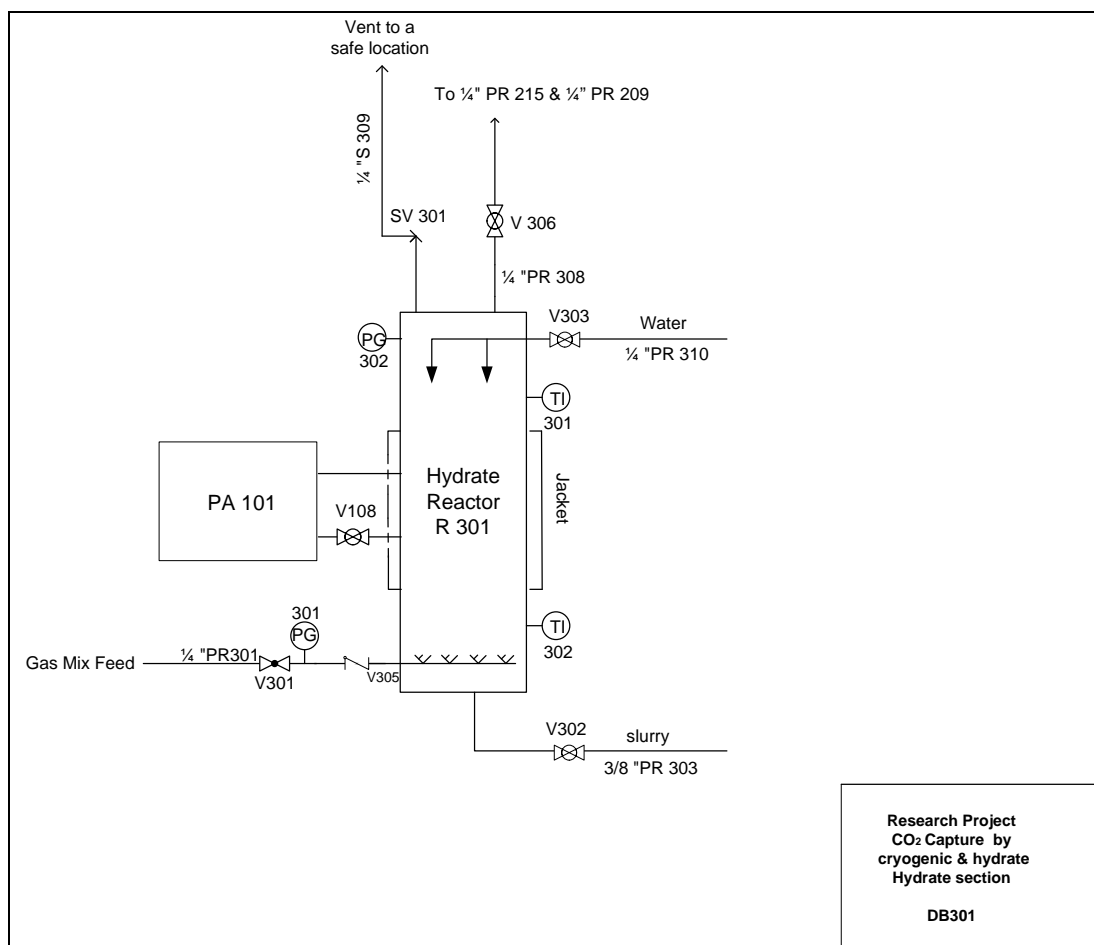


Figure 8. 5 Hydrate section

In the first arrangement, prepared gas is fed from the mixing drum D101 to the chiller E201 where desired low temperatures are achieved allowing for CO₂ condensation after which the two phases, liquid CO₂ and Hydrogen-enriched gas, are separated in cryogenic separator D201. The feed pressure is maintained at the desired level by high pressure regulator V116. The overhead stream is continuously passed through CO₂ analyser SP201 and the flow rate is controlled by the low pressure flow meter FI201 for which the pressure is reduced by the pressure regulator V209 to about 5 bar. The stream is heated in the hot water bath E202 prior to feeding into the flow meter and analyser to eliminate the risk of damaging the equipment. Liquefied CO₂ is drained to the collecting vessel V202 through the valve V203 in order to prevent overfilling of the separator, then taken through a hot water bath E203 and analysed by CO₂ analyser via sample point SP202.

In the second arrangement, the prepared mixture is directed from the mixing drum D101 to the hydrate reactor R301 which is partially filled with water-promoter solution through valve V303. The temperature of the reactor is maintained at 1°C by cooling package PA101. Gas mixture is supplied from the bottom of the vessel to allow better mass transfer and mixing. Once-through gas is continuously passed through the valve V306 to the CO₂ analyser SP201 and the flow rate is controlled by low pressure flow meter FI201. At the end of the experiment, the aqueous phase is analysed by sampling through valve V302.

8.3. Equipment and Specifications

All digital measuring equipment was connected to the displays shown in Figure 8.2. The temperature of each stream was measured by inline sensors and monitored using a six channel Shimaden controller with an accuracy of $\pm 0.1^\circ\text{C}$. Temperature in the cold Methanol-ice bath used as a heat exchanger was monitored by a Deluxe Dual Input Thermometer with an accuracy $\pm 0.1^\circ\text{C}$. The inlet pressure was controlled by Swagelok high pressure regulators. Swagelok pressure transmitters with a 0 to 120 bar range connected to a Shimaden controller were used for monitoring pressure with an accuracy of ± 0.1 bar. An Elster RVG G16 flow meter was used to measure and control gas flow at 1 kg/h with an accuracy of $\pm 1\%$ at pressure not exceeding 5 bar. A Gas Alarm Systems' CO₂ analyser was installed on the venting line after the flow meter. All measurements were carried out after reaching steady flow for 20 minutes.

All vessels used for experimental set-up are stainless steel vertically placed cylinders with the design pressure of 110 bar. Dimensions of the vessels are given in Table 8.1.

Table 8. 1 Dimensions of the vessels used in laboratory set-up

	Mixing drum	Cryogenic separator	Hydrate reactor
ID, in (cm)	7 (17.8)	2 (5.1)	4 (10.2)
Length, in (cm)	41 (104.1)	15 (38.1)	27.5 (69.8)

Gas supply and transport lines are all ¼ in. (6.4 mm) stainless steel pipes supplied by Swagelok; liquid CO₂ and hydrate slurry transport line is ⅜ in. stainless steel. Vent lines and safety lines are mostly ½ in. (12.7 mm).

Safety valves on all vessels have a discharge pressure of 100 bar, and the rupture disk before the low pressure flow meter has a 100 bar rating.

In our experimental equipment, heat exchanger E201 was simulated by chilling coils submerged in a Methanol with dry ice bath. The hydrate reactor outer chilling package PA301 was represented by a large water-ice top-open tank.

8.4. Operating Procedures

The entire system was evacuated for 3 to 4 hours prior to each experiment.

Gas mixtures were prepared in the mixing drum V101 (Figure 8.3) using industrial grade gases supplied by BOC Australia. For the first set of experiments on the cryogenic section, the pressure of each gas to be added was calculated taking into account its compressibility factor, and then adjusted to match the mol composition in the first two columns of Table 8.2 via a trial-and-error method. For the testing of the hydrate section, the amount of Argon and Nitrogen was left unchanged, and the pressure of the H₂ and CO₂ was adjusted to match the measured CO₂ mol% as shown in Table 8.2 (Second feed). An assumption was made that any impurity in the liquid CO₂ after condensation is dissolved Hydrogen.

Silica gel was placed inside the drum to ensure absence of any moisture in the feed, and it was recovered by heating to 95°C overnight prior to each experiment. CO₂ from the cylinder was passed through a hot water bath E101 pre-heated to 60°C in order to ensure that all of it was in the gas phase. The Hydrogen supply line was separated from other gases for safety reasons.

Table 8. 2 First and second feed gas compositions

Table 6.7-1 First and second feed gas compositions				
Test GE				
	First feed		Second feed	
	Mol% (given composition)	P, psia (matching composition)	Mol% (given composition)	P, psia (matching composition)
CO ₂	40.4	441	12	166
N ₂	0.6	10	Amount unchanged	11
Ar	0.8	13		16
H ₂	58.2	938		1300
Feed is supplied at 57 bar				
Test Shell-28				
	First feed		Second feed	
	Mol% (given composition)	P, psia (matching composition)	Mol% (given composition)	P, psia (matching composition)
CO ₂	37.1	400	No hydrate expected, pressure too low	
N ₂	5.6	89		
Ar	0.5	11		
H ₂	56.8	966		
Feed is supplied at 28 bar				
Test Shell-53				
	First feed		Second feed	
	Mol% (given composition)	P, psia (matching composition)	Mol% (given composition)	P, psia (matching composition)
CO ₂	37.1	400	13	166
N ₂	5.6	89	Amount unchanged	89
Ar	0.5	11		11
H ₂	56.8	966		
Feed is supplied at 53 bar				
Test Oxyfuel				
	First feed		Second feed	
	Mol% (given composition)	P, psia (matching composition)	Mol% (given composition)	P, psia (matching composition)
CO ₂	90.43	456	Not Applicable	
N ₂	1.58	9		
Ar	4.82	24		
O ₂	3.17	16		
Feed is supplied at 9 to 12 bar				

Argon and Nitrogen were first mixed together with about 30% of total Hydrogen in the mixing drum. After that CO₂ was added slowly allowing for faster stabilisation, and at the end the rest of the Hydrogen was admixed to the total pressure of about 100 bar. The mixture was left for 2 to 3 hours to reach equilibrium. The mixing drum

could be optionally cooled down to -10°C using the refrigeration package connected to it.

If CO_2 is added first or last, condensation occurs because Hydrogen in these cases forms a cushion for the Carbon Dioxide (Appendix G). This phenomenon was confirmed and demonstrated in a high pressure sapphire PVT cell, which allows for visual observations and described in Appendix A. Therefore, two samples from the top SP101 and the bottom SP102 respectively, of prepared mixture were taken to ensure even distribution of CO_2 concentration along the mixing drum. Uneven distribution of CO_2 in freshly prepared mixture was also observed by other researchers (Kumar et al, 2006).

Dry ice was constantly added into the Methanol chilling bath E201, and temperature was controlled by portable temperature indicator at not less than -55°C to prevent CO_2 freezing in the line. Dried Argon was passed through the chilling coils and separator at a flow rate of about 1 kg/h at supplying pressure of 40 bar in order to bring the temperature of the entire system to the desired level of -55°C . The separator was additionally chilled by pouring liquid Nitrogen on the outer shell of the vessel inside the insulation. After the required low temperature remained stable for at least 20 minutes, the feed was switched to process gas from the mixing drum at the pressure designated in Table 8.2. Liquid CO_2 bottom product was collected in the low temperature separator and removed to a collecting vessel (not shown in Figure 8.4). Condensed CO_2 at the end of the experiment was evaporated by passing it through a hot water bath and the composition was analysed. Lean overhead gas was passed through the analyser at near atmospheric pressure and a flow rate of 1 kg/h which allowed for mass balance calculations.

The quantity of mixture prepared in the mixing drum was sufficient to run the cryogenic section for 20 to 40 minutes each time; however this was insufficient to subsequently form any hydrate. Therefore, the hydrate stage was tested separately.

The hydrate reactor was cleaned, evacuated and filled with 1.5 to 2 litres of fresh water-promoter solution which constitutes approximately one-quarter of the total volume prior to each experiment. By passing cold Argon through the system and maintaining the temperature of the outer chilling package PA101 at 0 to 1°C , the inside temperature was brought down to 1 to 2°C which ensures the absence of any ice formation. After the temperature remained stable for 20 minutes, the flow was switched to the flue gas, prepared according to the composition denoted Second feed

in Table 8.2. The overhead once-through gas was constantly passed through the CO₂ analyser at a rate of 1 kg/hr. When the CO₂ content started rising after about 20 to 30 min, the reactor was insulated and left for 30 min to reach equilibrium. Then two types of experiments were performed. In one case, all gas was quickly vented through the analyser, the reactor was again insulated and left overnight to allow hydrate dissociation. CO₂ content in the released gas was analysed, and a conclusion about CO₂ capture was made. In the other case, the liquid phase was taken out through valve V302 into an open vessel, and a conclusion about hydrate presence was made.

8.5. Safety

The cylinders with pure gases were placed in an outdoor area and securely chained to the wall. Hydrogen was supplied through a separate line to avoid any possible contact with air.

Each vessel was equipped with a safety valve opening to a vent line, and check valves were placed on inlet lines to prevent backflow. Each vessel had insulating plug or ball valves, and the cryogenic separator had two insulating plug valves on the liquid-CO₂ drain line. Needle valves were used for fine control of the flow, especially through the CO₂ analyser.

All of the cryogenic section was properly insulated, and the Methanol with dry ice bath E201 was closed with a lid to prevent splashing of cold liquid. The hydrate reactor was insulated as well.

General personal protective equipment was worn every time during experiments.

8.6. Experimental Results and Discussion

The cryogenic and hydrate sections of the plant were tested separately due to the limited quantity of the feed which could be prepared.

8.6.1. Cryogenic Section

Performance of the cryogenic section was repeated 2 times for IGCC gas mixtures. Average results collected on stand-alone cryogenic separation of CO₂ from IGCC flue gases are summarised in Table 8.3. Insufficient volumetric capacity of the cryogenic separator and the collecting vessel caused the need to increase operational temperatures to -51°C, however as shown in Table 8.3 it did not have a negative

impact on CO₂ capture rates. From IGCC GE gas mixtures containing 40 mol% CO₂ in the feed, up to 80 mol% CO₂ was captured at 57 bar. The overhead stream contained 12 mol% CO₂ and essentially all of the Hydrogen, Nitrogen and Argon. Liquefied CO₂ obtained in this case was characterised by 95 mol% purity on average. Higher purity CO₂ was obtained at higher temperatures due to the smaller amount of liquid phase and therefore better separation of Hydrogen-rich overhead which leads to less Hydrogen dissolved in liquefied CO₂.

Table 8. 3 Summary of Cryogenic stage performance

Process characteristics			CO ₂ content, mol%			Net CO ₂ produced	
Name	Pressure, bar	Temperature, °C	Feed	Processed gas	Liquid	Mol/hr	Mol% capture
IGCC GE	57	-51	40	12	95	60	79
IGCC Shell	53	-51	38	12	97	54	77
IGCC Shell	28	-51	38	22	97	21.8	47
Oxy	10	-50	83	42	94		

CO₂ capture from the IGCC Shell gas mixture was investigated at two different pressures. In the first set of experiments, a pressure of 28 bar was applied. Conventionally, the Shell gasifier operates at pressures about 30 bar, and consequently, the syngas stream from the shift-reactor containing mainly Hydrogen and Carbon Dioxide was supplied at 28 bar. Up to 50 mol% CO₂ was captured at this pressure and -51°C. The overhead stream contained 22 mol% CO₂ and essentially all the Hydrogen, Nitrogen and Argon. In the second series, experiments were conducted at a pressure of 53 bar. At this elevated pressure and -51°C between 75 and 80 mol% CO₂ was captured from the IGCC Shell shifted syngas. CO₂ content was reduced to 12 mol% as in case of the GE mixture. The liquid bottom product contained 97 mol% CO₂ in both cases for the Shell IGCC gas. The higher purity compared to the GE case is due to the smaller amount of liquid collected in the separator and therefore sharper separation from the Hydrogen-rich gas phase.

The amount of liquid CO₂ produced at the cryogenic stage can be represented in terms of the molar flow as shown in Table 8.3. In the case of GE flue gas separation, 60 mol/hr liquid CO₂ is produced at the overhead gas rate of 1 kg/hr. Slightly less CO₂ is produced from the Shell mixture at 53 bar comprising 54 mol/hr, and at 28 bar the rate of liquefied CO₂ drain is 21.8 mol/hr.

In case of Oxyfuel-type feed gas, at the chosen overhead flow rate the separator quickly overfilled with condensed liquid allowing only 10 min of observation. The

CO₂ content in the overhead gas in this case stabilised at 42mol%, and analysis of the liquid phase has shown 94 mol% CO₂.

8.6.1. Hydrate Section

Gas mixtures for the hydrate formation experiments were prepared according to the last column in Table 8.2 which represents the composition shown in the penultimate column. It was assumed that this composition is the same as the overhead gas composition from the cryogenic separator. Experimental testing was conducted before the results presented in Chapter 4 were obtained.

8.6.1.1. Experimental Description

Results on CO₂ capture by hydrate have been obtained with 0.5 wt% aqueous solution of para-TolueneSulphonic acid (pTSA). This chemical was found to significantly promote Natural Gas hydrate formation (Gnanendran & Amin, 2004), and therefore was chosen for testing in this work. Only a slight reduction of the 12 mol% CO₂ overhead at the exit from the cryogenic separation unit to 10 to 11 mol% was achieved in both the Shell and GE feed mixtures at high pressures. The aqueous phase obtained at the end of the experiment resembled extremely sparkling water with very fine white particles; however, they disappeared quickly upon depressurisation. No solid evidence of hydrate formation was obtained, and the lowering in CO₂ concentration was attributed to its increased solubility in water in the presence of pTSA. For the case of the low pressure Shell mixture producing 22 mol% CO₂ in the Hydrogen stream after condensation, the PTSA-water solution was not capable of capturing of any additional CO₂, and the aqueous phase was just a sparkling water. In all cases, the concentration of CO₂ in the gas phase increased after the equilibrium gas was vented and ambient temperature was achieved.

8.6.1.2. Theoretical Modelling

Investigation of the promotion action of a number of different chemicals was conducted on a bench scale high pressure sapphire cell and the results are presented in Chapter 4. Assuming 1 wt% TBAC solution is used for further CO₂ reduction by hydrate, the following estimation can be done for the IGCC GE and high pressure IGCC Shell cases.

To ensure the absence of any error associated with the amount of water and total gas-to-water volume ratio, the hydrate reactor has to be filled with between 1.75 and 1.8 litres of water-promoter solution. The CO₂ content can be reduced from 13 to 8 mol% and from 11 to 7 mol% at pressures about 55 bar. Total CO₂ captured in 170 cc water is between 0.026 and 0.03 mol which in the upscaled case will be approximately one order of magnitude higher. This represents 27 mol% capture. Based on the above assumptions, the instant performance of the hydrate stage can be roughly described in terms of the values in Table 8.4.

Table 8. 4 Estimated Hydrate stage performance

Process characteristics		CO ₂ contents, mol%		Net CO ₂ captured	
Pressure, bar	Temperature, °C	Feed	Processed gas	Mol	Mol% capture
about 55	near 0	12	7.5	0.28	27

The rate of the gaseous CO₂ production as a result of the hydrate dissociation will depend on the flow rate of the exhaust gas as well as the water circulation rate. The latter will be determined by the rate of the slurry removal from the reaction zone into the hydrate dissociation drum. Experimental work has to be conducted in order to choose the optimum conditions for the CO₂ release and water circulation.

8.7. Conclusion

The experimental results show that the combined process is excellent for CO₂ capture from coal gasification systems where the shifted synthesis gas streams come out at high pressures providing ideal conditions for substantial condensation and CO₂ hydrate formation. The trial has confirmed that up to 80 mol% of CO₂ can be captured from IGCC GE process gas mixtures by cryogenic condensation at pressures of 50 to 60 bar and -50°C. Between 50 to 70 mol% of total CO₂ can be removed from the IGCC the Shell gas mixture at pressures between 30 and 53 bar at -50°C. The liquefied CO₂ is characterized by high purity of 95 to 97 mol% with a moderate amount of dissolved gas mainly Hydrogen of 3 to 5 mol% (Surovtseva et al., 2009).

A further reduction of CO₂ content of the gas leaving the condenser can be achieved by hydrate precipitation. The particular hydrate promoter identified in this work and described in Chapter 4 has the potential to reduce CO₂ reduction down to 7 mol% at 1 to 2°C and pressures above 50 bar which constitutes an additional 27 mol% CO₂ reduction in the flue gas.

Chapter 9. Case Study. Cool Energy Cryogenic CO₂ Removal

Project Developer Model

CryoCell® Technology (see Chapter 2.2.2.3) implemented at the Cool Energy demonstration site (Figure 9.1) was initially developed between 1999 and 2002 by Professor Robert Amin who conducted the laboratory tests on what was called Micro-Cell CO₂ removal technology. It is based on the cryogenic CO₂ removal from the process stream, involving condensation and partial freezing of Carbon Dioxide. The method developed in this thesis can be considered analogous as it revolves around the same principles. It is therefore considered worthwhile to look in detail at the development of the CryoCell® Technology, its performance characteristics and problems encountered and conduct a marketplace case study. The data presented in the Chapter has been extracted from the Cool Energy reports, presentations and media publications and from the recent analysis of CCS technologies report given by (Rubin, 2010).

Following successful laboratory tests CryoCell® Technology was placed on a commercialisation path by Curtin University of Technology through the formation of a spin-off company called Cool Energy. The CryoCell® Technology was developed, in part, from the Micro-Cell laboratory-scale work. The CryoCell® initially faced numerous challenges, both technical and financial, however these were overcome and Cool Energy received significant industry and academia support, as well as support from investors and the Australian Government.

Cool Energy and Shell signed an agreement in early June 2005 covering the granting of rights to patents and the sharing of technical results and certain further developments and use in commercial applications.

A 2 MMscf/D demonstration plant is in operation at ARC Energy's Xyris site in the Perth Basin to demonstrate Cool Energy's CO₂ capture technology (Figure 9.1).

In the three years since Cool Energy's conception, it has moved from a 'concept' based company to a position of readiness for commercial application of its revolutionary new CO₂ capture technology.



Figure 9. 1 CoolEnergy Demonstration Site

9.1. Introduction

The project developer model case study represents a robust business case on the basis of the Cool Energy technology for cryogenic gas sweetening called Cryocell® that is very similar to the current research in the sense of cryogenic CO₂ capture.

Cryocell® removes CO₂ from Natural Gas by cooling and depressurizing to a regime where CO₂ deposits from the vapour phase. The solid and condensed CO₂ drops to the bottom of a pressure vessel where it is subsequently drained away. Pipeline specifications are met during development of Natural Gas resources from conventional gas fields containing 10 to 60 mol% CO₂. Cryocell® has been successfully demonstrated in a 2 MMscf/D test plant. Scale-up risk to approximately 100 MMscf/D commercial applications is seen as relatively small. It is difficult to protect Cryocell® via patents, as gas sweetening via solid CO₂ drop out is already in the public domain.

Cryogenic technology offers a possible solution to processing gas streams that contain high concentrations of CO₂ and are supplied at high pressure. It is competing in two markets:

- The removal of CO₂ in order to produce high value gas. Historically this CO₂ has been vented to the atmosphere; and
- The emerging Carbon Capture and Storage market, where CO₂ is captured (rather than just removed) and either stored or used in other processes.

There are no competitive options in production of CO₂ ready for re-use or storage except for the legacy Ryan-Holmes process, however, in the first market the cryogenic technology competes directly with existing procedures and these can be generically classified as:

- Chemical solvents (such as amine based solvents, or the Benfield process)
- Physical solvents such as Selexol™, from Dow/UOP)
- Membranes (such as Natco's Cyanara or UOP's Separex products)
- Hybrid membrane/solvent processes (such as a combination of Cynara with mDEA, a tertiary amine)

Potential entrants to this market also include the CFZ process, Cimarex process and advanced solvents.

Whilst the removal of CO₂ is a common requirement and there are a number of technology options available, the cryogenic technology has an advantage over other processes for processing for a wide range of streams that contain CO₂ content of 10% and higher down to the requirements for sales into pipeline systems

The main benefits of cryogenic technology over existing CO₂ removal techniques can be summarised as follows:

- The cryogenic technology offers both capital (CAPEX) and operating (OPEX) expenditure savings over conventional technologies in a wide range of applications.
- The cryogenic technology is a “better product” than conventional CO₂ removal units in a wide variety of applications offering not only a lower cost, but also a more environmentally friendly process than its competitors.
- The cryogenic technology enables a resource owner to “future proof” its resource/processing facility in anticipation of increased environmental demands, and allows the capture of additional value from a carbon economy.
- The cryogenic technology is the only process offering the production of liquid, ready to inject CO₂ from its primary power generating plant. This is seen as a significant differentiator to conventional techniques which require

expensive “add-on” solutions to capture and make the CO₂ suitable for storage.

In this Chapter both the current market place and future markets for the Cryocell® Technology are analysed. The analysis of the current market place is further broken down into looking at comparisons with the existing practice of removing the CO₂ from the Natural Gas stream and venting it to the atmosphere, and also looking at comparisons when CO₂ capture and storage or further use is required.

9.2. Current Market Place Overview for CO₂ Removal Technologies

The market has historically vented the CO₂ removed from the gas into the atmosphere. With increasing awareness of climate change impacts, and calls for reductions in emissions it has been recognized that in future a differential will be placed on technologies which not only remove CO₂ from the gas stream, but also enable its capture in a form suitable for storage or further use. The current market will be examined under both venting and storage CO₂ scenarios.

While there be other existing technologies, six cryogenic CO₂ removal technologies have been identified that are under development, or have been commercialised, and a review is presented in this Chapter for each technology. Two of these processes are based on cryogenic freezing and four are based on cryogenic cooling. A competitive environment clearly exists. With the exception of the Ryan-Holmes process, the commercial rollout of cryogenic CO₂ removal technologies appears to be quite limited, with no more than a handful of licenses having been sold by each vendor. The IFP/Total technology is new and the ExxonMobil technology is still under development.

Chemical and physical solvents currently account for approximately 90% of all CO₂ removal gas conditioning systems, with membranes making up the bulk of the remaining 10%. Within each of these categories each particular solvent or membrane has specific capabilities and constraints, resulting in different application areas

9.2.1. Chemical Solvents

The nature of the chemical reaction between chemical solvents and CO₂ means that they are capable of removing CO₂ down to very low levels in the product. However, this reaction also produces a lot of heat, so although the solvent can be loaded quite heavily with CO₂ this ability is compromised by the need to dilute the solvent with

water as the loading increases. A large amount of heat is required to liberate the CO₂ from the solvent during regeneration. As a result, as the amount of CO₂ in the feed gas increases the required circulation rate and heat input increase significantly for these systems. Generically therefore, chemical solvents are best employed for feedstock with relatively low levels of CO₂ where the requirement is for a low residual CO₂ content in the gas stream. As a result amines are often used for gas streams containing up to 10 to 15% CO₂ and exclusively for LNG service.

Suppliers of amines include BASF (aMDEA[®]) and Dow Chemical (MDEA). There are many different types of amines in use, but the trend has been to move towards specialized and proprietary amines such as aMDEA. A previous study commissioned by Shell⁶ basically discounted primary and secondary amines due to the fact that tertiary amines have been specifically designed to maximize absorption capacity and minimize required circulation rates, and indicated that almost without exception amine based chemical solvents would not be used for CO₂ contents above approximately 20%. Cool Energy internal analysis supports this viewpoint.

There are also a number of suppliers of hot potassium carbonate products, including ExxonMobil's Flexsorb HP, Catacarb and UOP. The Benfield process (UOP) uses hot potassium carbonate as the solvent, and is capable of processing feed gas with higher concentrations of CO₂ down to pipeline specifications. A good example of this is the Moomba gas plant in the Cooper Basin in South Australia, where an incoming gas stream of 20 to 30% CO₂ is treated to an outgoing level of <4% in the product gas. It should be noted though that the Natural Gas industry is not the main market for the Benfield process, it is mainly applied in ammonia and ethylene oxide plants; of 700 plus applications worldwide only about 50 are in the Natural Gas industry. In the Natural Gas industry the Benfield process is regarded as something of a legacy process, and is generally found to be non-competitive with modern activated amine processes.

9.2.2. Physical Solvents

Physical solvents on the other hand have a limited capacity for loading due to the weaker nature of the interaction between the solvent and the CO₂. However they do not require dilution and regeneration is significantly easier. Nevertheless as CO₂ concentrations go up, the required circulation rates go up. Generically therefore,

⁶ Shell Global Solutions –KBR CO₂ Removal Study Report, KBR Job No: E-116, April 2007

physical solvents are best employed for feedstock with relatively high levels of CO₂ where the requirement is for a relatively high residual CO₂ content in the gas stream. As a result physical solvents are often used for gas streams containing 10 to 40% CO₂.

The most commonly quoted example is the Selexol process (marketed by both Dow Chemical and UOP). The Selexol process can be H₂S selective in the presence of CO₂. The solvent can be regenerated by flashing and/or stripping with steam or gas and can reduce the H₂S, COS and mercaptan contents to 1 ppm. The CO₂ content can be retained or reduced to any required level, although both companies indicate its suitability for bulk CO₂ removal. A limitation of this process is the relatively high solubility of hydrocarbons heavier than Ethane in the solvent which may result in valuable hydrocarbon losses if there is no recovery unit for the flash gas. The process operates best at high pressure with a lean gas.

It is worth noting that although Selexol has been available since the 1970s only about 100 plants⁷ have been built, most of which are not in Natural Gas service. Selexol appears to be more strongly targeted at acid gas removal (mainly H₂S and COS) from gasification projects.

9.2.3. Membranes

Membranes work on the principle of selective permeation of the gas constituents in contact with the membrane. The gases dissolve in the membrane material and move across the membrane barrier under an imposed partial pressure gradient. The pressure gradient is established by feeding high pressure gas to one side of the membrane while maintaining the permeate (waste) side at a much lower pressure. Gases are separated on the basis of their solubility and diffusivity through the membrane material. As a result membranes are best employed for feedstock with high levels of CO₂ where the requirement is for a high CO₂ residual content in the gas stream. As a result membranes are often employed where the CO₂ specification is very lenient, or for the bulk removal from streams with a high CO₂ content.

Polymers commonly used in gas separation membranes include cellulose derivatives, polySulphone, polyamides and polyimides. Generally membrane plants need careful pre-treatment design to minimize fouling which otherwise have been known to lead to prohibitive operational costs and the requirement to retrofit pre-treatment

⁷ Dow and UOP product brochures indicate about 45 and about 55 plants respectively

facilities. Because of co-permeation of hydrocarbons along with the CO₂, membrane systems are often characterized by high losses, or require significant and costly recycle streams in order to reduce these losses.

A good example of the application of membranes is the SACROC EOR facility in North America where CO₂ is separated and used for enhanced oil recovery. A Cynara membrane system reduces CO₂ content of an associated gas stream from around 80 to 85%, to 10%.

Examples of the use of membranes in these applications can also be found in offshore peninsular Malaysia where streams containing 30 to 40% CO₂ are treated down to a pipeline specification of <8% CO₂.

Membranes have been employed in commercial Natural Gas applications since the early 1980s. It is estimated that over 200 membrane systems have been installed.

9.2.4. Hybrid Membrane and Chemical Solvents

The application of a hybrid system works on the principle that both parts of the system are operating in the application most suited to them. Membranes are employed for bulk CO₂ removal and a chemical solvent (often mDEA) is used as the final polishing step. Generically therefore, hybrid membrane/chemical solvent systems are best employed for feedstock with high levels of CO₂ where the requirement is for a low residual CO₂ content in the gas stream. This would suggest best use for these systems for gas streams with >20% CO₂ and a stringent (<3%) outlet specification.

The SACROC facility was first designed at the existing Benfield plant, creating a hybrid plant with membranes carrying out bulk removal followed by a Benfield process for final polishing. It now still operates in series with a polishing step, but the Benfield plant has been replaced by an amine unit.

The Grissik Gas Plant in Sumatra, Indonesia is another example of a hybrid membrane solvent system, with membranes reducing the CO₂ concentration down from 30% to 15% and an amine solvent (mDEA) used for final clean up.

9.3. CryoCell® Position in the CO₂ Removal Market (vented to atmosphere)

9.3.1. Comparison with Chemical Solvents

Previous studies^{8,9} have shown quite clearly where CryoCell® advantages lay in relation to a generic chemical solvent (amine) processes. More recent in-house studies have confirmed the advantages.

Detailed studies based on lean gas cases with 20% and 35% CO₂ for a 50MMscf/D feed rate have shown that CryoCell® has a competitive advantage in terms of power consumption, and therefore fuel usage and hydrocarbon efficiency, which increases with the CO₂ content of the gas stream.

9.3.1.1. Capital Cost

From Figure 9.2 it can be seen that as the CO₂ content of a gas increases beyond about 17 to 18%, CryoCell® offers an increasing capital cost advantage compared with conventional technology when compared on capital cost alone if both processes are venting to the atmosphere. This advantage increases with increasing CO₂ content. In the examples used, benefits ranged from about 6% at 20% CO₂ up to about 30% at 35% CO₂.

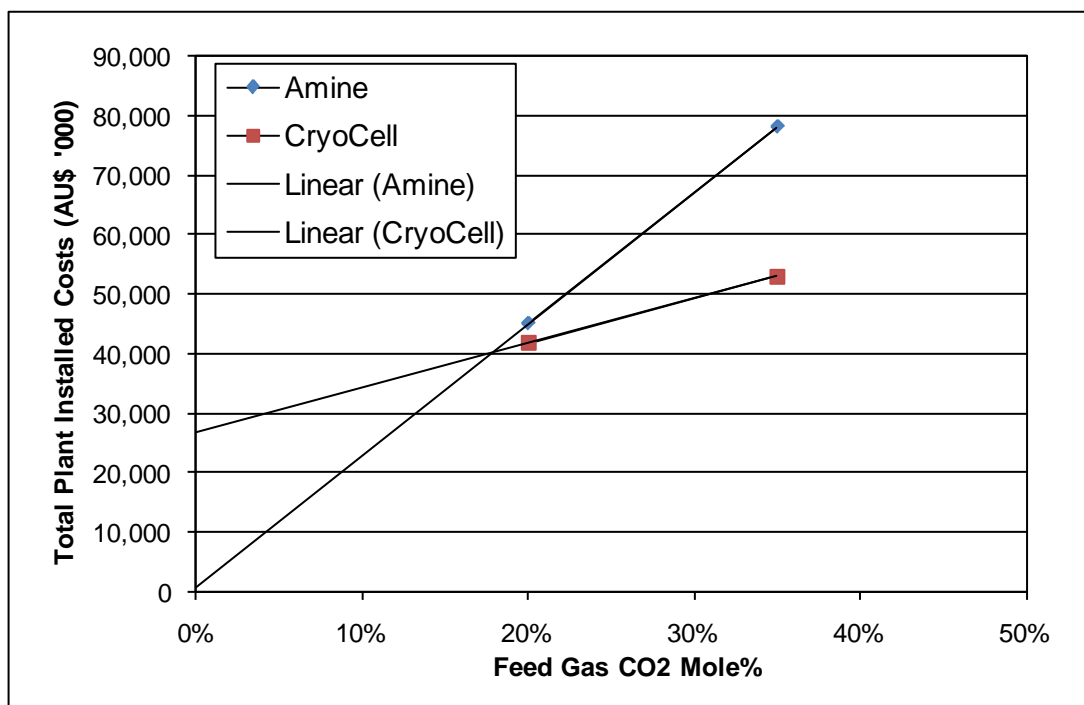


Figure 9. 2 Cost comparison between CryoCell and Amine for CO₂ removal only

⁸ CleanGas Feasibility Study, October 2007.

⁹ Evaluation of Cool Energy's CryoCell® Gas Processing Technology versus Conventional Technology, Presson Enerflex, October 2005 and updated from time to time in 2006 and 2007.

9.3.1.2. Operating Cost

CryoCell® offers advantages due to:

- Simpler operations
- No consumable chemicals used
- No water use
- Expected lower maintenance requirements due to elimination of corrosion potential

When overall costs are compared it is estimated that the impact of lower OPEX will reduce the “breakeven point” of CryoCell® by a further 2% from approximately 17 to 18% CO₂ to 15 to 16% CO₂ when comparing both processes venting to the atmosphere.

9.3.1.3. Conclusion for Chemical Solvents

The above analyses indicate that in a straight comparison for CO₂ removal (both processes venting to the atmosphere) CryoCell® Technology becomes competitive with amine processes at CO₂ levels above 15% and at levels above 20% appears to have a clear advantage.

It should be remembered that this comparison has been made against a generic amine (tertiary) process, and that there are a number of proprietary amine based technologies available. Each of these proprietary technologies has been designed to perform better than a generic process under certain conditions (e.g. Sulfinol® is designed to remove H₂S at the same time as removing CO₂), but because of the proprietary nature of these products it is not possible to carry out a detailed comparison such as the above for each.

Given the above, it has been assumed that the generic comparison is a reasonable basis for all chemical solvents, however, it cannot be ruled out that in an individual situation a proprietary technology may offer a more cost effective solution than CryoCell®.

9.3.2. Comparison with Physical Solvents and Membranes

Due to the proprietary nature of the information, it is not possible to directly compare CryoCell® to the proprietary physical solvents and membrane processes, some of which are, or can be focused on specific applications (e.g. Selexol™ can be tailored

to remove both H₂S and CO₂). However given their basic positioning within the markets a number of conclusions can be drawn.

CryoCell® Technology clearly has an advantage over chemical solvents when looking at processing a feed gas with a high CO₂ content to a pipeline specification. Physical solvents and membranes also appear to have an advantage over chemical solvents in this area. Given this it is reasonable to assume that CryoCell® technology will be competing directly with physical solvents, membranes and membrane-chemical solvent hybrids in its current market application.

Whilst it is difficult to determine quantitative differences in either cost or emissions performance some qualitative statements can be made:

- In general, physical solvents have a low loading capacity and therefore high solvent circulation, this generally means that they are only competitive against chemical solvents above 15 to 20% CO₂. Given the linear relationship of the circulation rate with CO₂ removal, this leads to the conclusion that CryoCell® will have a similar cost advantage over physical solvents to that over chemical solvents.
- To date we can find no evidence that any solvent processes (physical or chemical) have been used on Natural Gas streams with a CO₂ concentration above 30%.
- Membrane systems in general need significant recycle capacity and multiple stages in order to reach a pipeline gas specification, leading to a high cost of installation.
- Many commercial applications of membranes in Natural Gas conditioning have been plagued by fouling caused by insufficient pre-treatment, leading to a high operating cost, and in the worst cases to further significant capital expense.
- Hybrid systems are designed to capture the “best of both applications” and so would be expected to have advantages over both solvents and membranes in specific areas of application. However it entails the installation of two separate and discrete processing steps each of which has issues previously identified, leading to both high installation and operating costs.

9.3.3. CryoCell® Competitive Position for CO₂ Removal

Based on this analysis Cool Energy concludes that in a straight comparison CryoCell® has a competitive advantage over existing competitive technologies for processing Natural Gas streams with high CO₂ content (>15% CO₂) down to pipeline specifications.

Notwithstanding the above analyses, CryoCell® technology retains a number of distinct advantages over all the other processes:

- The process does not have significant consumables. Solvents require make-up and change-out, and membranes have a limited life.
- The operation is simpler than solvent processes: the main control points are temperature and pressure, there is no requirement to control concentration or circulation rate of a solvent.
- Both solvent and membrane processes have the potential for performance to be “spoilt” due to degradation, this is not present in a CryoCell® plant.

However the single biggest advantage that the CryoCell® plant offers is the issue of obtaining CO₂ in a ready to inject form. The CryoCell® process captures CO₂ as a pressurized liquid and is therefore ready for transport and injection. All the other processes release CO₂ as a warm and wet atmospheric gas which must then be captured, dried and compressed to be ready for storage. This will be looked at more closely in the following section.

9.4. Competing Technologies in the CO₂ Capture Market (Geological storage, EOR, etc.)

None of the competing technologies listed in the previous section involve CO₂ capture. The focus of each of these technologies is on removing CO₂ from the gas stream. In all solvent and membrane based processes this CO₂ and any associated contaminants are then vented to the atmosphere at low pressure.

In order to capture the CO₂ into a usable or storable form, further processing is required in the form of compression and cooling and often dehydration. This add-on solution is not seen as attractive within the industry, and technologies that capture the CO₂ in a liquid form are being sought.

CryoCell® captures the CO₂ as a dehydrated pressurized liquid, and so has distinct advantages over the technologies already discussed.

This is a new industry area and there are very few competitors that can be identified. This section looks at other technologies currently in the CO₂ capture market, including comparison with conventional technologies plus compression.

9.4.1. Cryogenic Distillation (Ryan-Holmes)

The Ryan-Holmes process operates under similar conditions to the CryoCell®; that is, it operates at temperatures and pressures where solid CO₂ will form. The process, however, prevents the formation of solid CO₂ through the use of a liquid hydrocarbon additive. It also recovers CO₂ as a pressurized liquid.

The Ryan-Holmes is basically a series of distillation columns through which a dry feed gas is treated; in the first column Propane and heavier components are removed (de-ethaniser), in the second column Ethane and bulk CO₂ are removed from the Methane, and in the third column the remaining CO₂ is removed from the Methane (demethaniser), which is then suitable for sale. Solid formation is prevented via the use of the liquid additive as reflux. A fourth column acts as the additive regenerator feeding liquid reflux back to the first and third columns. The CO₂-Ethane stream off the bottom of the second column is recovered as a liquid at pressure.

The Ryan-Holmes process was first registered in the early 1980s and the technology appears to be owned by Chart Industries. Information about applications is difficult to come by, but it appears to have been employed in at least a handful of applications exclusively associated with enhanced oil recovery from associated gas. There is no reference to the process on the Chart website, and there is little indication that they are currently targeting the Natural Gas conditioning market.

9.5. CryoCell® position in the CO₂ capture Market (CO₂ in injectable form)

9.5.1. Comparison with Solvents and Membranes

The previous section showed comparisons based on CO₂ removal only. When the need for capture and storage or use of the CO₂ (for CCS or EOR) is included then the advantages of CryoCell® increase significantly.

Table 9.1 gives a detailed comparison of CryoCell® against an amine plant, showing the advantages in terms of power, fuel use and hydrocarbon efficiency.

Table 9. 1 Comparison of CryoCell and Amine plant fuel and power requirements

	Amine		CryoCell [®]	
	20 mol%	35mol%	20mol%	35 mol%
CO ₂ for Storage (t/D)	460	859	460	859
Sales Gas Rate (MMscf/D)	37.7	27.8	38.2	29.6
Fuel Gas Rate (MMscf/D)	2.8	5.1	1.3	2.0
Hydrocarbon Efficiency* (%)	91	85	91	88
Electrical Load (MW)	1.3	2.2	0.2	0.3
Compression Power (MW)	1.9	3.8	4.3	7.0
Process Heating (MW)	19	35	<0.1	<0.1

9.5.1.1. Capital Cost

When the costs associated with capture and storage are added into the picture the cost advantages of CryoCell[®] compared to conventional technologies increase. Comparison of Figure 9.2 and Figure 9.3 shows the increasing cost advantage over amines when CO₂ capture is included. For CO₂ contents above about 12 to 13% CryoCell[®] shows an increasing advantage.

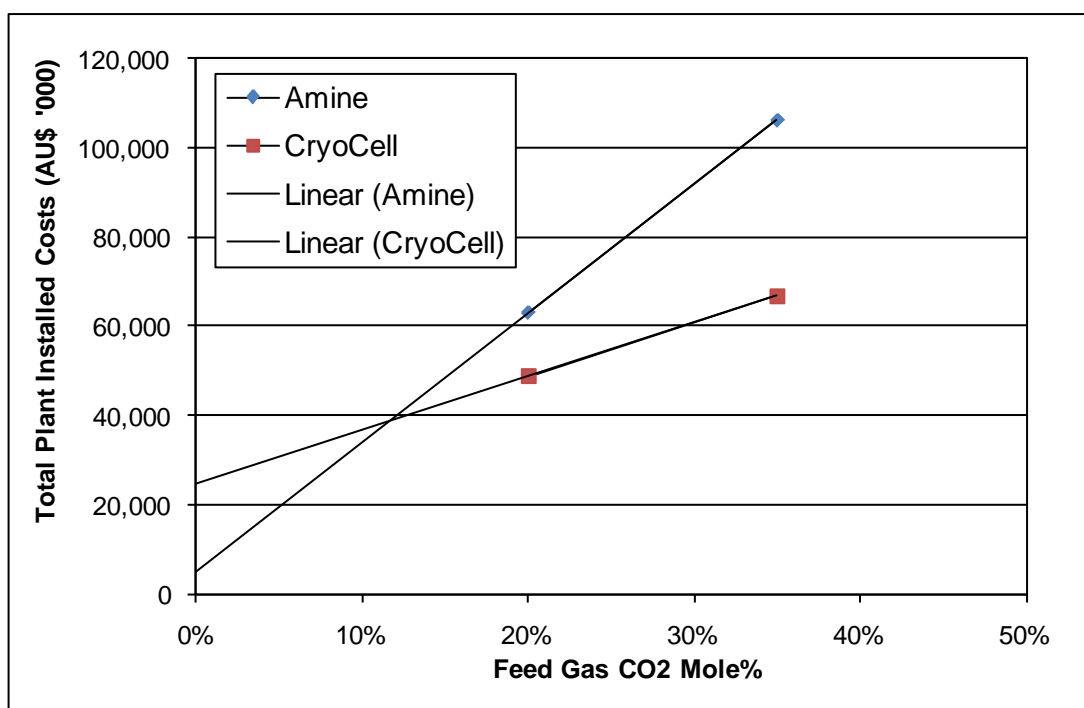


Figure 9. 3 Cost comparison of CryoCell[®] and amine including CO₂ capture (Hart & Gnanendran, 2008a)

9.5.1.2. Operating Cost

CryoCell® offers advantages due to:

- Simpler operations
- No consumable chemicals use
- No water use
- Expected lower maintenance requirements due to elimination of corrosion potential.

As in the previous section it is estimated that the impact of lower OPEX will reduce the “breakeven point” of CryoCell® by a further 2% from approximately 12 to 13% CO₂ to 10 to 11% CO₂.

9.5.1.3. Emissions from fuel gas

Comparisons between CryoCell® Technology and amine show that the emissions from each type of plant vary significantly with both CO₂ content and heavy hydrocarbons.

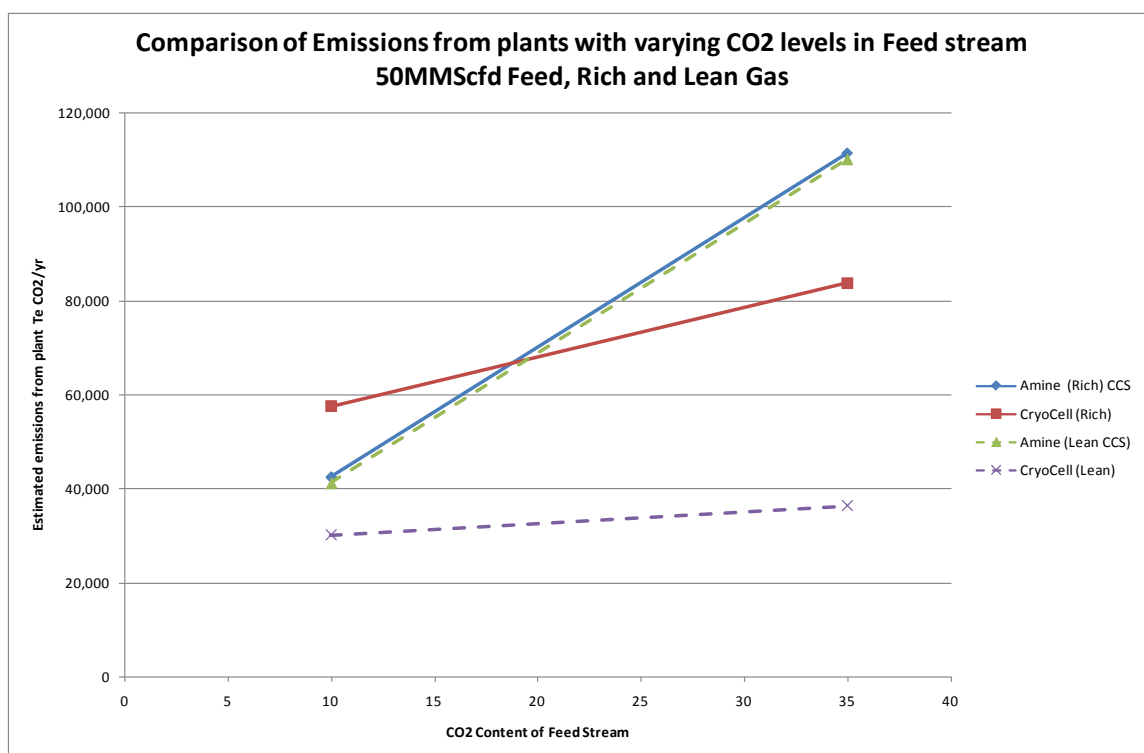


Figure 9. 4 Comparison of emissions from fuel gas for CryoCell and Amine plants (Hart & Gnanendran, 2008b)

For a lean gas, emissions from a CryoCell® plant are significantly lower than from an amine plant at CO₂ content levels below 10%, but for a rich gas the emissions advantage does not come in until about 20% CO₂.

9.5.2. Comparison with Ryan-Holmes

Cool Energy's knowledge of cryogenic processing allows some insights into the Ryan-Holmes process. The first and second columns appear to act in a manner similar to the CryoFrac and DeCO₂aniser columns in a CryoCell plant treating rich gas streams.

Cool Energy analysis has shown that it is more efficient to remove bulk CO₂ along with all the NGLs and then separate the CO₂ from this stream, rather than removing the NGLs and then the CO₂.

The CO₂ rich liquid stream from the bottom of the demethaniser is recycled to the first column, introducing a significant (CO₂-Hydrocarbon) recycle stream into the system. Given the above, Cool Energy would expect to have significant energy and efficiency advantages over this process.

Based on this, and on the current understanding that this process has to date been employed exclusively on EOR projects, Cool Energy does not view the Ryan-Holmes process as a direct competitor at this stage.

9.5.3. CryoCell® Competitive Position for CO₂ Capture

Based on the above analysis Cool Energy concludes that CryoCell® has a competitive advantage over existing technologies for processing Natural Gas streams with high CO₂ content (>10% CO₂) down to pipeline specifications where there is a requirement to capture the CO₂.

9.6. Potential Competition in the CO₂ Capture Market

There are other technologies being investigated in the area of CO₂ capture, and these are discussed in this section. It is important to note that the CryoCell® technology appears to be more advanced than most.

9.6.1. CFZTM – Controlled Freeze Zone



ExxonMobil carried out tests on this technology in 1986 and the schematic is given in Figure 2.6. However the test work was shelved (due to the lack of need or desire to develop high CO₂ gas fields) and no significant work was done in this area for over 20 years. In April 2008 ExxonMobil announced that they would build a demonstration facility to recommence testing this technology, with the aim of commercialisation.

Figure 9. 5 CFZ Clear Lake Pilot Plant (Scott Northrop, 2004)

Whilst this is a potential direct competitor for CryoCell® as its technology base is very similar, Cool Energy analysis is that it is unlikely to present itself as a direct competitor for a number of years.

The demonstration plant will have to undergo the same series of tests that CryoCell has already conducted and completed in 2007. The test facility is expected to start up sometime in 2009 and Cool Energy expects that there will be at least a 12 month testing program. This puts Cool Energy approximately 3 years ahead of ExxonMobil. The CFZTM process is also targeting H₂S removal in a single step column.

ExxonMobil is a large multinational and as such operates in a different market area to Cool Energy. ExxonMobil has stated in industry papers (Valencia et al., 2008) that it is targeting the use of this technology at scales up to 1,000 MMscf/D. It is unlikely that they will be looking at small to medium scale developments such as those currently planned by Cool Energy.

Cool Energy regards the choice of CFZ for further development as an endorsement of the cryogenic CO₂ capture route by another major and well-respected company. However given the time-scale of the research and development work, and the nature of the company, Cool Energy does not view CFZ as a potential direct competitor unless ExxonMobil decides to license the technology to another technology provider (e.g. UOP or BASF). Cool Energy intends to maintain a watching brief on the development of CFZ.

9.6.2. The Cimorex Process

The process utilized by Cimorex appears to be a refrigerated physical solvent process, employing first a cold fractionation step to remove bulk CO₂ and then cold Methanol to absorb the remaining CO₂. The developer BCCK claim that the resultant gas stream will contain CO₂ at levels of 1 to 5ppm and is suitable for feed into an LNG plant. However there is no documentary evidence of any tests on either laboratory or pilot plant scale to support this claim, and the first application of this technology will be to produce pipeline specification gas at a plant in Wyoming, USA.

Given that this process looks remarkably similar to the proposed CryoZorb™ design for a high CO₂ content gas (see section 9.7.1) without the CryoCell® separation step (in between the fractionation step and the Methanol polishing step), Cool Energy has a number of insights into this process. The following observations can be made:

The modelling has confirmed the capability of Methanol absorption to obtain the required CO₂ removal to enable liquefaction however it is anticipated that residual levels will be in the order of 50 to 100 ppm from the Methanol absorption step.

It is unlikely that the Cimorex process will be operating at temperatures as low as those proposed for CryoZorb. The absorption of CO₂ in Methanol improves with decreasing temperature, and therefore the amount of CO₂ absorbed in the Cimorex process will be less than expected for CryoZorb.

The fractionation step can only reduce CO₂ levels down to about 15%; the CryoCell step reduces this further to less than 3%.

Without the CryoCell step, and operating at higher temperatures, Cool Energy has doubts that the claims made for the Cimorex process (1 to 5 ppm CO₂) can be achieved. Even if this result could be achieved, the amount of Methanol circulation, and CO₂ recycle that would be needed would be economically prohibitive.

Cool Energy analysis suggests that this is more likely to be a competitor in the current market of producing pipeline specification. As such the comments made regarding physical solvents can also be applied to the Cimarex process.

9.6.3. Advanced Solvents

There has already been significant progress in solvent technologies, with the development of both tertiary amines and proprietary cocktails of chemical and physical solvents. Nevertheless there is a continuing focus on the development of new solvents, in part driven by the climate change debate and the need to reduce costs to capture CO₂ from flue gas.

Since amines form the basis of most current flue gas capture work most of the work in this area is currently focused on developing new chemical solvents to better capture CO₂ from flue gas. However, any successes in this area could transfer back into the Natural Gas arena offering a new solvent with better absorption and/or regeneration properties and thus could present a new competitor for CryoCell.

Currently there have been no really significant developments of either chemical or physical solvents; however there is significant work ongoing. A recent article (Heldebrant, 2008) in *Energy and Environmental Science* indicates an example of what might develop in the future. Some success in research into CO₂ binding organic liquids (CO₂ BOLs) as potential alternatives to amine based scrubbers has been reported in the US. The authors claim to have discovered CO₂ BOLs which can store almost 20% of their own weight of CO₂ – almost treble the gravimetric capacity of aqueous amine – and which require only half the amount of energy to release the CO₂ on regeneration.

Although only laboratory scale at present, this could develop into a competitive threat if it could be proved at a larger scale.

9.6.4. IFPexol IFPex 2

The IFPex 2 process from IFP/Prosernat is described in the literature and uses a refrigerated Methanol stream to remove acid gas in upstream developments. In this aspect it is similar to Rectisol. Regeneration is carried out in a stripper. Removal of CO₂ down to 1% is claimed.

The technology was licensed by IFP in 1992, but we have been unable to find a commercial application of IFPexol2, and it is not listed on either the IFP or Prosernat websites.

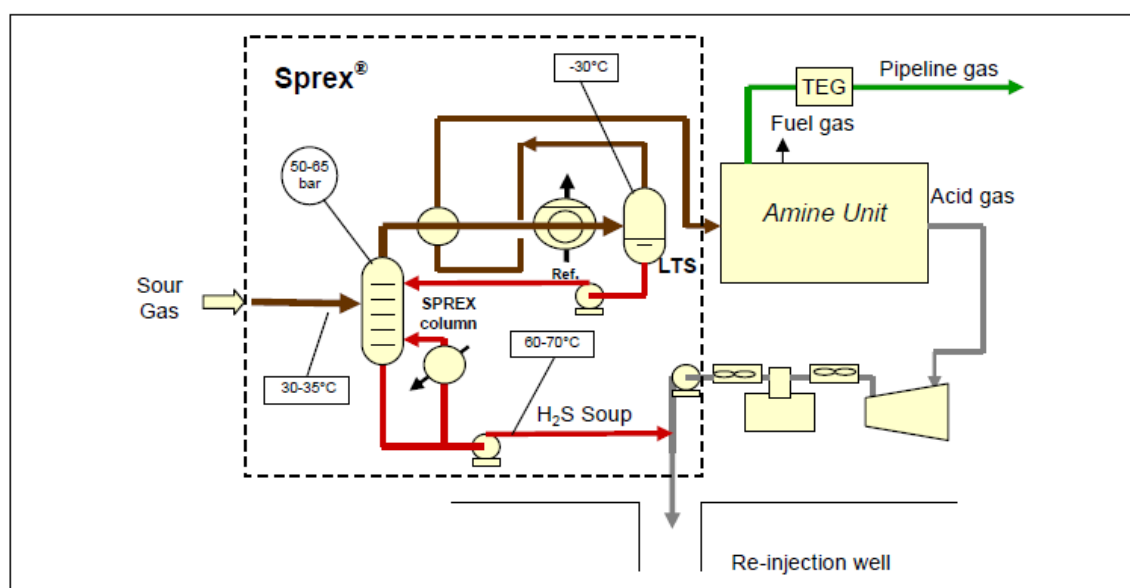
Given the lack of material and data on this process Cool Energy assumes it is no longer available, and therefore is not a competitor to the CryoCell technology.

9.6.5. Sprex® CO₂

Total, IFP and Prosernat have teamed up to develop a process to remove CO₂.

This is still in the research and development phase, and is described by Total as a hybrid solvent and membrane process that will reduce CO₂ content from above 35% to below 20%.

At first sight this doesn't look to be offering an immediate solution to getting to pipeline specification, and in any case is a proprietary example of a hybrid process that is already covered under existing competitor discussions.



Source: Total: 50 years in Sour Gas Production, November 2007. Total

Figure 9. 6 Simplified Sprex Process Flow Diagram

9.7. Future Markets Overview

Cool Energy is just embarking on a series of trials to remove and capture CO₂ from Natural Gas streams to the level required to enable LNG production.

Beyond this, the technology development staircase and a broadening of applications could move Cool Energy into a number of markets, including Landfill, syngas, Oxyfuels, etc. Competition across some of the more likely of these will be discussed in this section.

9.7.1. Competing Technologies in LNG Market

CryoZorb™ can be viewed as a hybrid CryoCell®-physical solvent process, since the initial CryoCell separation step is followed by a Methanol absorption step to remove the remaining CO₂. A successful result from the CryoZorb™ trials will open up new markets for Cool Energy based on an ability to produce LNG directly from the plant. The only real competitors in this market space in terms of CO₂ removal are amines and proprietary chemical and physical solvent cocktails such as the Shell Sulfinol solvent.

However, in developing an LNG application Cool Energy is taking the CryoCell® technology into a different arena, and in effect will be developing a new LNG process where the CO₂ removal step is integral in the cooling process rather than a separate “front-end” process. As such the competitive arena will be the whole LNG production process, from feed gas to final product.

For the purposes of this discussion the LNG Market is broken down into 3 distinct areas:

- Large Scale LNG (>1000T/D (0.3MTPA))
- Medium Scale LNG (100-1000T/D)
- Small Scale LNG (<100T/D)

9.7.1.1. Large Scale LNG

From the initial world's first export LNG plant (about 1 megatonnes per annum (MTPA)) built in Algeria through to the last plant commissioned on the Australian North-West shelf in 2008 (about 4.5 MTPA), without exception all the LNG plants have utilized amines of some sort to remove CO₂ prior to liquefaction.

The majority have employed straight amines (normally a tertiary amine), but on occasions, where some H₂S removal has been required, or for other commercial reasons, Sulfinol, a mixed amine and physical solvent has also been employed.

Given Cool Energy's licensing position the largest scale plant likely to be considered is of the order of 1.5 MTPA (4500T/D).

In this context CryoZorb™ is competing against “standard” LNG facilities. The integration of CryoZorb™ into an LNG facility offers a number of potential advantages:

- Replacement of the whole “front end scrubbing” amine section

- Removal of the cost differential for dehydration that is a penalty for CryoCell in the pipeline gas market.
- Removal of end compression costs
- Integration of refrigeration requirements
- Other identified advantages of CryoCell technology over amines.

These have all been documented in more detail in a recent paper¹⁰, and suggest that CryoZorb™ should have a significant advantage over amines in a range of LNG applications.

9.7.1.2. Medium Scale LNG

This is a slightly different arena. This scale of LNG plant was initiated in the US and is now starting to be employed around the world. Examples of small scale LNG can be found in Western Australia at the Wesfarmers Kwinana LNG plant and the Energy Developments West Kimberley Power Project at Maitland in Karratha (both about 200T/D). This scale is aimed at providing LNG to fuel stationary but isolated power requirements.

To date all medium scale LNG plants take their feed from pipeline gas (with <3 to 4% CO₂), and therefore an amine CO₂ removal unit has been the obvious solution for CO₂ removal. Competitors in this arena include Kryopak (West Kimberley) and Linde (Kwinana).

CryoZorb™ could compete directly with the existing medium scale LNG applications taking gas from the pipeline and converting it to LNG – in this case the CryoCell separator step would be unnecessary and only the absorption section would be employed. Whilst this is a possibility, Cool Energy would in effect be offering a physical solvent process to replace the amine process. Results from the CryoZorb™ trials should enable an evaluation of whether this will offer significant advantages. In addition CryoZorb™ will, in effect, carve out a new and unique opportunity: the ability to produce LNG directly from an initial (and potentially remote) processing facility. There are currently no competitors operating in this space.

¹⁰ CryoZorb™ : CryoCell® - Methanol Absorber Field Trials. Cool Energy Board Paper, October 2008.

9.7.1.3. *Small scale LNG*

Very small scale LNG plants are aimed directly at the transport fuel market. Gas sources for this scale of plant currently range from pipeline gas to biogas from landfill. This is recognized as a growing area and some competitors and competing technology is identified below.

Prometheus Energy Landfill to LNG Facility

Prometheus Energy have built a processing plant at the Bowerman Landfill site in California that takes landfill gas and processes it to produce LNG. The plant capacity is approximately 1.3 MMscf/D (slightly smaller in capacity than the CryoCell[®] Demonstration Plant), and produces approximately 5000 gallons per day of LNG (about 10 T/D). They are looking to expand this plant to a potential size of 40,000 gallons per day (about 80 T/D). Whilst they are both currently in a different market and small in scale, the technology includes the following:

- A pre-purification module, which removes Sulphur compounds.
- A bulk purification module, which removes CO₂ using a “proprietary cryogenic freezing technique that simultaneously pre-cools the Methane and any Nitrogen while freezing out the CO₂”.
- A liquefaction and post purification module, where the gas is liquefied and Nitrogen removed through flashing.

The technology is based on a semi-continuous process analogous to the molecular sieve dehydration process. In this process two identical heat exchangers are operated in a cyclic process, one in operation and one in regeneration mode. In the operation mode the heat exchanger is cooled to approximately -120 to -130°C by a refrigerant (in the tube side), and operated at approximately 13 to 15 bar, the CO₂ rich gas stream is fed into the exchanger, solid CO₂ is allowed to form on the surface of the heat exchanger and LNG is drawn out of the other end of the exchanger.

In the regeneration mode the pressure in the heat exchanger is reduced to atmospheric, and the exchanger is heated by replacing the refrigerant flow with the incoming gas stream which pre-cools the incoming gas. CO₂ sublimates from the surface of the exchanger.

Over time the performance of the heat exchanger in operation will deteriorate as the increasing layer of solid CO₂ reduces heat transfer capacity. Once this reaches a certain point the heat exchangers will be switched.

It is thought that the resulting CO₂ stream is either burnt or emitted to the atmosphere.

Their website does indicate that they regard the technology as suitable for stranded gas, and coal bed Methane, which would put them in potential competition with Cool Energy. However all their current projects are focused on landfill gas, and the process patent is clearly focused on a scale of less than 2 MMscf/D.

Cool Energy recognizes the similarities of the Prometheus technology to CryoCell®. Initial analysis of this process indicates the following key differences:

- The reliance on a cyclic process which allows solid CO₂ to form on a heat exchange surface indicates that scale up of this process would be difficult. This is backed up by statements made in the patent which clearly indicate that the inventors see this as a small scale technology.
- This process produces CO₂ as a gas at atmospheric conditions and is therefore vented.

Given the above, Cool Energy does not regard the Prometheus process as a direct competitor. However, should Cool Energy move into landfill gas applications they would be in direct competition with Prometheus.

Cool Energy recognizes the Prometheus technology as a potential competitor and is intending to keep a close eye on any future developments.

CO₂ Wash®

At first sight CO₂ Wash® from Acrion is similar to Prometheus as it has a demonstration plant producing LNG from Landfill gas with its CO₂ Wash® process. However the process technology is markedly different. The CO₂ Wash® process is a refrigerated column that produces food grade CO₂ and a Methane rich stream from a dehydrated landfill gas feed. The resulting Methane rich gas stream however still contains upwards of 30% CO₂. In order to create LNG from this stream Acrion have employed Air Liquide MEDAL membranes to reduce the CO₂ concentration down to 50 ppm. The liquefaction occurs through exchange with liquid Nitrogen which presumably is boiled off.

The size of this process appears to have been approximately 150 to 200 gallons of LNG per day (or 50,000 scf/D), less than the size of the lab scale microcell tests on which CryoCell is based.

Cool Energy analysis suggests that this technology is not a direct competitor to CryoCell®, or directly transferable to the Natural Gas market. In any case the main CO₂ removal is carried out by membranes, and these are covered under existing competitor discussions.

This technology may in fact be complementary to CryoZorb for Landfill sites if the scales can be matched. Cool energy will maintain a watching brief on this.

9.7.2. Other Technologies in Syngas and Other Potential Markets

9.7.2.1. Rectisol and Purisol

Both solvents were first described in (Hochgesand, 1970). Rectisol is a physical solvent based process offered by both Lurgi (Air Liquide) and Linde. It employs refrigerated Methanol as the solvent for stripping acid gases out of syngas from gasification plants.

Due to the use of refrigerated Methanol there are many similarities between this application and the CryoZorb process, however Rectisol is firmly targeted at the clean up of syngas from gasification plants, where it has approximately 75% of the market. As such it does not represent a direct competitor to CryoCell technology. The Rectisol process also operates at much higher temperatures (similar to the Cimarrex process).

When Cool Energy develops the CryoCell technology further into the syngas market, Rectisol would become a competitor.

The Lurgi Purisol® process is used for bulk removal of acid gases by physical absorption in amine-based solvent. It is ideal for the selective desulfurization of raw gases from the partial oxidation of heavy oils or from coal gasification. As the solubility of H₂S is significantly higher than that of CO₂, only very little CO₂ is co-absorbed.

Purisol is not a competitor to the CryoCell® technology

9.7.2.2. Cansolv

Cansolv is a “global provider of high efficiency air pollution control and capture solutions” (Cansolv corporate website) and look to be targeting post combustion capture using a proprietary amine.

This is potentially a new generation amine; the claims are low effluent, low water consumption, low energy requirement and ‘commercially available’.

Currently this is clearly focused on the post combustion capture of CO₂ from flue gas, nevertheless this claimed improvement could be transferred back to the Natural Gas market, in which case this would become a competitor to CryoCell under the banner of advanced solvents.

Cool Energy will maintain a watching brief on this and other solvent developments.

9.7.2.3. Molecular Gate®

This is a solid adsorption system from BASF. Pressure swing adsorption (PSA) is used to first adsorb the CO₂ from the gas stream onto the solid bed, and then remove it in a regeneration process.

Pressure swing adsorption systems have, in a few instances, been used for the bulk removal of Carbon Dioxide from Methane, such as through the use of activated carbon adsorbent. The advantages of PSA are in its simplicity but the technology is limited by a relatively low selectivity between Methane and Carbon Dioxide using conventional adsorbents. This means that a large amount of Methane is co-adsorbed along with the Carbon Dioxide leading to high losses of Methane into the tail gas and larger adsorbent inventories.

The Molecular Gate was originally designed as a Nitrogen rejection unit, but has been adapted to Carbon Dioxide removal.

The Molecular Gate–Carbon Dioxide Removal system tailors the pore sizes of the adsorbent resulting in a design for a low Methane adsorption level on the adsorbent. Using a single stage vacuum pump for regeneration as well as a recycle to feed of a Methane rich stream further enhances this inherent adsorbent selectivity to provide high Methane recovery rates.

Guild Associates have built one operational plant at the Tidelands oil facility in California. The plant was built in 2002 and has a capacity of 1.0 MMscf/D, and reduces the CO₂ content from over 30% to less than 2%. The molecular gate operates at a low pressure of 4 to 8 bar.

Cool Energy analysis shows that this technology is not a direct competitor in the current market place, but is a potential competitor for the coal seam Methane market.

9.7.2.4. Gastreatment Power Package (GPP)

Gastreatment BV has developed a cryogenic process for the upgrading of biogas into gas of pipeline specification.

They have built a pilot plant which operates at a rate of 25 mscf/D (1/10th of the scale of the original MicroCell lab tests) at 10 barg. This has been tested on sewage gas in the Netherlands and on landfill gas in Hong Kong. Based on this they have developed designs for commercial scale plants of 0.5 to 10 MMscf/D operating at 18 to 25 barg.

Whilst they are both currently in a different market and small in scale, the technology includes the following:

- Pre-compression
- A total contaminant removal (TCR) step which is a basic cooling and condensing process designed to take the gas down to -25°C and remove NGLs, water and other contaminants
- A catalytic filtration step where Siloxanes are removed
- A final 2-stage cooling step where in the first stage bulk CO₂ is removed as a liquid and in the second the remaining CO₂ is removed as a solid.

This technology is also based on the concept of semi-continuous operation for both the TCR and the CO₂ removal steps.

In the TCR step the gas is cooled down to a level where water freezes out and hydrates would also probably form. This is apparently accepted and a dual heat exchanger configuration is proposed, one in operation and one in de-frost (it is not apparent where the defrosted gas/liquid is routed).

The CO₂ removal section also operates (like Prometheus) with two heat exchangers, one in operation and one in defrost. The CO₂ from the defrost is first captured as a liquid and then vaporized to cool the gas stream.

Although the CO₂ coming off this process is a vapour, it could be altered (with extra refrigeration) to produce a liquid CO₂ stream.

As with the Prometheus technology, given the reliance on a cyclic process that allows the build-up of a solid in the system, it appears that the scale up of this process would be difficult. In addition the issues of both hydrate formation and water dew-point do not appear to have been fundamentally addressed.

Given the above, Cool Energy does not regard the GPP process as a direct competitor. However, should Cool Energy move into biogas applications they would be in direct competition with Gastreatment Services BV.

Cool Energy recognizes the GPP technology as a potential competitor if it is proven at a larger scale and transitions into the Natural Gas market, and is intending to keep a close eye on any future developments.

9.7.2.5. Flexsorb SE

The Flexsorb SE and SE plus solvent is a proprietary gas treating agent that was developed by the ExxonMobil Research and Engineering Company specifically for selective H₂S removal, where low concentrations of H₂S are required in the treated gas. The amine does not degrade in the presence of CO₂, H₂S or COS and therefore does not require reclaiming.

Flexsorb is not a competitor to the CryoCell[®] Technology.

9.7.2.6. Econamine FG

Econamine is an amine based proprietary solvent developed by Fluor specifically targeting CO₂ removal from flue gas. It has been applied in over 20 flue gas applications.

Most alkanolamine systems cannot operate in a flue gas environment, because the amine will rapidly degrade in the presence of Oxygen. This is prevented through a proprietary inhibitor in the amine (MEA). The solvent formulation is specially designed to recover CO₂ from low pressure, Oxygen-containing streams, such as burner flue gas streams.

Econamine is not a competitor to the CryoCell technology. However should Cool Energy develop the technology further and move into the flue gas separation market, Econamine would be a competitor.

9.8. Conclusion

Present and future marketplace and competitiveness of cryogenic technology with and without process integration for more efficient CO₂ removal is discussed. Comprehensive analysis of the “current” techniques becomes quickly outdated, therefore in this case study only the most advanced methods were included.

Cryogenics has an obvious advantage of a wide range of operating conditions such as pressure and range of concentrations compared to other technologies suitable only for a limited field of applications.

Another distinctive feature of the cryogenic process is the ability to process large quantities of treated fluid with relatively low cost excess. This is stipulated by the absence of chemical treatment and as well, no water is consumed anywhere in the process.

CryoCell combined with CryoZorb is very similar to the cryogenic and hydrate method developed in this research in terms of the combination of the two low temperature processes for CO₂ capture in a form amenable for injection and underground storage. In the first stage the bulk quantity of CO₂ is removed in liquid form, and in the next stage the desired low level of acidity is reached by means of another technique. The use of hydrates is prospectively less energy demanding than dissolving in Methanol due to significantly higher temperatures used and easier regeneration of the absorbent.

The case study conducted herein can be applied to assess the place which the combined cryogenic and hydrate process can take among the other techniques used for acid gas removal. This process, however, is developed for syngas processing and significant research will be necessary to adopt the procedure for other sources containing CO₂ such as natural and landfill gas.

Chapter 10.

Conclusion and Recommendations

Carbon Capture and Storage technology for the power generation sector has the potential to solve up to one-half of the global greenhouse gas problem.

Flue gas carbon capture R&D activities are being pursued by energy companies, oil majors, power plant and generation equipment providers, process plant contractors and entrepreneurial start-up companies. The technologies under development range from laboratory stage to test demonstration trials and to full scale commercial demonstration plants. Significant long term investments and commitments are being made in the area of carbon capture by power generation companies and related service companies supporting their needs.

Energy companies stand to offset heavy carbon emission related costs if they can develop Carbon Capture and Storage solutions in conjunction with more efficient power technologies. Focus on these technologies is most evident in developed countries where governments are contemplating the introduction of, or have introduced, harsh regulatory environments.

This thesis presented a comprehensive discussion comprising an overview of research and development activities in the area of carbon capture from flue gas streams. The discussion includes a review of the emerging competitive environment in the area of flue-gas carbon capture, the commercial drivers behind this activity and an overview of companies that have developed, or are developing, carbon capture technology that is beyond the laboratory stage.

Power Generation in Perspective

Carbon emissions from the power generation sector account for approximately one-third of global CO₂ emissions (Figure 10.1) (IPCC Fourth Assessment Report, 2007). Carbon Capture and Storage technologies therefore have the potential to deliver the answer to up to one-third of the greenhouse gas problem. In Victoria, Australia, 55% of greenhouse gas emissions are generated by the burning of coal by power utilities. In New South Wales, the figure is 35%. In the UK, the figure is 32% (2002 data). To fully understand the importance of this research, especially for the power industry, we need to review the power generation carbon capture processes.

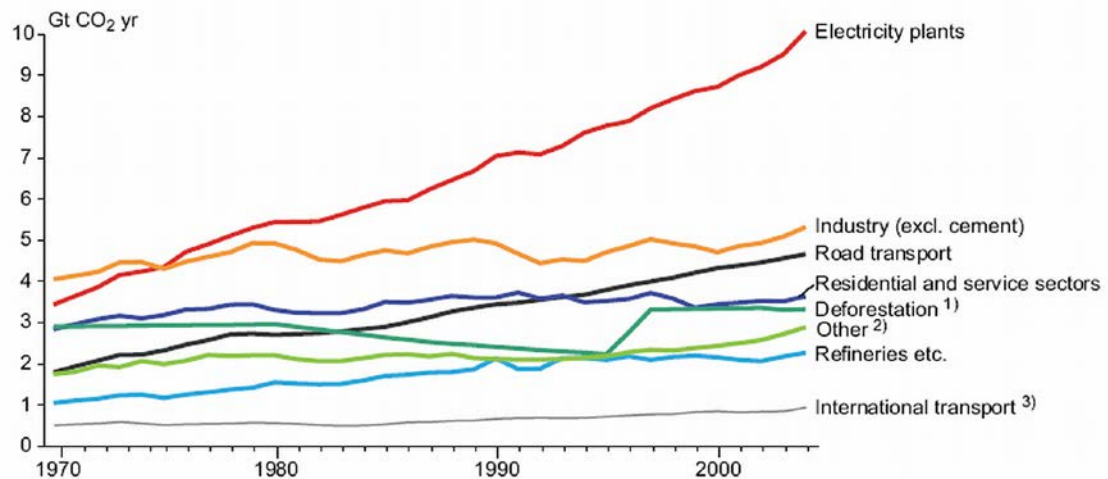


Figure 10. 1 Contribution to CO₂ emissions from various sources
(IPCC Fourth Assessment Report, 2007, p.104)

Power Generation Carbon Capture Processes

Three options exist and are being developed for carbon capture from power stations

- Post-combustion Capture

Post-combustion capture is a mature technology, but also the most costly of the three techniques, and is appropriate for existing installations. It involves separating the CO₂ from combustion gases, usually by means of a liquid solvent.

- Pre-combustion Capture

Pre-combustion capture yields separate streams of Hydrogen and CO₂, thereby facilitating CO₂ capture. The process consists of treating the fuel either with steam and air (steam reforming) or with Oxygen (partial oxidation) to produce a synthesis gas that contains mainly carbon Monoxide (CO) and Hydrogen. A second step converts the CO in the presence of water (H₂O) and then separates the resulting CO₂ for capture and storage.

- Oxyfuel

Oxyfuel combustion capture is still in the pilot phase. This technique yields a combustion gas highly concentrated in CO₂ and could constitute a suitable retrofit technology for existing installations. The process uses high-purity Oxygen instead of air for combustion, the main difficulty being to extract the Oxygen from the air. Due to the high cost of this separation step, a chemical looping process is being investigated in which the Oxygen supply is derived from a reaction involving a metal oxide, using metal particles which would serve as the Oxygen carrier from air to fuel.

10.1. Research Summary

Several methods to enhance the purity of Hydrogen have been cited in the literature. A slight advancement in the commercial method of Hydrogen production has been to remove the Carbon Dioxide from the reaction mixture between the two stages of the shift reaction.

The main purpose of this research work was to develop a new combined cryogenic and hydrate-based gas separation process for efficiently recovering CO₂ from IGCC or Oxyfuel gases. Numerous temperature and pressure conditions for each of the process have been tested and reported in this thesis.

Process integration of the well known cryogenic technique with the novel concept of utilisation of gas hydrates formation for CO₂ removal was systematically developed and trial-tested in this research for H₂-CO₂ separation necessary at the IGCC power stations. Initially the majority of Carbon Dioxide was removed by cryogenic condensation and the estimation of the effectiveness of this method at temperatures down to -55°C was made based on bench-scale experiments (Chapter 3). Assessment of the freeze-out conditions which can be encountered and behaviour of the frozen matter was conducted therein. The best hydrate promoter, Tetrabutyl Ammonium Chloride (TBAC), was selected in Chapter 4, and the optimum conditions for operation including hydrate formation temperature and the TBAC concentration were also determined. Methodology of detection of the hydrate formation conditions is described in Chapter 5. Discussion of the effect of the presence of a third phase on hydrate is also given in this Chapter. The importance of chemical-water interaction is outlined. Chapter 6 analyses in depth the issues associated with multiphase flow and the effect of liquid and solid phases on hydrate. Based on the gathered experience and results, a laboratory scale pilot plant was designed for up to 87 mol% removal of CO₂ from IGCC GE and Shell flue gases at the process pressure (Chapter 7). A laboratory rig has been constructed at Clean Gas Technologies Australia (formerly the Woodside Research Foundation) and the operating techniques and the results are described in Chapter 8. Finally, Chapter 9 gives an extensive overview of the current marketplace for CO₂ removal techniques, and the competitiveness of a process integrated cryogenic method is assessed

10.2. Significance

The key findings of this research are outlined below:

- Significant discrepancy can be found between commercial computer software when the phase envelope of gas mixtures presented essentially by CO₂ and H₂ has to be estimated (the results will be published).
- A ceramic coating for stainless steel parts is proposed by this research as the most favourable in the environments where CO₂ freezing can be encountered due to the total absence of adherence of the frozen matter to the surface.
- The presence of hydrotrope Tetrabutyl Ammonium Chloride was shown to influence the hydrate equilibrium in the water-Hydrogen-CO₂ -hydrate system and shift the dissociation curve to the left compared to that for pure water (the results will be published).
- TBAC enables utilisation of water above the freezing point for hydrate encapsulation from very low CO₂ environments which provides unambiguous advantages to the process design, hydrate transportation and storage.
- The research proposes TBAC to be a more viable promoter for large scale CO₂ abatement than common micelle surfactants due to three reasons: 1) an open structure solubilisation mechanism enables higher solubility of the CO₂, 2) a very low concentration of TBAC is necessary and its low volatility prevents any contamination of the CO₂ released from the hydrate, and 3) a low foaming factor allows for the safe recirculation of the promoter solution in a closed system.
- Hydrate formation/dissociation conditions predicted by commercial computer software can differ by up to 10°C, therefore a thorough experimental investigation in accredited laboratories is vital for the prudent choice of operating conditions where hydrate formation is expected (submitted a paper 'Selection of Hydrate Curve for Deep Sea Development Design' is submitted to the Fluid Phase Equilibria Journal).
- The presence of the condensed liquids and precipitating solids can promote hydrate deposition and delay the decomposition of plugs (a paper 'Experimental Hydrate Dissociation Curves: Effect of Wax Presence and Hydrate Software Prediction Assessment' is submitted to the Fluid Phase Equilibria Journal).

- This research, for the first time states that the hydrate formation can be accurately determined in a hydrate-forming system via observation of viscosity changes in aqueous media.
- The pilot plant testing was successful in demonstrating the effectiveness of CO₂ capture by integrated cryogenic and hydrate techniques (Surovtseva et al., 2010).
- The cryogenic method with process integration is very competitive in the current market place for CO₂ capture and storage.

10.3. Recommendations

This project has demonstrated the viability of the combined low temperature condensation and hydrate precipitation method for separating CO₂ from shifted synthesis gas. The potential of this technique for storage of captured CO₂ was identified throughout this thesis to emphasise the commercial implications of this work. The following can be recommended for future academic research in this area.

- The model for phase envelope prediction can be improved to better fit experimental data for H₂-CO₂ systems.
- TBAC is classified as a hydrotrope, an amphiphilic surface-active chemical containing a relatively large hydrophilic part and a bulky hydrophobic part too small to cause self-aggregation. Hydrotropes form very loose structures compared to common surfactants, therefore enabling higher solubility of hydrophobic molecules. Further development of hydrotropes for promoting hydrate formation is worthwhile.
- The optimum concentration of any known hydrate-promoting surfactant including hydrotropes is substantially lower than the reported value of the critical micelle concentration. Therefore, the exact nature of the aggregation phenomena and the dissolving mechanism at hydrate formation conditions is yet to be investigated at the micro-scale level.
- The bulk properties of the aqueous phase, particularly viscosity, change dramatically during the hydrate formation. An extensive study of such properties will allow for modelling of hydrate slurries of certain compositions and properties.

- Phase separation in a pipeline can affect hydrate formation/decomposition. This research has shown unambiguously that solid deposition will promote hydrate formation; however, the effect of the condensate needs to be studied more thoroughly.
- Future experimentations on the pilot plant should be supplemented with automatic control, digital data acquisition and recording features.
- The two systems of the pilot plant were operated separately in a semi-batch steady-state isobaric-isothermal system. More accurate dynamic results need to be collected from the two stages run simultaneously to enable an accurate proposal for a scaled-up unit.
- Utilisation of the heat integration system proposed in Chapter 7 describing the design of the plant will allow for comprehensive assessment of the proposed technology in terms of the energy consumption and cost.
- The process optimisation considered in this thesis is based on the bench-scale experimentation and scaled-up to a laboratory scale rig. Further study should be conducted in a dynamic mode to better understand the milestones of the combined cryogenic and hydrate technique for CO₂ capture.

The common observation emphasised throughout this thesis is that the theoretical modelling using the modern computer software has shown the unavoidability of experimental testing for reasonable design and assessment.

The outcomes of this research will justify the feasibility of commercialisation of the low-temperature concept for large-scale CO₂ capture. In this regard, the following points will play a crucial role:

- Produced liquid CO₂ needs to be pumped either to the deep ocean or to the depleted oil and gas reservoirs for storage. Some of the associated issues can be found, for example, in (Fogarty & McCally, 2010).
- The preservation capability for permanent storage of CO₂ in the form of hydrates should be verified.
- Accurate determination of the hydrate stability region will be essential in the experiment with continuous hydrate slurry removal from the reacting zone.
- Kinetic investigation of the hydrate decomposition rates is vital for both transportation of the CO₂ hydrate slurry and re-gasification.

- Economic estimation will make the major contribution to the final decision regarding the viability of the technology in the current market.

Reference List

- Abdoul, W., E. Rauzy, and A. Peneloux, (1991), 'Group Contribution Equation of State for Correlating and Predicting Thermodynamic Properties of Weakly Polar and Non-Associating Mixtures. Binary and Multicomponent Systems', *Fluid Phase Equilibria*, 68, 47-102.
- Acrion Technologies Inc. website www.acrion.com (last accessed November 2010).
- Al-Sahhaf, T.A., A.J. Kidnay, and E.D. Sloan, (1983), 'Liquid + Vapor Equilibria in the $N_2+CO_2+CH_4$ System', *Ind. Eng. Chem. Fundam.*, 22, 372-380.
- Aman, Z.M., L.E. Dieker, G. Aspenes, C.A. Koh, A.K. Sum, and E.D. Sloan, (2009), 'Composition-Dependent Adhesion Forces Between Cyclopentane Hydrate Particles', In: *2009 AIChE annual meeting proceedings*, 8-13 November, Nashville, TN.
- Amin, R., A. Jackson, and A.F. Kennaird, (2005), 'The Cryocell: An Advanced Gas-Sweetening Technology', *International Petroleum Technology Conference*, 21-23 November, Doha, Qatar.
- Amin, R., and A.F. Kennaird, (2008), 'Process and Device for Production of LNG by Removal of Freezable Solids', US Patent 7.325.415 B2.
- Anderson, F.E., and J.M. Prausnitz, (1986), 'Inhibition of Gas Hydrates by Methanol', *American Institute of Chemical Engineers Journal*, 32 (8), 1321-1233.
- Arai, Y., G.-I. Kaminishi, and Sh. Saito, (1971), 'The Experimental Determination of the P-V-T-X Relations for the Carbon Dioxide-Nitrogen and the Carbon-Dioxide-Methane Systems', *Journal of Chemical Engineering of Japan*, 4 (2), 113-122.
- Arjmandi, M., A. Chapoy, and B. Tohidi, (2007), 'Equilibrium Data of Hydrogen, Methane, Nitrogen, Carbon Dioxide, and Natural Gas in Semi-Clathrate Hydrates of Tetrabutyl Ammonium Bromide', *J. Chem. Eng. Data*, 52, 2153-2158.

- Arjmandi, M., S. Ren, B. Tohidi, (2003), 'Progress in Design and Assessment of Low Dosage Hydrate Inhibitors', In: *Proceedings of the 6th Offshore Mediterranean Conference*, 26–28 March, Ravenna, Italy.
- Balasubramanian, D., V. Srinivas, V.G. Gaikar, and M.M. Sharma, (1989), 'Aggregation Behavior of Hydrotropic Compounds in Aqueous Solution', *J. Phys. Chem.*, 93 (9), 3865-3870.
- Ballard, A.L., and E. D. Sloan Jr., (2002) 'The next generation of hydrate prediction I. Hydrate standard states and incorporation of spectroscopy', *Fluid Phase Equilibria*, 194-197, 371-383,.
- Ballou, D., (2009), 'Update on Cimarex Helium-Methane Project', *Pinedale Online!*, 27 August.
- Bantrel corporate website <http://www.bantrel.com> (last accessed November 2010).
- Barclay, M.A., T.C. Brook, J.A. Barclay, and R.R. Tison, (2000), 'Apparatus and method for purifying natural gas via cryogenic separation', US Patent 6,082,133.
- Battah, S.J., (2002), 'Natural Gas Hydrate Redustion', *MS Thesis*, Department of Petroleum Engineering, Curtin University of Technology.
- Bazant, M.Z., and B. L. Trout, (2001), 'A method to extract potentials from the temperature dependence of Langmuir constants for clathrate-hydrates', *Physica Acta*, 300, 139-173.
- BCCK Engineering Inc. corporate website www.bcck.com (last accessed November 2010).
- Behar, E., P. Bourmayer, A. Sugier, and M. Thomas, (1991), 'Advances in hydrate control', In: *Proceedings Annual Convention - Gas Processors Association*, 11-12 March, San Antonio, TX, 115-120.
- Benesh, M.E., (1942), Patent 2.270.016 cited in Guo, B., R.E. Bretz and R.L. Lee, (1995), 'Method and apparatus for generating, transporting and dissociating gas hydrates', Patent US5473904.

- Berro, C., L. Barna, and E. Rauzy, (1996), 'A group-contribution equation of state for predicting vapour-liquid equilibrium and volumetric properties of carbon dioxide-hydrocarbons systems', *Fluid Phase Equilibria*, 114 (1-2), 63-87.
- Bezanehtak, K., G.B. Combes, F. Dehghani, and N.R. Foster, (2002), 'Vapor-Liquid Equilibrium for Binary Systems of Carbon Dioxide + Methanol, Hydrogen + Methanol, and Hydrogen + Carbon Dioxide at High Pressures', *J. Chem. Eng. Data*, 47, 161-168.
- Bishnoi, P.R., and V. Natarajan, (1996), 'Formation and Decomposition of Gas Hydrates', *Fluid Phase Equilibria*, 117, 168-177.
- Bocquet, Ph.E., (1959), 'Process of Removing Carbon Dioxide from Natural Gas', US Patent 2,888,807.
- Bouchemoua, A., A. Fezoua, Y. Ouabbas, F. Chauvy, A. Cameirao, and J.-M. Herri, (2009), 'CO₂ Capture by Gas Mixtures Hydrate Crystallisation', *XII Congrès de la Société Française de Génie des Procédés Pour relever les défis industriels du XXI*, Marseille, France.
- Brdar, R.D. and R.M. Jones, 'GE IGCC Technology and Experience with Advanced Gas Turbines', report GER-4207, GE Energy (retrieved 13 January 2010).
- Buhre, B.J.P., L.K. Elliott, C.D. Sheng, R.P. Gupta, and T.F. Wall, (2005), 'Oxy-fuel Combustion Technology for Coal Fired Power Generation', *Progress in Energy and Combustion Science*, 31, 283-307.
- Burshears M., T.J. O'Brien and R.D. Malone, (1986), 'A multiphase multi-dimensional, variable composition simulation of gas production from a conventional gas reservoir in contact with hydrates', In: *SPE unconventional gas technologies symposium*, 18-21 May, Louisville, KY.
- Business Wire News, (2008), 'ExxonMobil to Build Commercial Demonstration Plant to Remove Carbon Dioxide from Natural Gas', 5 May, retrieved from <http://www.businesswire.com/news/home/20080505006145/en/ExxonMobil-Build-Commercial-Demonstration-Plant-Remove-Carbon> (retrieved 10 November 2010).

Callide Oxyfuel Project Schedule

<http://www.callideoxyfuel.com/When/Schedule/tabid/83/Default.aspx>

(retrieved 22 September 2010).

Cansolv corporate website www.cansolv.com (last accessed November 2010).

Carroll, J.J., (2002), *Natural Gas Hydrates*, Elsevier Science & Technology Books.

Chatti, I., A. Delahaye, L. Fournaison, and J.-P. Petitet, (2005), 'Benefits and Drawbacks of clathrate hydrates: a review of their areas of interest', *Energy Conversion and Management*, 46, 1333-1343.

Chen, G.-J., and T.-M. Guo, (1996), 'Thermodynamic Modelling of Hydrate Formation Based on New Concepts', *Fluid Phase Equilibria*, 122 (1-2), 43-65.

Chui, E.H., M.A. Douglas, and Y. Tan, (2003), 'Modelling of Oxy-fuel Combustion for a Western Canadian sub-Bituminous Coal', *Fuel*, 82, 1201-1210.

Chung, T.H., M. Ajlan, L.L. Lee, and K.E. Starling, (1988), 'Generalised multiparameter Correlation for Nonpolar and Polar Fluid Transport Properties', *Ind. Eng. Chem. Res.*, 27 (4), 671-679.

Clarke, M.A., and P.R. Bishnoi, (2005), 'Determination of the intrinsic kinetics of CO₂ gas hydrate formation using in situ particle analysis', *Chem. Eng. Sci.*, 60, 695-709.

Cole, E.T., E.R. Thomas, R.R. Bowen, (1999), 'Process for Liquefying a Natural Gas Stream Containing at least One Freezable Component', US Patent 5,956,971.

CoolEnergy Limited corporate website <http://www.coolenergy.com.au/> (last accessed November 2010).

Cormos, C. C., F. Starr, E. Tzimas, S. Peteves, and A. Brown, (2007), 'Gasifier Concepts for Hydrogen and Electricity Co-Production with CO₂ Capture', *Third International Conference on Clean Coal Technologies for our Future*, 15 - 17 May, Cagliari, Sardinia, Italy.

- Cottrell, A., J. Nunn, D. Palfreyman, D. Urfer, P. Scaife, L. Wibberley, (2003), 'System Assessment of Future Electricity Generation Options for Australia', Technical Assessment Report 32, *CRC for Coal in Sustainable Development*.
- Croiset E, K.V. Thambimuthu, (2001), 'NO_x and SO_x emissions in O₂/CO₂ recycle coal combustion', *Fuel*, 80, 2117–2121.
- Croiset E., and K.V. Thambimithu, (1998), 'Coal combustion with flue gas recirculation for CO₂ recovery', *Proceedings of the fourth international conference on greenhouse gas control technologies*, Interlaken, Switzerland, 581.
- Cryogenic Carbon Capture Technology, (2009), *Carbon Capture Journal*, 10, 18-21.
- Cuevas-Cubria, C., A.Schultz, R. Petchey, A. Maliyasena, and S. Sandu, (2010), *Energy in Austarlia*, 87.
- Da Silva, R.C, M. Spitzer, L.H.M. da Silva, and W.Loh, (1999), 'Investigation on the Mechanism of Aqueous Solubility Increase Caused by some Hydrotropes', *Thermochimica Acta*, 328 (1-2), 161-167.
- Davalath, S. Patni, T. Chen, B. Bryson, (2004), 'Bijupira Salema: Flow Assurance Analysis to Support Operating Strategy', *Offshore Technology Conference*, 3-6 May, Houston, Texas.
- Davies, S.R., J.A. Boxall, C.A. Koh, E.D. Sloan, P.V. Hemmingsen, K.J. Kinnari and Zh.-G. Xu, (2008), 'Predicting Hydrate Plug Formation in a Subsea Tieback', *SPE Annual Technical Conference and Exhibition*, 21-24 September, Denver, CO.
- Davis, J.A., N. Rodewald, and F. Kurata, (1962), 'Solid-Liquid-Vapor Phase Behavior of the Methane-Carbon Dioxide System', *American Institute of Chemical Engineers Journal*, 8 (4), 537-539.
- Davison, J., L. Bressan, and R. Domenichini, (2004), 'CO₂ Capture in Coal-Based IGCC Power Plants', *7th International Conference on Greenhouse Gas Control Technologies*, 5-9 September, Vancouver, Canada.

- Dayalath, J., S. Patni, T. Chen, and B. Bryson, (2004), *Offshore Technology Conference*, 3-6 May, Houston, TX.
- Deppe, G. J., and G. Anderson, (2001), 'A High Pressure Carbon Dioxide Separation Process for IGCC Plants', *First National Conference on Carbon Sequestration*, 14-17 May, Washington DC.
- Deppe, G., S.S. Tam, R.P. Currier, J.S. Young, G.K. Anderson, L. Le, et al., (2004), 'Developments in the SIMTECHE Process CO₂ Capture by Formation of Hydrates', *Third Annual Conference on Carbon Capture and Sequestration*, 3-6 May, Washington DC.
- Dillon, W.P., R.F. Mast, K.L. Fehlhaber, M.W. Lee and L.M.H. Carter, (1992), 'Gas hydrates in deep ocean sediments offshore Southeastern United States; a future resource?', In: *Program and Abstracts of the 8th V. E. McKelvey forum, Mineral and Energy Resources, USGS research on energy resources*, Houston, TX, 18-21.
- Donnelly, H.G., and D.L. Katz, (1954), 'Phase Equilibria in the Carbon Dioxide-Methane System', *Ind. Eng. Chem.*, 46 (3), 511-517.
- Durr, Ch.A., D.B. Manley, R.L. McKee, (1994), 'Carbon Dioxide Recovery Process', US Patent 5,335,504.
- Eakman, J.M., and H.A. Marshall, (1979), 'Separation of Carbon Dioxide and other Acid Gas Components from Hydrocarbon Feeds', US Patent 4,149,864.
- Edmonds, B., R.A.S. Moorwood, and R. Szczepanski, (1996), 'A Practical Model for the Effect of Salinity on Gas Hydrate Formation', *European Production Operations Conference & Exhibition*, 16-17 April, Stavanger, Norway.
- Eggeman, T., and E. Chafin, (2003), 'Pitfalls of CO₂ Freezing Prediction', 82nd *Annual Convention of the Gas Processors Association*, 10 March, San Antonio, TX.
- Eggeman, T., and S. Chafin, (2005), 'Beware the Pitfalls of CO₂ Freezing Prediction', *Chemical Engineering Progress*, 101 (3), 39-44.

- Electric power research institute & Bevilacqua-Knight, Inc., (2008), 'Advanced Coal Power Systems with CO₂ Capture: EPRI's CoalFleet for Tomorrow Vision', 6.
- Electric power research institute, (2009), *Prism/MERGE Analyses 2009 Update*, 20.
- Fogarty, J., and M. McCally, (2010), 'Health and safety risks of carbon capture and storage', *The Journal of the American Medical Association*, 303(1), 67-68.
- Gao, Sh., (2008), 'Investigation of Interactions between Gas Hydrates and Several Other Flow Assurance Elements', *Energy & Fuels*, 22, 3150-3153.
- Gas Processors Suppliers Association, (2004), Engineering Data Book, 821.
- Gayet., P., C. Dicharry, G. Marion, A. Graciaa, J. Lachaise, and A. Nesterov, (2005), 'Experimental Determination of Methane Hydrate Dissociation Curve up to 55 MPa by Using a Small Amount of Surfactant as Hydrate Promoter', *Chem. Eng. Sci.*, 60, 5751-5758.
- GE Energy, 'Product of Ecomagination',
http://www.gepower.com/prod_serv/products/gasification/en/app_power.htm
 (retrieved 18 May 2010).
- Giavarini, C., F. Maccioni, M. Politi, and M.L. Santarelli, (2007), 'CO₂ Hydrate: Formation and Dissociation Compared to Methane Hydrate', *Energy&Fuels*, 21, 3284-3291.
- Gnanendran, N., and R. Amin, (2003), 'The Effect of Hydrotropes on Gas Hydrate Formation', *J. Petroleum Science and Engineering*, 40, 37-46.
- Gnanendran, N., and R. Amin, (2004), 'Modelling hydrate formation kinetics of a hydrate promoter-water-natural gas system in a semi-batch spray reactor', *Chem. Eng. Sci.*, 59 (18), 3849-3863.
- Goddin, C.S., (1984), 'Cryogenic Distillative Removal of CO₂ from High CO₂ Content Hydrocarbon Containing Streams', US Patent 4,459,142.

- Goddin, C.S., and R.L. McGalliard, (1983), 'Process for Separating Relatively Pure Fractions of Methane and Carbon Dioxide from Gas Mixtures', US Patent 4,370,156.
- Gottier, G.N., (1988), 'Process for Removal of Carbon Dioxide from Mixtures Containing Carbon Dioxide and Methane', US Patent 4,747,858.
- Gross, D.M., (2002a), 'Oxy-fuel Combustion System and Uses Thereof', US Patent 6,436,337.
- Gross, D.M., (2002b), 'Method for Oxy-fueled Combustion', US Patent 2002/0180122 A1.
- Guo, X., Zh. Dai, X. Gong, X Chen, H. Liu, F. Wang, and Z. Yu, (2007), 'Performance of an Entrained-Flow Gasification Technology of Pulverised Coal in Pilot-Scale Plant', *Fuel Processing Technology*, 88, 451-459.
- Hammerschmidt, E.G., (1934), 'Formation of gas hydrates in natural gas transmission lines', *Ind. Eng. Chem.*, 26 (8), 851-855.
- Hart, A. And N. Gnanendran, (2008a), 'Cryogenic CO₂ Capture from Natural Gas', *9th International Conference on Greenhouse Gas Control Technologies*, 20 November, Washington DC.
- Hart, A. And N. Gnanendran, (2008b), 'Cryogenic CO₂ Capture from Natural Gas', *Energy Procedia*, Volume 1, Issue 1, February 2009, Pages 697-706.
- Hart, A., and R. Amin, (2007), 'Process and Apparatus for Removal of Sour Species from a Natural Gas Stream', WIPO Patent WO/2007/030888.
- Haut, R.C., E.R. Thomas, and R.D. Denton, (1991), 'Method and Apparatus to Start-up Controlled Freezing Zone Process and Purify the Product Stream', US Patent 5,062,270.
- Haut, R.C., R.D. Denton, and E.R. Thomas, (1989), 'Development and Application of the Controlled-Freeze-Zone Process', *SPE Production Engineering*, August, 265-271.

- Heichberger, A.N., (1987), 'Method and Apparatus for Carbon Dioxide Liquefaction and Evaporation', US Patent 4,639,262.
- Heldebrant, D.J., C.R. Yonker, P.G. Jessop and L. Phan, (2008), 'Organic liquid CO₂ capture agents with high gravimetric CO₂ capacity', *Energy Environ. Sci.*, 1, 487.
- Hlavinka, M.W., V.N. Hernandez, and D. McCartney, (2005), 'Proper Interpretation of Freezing and Hydrate Prediction Results from Process Simulation', Bryan Research & Engineering, Inc., Technical Paper.
- Hochgesand, G., (1970), 'Rectisol and Purisol', *Ind. Eng. Chem.*, 62 (7), 37-43.
- Holder G.D., S.P. Zetts and N. Pradhan, (1988), 'Phase behavior in systems containing clathrate hydrates', *Rev Chem Eng*, 5 (1-4), 1-70.
- Holder, G.D., and D.J. Manganiello, (1982), 'Hydrate Dissociation Pressure Minima in Multicomponent System', *Chem. Eng. Sci.*, 37 (1), 9-16.
- Holder, G.D., G. Corbin, and K.D. Papadopoulos, (1980), 'Thermodynamic and Molecular Properties of Gas Hydrates from Mixtures Containing Methane, Argon, and Krypton', *Ind. Eng. Chem. Fundam.*, 19, 282-286.
- Holder, G.D., L.P. Mokka, and R.P. Warzinski, (2001), 'Formation of Gas Hydrates from Single-Phase Aqueous Solutions', *Chem. Eng. Sci.*, 56, 6897-6903.
- Holmes, A.S., and J.M. Ryan, (1982a), 'Cryogenic Distillative Separation of Acid Gases from Methane', US Patent 4,318,723.
- Holmes, A.S., and J.M. Ryan, (1982b), 'Distillative Separation of Carbon Dioxide from Light Hydrocarbons', US Patent 4,350,511.
- Huyghe, R., E. Lemaire, P. Mougins, X. Renaud, and G. Elbaz, (2008), 'Operational Validation of the Spretex® Process for Bulk H₂S and Mercaptans Removal', *OAPEC-IFP Joint Seminar The Gas Industry: Current & Future*, 17-19 June, Rueil-Malmaison, France.

- Hwang, M.-J., G. D. Holder and S. R. Zele, (1993), 'Lattice Distortion by Guest Molecules in Gas-Hydrates', *Fluid Phase Equilibria*, 83, 437-444.
- Hwang, Sh.-Ch., H.-M. Lin, P.S. Chapple, and R. Kobayashi, (1976), 'Dew Point Study in the Vapor-Liquid Region of the Methane-Carbon Dioxide System', *J. of Chemical and Engineering Data*, 21 (4), 493-497.
- Imai, Sh., K. Okutani, R. Ohmura, and Y.H. Mori, (2005), 'Phase Equilibrium for Clathrate Hydrates Formed with Difluoromethane + either Cyclopentane or Tetra-n-butylammonium Bromide', *J. Chem. Eng. Data*, 50 (5), 1783-1786.
- IPCC Fourth Assessment Report, (2007), *Climate Change 2007: Mitigation of Climate Change*, Cambridge University Press, Cambridge, United Kingdom and New York, NY, USA.
- Jackson, A., and R. Amin, (2004), 'Method for Separation of Non-Hydrocarbon Gases from Hydrocarbon Gases', US Patent 2004/0074389 A1.
- Jadhawar P., A.H. Mohammadi, J. Yang and B. Tohidi, (2006), 'Subsurface Carbon Dioxide Storage through Clathrate Hydrate Formation', *NATO Science Series*, 65 part II, 111-126.
- Jager, M.D., R.M. De Deugd, C.J. Peters, J. de Swaan Arons, and E.D. Sloan, (1999), 'Experimental determination and modelling of structure II hydrates in mixtures of Methane+ water+ 1, 4-dioxane', *Fluid Phase Equilibria*, 165 (2), 209-223.
- John, V.T., K.D. Papadopoulos, and G.D. Holder, (1985), 'A Generalised Model for Predicting Equilibrium Conditions for Gas Hydrates', *American Institute of Chemical Engineers Journal*, 31 (2), 252-259.
- Jones, R.M., and N.Z. Shilling, 'IGCC Gas Turbines for Refinery Applications', report GER-4219, GE Energy (retrieved 21 October 2009).
- Kalogerakis, N., A.K.M. Jamaluddin, P.D. Dholabhai, and P.R. Bishnoi, (1993), 'Effects of Surfactants on Hydrate Formation Kinetics', *SPE International Symposium on Oilfield Chemistry*, 2-5 March, New Orleans, Louisiana.

- Kang, S.-P., H. Lee, (2000), 'Recovery of CO₂ from Flue Gas Using Gas Hydrate: Thermodynamic Verification through Phase Equilibrium Measurements', *Environ. Sci. Technol.*, 34, 4397-4400.
- Kang, S.-P., H. Lee, C.-S. Lee and W.-M. Sung, (2001), 'Hydrate phase equilibria of the guest mixtures containing CO₂, N₂ and Tetrahydrofuran', *Fluid Phase Equilibria*, 185, 101-109.
- Karaaslan, U., and M. Parlaktuna, (2000), 'Surfactants as Hydrate Promoters?', *Energy&Fuels*, 14, 1103-1107.
- Karaaslan, U., and M. Parlaktuna, (2001), 'On the Dissociation of Natural Gas Hydrates from Surfactant Solutions', *Energy Fuels*, 15 (1), 241-246.
- Karaaslan, U., E. Uluneye, M. Parlaktuna, (2002), 'Effect of an Anionic Surfactant on Different Type of Hydrate Structures', *J. Petrol. Sci. Eng.*, 35, 49-57.
- Kashchiev, D., and A. Firoozabadi, (2002a), 'Driving force for crystallisation of gas hydrates', *J. of Crystal Growth*, 241, 220-230.
- Kashchiev, D., and A. Firoozabadi, (2002b), 'Nucleation of Gas Hydrates', *J. of Crystal Growth*, 243, 476-489.
- Kashchiev, D., and A. Firoozabadi, (2003), 'Induction time in crystallisation of gas hydrates', *J. of Crystal Growth*, 250, 499-515.
- Katz, D.L., (1945), 'Prediction of Conditions for Hydrate Formation in Natural Gases', *Petroleum Transactions of American Institute of Mining Engineers*, 160, 140-149.
- Kelland, M.A, (2006), 'Hystory of the Development of Low Dosage Hydrate Inhibitors', *Energy Fuels*, 20 (3), 825-847.
- Kelland, M.A., T.M. Svaftaas and L. Dybvik, (1995), 'A New Generation of Gas Hydrate Inhibitors', *SPE Annual Technical Conference*, 22-25 October, Dallas, TX.

- Khokhar, A.A., J.S. Gudmundsson, and E.D. Sloan, (1998), 'Gas Storage in Structure H Hydrates', *Fluid Phase Equilibria*, 150-151, 383-392.
- Kihara, T., (1953), 'Virial Coefficients and Models of Molecules in Gases', *Review of Modern Physics*, 25 (4), 831-843.
- Kim, H.C., P.R. Bishnoi, R.A. Heidemann, and S.S.H. Rizvi, (1987), 'Kinetics of Methane Hydrate Decomposition', *Chem. Eng. Sci.*, 42 (7), 1645-1653.
- Kim, H.K., Y. Kim, S.M. Lee, and K.Y. Ahn, (2007), 'NO Reduction on 0.03-0.2 MW Oxy-fuel Combustor Using Flue Gas Recirculation Technology', *Proceedings of the Combustion Institute*, 31, 3377-3384.
- Klara, J.M., and J.G. Wimer, (2007), 'Cost and Performance Baseline for Fossil Energy Plants', DOE/NETL-2007/1281, May.
- Klara, S. M., R.D. Srivastava, (2002), 'US DOE integrated collaborative technology development program for CO₂ separation and capture', *Environ. Prog.*, 21 (4), 247-253.
- Kobayashi, R., K.Y. Song, and E.D. Sloan, "Phase Behavior of Water/Hydrocarbon Systems", in Lake, L.W., (1987), *Petroleum Engineers Handbook*, Society of Petroleum Engineers.
- Koh, C.A., (2002), 'Towards a Fundamental Understanding of Natural Gas Hydrates', *Chem. Soc. Rev.*, 31, 157-167.
- Kumar, R., H.-J. Wu, and P. Englezos, (2006), 'Incipient Hydrate Phase Equilibrium for Gas Mixtures Containing Hydrogen, Carbon Dioxide and Propane', *Fluid Phase Equilibria*, 244, 167-171.
- Kumar, R., P. Englezos, and J. Ripmeester, (2008), 'The Gas Hydrate for Separation of CO₂ from Fuel Cell Gas Mixture: Macro and Molecular Level Studies', In: *Proceedings of the 6th International Conference on Gas Hydrates*, 6-10 July, Vancouver, British Columbia, Canada.

- Lachance, J.W., E.D. Sloan, and C.A. Koh, (2009), 'Determining Gas Hydrate Kinetic Inhibitor Effectiveness Using Emulsions', *Chem. Eng. Sci.*, 64, 180-184.
- Lamorena, R.B., and W. Lee, (2009), 'Effect of pH on Carbon Dioxide Hydrate Formation in Mixed Soil Mineral Suspensions', *Environ. Sci. Technol.*, 43, 5908-5914.
- Lederhos, J.P., J. P. Long, A. Sum, R. L. Christiansen and E. D. Sloan, (1996), 'Effective Kinetic Inhibitors for Natural Gas Hydrates', *Chem. Eng. Sci.*, 51 (8), 1221-1229.
- Lee S.Y. and G.D. Holder, (2001), 'Methane hydrates potential as a future energy source', *Fuel Process Technol.*, 71, 181–186.
- Lee, H., and S.-P. Kang, (2001), 'Method for Separation of Gas Constituents Employing Hydrate Promoter', US Patent 2001/0052288 A1, December.
- Lee, S.-Y., and G.D. Holder, (2000), 'A Generalised Model for Calculating Equilibrium States of Gas Hydrates: Part II', *Annals of the New York Academy of Sciences*, 912, 614-622.
- Lee, S.-Y., and G.D. Holder, (2002), 'Model for Gas Hydrate Equilibria Using a Variable Reference Chemical Potential: Part I', *American Institute of Chemical Engineers Journal*, 48 (1), 161-167.
- Li, X.-S., Zh.-M. Xia, Zh.-Y. Chen, K.-F. Yan, G. Li, and H.-J. Wu, (2010), 'Equilibrium Hydrate Formation Conditions for the Mixtures of $\text{CO}_2 + \text{H}_2 + \text{Tetrabutyl Ammonium Bromide}$ ', *J. Chem. Eng. Data*, 55 (6), 2180-2184.
- Linga, P., R. Kumar, P. Englezos, (2007), 'The Clathrate Process for Post and Pre-Combustion Capture of Carbon Dioxide', *J. of Hazardous Materials*, 149, 625-629.
- Link, D.D., P.E. Ladner, H.A. Elsen and C.E. Taylor, (2003), 'Formation and dissociation studies for optimizing the uptake of Methane by Methane hydrates', *Fluid Phase Equilibria*, 211, 1–10.

- Liu H, K. Okazaki, (2003), 'Simultaneous easy CO₂ recovery and drastic reduction of SO_x and NO_x in O₂/CO₂ coal combustion with heat recirculation', *Fuel*, 82, 1427–1436.
- Lo, C., J. Zhang, A. Couzis, P. Somasundaran, and J.W. Lee, (2009), 'Surfactant Adsorption on Structure II and Semi-Clathrate Hydrates', In: *2009 AIChE annual meeting proceedings*, 8-13 November, Nashville, TN.
- Long, J.P., J.P. Lederhos, A. Sum, R.L. Christiansen and E.D. Sloan, (1994), 'Kinetic inhibitors of natural gas hydrates', In: *Proceedings of the 73rd Gas Processors Association Annual Convention*, 7-9 March, New Orleans, 85–93.
- Makogon, Y. F., (1994), 'Russia's Contribution to the Study of Gas Hydrates', *Annals of the New York Academy of Sciences*, 715, 119–145.
- Makogon, Y.F., (1997), *Hydrates of Hydrocarbons*, PennWell Books, Tulsa OK.
- McKoy, V., and O. Sinanoglu, (1963), 'Theory of Dissociation Pressures of Some Gas Hydrates', *Journal of Chem. Phys.*, 38 (12), 2946-2956.
- Mehta, A., J. Walsh, and S. Lorimer, (2006), *Annals of the New York Academy of Sciences*, 912, 366.
- Michelsen, M.L., (1982a), 'The Isothermal Flash Problem. Part I. Stability', *Fluid Phase Equilibria*, 9, 1-19.
- Michelsen, M.L., (1982b), 'The Isothermal Flash Problem. Part II. Phase-Split Calculation', *Fluid Phase Equilibria*, 9, 21-40.
- Miller J.W. and E.R. Strong, (1946), 'Hydrate storage of natural gas', *American Gas Association Monthly*, 28, 63-67.
- Minkinen, A., D. Benayoun, and Y. Barthel, (1996), 'Process for the Pretreatment of a Natural Gas Containing Hydrogen Sulphide', US Patent 5,520,249.
- Minkinen, A., J. Larue, and P. Capron, (1998), 'Process and Apparatus for Eliminating at least One Acid Gas by means of a Solvent for the Purification of Natural Gas', US Patent 5,735,936.

- Munck, J., S. Skjold-Jorgensen and P. Rasmunssen, (1988), 'Computations of the Formation of Gas Hydrates', *Chem. Eng. Sci.*, 43 (10), 2661-2672.
- Natarajan, V., P.R. Bishnoi, and N. Kalogerakis, (1994), 'Induction phenomena in Gas Hydrate Nucleation', *Chem. Eng. Sci.*, 49 (13), 2075-2087.
- Ng, H.-J., and D.B. Robinson, (1985), 'Hydrate formation in systems containing Methane, Ethane, Propane, Carbon Dioxide or Hydrogen Sulphide in the presence of Methanol', *Fluid Phase Equilibria*, 21 (1-2), 145-155.
- Nielsen, R.B., and R.W. Bucklin, (1983), 'Why not use Methanol for hydrate control?', *Hydro Proc*, 55 (4), 71-75.
- Northrop P.S., and J.A. Valencia, (2009), 'The CFZTM process: A cryogenic method for handling high-CO₂ and H₂S gas reserves and facilitating geosequestration of CO₂ and acid', *Energy Procedia* (1), 171-177.
- Northrop, P.S., and R.F. Bialek, (2004), 'Cryogenic Sour Gas Process Attractive for Acid Gas Inject Applications', 83d Annual GPA Convention, 14-17 March, New Orleans, LA.
- O'Brien, J.V., (1983), 'Distillative Separation of Methane and Carbon Dioxide', US Patent 4,383,842.
- O'Brien, J.V., A.S. Holmes, and R.B. Hopewell, (1987), 'Process for the Separation of Landfill Gas', US Patent 4,681,612.
- Ochs, T, D. Oryshchyn, R. Woodside, C. Summers, B. Patrik, D. Gross, et al., (2009), 'Results of Initial Operation of the Jupiter Oxygen Corporation Oxy-fuel 15 MWth Burner Test Facility', *Energy Procedia*, 1, 511-518.
- Ochs, T., D. Oryshchyn, D. Gross, B. Patrik, A. Gross, C. Dogan, et al., (2004), 'Oxy-Fuel Combustion Systems for Pollution Free Coal Fired Power Station', *Clearwater conference*, 18-22 April, Florida.
- Ozero, B. J., M.P. Czaikowski, and H.E. Gimpel, (1986), 'CO₂ Methane Separation by Low Temperature Distillation', US Patent 4,595,404, June.

- Pakulski, M., (2007), 'Accelerating Effect of Surfactants on Gas Hydrates Formation', *International Symposium on Oilfield Chemistry*, 28 February - 2 March, Houston, TX.
- Parent, J.D., (1948), 'The Storage of Natural Gas as Hydrate', Institute of gas technology, *Research Bulletin No. 1*, January, 40.
- Peneloux, A., and E. Rauzy, (1982), 'A Consistent Correction for Redlich-Kwong-Soave Volumes', *Fluid Phase Equilibria*, 8, 7-23.
- Peng, D.-Y., and D.B. Robinson, (1976), 'A New Two Constant Equation of State', *Ind. Eng. Chem. Fundam.*, 15 (1), 59-64.
- Potts, W.A., and E.R. Thomas, (1992), 'Method for Separating a Multi-Component Feed Stream Using Distillation and Controlled Freezing Zone', US Patent 5,120,338.
- Profio, P.D., S. Arca, R. Germani, and G. Savelli, (2005), 'Surfactant Promoting Effects on Clathrate Hydrate Formation: Are Micelles Really Involved?', *Chem. Eng. Sci.*, 60, 4141-4145.
- R.Amin, (2006), 'Method of Removing Solid Carbon Dioxide', US Patent 2006/0144079 A1.
- Radhakrishnan R., and B.L. Trout, (2002), 'A new approach for studying nucleation phenomena using molecular simulations: Application to CO₂ hydrate clathrates', *J. of Chem. Phys.*, 117 (4), 1786-1796.
- Renon, H., and J.M. Prausnitz, (1968), 'Local Compositions in Thermodynamic Excess Functions for Liquid Mixtures', *American Institute of Chemical Engineers Journal*, 14 (1), 135-144.
- Ripmeester, J.A. and C.I. Ratcliffe, (1990), 'Xenon-129 NMR studies of clathrate hydrates: new guests for structure II and structure H', *J. Phys. Chem.*, 94 (25), 8773-8776.
- Rodger, P.M., (1990), 'Stability of Gas Hydrates', *J. Phys. Chem.*, 94, 6080-6089.

- Rovetto, L.J., T.A. Strobel, C.A. Koh, and E.D. Sloan, (2006), 'Is Gas Hydrate Formation Thermodynamically Promoted by Hydrotrope Molecules?', *Fluid Phase Equilibria*, 247, 84-89.
- Rubin, E.S., A. Marks, H. Mantripragada, P. Versteeg and J. Kitchin, (2010), 'Prospects for Improved Carbon Capture Technology', *Report to the Congressional Research Service Washington DC from Carnegie Mellon University*, June, Department of Engineering and Public Policy Pittsburgh, Pennsylvania 15213.
- Sapper, R, (1987), 'Separation of CO₂ from a Gaseous Mixture', US Patent 4,695,304.
- Sapper, R., and H. Kick, (1987), 'Process for Separating CO₂ from a Gaseous Mixture', US Patent 4,710,213.
- Seo, Y.-T., S.-P. Kang and H. Lee, (2001), 'Experimental determination and thermodynamic modelling of Methane and Nitrogen hydrates in the presence of THF, propylene oxide, 1,4-dioxane and acetone', *Fluid Phase Equilibria*, 189, 99-110.
- Skovborg, P., and P. Rasmussen, (1994), 'A Mass Transport Limited Model for the Growth of Methane and Ethane Gas Hydrates', *Chem. Eng. Sci.*, 49 (8), 1131-1143.
- Sloan, E.D and C.A. Koh, (1998), *Clathrate Hydrates of Natural Gases*, 2nd edition, New York: Marcel Dekker.
- Sloan, E.D. and C.A. Koh, (2008), *Clathrate hydrates of natural gases*, 3d edition, CRC press.
- Sloan, E.D., (2003), 'Fundamental Principles and Applications of Natural Gas Hydrates', *Nature*, 426, 353-359.
- Spano, J.O., C.K. Heck, and P.L. Barrick, (1968), 'Liquid-Vapor Equilibria of the Hydrogen – Carbon Dioxide System', *J. Chem. Eng. Data*, 13 (2), 168-171.

- Spencer, D.F., (1997), 'Methods of Selectively Separating CO₂ from a Multicomponent Gaseous Stream', US patent 5,700,311.
- Spencer, D.F., and W.J. North, (1996), 'Methods for the Production of Carbon Dioxide Hydrates', US patent 5,562,891.
- Starr F., E. Tzimas, and S.D. Peteves, (2006), 'Near-Term IGCC and Steam Reforming Processes for the Hydrogen Economy: The Development Issues', *Joint Research Centre Institute for Energy*, July.
- Storr, M.T., P.C. Taylor, J.-P. Monfort, and P.M. Rodger, (2004), 'Kinetic Inhibitor of Hydrate Crystallisation', *Journal American Chemical Society*, 126, 1596-1576.
- Streater, S., (2010), 'OIL & GAS: Woy. Gas plant sets high bar for CO₂ sequestration', *Environment & Energy Daily*, 28 January.
- Sun, R., and Zh. Duan, (2005), 'Prediction of CH₄ and CO₂ Hydrate Phase Equilibrium and Cage Occupancy from ab initio Intermolecular Potentials', *Geochimica et Cosmochimica Acta*, 69 (18), 4411-4424.
- Sun, Zh.-G., R. Wang, R. Ma, K. Guo., and Sh. Fan, (2003), 'Natural Gas Storage in Hydrates with the Presence of Promoters', *Energy Conversion and Management*, 44, 2733-2742.
- Surovtseva, D, A. Barifcani and R. Amin, (2009a), 'CO₂ Separation by Cryogenic Condensation from the IGCC and Oxyfuel Flue Gases using PVT Sapphire Cell', Progress Report RPT09-1568, CO2CRC.
- Surovtseva, D, A. Barifcani and R. Amin, (2009b), 'Cryogenic condensation capture of CO₂ from IGCC flue gases', *Program and abstracts, CO2CRC Research Symposium*, Cooloom, Australia, 1-3 December. CO2CRC, Canberra, 67.
- Surovtseva, D., R. Amin, and A. Barifcani, (2010), 'Design and Operation of Pilot Plant for CO₂ Capture from IGCC Flue Gases by Combined Cryogenic and Hydrate Method', *Chemical Engineering Research and Design*, in press.

- Tabatabaei, A.R., A. Danesh, B. Tohidi, and A.C. Todd, (2000), 'A Consistent Thermodynamic Model for Predicting Combined Wax-Hydrate in Petroleum Reservoir Fluids', *Annals of the New York Academy of Sciences*, 912, 392-402.
- Takahashi, H., T. Yonezawa and E. Fercho, (2003), 'Operation Overview of the 2002 Mallik Gas Hydrate Production Research Well Program at the Mackenzie Delta in the Canadian Arctic', In: *Offshore Technology Conference*, 5-8 May, Houston, TX.
- Takeuchi, Y., Sh. Hironaka, Y. Shimada, and K. Tokumasa, (2000), 'Study on Solidification of Carbon Dioxide Using Cold Energy of Liquefied Natural Gas', *Heat Transfer – Asian Research*, 29 (4), 249-268.
- Tan, Y., E. Croiset, M.A. Douglas, K.V. Thambimuthu, (2006), 'Combustion Characteristics of Coal in a Mixture of Oxygen and Recycled Flue Gas', *Fuel*, 85, 507-512.
- Theiry, R., A. Van der Kerkhof, and J. Dubessy, (1994), 'vX Properties of CH₄-CO₂ and CO₂-N₂ Fluid Inclusions: Modelling for T<31°C and P<400 bars', *Eur. J. Mineral*, 6, 753-771.
- Thompson, A.-M., (2005), 'CANMET Energy Technology Centre R&D Oxyfuel Combustion for CO₂ Capture', *1st International Workshop on CSLF Projects*, 29 September, Postdam, Germany.
- Uchida, T., T. Ebinuma, J. Kabawata, and H. Narita, (1999), 'Microscopic observations of Formation Process of Clathrate-Hydrate Films at an Interface between Water and Carbon Dioxide', *J. of Crystal Growth*, 204, 348-356.
- Urdahl, O., A. Lund, P. Mork, and T.-N. Nilsen, (1995), 'Inhibition of Gas Hydrate Formation by Means of Chemical Additives – I. Development of an Experimental Set- up for Characterisation of Gas Hydrate Inhibitor Efficiency with Respect to Flow Properties and deposition', *Chem. Eng. Sci.*, 50 (5), 863-870.

US DOE NETL, (2008), 'Carbon Dioxide Hydrate Process for Gas Separation from a Shifted Synthesis Gas Stream', *Project Facts: Sequestration and Gasification Technologies*, April.

US DOE Office of Fossil Energy, (generated 2d November 2009), 'CO₂ Hydrate Process for Gas Separation from a Shifted Synthesis Gas Stream', Project Fact Sheet.

US DOE Office of Fossil Fuels, 'Pioneering Gasification Plants',
<http://www.fossil.energy.gov/programs/powersystems/gasification/gasificationpioneer.html> (retrieved 5 March 2010).

Valencia, J.A., and D.Denton, (1985), 'Method of Separating Acid Gases, Particularly Carbon Dioxide, from Methane by the Addition of a Light Gas such as Helium', US Patent 4,511,382.

Valencia, J.A., and D.J. Victory, (1990), 'Method and Apparatus for Cryogenic Separation of Carbon Dioxide and Other Acid Gases from Methane', US Patent 4,923,493.

Valencia, J.A., and R.D. Denton, (1985), 'Method and Apparatus for Separating Carbon Dioxide and Other Acid Gases from Methane by the Use of Distillation and a Controlled Freezing Zone', US Patent 4,533,372.

Valencia, J.A., P.S. Northrop, and C.J. Mart, (2008), 'Controlled Freeze ZoneTM Technology for Enabling Processing of High CO₂ and H₂S Gas Reserves', *International Petroleum Technology Conference*, 3-5 December, Kuala Lumpur, Malaysia.

Van der Kerkhof, A., and R. Thiery, (2001), 'Carbonic Inclusions', *Lithos*, 55, 49-68.

Van der Waals, J.H., and J.C. Plateeuw, (1959), 'Clathrate solutions', *Advances in Chemical Physics*, 2, 1-57.

van Hassel, B.A., J. Li, L. Switzer, G.M. Christie, and J. Sirman, (2005), 'Advanced Oxy-fuel Boilers for Cost-Effective CO₂ Capture', *4th Annual Conference on Carbon Capture & Sequestration*, 2-5 May, Alexandria, Virginia.

Van Konynenburg, P.H., and R.L. Scott, (1980), 'Critical Lines and Phase Equilibria in Binary Van der Waals Mixtures', *Philosophical Transactions of the Royal Society of London. Series A, Mathematical and Physical Sciences*, 298 (1442), 495-540.

Vattenfall corporate website <http://www.vattenfall.com> (last accessed November 2010).

von Stackelberg, M., (1949), 'Feste gashydrate', *Naturwissenschaften*, 36, 327-333

Watanabe, K., Sh. Imai., and Y.H. Mori, (2005), 'Surfactant Effects on Hydrate Formation in an Unstirred Gas/Liquid System: An Experimental Study Using HFC-32 and Sodium Dodecyl Sulfate', *Chem. Eng. Sci.*, 60 (17), 4846-4857.

Wu, S., A. Kukoski, P. Jin, K.-D. Tiggers, F. Klauke, C. Bergins, et al., 'Development of Oxyfuel Combustion Technology for Existing Power Plants', Hitachi Power Systems America, Ltd. www.hitachipowersystems.us (last accessed November 2010).

Xhang, J.S., C. Lo, A. Couzis, P. Somasundaran, J. Wu and J. W. Lee, (2009), 'Adsorption of Kinetic Inhibitors on Clathrate Hydrates', *J. Phys. Chem.*, 113, 17418-17420.

Zhang, C.S., S.S. Fan, D.Q. Liang, and K.H. Guo, (2004), 'Effect of Additives on Formation of Natural Gas Hydrate', *Fuel*, 83, 2115-2121.

Zhang, J.S., C. Lo, A. Couzis, P. Somasundaran, J. Wu, and J.W. Lee, (2009), 'Adsorption of Kinetic Inhibitors on Clathrate Hydrates', *J. Phys. Chem.*, 113, 17418-17420.

Zhang, Y., (2003), 'Formation of Hydrate from Single-Phase Aqueous Solutions', *MS thesis*, School of Engineering, University of Pittsburgh.

Zheng, L., and E. Furinsky, (2005), 'Comparison of Shell, Texaco, BGL and KRW Gasifiers as Part of IGCC Plant Computer Simulations', *Energy Conversion and Management*, 46, 1767-1779.

Zhong, Y., and R.E. Rogers, (2000), 'Surfactant Effects on Gas Hydrate Formation',
Chem. Eng. Sci., 55 (19), 4175-4187.

Every reasonable effort has been made to acknowledge the owners of copyright material. I would be pleased to hear from any copyright owner who has been omitted or incorrectly acknowledged.

Appendix A.**High Pressure Full-Vision Sapphire PVT Cell**

Figure A. 1 Photograph of the Sapphire Cell



Figure A. 2 Temperature Controlled Air Bath wherein the Sapphire Cell is contained

Figure A.3 presents a schematic of the hydrate testing cell. A high pressure sapphire cell (A) of 60 cc internal volume capacity contained inside a temperature controlled air bath (E) capable of achieving temperatures from -160°C to $+100^{\circ}\text{C}$ with an accuracy of 0.1 degree was used for the laboratory-scale experiments. Temperature of air bath and rate of cooling/heating was set via specially designed computer

software connected to the cell computer. Pressure maintenance at required levels during experiments was achieved by using a computer controlled positive displacement pump (K) having a 500 cc internal volume. A stainless steel magnetic stirrer (B) placed inside the cell and driven by motor drive (L) was used for agitation in the hydrate experiments. In the condensation experiments, the mixer was replaced with a calibrated measuring cylinder which allowed for an estimation of the quantities of liquid collected. The cell was equipped with a fibre optic system (F) to detect the dew point and the appearance of solids.

In the hydrate experiments, all liquids were fed into the evacuated cell, first through inlet (H), and after that the gas mixture was added.

Sample points (J) were used to analyse the feed gas prior to feeding it to the cell. Other sample points (I) were used for analysis of gas and liquid equilibrium phases. The conditions inside the cell were monitored via thermocouples T1, P1 and T2, P3 and pressure indicators on bottom and top of the cell respectively. Each experiment was recorded by one of the two digital cameras C through 5x magnifying lens.

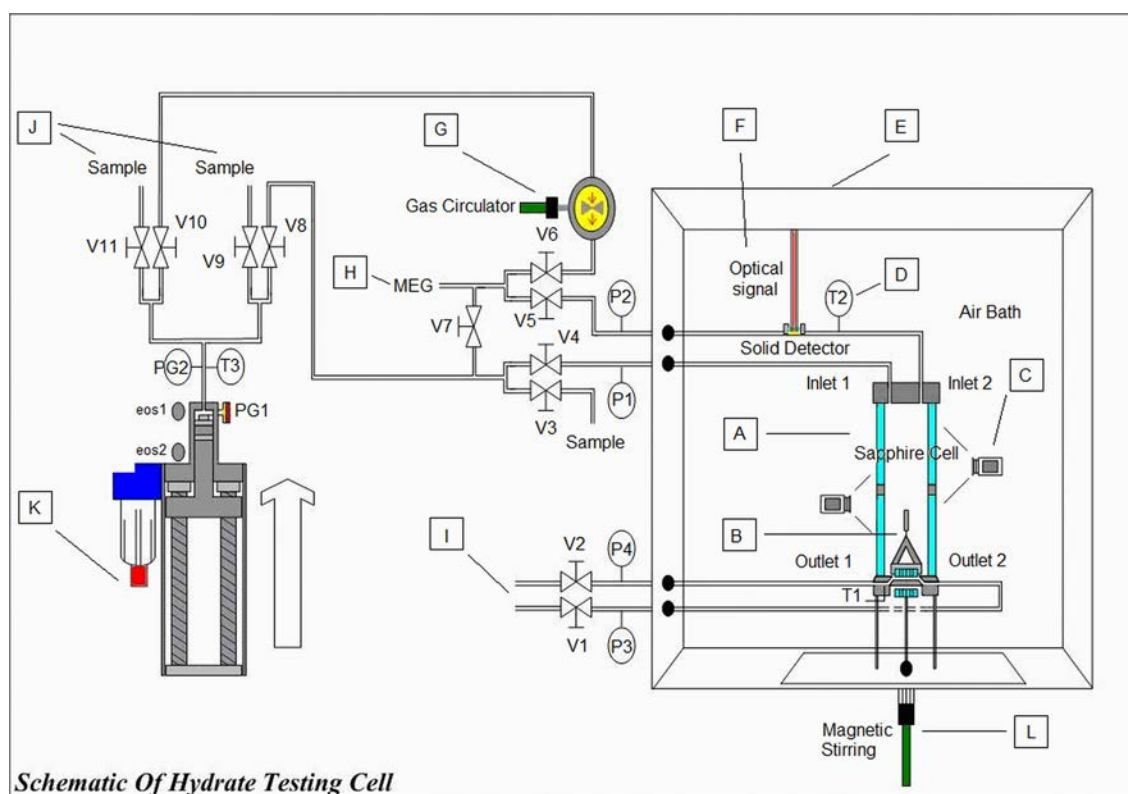


Figure A. 3 Schematic of the Hydrate Testing System

A - High-pressure variable-volume optical cell;

B - Magnetic Stirrer;

- C - Visualization video camera x2;
- D - Temperature measurement;
- E - Climatic Air Bath;
- F - Optical Solid Detection System;
- G - Gas Circulation System;
- H – Liquid Sample transfer systems;
- I - Liquid phase sampling system;
- J - Feed Sampling systems;
- K - Positive Displacement Pump for Gas Pressure Control;
- L - Motor drive for the magnetic stirrer.



Figure A. 4 Working Process

Appendix B.

Gas Sample Preparation and Transfer Procedure

Equipment used for preparation of gas mixtures is described in Table B.1.

Table B. 1 Equipment used for sample preparation

Equipment	Manufacturer	Model	Capacity	Accuracy
Vacuum pump	Edwards	E2M2	Ultimate pressure 1×10^{-3} mbar	
Pressure transmitter	Hinco Instruments Pty Ltd	892.23.510-300 (IS-20-S)	0...250 bar	≤ 0.5 % span
Balances	Shimadzu	UW6200H	0...6200 g	0.01 g
Gas booster	Haskel	AA-30	Compression ratio 30:1	
CO ₂ and CH ₄ analyser	Gas Alarm Systems	MGC-03	0...100 mol %	5% above 30 ppm

Each composition used for experiments was prepared in the following manner:

- 1) Evacuate residual gas from sample bottles
- 2) Weigh each cylinder
- 3) Estimate the required amount of each component to be added according to the desired mol composition
 - 3.1) Using the equation of state for an ideal gas and knowing the volume of the sample bottles, determine the approximate pressure of each component in a bottle
 - 3.2) Adjust the amount of components so that maximum pressure in a bottle doesn't exceed the design pressure of a bottle (120 bar)
- 4) Fill the bottles with the components according to the estimated pressures
- 5) Weigh the bottles to ensure correct composition

Because the compressibility factor was not taken into account for calculation of the amount of each component, a small error in mass occurred in some cases.

Prepared sample was loaded into the cell following the steps described below:

- 1) Evacuate any gas from the pump-cell system and manifold
- 2) Open bottles into the manifold and leave for 1 hour to let the gases mix
- 3) Using the gas booster, transfer gas mixture into the pump-cell system

- 4) Let the temperature and pressure stabilise and pass a sample through the gas analyser

- 5) Pressurise the cell to the desired pressure

All compositions were prepared on a weight basis. The estimated mass of each gas was weighed in a separate bottle of 500cc capacity, as commonly used in industry for transporting samples. Prior to transferring the sample into the PVT cell, the gases were mixed in a manifold and the total pressure was monitored via a pressure indicator. The mixture was then transferred via the positive displacement pump, and the pressure was monitored by the pressure indicator. The sample was then transferred into the cell and the pressure observed via the pressure indicator. Total CO₂ composition was verified by sampling prior to each experiment and using a Gas Alarm Systems' CO₂ analyser. Gas and liquid phases were sampled and the CO₂ content was determined directly.

Appendix C.

CO₂ condensation and freezing

1. Gas compositions

All gas compositions were prepared on a weight basis as described in Appendix B. Table C.1 shows in detail the amount of each component added to prepare the experimental compositions. Differences in measurements taken after loading the sample into the cell are attributable to the challenges of transferring the gases from the bottles.

Table C. 1 Gas composition for CO₂ freezing testing

CO ₂ mol% in the final mixture	Component mass, g. Common error ± 0.1 g except for H ₂ ± 0.05 g					
	CO ₂	NG	H ₂	Ar	N ₂	O ₂
23	21.00		3.33	0.58	0.31	
27 (and 28)	15.40		2.17	0.68	0.48	
29 (and 30)	20.40		2.71	0.72	0.51	
37	25.91		1.88	0.31	1.38	
37	25.40		1.66	0.46	0.24	
40 (and 41)	24.06		1.49	0.43	0.22	
43	43.59		2.42	0.66	0.35	
45	26.41		1.43	0.43	0.22	
52	44.01		1.29	0.53	0.28	
84	68.32			3.21	0.74	1.69
88 (and 93)	80.61			3.21	0.74	1.69
20	10.00	18.00				
45	35.00	18.13				
70	35.00	6.26				

2. Properties of Solid CO₂ at Various Pressures, Temperatures and Concentrations

The visualization experiment was done using a high-speed video camera on a continuous basis. The whole process of the mixture condensation and CO₂ freezing was recorded on the video tapes at the same time the pressure and temperatures were logged.

The experiments were conducted for three gas mixtures specified above in Table C.1 and observations on CO₂ freezing and the stickiness pattern were recorded on video. Multiple pressure–temperature conditions detailed in Table C.2 were tested with a stainless steel stirrer in the cell, coated with Teflon, ceramic or polymer.

Table C. 2 Experimental conditions for CO₂ stickiness experiments

Pressure, bar	12	18	30
Temperatures observed, °C	-60; -65; -70; -80; -100	-60; -65; -90	-60; -65; -90

Particular attention was paid to the solid behaviour at temperatures between -60°C and -65°C because these conditions are most likely to appear during cold start up and extended shut-in.

2.1. Observations from stainless steel test (SS)

2.1.1. For (SS) 20% CO₂ composition mixture

12 bar (-100°C)

- Mostly a very fine, thin layer of solid CO₂ on the sapphire cell walls
- Solid build up on the stirrer at the bottom of the cell restricting the movement of the stirrer and finally causing the blockage of the movement
- Solid was not movable from the stainless steel metal



12 bar (-80°C)

- Solid formation starts at the gas-liquid interface
- A thin film of solid on the sapphire cell walls plus some granola-like solid on other parts of the sapphire wall. Some solids on the bottom
- Forms sticky agglomerate solid phase after 60 minutes in a static condition

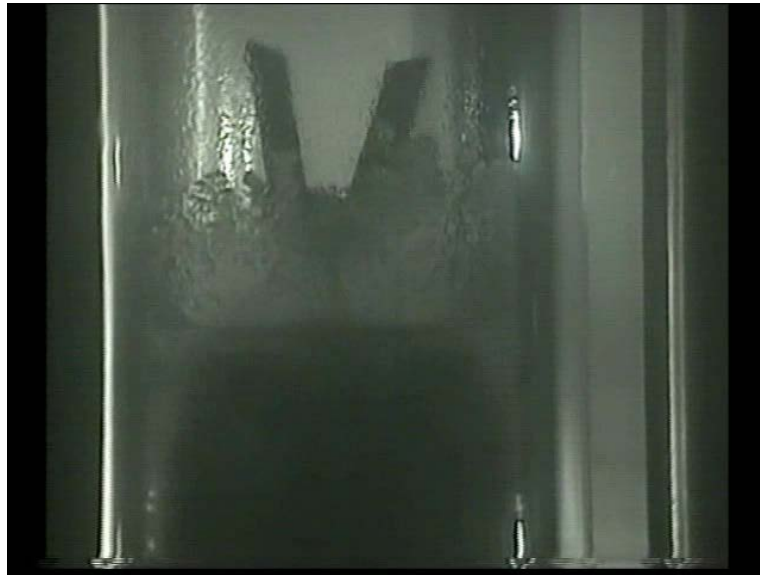
12 bar (-60°C)

- Extremely fine, wet thin film on the sapphire cell walls. No evidence of any solid deposition on the metal



18 bar (-90°C)

- Solid CO₂ forming at the gas-liquid interface
- Solid phase deposition on the stirrer but removable at high speed stirring with some difficulties over time
- Forms sticky agglomerate solid phase after 60 minutes in a static condition

18 bar (-60°C)

- Extremely very fine wet thin film on the sapphire cell walls
- No evidence of deposition on the metal



30 bar (-90°C)

- Slightly more consolidated solid CO₂ forming on the sapphire cell walls
- Adhering to the metal, but can be moved around by the stirrer at high velocity with some delay
- Forms sticky agglomerate solid phase after 60 minutes in a static condition

30 bar (-60°C)

- Fine wet thin film on the sapphire cell walls
- Very little condensation



2.1.2. For (SS) 70% CO₂ composition mixture:

12 bar (-65°C)

- Transparent frozen film of CO₂ on the sapphire cell walls
- Adhering slightly to the (stirrer) metal or the sapphire walls but can moved around by the stirrer
- The sapphire walls inside the liquid phase is clear of solid because of the shear of the liquid



18 bar (-65°C)

- Solid CO₂ starts to form on the interface
- Not adhering strongly to the (stirrer) metal or the sapphire cell walls and can moved around by the stirrer
- Forms sticky agglomerate solid phase after 60 minutes in a static condition



30 bar (-65°C)

- Very fine white solid crystals forming near the sapphire cell walls, falling after forming critical mass.
- Not adhering strongly to the (stirrer) metal or the sapphire cell walls and can moved around by the stirrer
- Forms sticky agglomerate solid phase after 60 minutes in a static condition

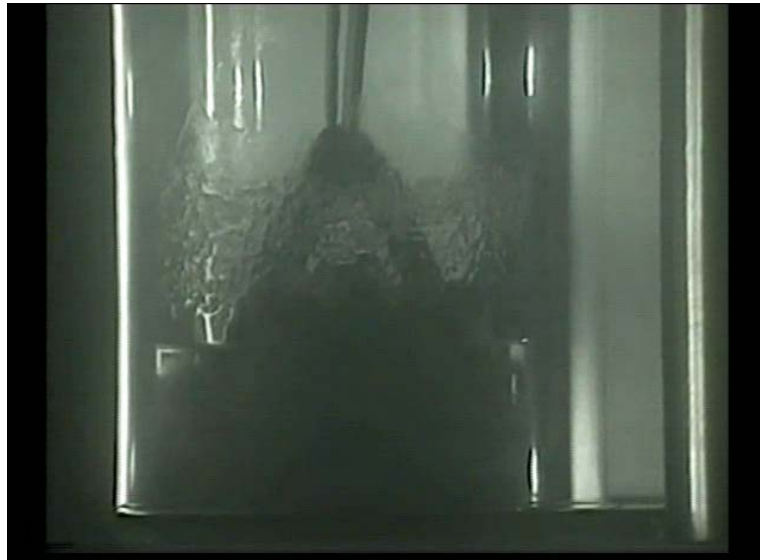
***2.1.3. For (SS) 45% CO₂ composition mixture:***12 bar (-70°C)

- Solid CO₂ formation at the interface and the sapphire cell walls
- Adhering slightly to the (stirrer) metal or the sapphire cell walls but can moved around by the stirrer
- Forms sticky agglomerate solid phase after 60 minutes in a static condition



12 bar (-65°C)

- Clear solid CO₂ film forming at the sapphire cell walls
- Adhering slightly to the metal (stirrer) or the sapphire cell walls but can be moved around by the stirrer
- Forms sticky agglomerate solid phase after 60 minutes in a static condition

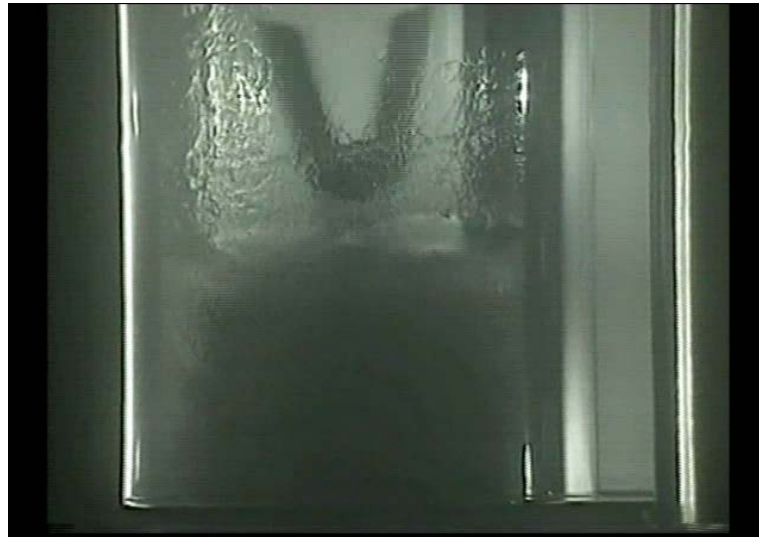
18 bar (-65°C)

- Very fine clear transparent solid CO₂ crystals forming at the liquid-gas interface
- The solid on the metal can be removed by the below liquid level by the shear of the stirrer
- Forms sticky agglomerate solid phase after 60 minutes in a static condition



30 bar (-65°C)

- Very fine clear solid CO₂ crystals forming at the liquid-gas interface
- The solid on the metal can be removed by below liquid level by the shear of the stirrer
- Forms sticky agglomerate solid phase after 60 minutes in a static condition

**2.2. Observation from Teflon coated (SS) test****2.2.1. For (Teflon) 20% CO₂ composition mixture:**12 bar (-60°C)

- Only thin wetting on the sapphire cell walls, no solid.



12 bar (-80°C)

- Some solid crystalline thin solid on the sapphire cell walls, one side only.
- Solid stayed on the sapphire cell walls
No enough liquid to test the stickiness of the solid.
- No solid deposition on the Teflon coated metal

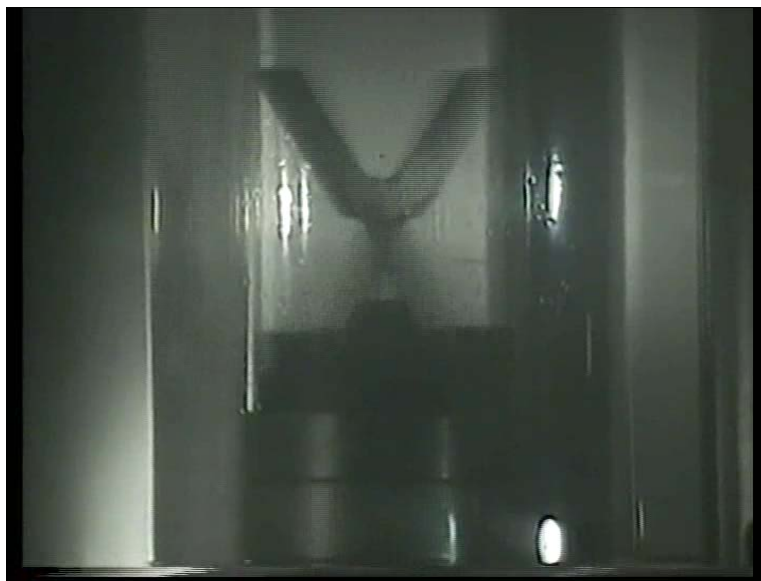
12 bar (-100°C)

- Mostly very fine thin layer of solid CO₂ on one side of the sapphire cell walls
- Solid was not movable from the walls because of a lack of liquid
- No immediate stickiness on the Teflon was documented
- Forms sticky agglomerate solid phase after 60 minutes in a static condition

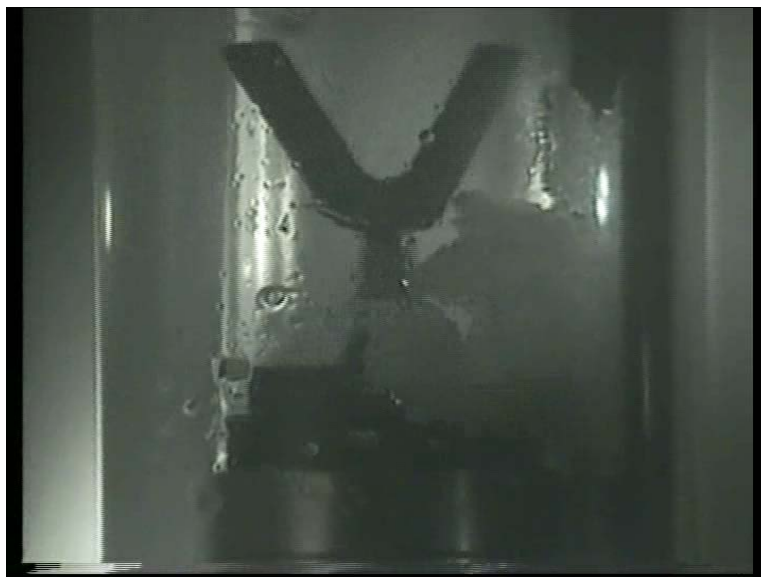


18 bar (-60°C)

- Only thin wetting on the sapphire cell walls, no solids

18 bar (-90°C)

- Solid CO₂ forming of the sapphire cell walls
- Some solid phase deposition on the stirrer but removable at high speed stirring
- Forms sticky agglomerate solid phase after 60 minutes in a static condition



30 bar (-90°C)

- Consolidated/agglomerated solid CO₂ forming on the sapphire cell walls
- Solid adhering to the Teflon coated stirrer restricting its movement
- Forms sticky agglomerate solid phase after 60 minutes in a static condition

30 bar (-60°C)

- Only thin wetting film on the sapphire cell walls, no solids



2.2.2. For (Teflon) 70% CO₂ composition mixture:

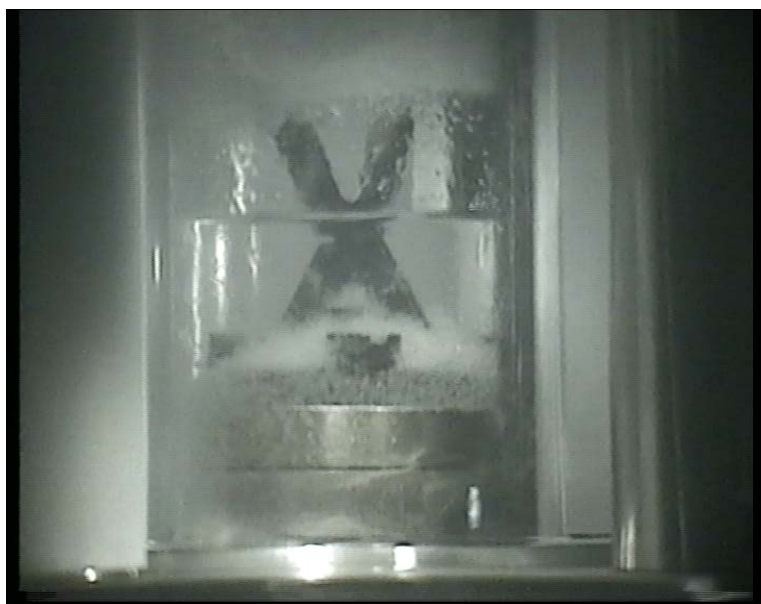
12 bar (-65°C)

- CO₂ crystals forming in the liquid phase, some CO₂ crystals on the sapphire cell walls
- Some solid phase deposition on the stirrer but removable at high speed



18 bar (-65°C)

- CO₂ crystals forming in the liquid phase, some CO₂ crystals on the sapphire cell walls
- Some solid phase deposition on the stirrer but removable at high speed



30 bar (-65°C)

- Some white solid CO₂ crystals forming near the sapphire cell walls and the interface.
- Fine solid CO₂ particles can be seen in the liquid phase moving freely with the stirrer
- Solid CO₂ blocked the Teflon coated stirrer after 5 minutes
- Solid CO₂ can be seen on the tip of the Teflon coated stirrer



2.2.3. For (Teflon) 45% CO₂ composition mixture:

12 bar (-70°C)

- Clear solid CO₂ film forming at the sapphire cell walls and the interface
- Solid CO₂ sticking to the Teflon coated stirrer in the middle below the liquid level, the Teflon coated stirrer could not remove it
- Forms sticky agglomerate solid phase after 60 minutes in a static condition



12 bar (-65°C)

- Clear solid CO₂ film forming at the sapphire cell walls
- Solid CO₂ sticking to the Teflon, the stirrer cannot remove it
- Forms sticky agglomerate solid phase after 60 minutes in a static condition

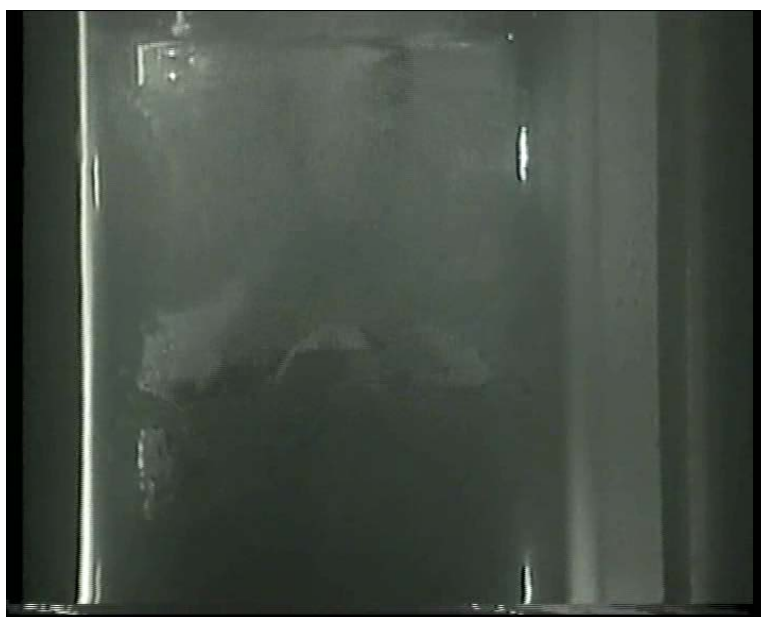


18 bar (-65°C)

- Very fine clear solid CO₂ crystals forming at the liquid-gas interface
- Evidence of stickiness to the Teflon by restricting the movement of the stirrer
- Forms sticky agglomerate solid phase after 60 minutes in a static condition

30 bar (-65°C)

- Transparent solid CO₂ crystals forming at the liquid-gas interface
- Sticky solid phase can be observed in the middle of Teflon coated metal
- Forms sticky agglomerate solid phase after 60 minutes in static condition



2.3. Ceramic coated (Aluminium Oxide) stirrer

As mentioned in the main body of Chapter 3 it can be confirmed that the CO₂ solid formation on the walls is related only to the equilibrium as experiments were conducted at highspeed cooling where the sapphire wall was colder than the fluid inside. Under these conditions the growth always started on the walls, whereas the growth for the slower cooling speed started as fine crystals from the liquid phase.

Unlike all the other tests, no solid CO₂ deposited on the ceramic coated stirrer, even after 60 minutes, although at the same time it was sticking to the bottom of the stirrer made of stainless steel.

2.3.1. For (Ceramic) 70% CO₂ composition mixture:

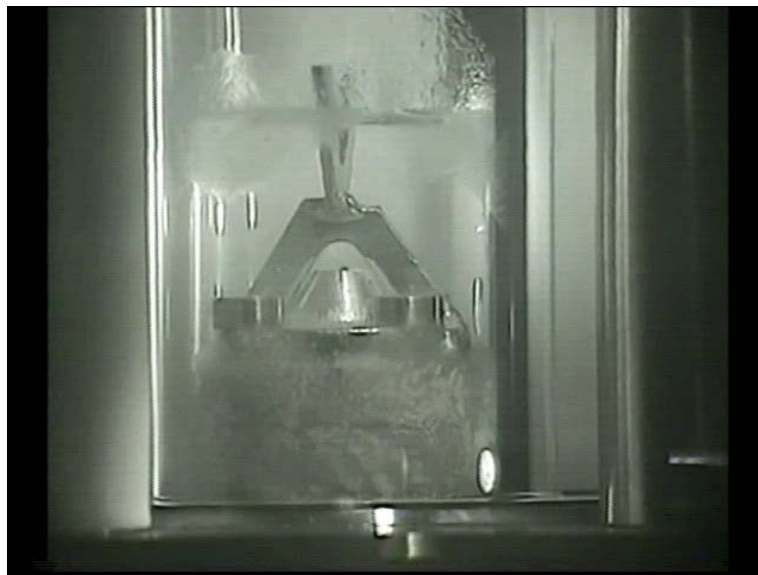
30 bar (-65°C)

- Solid formation started in the liquid phase at the bottom of the cell
- Fine solid CO₂ particles can be seen in the liquid phase moving freely with the stirrer
- No CO₂ was sticking to the walls (conducted at low cooling rate)
- No solid stickiness on the ceramics stirrer was observed even after 60 minutes



18 bar (-65°C)

- Very fine clear transparent solid CO₂ crystals forming at the liquid-gas interface
- Some solid crystals moving freely in the liquid phase
- No solid stickiness on ceramics stirrer was observed even after 60 minutes
- Some transparent solid CO₂ on the sapphire walls



12 bar (-65°C)

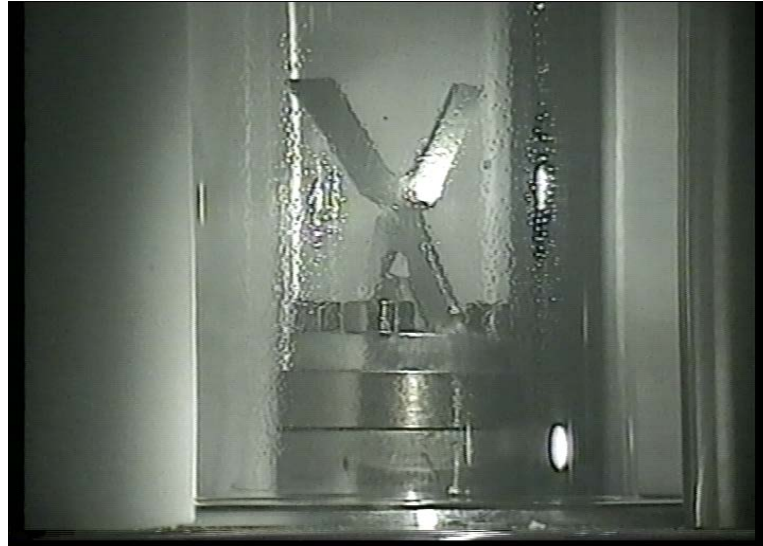
- Solid CO₂ crystals forming in the liquid phase starting at the bottom of the cell
- Adhering slightly to the sapphire cell walls but can be moved around by the stirrer in the liquid covered area, some solid splash on the gas area
- Solid sticking to the bottom of the stirrer made of stainless steel
- No solid stickiness on ceramic stirrer was observed even after 60 minutes
- Forms sticky agglomerate solid phase after 60 minutes on the stainless steel part of the stirrer (bottom)



2.3.2. For (Ceramic) 20% CO₂ composition mixture:

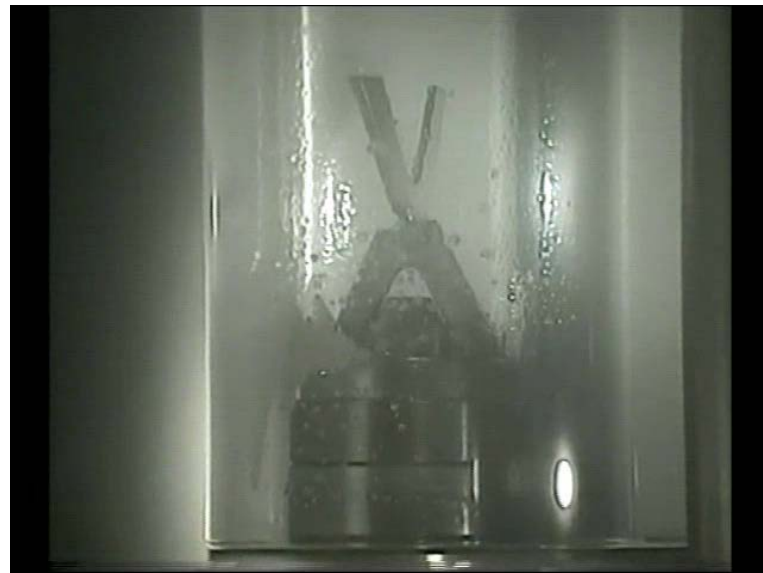
12 bar (-60°C)

- Thin film on the sapphire cell wall
- Very fine crystals, not sure if it solid



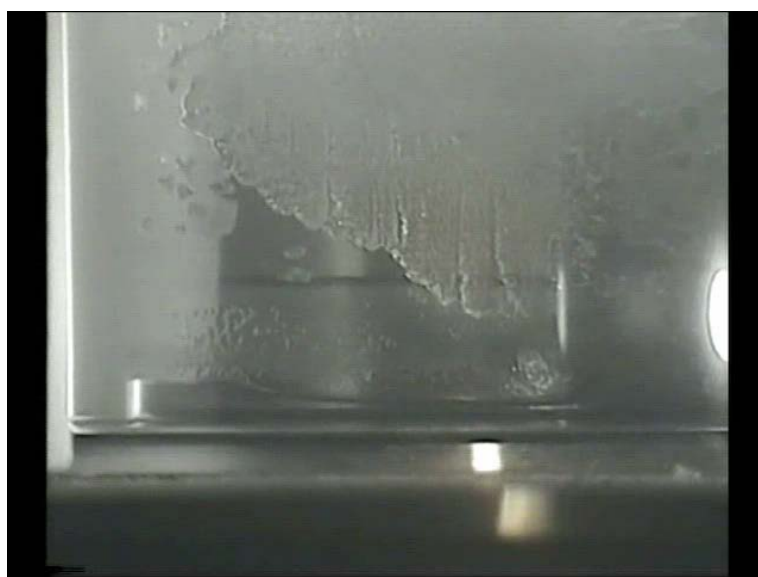
12 bar (-80°C)

- Solid CO₂ crystals forming on the sapphire cell wall
- No solid stickiness on ceramic stirrer was observed even after 60 minutes
- Not enough liquid to test the stickiness on the sapphire wall



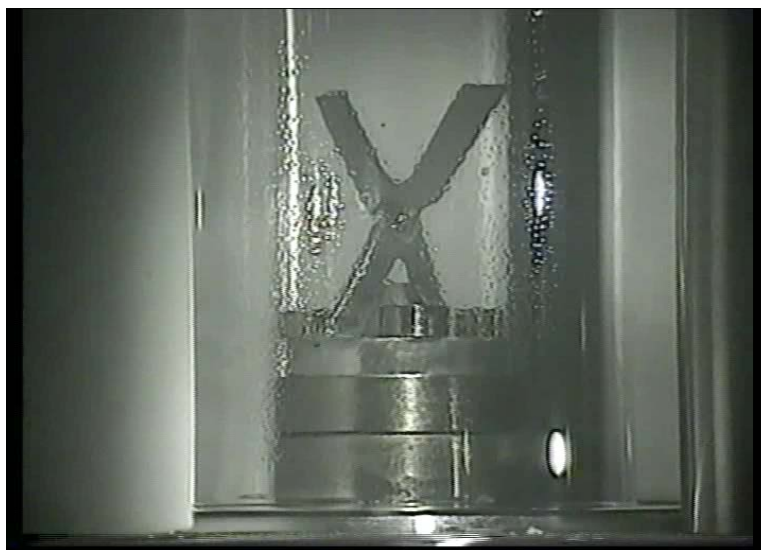
12 bar (-100°C)

- Solid agglomerated CO₂ crystals forming on the sapphire cell wall
- The solid looks like it is wetted by the hydrocarbon liquid film
- The solid was moved at high-speed stirring by the gas phase (Photograph 2)
- No solid stickiness on ceramic stirrer was observed even after 60 minutes



18 bar (-60°C)

- Thin film on the sapphire cell wall
- Very fine crystals, not sure if it solid

18 bar (-90°C)

- Solid CO₂ Crystals on the sapphire cell wall
- No solid precipitated on the ceramic stirrer
- The solid looks like it is wetted by the hydrocarbon liquid film

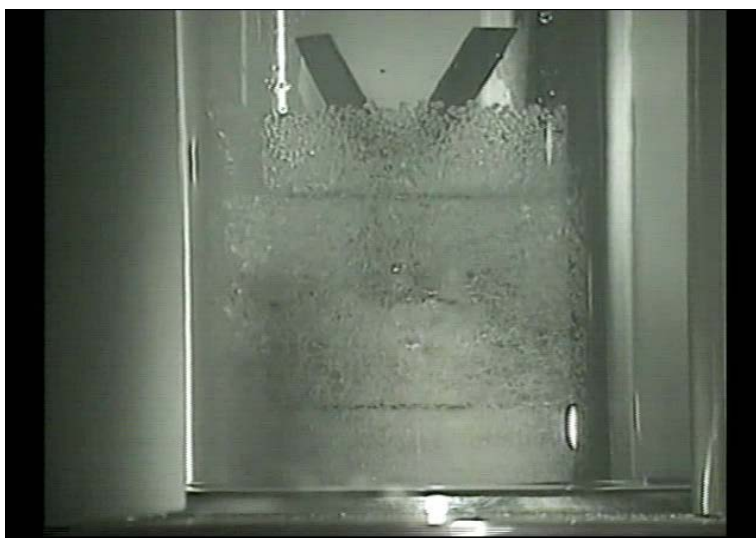


30 bar (-60°C)

- Thin film on the sapphire cell wall
- Very fine crystals, not sure if it solid

30 bar (-90°C)

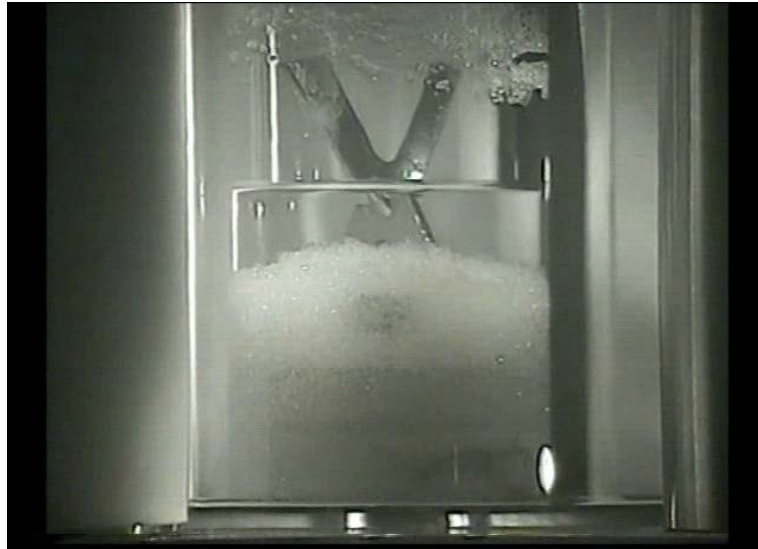
- Solid CO₂ crystals forming on the sapphire cell wall
- The solid looks like it is wetted by the hydrocarbon liquid film
- No solid stickiness on ceramic stirrer was observed even after 60 minutes



2.3.3. For (Ceramic) 45% CO₂ composition mixture:

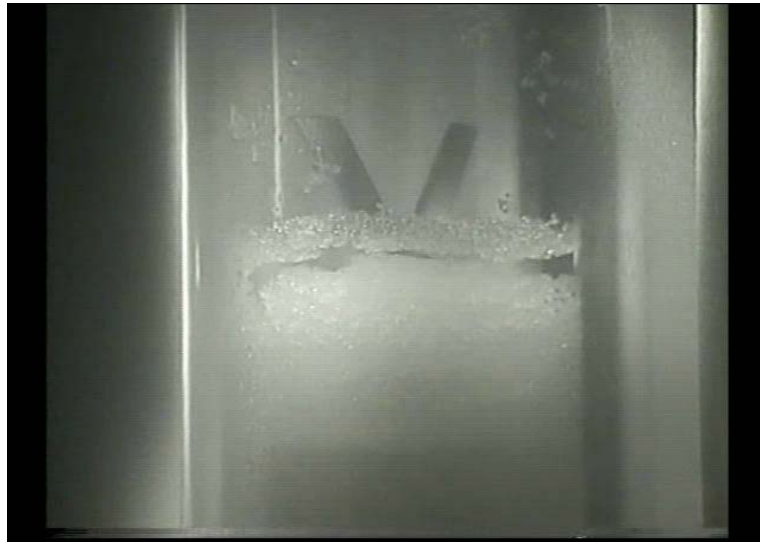
30 bar (-65°C)

- Some CO₂ crystals forming on the sapphire cell wall from the gas phase
- Fine solid CO₂ crystals formed in the liquid phase
- No solid on the sapphire cell wall inside the liquid phase
- Some minor solid deposited on the ceramic stirrer tip after 30 minutes. This could be related to some erosion on the ceramic coating, this was investigated after opening the cell



18 bar (-65°C)

- Some minor CO₂ crystals forming on the sapphire cell wall from the gas phase
- Fine solid CO₂ crystals formed in the liquid phase
- No solid on the sapphire cell wall inside the liquid phase
- No solid deposition on the ceramic stirrer

12 bar (-65°C)

- Some minor CO₂ crystals forming on the sapphire cell wall from the gas phase
- Fine solid CO₂ crystals formed in the liquid phase
- No solid on the sapphire cell wall inside the liquid phase



12 bar (-70°C)

- Some minor CO₂ crystals forming on the sapphire cell wall from the gas phase
- Fine solid CO₂ crystals formed in the liquid phase
- No solid on the sapphire cell wall inside the liquid phase

**2.4. Observation from polymer coated (SS) test****2.4.1. For (Polymer) 20% CO₂ composition mixture:**12 bar (-60°C)

- Only thin wetting on the sapphire cell walls, no solid.



12 bar (-80°C)

- Thin solid on the sapphire cell walls
No enough liquid to test the stickiness of the solid.
- No solid deposition on the Polymer coated metal

12 bar (-100°C)

- Mostly very fine thin layer of solid CO₂ on one side of the sapphire cell walls
- Fine thin solid film on the polymer
- Forms sticky agglomerate solid phase after 60 minutes in static condition



18 bar (-60°C)

- Only thin wetting on the sapphire cell walls, no solids

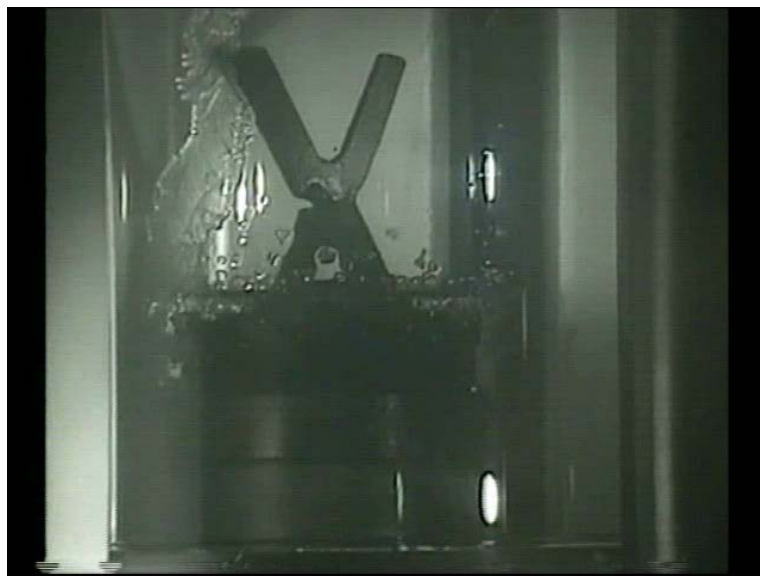
18 bar (-60°C)

- Solid CO₂ forming of the sapphire cell walls
- Some thin solid deposition on the stirrer, removable at high speed stirring
- Forms sticky agglomerate solid phase after 60 minutes in a static condition



30 bar (-90°C)

- Consolidated icy looking solid CO₂ on the sapphire cell walls
- Some solid crystals to the polymer coated stirrer
- Forms sticky agglomerate solid phase after 60 minutes in a static condition

30 bar (-60°C)

- Only thin wetting film on the sapphire cell walls, no solids



2.4.2. For (Polymer) 70% CO₂ composition mixture:

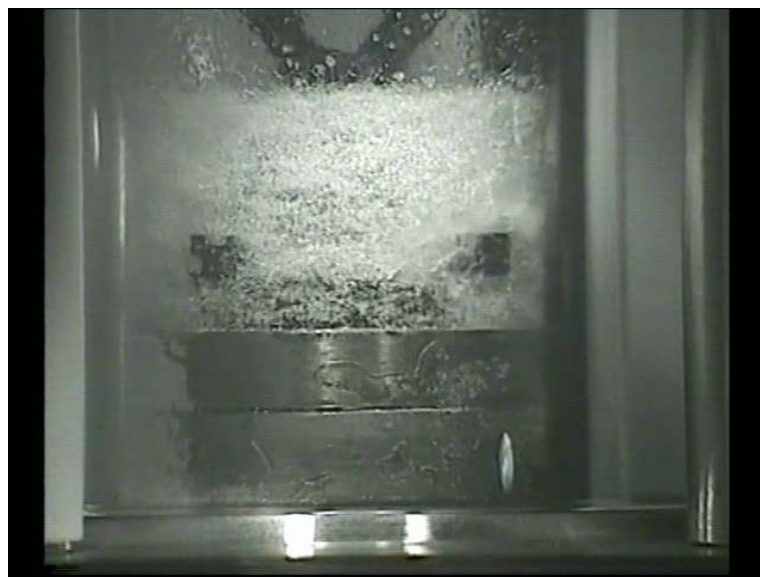
12 bar (-65°C)

- Thick CO₂ crystals forming in the liquid phase, CO₂ crystals on the sapphire cell walls
- Solid phase deposition on the stirrer



18 bar (-65°C)

- CO₂ crystals forming in the liquid phase, CO₂ crystals on the sapphire cell walls
- Thick solid phase deposition on the stirrer



30 bar (-65°C)

- White solid CO₂ crystals forming on the sapphire walls and liquid interface.
- Fine solid CO₂ particles can be seen in the liquid phase moving freely with the stirrer
- Solid CO₂ blocked the Polymer coated stirrer
- Solid CO₂ can be seen on the tip of the Polymer coated stirrer



2.4.3. For (Polymer) 45% CO₂ composition mixture:

12 bar (-70°C)

- Clear icy solid CO₂ forming at the sapphire cell walls and the interface
- Solid CO₂ sticking to the polymer coated stirrer in the middle below the liquid level and the stirrer cannot remove it
- Forms sticky agglomerate solid phase after 60 minutes in a static condition



12 bar (-65°C)

- Clear solid CO₂ film forming on the sapphire cell walls
- Solid CO₂ sticking to the polymer, the stirrer cannot remove it
- Forms sticky agglomerate solid phase after 60 minutes in a static condition



18 bar (-65°C)

- Fine clear solid CO₂ crystals forming at the liquid-gas interface
- Solid CO₂ ticking to the polymer coated stirrer
- Forms sticky agglomerate solid phase after 60 minutes in a static condition

30 bar (-65°C)

- Thick transparent solid CO₂ crystals forming on the cell walls and liquid-gas interface
- Sticky solid phase can be observed in the middle of the polymer coated metal



Appendix D.

Gas Compositions for Hydrate Testing.

1. CO₂ Hydrate Testing

CO₂ hydrate testing was performed for binary mixtures of CO₂ with Hydrogen prepared on a weight basis as specified in Table D.1. The composition was prepared in one cylinder and was confirmed by sampling through the Gas Alarm Systems' CO₂ analyser. First about 20% of Hydrogen was added to the bottle, then it was pressurised with all the CO₂ and finally the rest of the Hydrogen was transferred. The results are discussed in Chapter 4.

Table D. 1 Gas composition for CO₂ hydrate testing

Component	Pressure	Mass, g
CO ₂	~300psi	7.4±0.1
Hydrogen	To total 69 bar	2.3±0.05

2. Complex Hydrate Testing

The CO₂ hydrate testing discussed in Chapters 5 and 6 was performed for gas mixtures prepared on a weight basis detailed in Table D.2. The composition was confirmed by chromatographic analysis conducted at Core Labs. Sample S1 was obtained from the field.

Table D. 2Compositions prepared for hydrate testing

Gas Sample	S2	S3
Component	Mass of component, g	
Nitrogen	6.53	0.63
Carbon Dioxide	2.50	9.4
Methane	38.16	36±0.15
Ethane	3.35	4.79
Propane	1.76	2.52
Butanes	1.13	1.67
Pentanes	0.60	1.83
C6 fraction	0.40	1.56
C7 fraction	0.50	

Appendix E.

Gas Hydrate observations

1. Sample S1 hydrates

1.1. Some common observations

When cooling was performed at stagnant conditions, the hydrate crystallisation occurred only after the system was exposed to vigorous stirring.

At lower concentration of MEG (40 wt%), the hydrate was formed as a very viscous slurry, and some of it deposited on the walls of the cell (see Figure E.1). At pressures under 100 bar, however, the hydrate slurry was too loose to stick to the walls (see Figure E.2). In the presence of 45 wt% MEG, very watery slurry was formed in all cases and no hydrate was sticking to the walls (see Figure E.3).



Figure E. 1 Splashed hydrate is sticking to the walls at 200 bar in the presence of 40 wt% MEG

During experiments separation of different types of hydrate was observed (see Figure 5). A light hydrocarbon fraction formed less dense hydrate which tends to separate from MEG and float on top of it. Heavier hydrocarbons such as C4 and C5 form more dense chunks of hydrate which are submerged deeper in the liquid phase. The latter type of hydrate melted at temperatures about 1.5°C lower than the former.

At pressures less than 100 bar, some condensate collected on top of the hydrate slurry. This condensate layer was found to 'hold' hydrate and inhibit its dissociation, which was particularly the case for the experiment with 45 wt MEG at 75.6 bar. Hydrate stayed in form of very thick slurry up to temperatures 1°C higher than the beginning of dissociation (this was captured on video).



Figure E. 2 Low viscosity hydrate slurry at 70 bar in the presence of 40 wt% MEG



**Figure E. 3 Heavy hydrocarbons hydrate flock submerged in MEG at 170 bar
in the presence of 45 wt% MEG**

1.2. Hydrate appearance with 40 wt% MEG

220 bar



200 bar



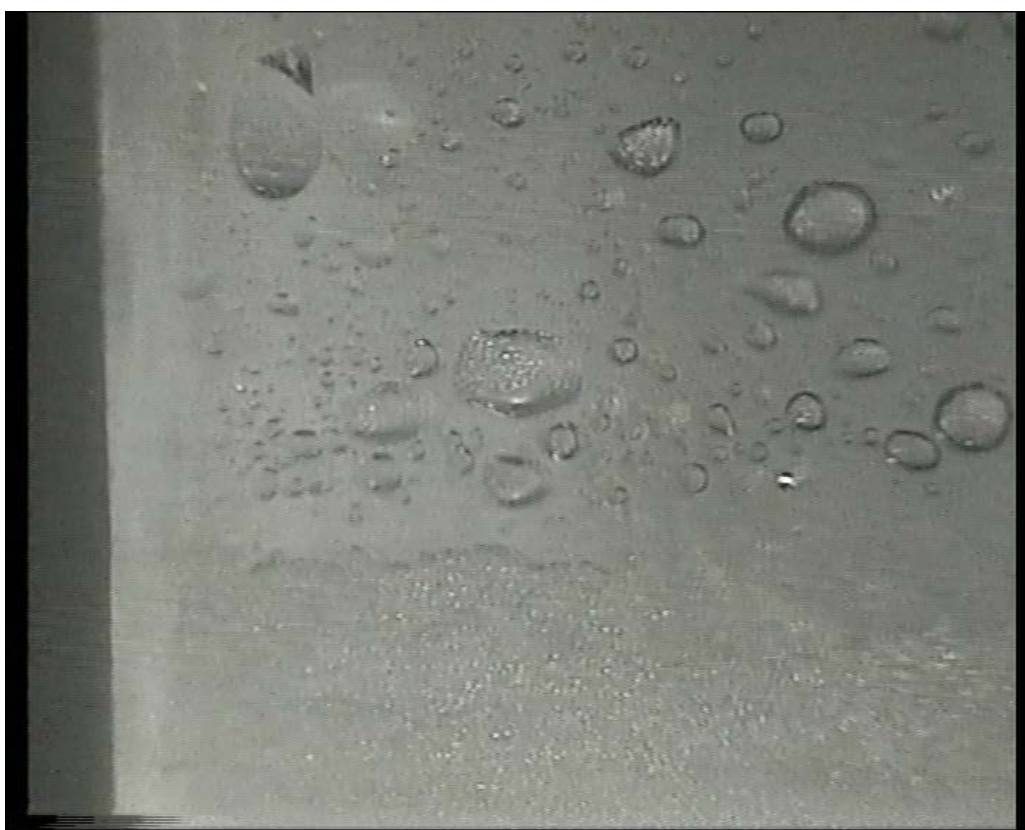
186 bar



140 bar

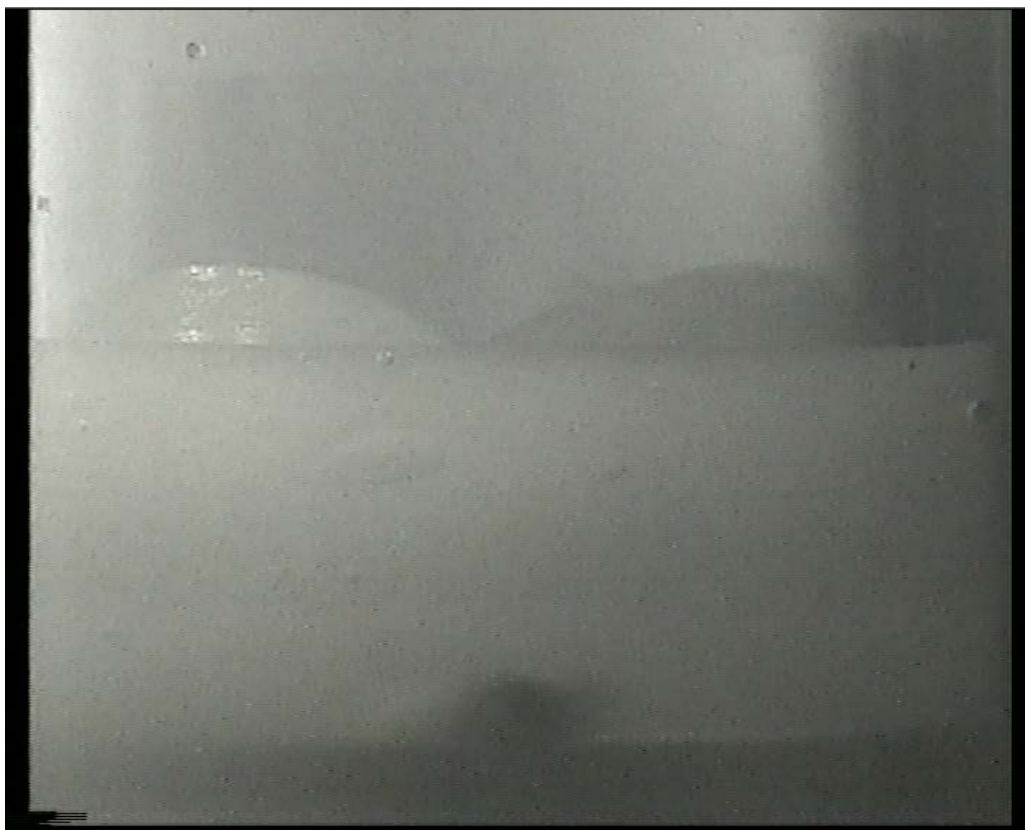


100 bar



70 bar



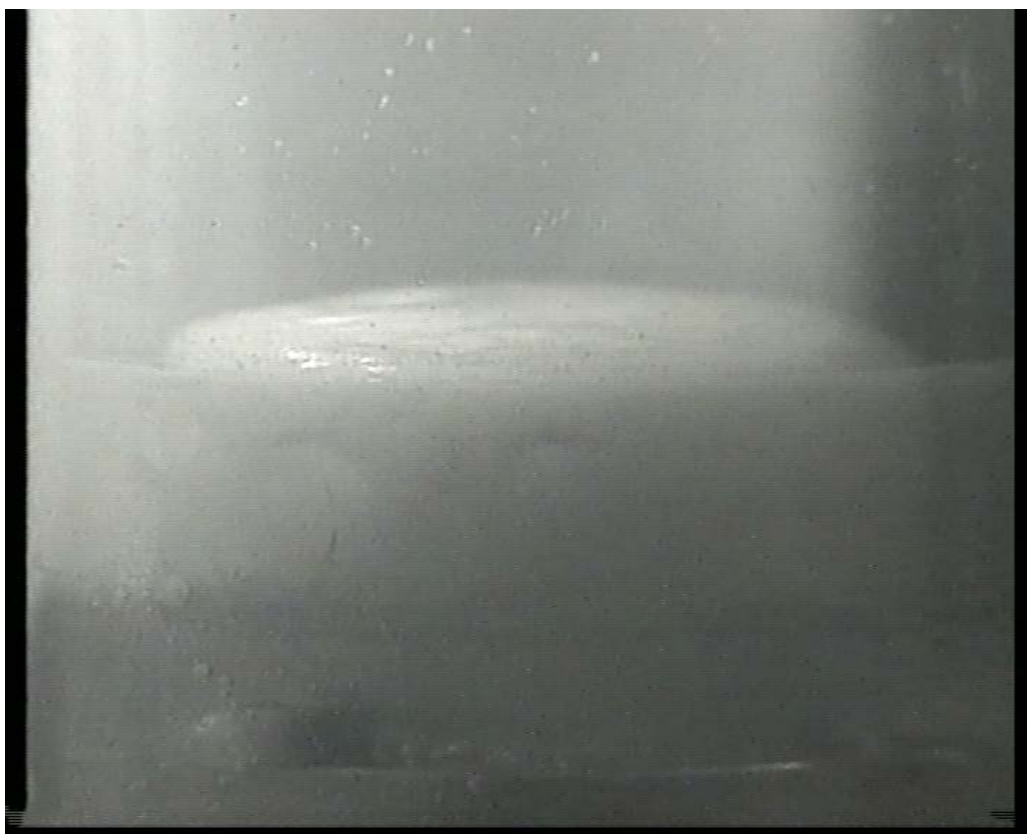
1.3. Hydrate appearance with 45 wt% MEG230 bar

200 bar

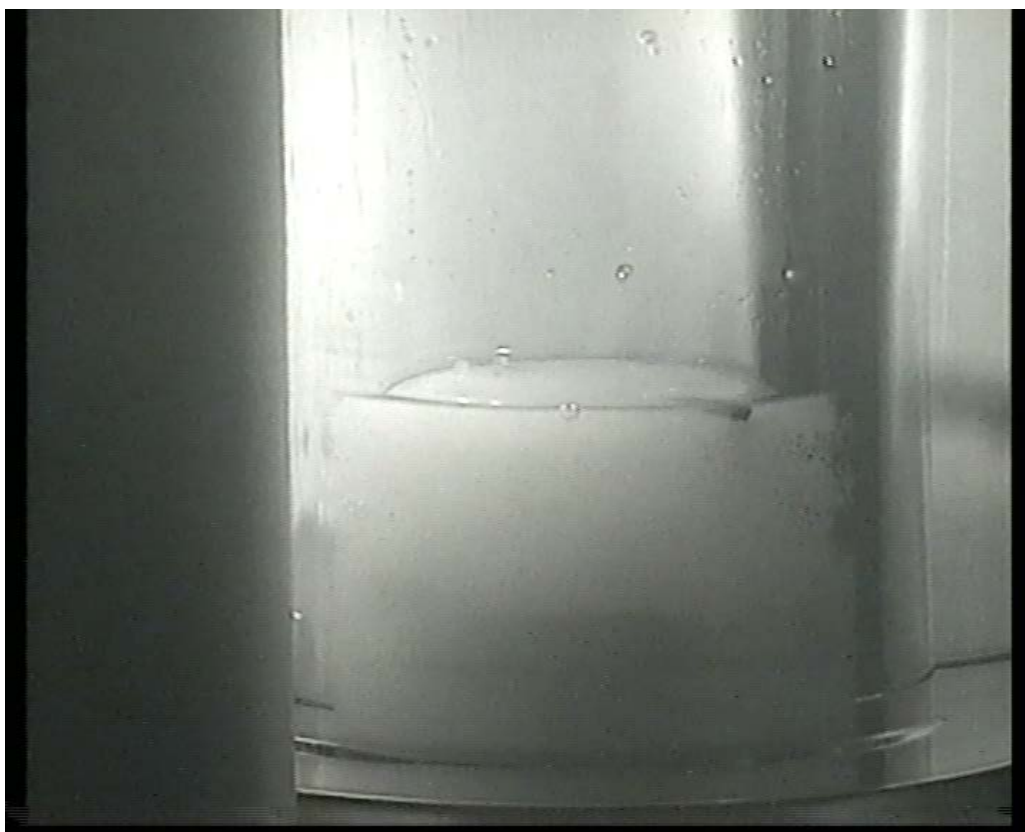


170 bar



150 bar130 bar

93 bar



75 bar



Appendix F.

CO₂-Natural Gas Multiphase Flash Model

Input Data

Temperature (K):

$$T_{\text{cel}} := -70 \quad T := 273.15 + T_{\text{cel}}$$

Pressure (kPa) $P := 3500$

Gas Composition:

$$\text{CO}_2 := 0.207235$$

$$\text{N}_2 := 0.018943$$

$$\text{C}_1 := 0.701464$$

$$\text{C}_2 := 0.053496$$

$$\text{C}_3 := 0.015285$$

$$i\text{-C}_4 := 0.001301$$

$$n\text{-C}_4 := 0.001626$$

$$i\text{-C}_5 := 0.000244$$

$$n\text{-C}_5 := 0.000244$$

$$\text{C}_6 := 0.00163$$

Basic Constants

Ref. Temperature (K):

$$T_o := 273.15$$

Boltzmann Constant:

$$k := 1.380658 \cdot 10^{-26} \text{ kJ/K}$$

Gas Constant:

$$R_c := .0083143 \text{ (kPa}\cdot\text{m}^3/\text{mol}\cdot\text{K)}$$

Critical Properties of Gas Components

	$^{\circ}\text{K}$	kPa	
$x := \begin{pmatrix} \text{CO}_2 \\ \text{N}_2 \\ \text{C}_1 \\ \text{C}_2 \\ \text{C}_3 \\ i\text{-C}_4 \\ n\text{-C}_4 \\ i\text{-C}_5 \\ n\text{-C}_5 \\ \text{C}_6 \end{pmatrix}$	$T_c := \begin{pmatrix} 304.1 \\ 126.1 \\ 190.6 \\ 305.4 \\ 369.8 \\ 408.2 \\ 425.2 \\ 460.4 \\ 469.7 \\ 507.5 \end{pmatrix}$	$P_c := \begin{pmatrix} 7382 \\ 3394 \\ 4599 \\ 4872 \\ 4248 \\ 3648 \\ 3796 \\ 3058 \\ 3370 \\ 3025 \end{pmatrix}$	$w := \begin{pmatrix} 0.2276 \\ 0.0403 \\ 0.0115 \\ 0.0995 \\ 0.1523 \\ 0.1770 \\ 0.2002 \\ 0.2275 \\ 0.2515 \\ 0.3013 \end{pmatrix}$

Binary Interaction coefficients for SRK EOS

$$\delta := \begin{pmatrix} 0 & 0 & 0 & 0 & 0 & 0 & 0 & 0 & 0 & 0 \\ 0 & 0 & 0 & 0 & 0 & 0 & 0 & 0 & 0 & 0 \\ .0311 & .107 & 0 & 0 & 0 & 0 & 0 & 0 & 0 & 0 \\ .0515 & .1322 & .0026 & 0 & 0 & 0 & 0 & 0 & 0 & 0 \\ .0852 & .12413 & .014 & .0011 & 0 & 0 & 0 & 0 & 0 & 0 \\ .1 & .14 & .0256 & -.0067 & -.0078 & 0 & 0 & 0 & 0 & 0 \\ .0711 & .1333 & .0133 & .0093 & .0033 & 0 & 0 & 0 & 0 & 0 \\ .1 & .14 & -.0056 & .008 & .0111 & -.004 & .017 & 0 & 0 & 0 \\ .1 & .14 & .0236 & .0078 & .012 & .002 & .017 & 0 & 0 & 0 \\ .1496 & .145 & .0422 & .014 & .0267 & .024 & .0174 & 0 & 0 & 0 \end{pmatrix}$$

Gas Phase Fugacity coefficient calculations using Soave-Redlich-Kwong Equation of State

$$i := 0..9$$

$$j := 0..9$$

$$q_i := \left[0.48508 + 1.55171 \cdot w_i - 0.15613 \cdot (w_i)^2 \right]$$

$$\alpha_i := \left[1 + q_i \cdot \left[1 - \left(\frac{T}{T_{c_i}} \right)^{0.5} \right] \right]^2$$

$$aT_i := 0.42747 \cdot \frac{(R_c \cdot T_{c_i})^2 \cdot \alpha_i}{P_c}$$

$$b_i := 0.08664 \cdot R_c \cdot \frac{T_{c_i}}{P_c}$$

CO₂ Properties**Solid CO₂ Vapour Pressure**

$$V_p := \exp \left[\frac{-6030}{1.98588} \cdot \left(\frac{1}{T} - \frac{1}{273.15 - 78.5} \right) \right] \cdot 101$$

$$V_p = 193.992$$

Fugacity Coefficient of Pure CO₂ at Vp

$$\begin{aligned}
 F_{\text{CO}_2}(P) &:= \begin{aligned} &i \leftarrow 0 \\ &A \leftarrow 0.42747 \cdot \frac{P}{P_c} \cdot \frac{\alpha_i}{\left(\frac{T}{T_{c_i}}\right)^2} \\ &B \leftarrow 0.08664 \cdot \frac{P}{T} \cdot \frac{T_{c_i}}{P_c} \\ &Z \leftarrow \begin{pmatrix} -A \cdot B \\ A - B - B^2 \\ -1 \\ 1 \end{pmatrix} \\ &Z_0 \leftarrow \text{polyroots}(Z) \\ &f \leftarrow \exp \left[(Z_0 - 1) - \ln(Z_0 - B) - \frac{A}{B} \cdot \ln \left(1 + \frac{B}{Z_0} \right) \right] \end{aligned}
 \end{aligned}$$

$$F_{\text{CO}_2}(V_p) = 0.97$$

Solid CO₂ Molar Volume

$$V_m := \frac{(6 \cdot 10^{-6} \cdot T^2 + 0.0017 \cdot T + 0.7367)}{10^6} \cdot 44.01$$

$$V_m = 5.852 \times 10^{-5}$$

Z Factors

$$\begin{aligned}
 Z(y) &:= \begin{aligned} &a_m \leftarrow \sum_i \sum_j y_i \cdot y_j \cdot (a_{T_i} \cdot a_{T_j})^{0.5} \cdot (1 - \delta_{i,j}) \\ &b_m \leftarrow \sum_i y_i \cdot b_i \\ &A \leftarrow \frac{a_m \cdot P}{(R_c \cdot T)^2} \\ &B \leftarrow \frac{b_m \cdot P}{R_c \cdot T} \\ &Z \leftarrow \begin{pmatrix} -A \cdot B \\ A - B - B^2 \\ -1 \\ 1 \end{pmatrix} \\ &Z_0 \leftarrow \text{polyroots}(Z) \end{aligned}
 \end{aligned}$$

$$Z(z) = \begin{pmatrix} 0.095 \\ 0.452 + 0.334i \\ 0.452 - 0.334i \end{pmatrix}$$

Gas phase Fugacity Calculations

$$\begin{aligned} \text{Fcg}(y) := & \left| \begin{array}{l} \text{am} \leftarrow \sum_i \sum_j y_i \cdot y_j \cdot (aT_i \cdot aT_j)^{0.5} \cdot (1 - \delta_{i,j}) \\ \text{bm} \leftarrow \sum_i y_i \cdot b_i \\ A \leftarrow \frac{\text{am} \cdot P}{(Rc \cdot T)^2} \\ B \leftarrow \frac{\text{bm} \cdot P}{Rc \cdot T} \\ Z \leftarrow \begin{pmatrix} -A \cdot B \\ A - B - B^2 \\ -1 \\ 1 \end{pmatrix} \\ Z_0 \leftarrow \text{polyroots}(Z) \\ \text{rZo} \leftarrow \begin{cases} aZ_0 \leftarrow \text{Im}(Z_0) \\ \text{rZo} \leftarrow Z_{00} & \text{if } (aZ_{00} = 0) \cdot Z_{00} > 0 \\ \text{rZo} \leftarrow Z_{02} & \text{otherwise} \\ \text{rZo} \end{cases} \\ \text{for } s \in 0..9 \\ f_s \leftarrow \exp \left[(rZo - 1) \cdot \frac{b_s}{bm} - \ln(rZo - B) - \frac{A}{B} \cdot \left[\frac{2 \cdot \sum_j (aT_s \cdot aT_j)^{0.5} \cdot (1 - \delta_{sj}) \cdot y_j}{am} - \frac{b_s}{bm} \right] \cdot \ln \left(1 + \frac{B}{rZo} \right) \right] \\ f \end{array} \right| \end{aligned}$$

Liquid phase Fugacity Calculations

$$\begin{aligned}
 \text{Fcl}(y) &:= \left| \begin{array}{l}
 am \leftarrow \sum_i \sum_j y_i \cdot y_j \cdot (aT_i \cdot aT_j)^{0.5} \cdot (1 - \delta_{i,j}) \\
 bm \leftarrow \sum_i y_i \cdot b_i \\
 A \leftarrow \frac{am \cdot P}{(Rc \cdot T)^2} \\
 B \leftarrow \frac{bm \cdot P}{Rc \cdot T} \\
 Z \leftarrow \begin{pmatrix} -A \cdot B \\ A - B - B^2 \\ -1 \\ 1 \end{pmatrix} \\
 Zo \leftarrow \text{polyroots}(Z) \\
 rZo \leftarrow \left| \begin{array}{l}
 aZo \leftarrow \text{Im}(Zo) \\
 rZo \leftarrow Zo_2 \quad \text{if } aZo_2 = 0 \\
 rZo \leftarrow Zo_0 \quad \text{otherwise} \\
 rZo
 \end{array} \right. \\
 \text{for } s \in 0..9 \\
 f_s \leftarrow \exp \left[(rZo - 1) \cdot \frac{b_s}{bm} - \ln(rZo - B) - \frac{A}{B} \cdot \left[\frac{2 \cdot \sum_j (aT_s \cdot aT_j)^{0.5} \cdot (1 - \delta_{s,j}) \cdot y_j}{am} - \frac{b_s}{bm} \right] \cdot \ln \left(1 + \frac{B}{rZo} \right) \right] \\
 f
 \end{array} \right.
 \end{aligned}$$

Solubility

$$x_2(T) := \frac{V_p \cdot \text{FcgcO}_2(V_p)}{P \cdot \text{Fcl}(z)_0} \cdot \exp \left[\frac{V_m}{Rc \cdot T} \cdot (P - V_p) \right]$$

$$x_2(T) = 0.58$$

Freezing Point of the Mixture

$$T_{fr} := \frac{V_m}{Rc} \cdot \frac{(P - V_p)}{\ln \left[\frac{(z_0) \cdot \text{Fcgc}(z)_0 \cdot P}{V_p \cdot \text{FcgcO}_2(V_p)} \right]}$$

$$T_{fr} - 273.15 = -65.71$$

Michelsen VLE Phase Stability Algorithm

$i := 0..9$

Initial liquid Phase Composition:

$$gK_i := \frac{P_{Ci}}{P} \cdot \exp \left[5.42 \cdot \left(1 - \frac{T_{Ci}}{T} \right) \right]$$

$$ly_i := gK_i \cdot z_i$$

$l := 0..9$

$$lz_l := \ln(z_l \cdot Fcg(z)_l)$$

$$lk := \ln(ly) + \ln(Fcl(ly)) - lz$$

$$mY_i := ly_i \cdot \exp(-lk_i)$$

```

sb:=
  n ← 0
  st ← 0
  sb ← 0
  Yn ← mY
  yn ← ly
  while n < 100
    G ← ln(Yn) + ln(Fcl(yn)) - lz
    tG ← ∑i |Gi|
    st ← st + 1 if tG < 10-12
    sb ← 1 if (tG < 10-12) · [∑i (Yn)i ≤ 1]
    Yn+1 ← exp(lz - ln(Fcl(yn)))
    n ← n + 1
    yn ←  $\frac{Y_n}{\sum_i (Y_n)_i}$ 
  (st sb n)
sb = (90 0 100)

```

(Note: sb = 1 is stable, sb = 0 unstable)

Initial Guess Value for y

```

yr := | m ← 0
      | ym ← 0 if sb0,1 = 1
      | otherwise
      |   ym ← ly
      |   while m ≤ sb0,0
      |     | Ym+1 ← exp(lz - ln(Fcl(ym)))
      |     | m ← m + 1
      |     | ym ←  $\frac{Y_m}{\sum_i (Y_m)_i}$ 
      | ym

```

Michelsen VLE Flash Calculations

```

i := 0..9
F(β, K) :=  $\sum_i \frac{z_i \cdot (K_i - 1)}{[1 + (K_i - 1) \cdot \beta]}$ 
β := 0.5
st(K) := root(F(β, K), β)
fx(K, i) :=  $\frac{z_i}{[1 + (K_i - 1) \cdot st(K)]}$ 
fy(K, i) :=  $\frac{K_i \cdot z_i}{[1 + (K_i - 1) \cdot st(K)]}$ 
x(K) := for i ∈ 0..9
        | mxi ← fx(K, i)
        | mx
y(K) := for i ∈ 0..9
        | myi ← fy(K, i)
        | my
eK(K, i) :=  $\frac{Fcl(x(K))_i}{Fcg(y(K))_i}$ 

```

```

Keq := sK ← 0 if yr = 0 ∨ sb0,1 = 1
      otherwise
        m ← 0
        tdK ← 1
        for i ∈ 0..9
          Koi ←  $\frac{yr_i}{z_i}$ 
        Km ← Ko
        while tdK > 10-7
          break if st(Km) ≥ 1
          sK ← for i ∈ 0..9
                sKi ← eK(Km, i)
          sK
          dK ← sK - Km
          tdK ←  $\sum_i |dK_i|$ 
          Km+1 ← sK
          m ← m + 1
        sK

```

Composition of Gas and Liquid Phase

Vapour Fraction:

$$st(Keq) = 0.029$$

Freezing Point of Vapour

$$T_{frV} := \frac{V_m}{R_c} \cdot \frac{(P - V_p)}{\ln \left[\frac{(y(Keq)_0) \cdot F_{cg}(y(Keq))_0 \cdot P}{V_p \cdot F_{cgCO_2}(V_p)} \right]}$$

$$T_{frV} - 273.15 = -78.959$$

Freezing Point of Liquid

$$T_{frL} := \frac{V_m}{R_c} \cdot \frac{(P - V_p)}{\ln \left[\frac{(x(Keq)_0) \cdot F_{cl}(x(Keq))_0 \cdot P}{V_p \cdot F_{cgCO_2}(V_p)} \right]}$$

$$T_{frL} - 273.15 = -78.959$$

Appendix G.

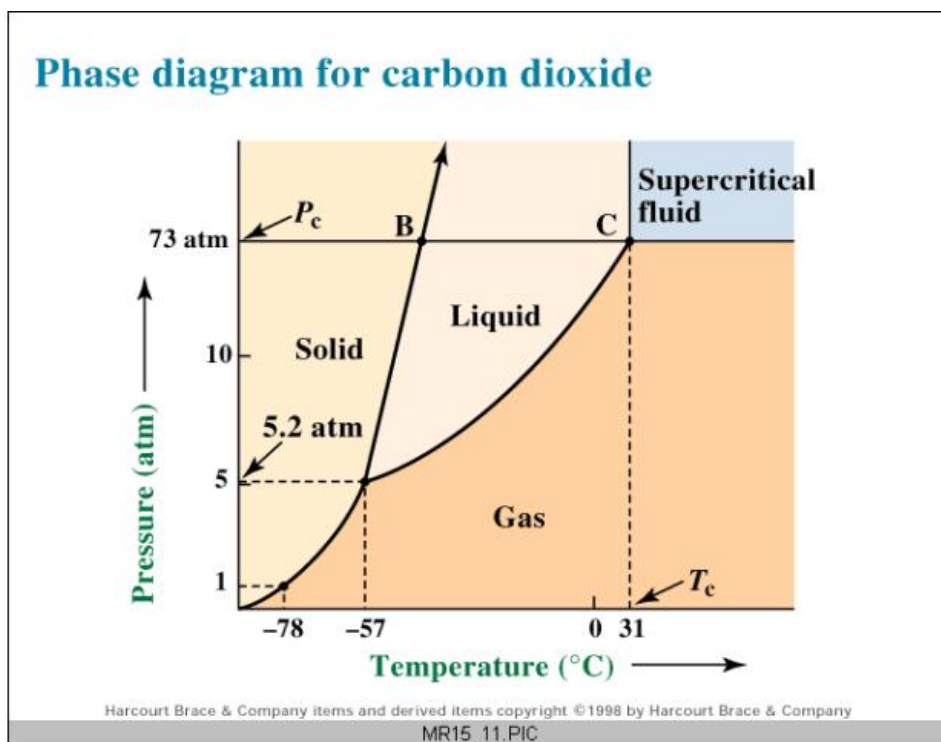
Observations During Gas Mixture Preparation

The mixture is usually prepared by pressurising the mix drum from the top and as follows:

- 1) All gas is evacuated from the system using a vacuum pump
- 2) Add Nitrogen to 10 psi and Argon to 23 psi
- 3) Add CO₂ to 603 psi (max achievable pressure)
- 4) Add Hydrogen to 1470 psi

With this sequence the analytic results of the gas samples taken from top and bottom of the mix drum were consistently such that the CO₂ concentration was significantly higher at the bottom and that the top sample showed very low or no CO₂. This suggested condensation during loading of the gases.

In Step 3 and particularly Step 4, CO₂ condenses in the mix drum according to the phase diagram in Figure G.1 and because the Hydrogen acts as a cushion, it basically compresses the CO₂ which is already in the vessel.



Dr. S. M. Condren

CBU
Chemistry

Figure G. 1 CO₂ phase diagram

In order to prove the appearance of liquid CO_2 as well as to determine the effectiveness of the proposed solutions, a batch experiment was conducted using a sapphire cell.

The CO_2 started condensing immediately when the Hydrogen started entering the cell and a further increase in pressure lead to a significant amount of liquid condensing, as illustrated in Figure G.2.

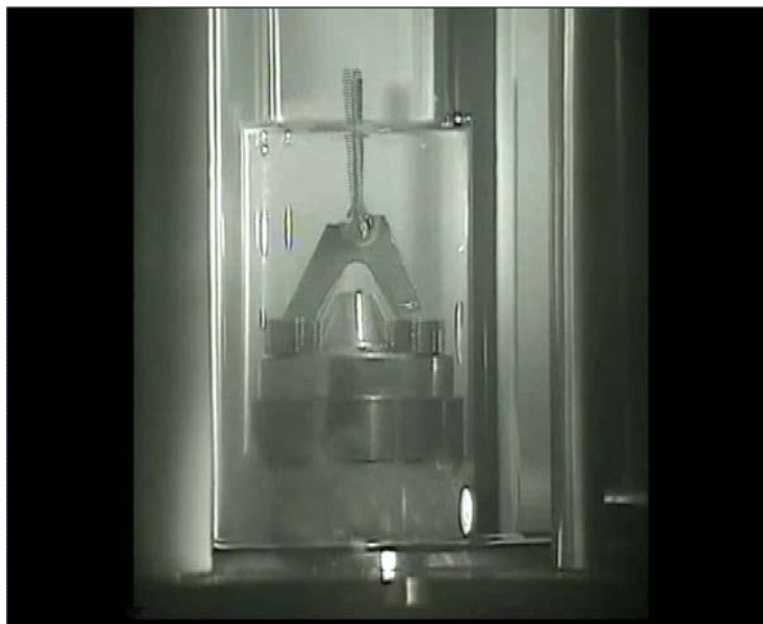


Figure G. 2 CO_2 condenses with Hydrogen acting as a press

When Hydrogen is added to the liquid CO_2 , some time is required for evaporation of all Carbon Dioxide. The cell was exposed to vigorous stirring overnight, however this was insufficient to evaporate all CO_2 .

The proposed solution to this problem was:

- 1) All gas is evacuated from the system using a vacuum pump
- 2) Add Nitrogen to 10 psi and Argon to 23 psi
- 3) Add Hydrogen to approximately 400 psi
- 4) Add CO_2 to approximately 900 psi using the booster pump
- 5) Add the rest of the Hydrogen slowly from the bottom of the vessel to allow for better mixing to 1470 psi
- 6) Leave the mixture in a well heated room overnight prior to the experiment